The Generation of Cavitation for the Removal of Fouling on Submerged Structures Using High Power Ultrasonic Transducers

Habiba Lais

A thesis submitted for the degree of

Doctor of Philosophy

Brunel University London

Institute of Materials and Manufacturing

College of Engineering, Design and Physical Sciences

Department of Mechanical, Aerospace and Civil Engineering

21 08 2019

I, Habiba Lais, confirm that the work presented in this thesis is my own. Where information has been derived from other sources, I confirm that this has been indicated in this work.

Abstract

Institute of Materials and Manufacturing

College of Engineering, Design and Physical Sciences

Department of Mechanical, Aerospace and Civil Engineering

Doctor of Philosophy

by Habiba Lais

The accumulation of fouling is a well-known problem in industry which can occur on various different structures depending on the surrounding environmental conditions. The removal of this fouling can be very costly and has resulted in many attempts to mitigate, monitor and remove fouling accumulation in a cost-effective manner. As mitigating techniques cannot guarantee 100% fouling removal of a structure, another approach is to detect and monitor the fouling accumulation to assist in carrying out de-fouling procedures. Current detection methods such as PIGging can also require halts in production to carry out monitoring. In recent years, the application of Ultrasonic Guided Waves (UGW) for fouling detection has been recognised as a promising and non-invasive technique; however, its research is still in its early stages. To complement a non-invasive fouling detection technique, the application of high power ultrasounds has gained much attention from the industry for in-situ fouling removal. Much research has been conducted to advance the knowledge on the potential uses of ultrasonics across different fouling applications, primarily in reverse osmosis membranes and heat exchangers. However, improvements of the in-situ ultrasonic fouling removal technique has not yet been investigated and is also in its infancy. This research arises as a continuation from the InnovateUK funded CleanMine project and as part of the InnovateUK funded HiTClean project. This thesis elaborates on the fundamentals of High Power Ultrasonic Transducers (HPUT) used for generating acoustic cavitation bubbles for achieving ultrasonic cleaning. This knowledge is used in the development of a Finite Element (FE) model which is validated using experimental characterisation of the impedance. The HPUT FE model is used to further understand the design and development of sonotrode attachments for future improvements of the ultrasonic cleaning technique. The FE model is expanded for the prediction of cavitation generation to determine cleaning patterns and is validated in laboratory conditions. By utilising controlled fouling generation capabilities, fouling detection using UGW is investigated and an FE model is used to further characterise variables that can quantify the detection of fouling accumulation with potential applications of monitoring fouling removal. The FE method for fouling removal predictions is used to optimise an HPUT configuration for achieving long-distance fouling removal coverage on a 6.2 meter long, 6 inch diameter schedule 40 (168 mm outer diameter and 7.11 mm wall thickness) carbon steel pipe. The confirmed 4-HPUT configuration is developed for laboratory validation and demonstrates wave propagation up to ± 3 meters from a single HPUT location.

Dedicated to my nieces;

Anika Laila Hasnat,
Alia Tara Hasnat,
Amelia Lais Al Balushi,
and Aria Lais Al Balushi

In life, nothing lasts forever. You only live once, so why waste it on living someone else's life and dream? Take chances, make mistakes but never regret. Never be late to do something you want to do right now. Stop chasing happiness, instead, find it in the moment that you are living in. Because one day you will realise that everything you did will define exactly who you are and who you will become.

Contents

Figures

Tables

Acknowledgements

My gratitude goes to my supervisory team; Prof. Luiz Wrobel (hope you are enjoying Brazil), Prof. Tat-Hean Gan (have fun in Singapore!), Dr. Makis Livadas (keep enjoying them sweeties) and Mr. Jamil Kanfoud (my road trip buddy). My biggest thanks goes to Dr. Shehan Lowe for his charity work as a volunteer mentor throughout this PhD, I wouldn't have gotten this far without you! Do not forget the impact you have made on my life and I wish you all the best in the future. Thanks to everyone that has helped me join BIC as a member of staff. Thanks to Prof. Bala for checking up on me regularly (to make sure I still had a pulse) and reading my thesis.

I would like to give my appreciations to Marcus and Gareth for putting up with all of my ridiculous experiments (especially when it came to the clean-up), Plant Integrity Ltd. and InnoTecUK. Project Technical Assistants (Jimmy, Girthan, Veena, Bradley, Joash, Daniel and Aris), not forgetting the O.G. Adrian Waka, thanks for the blue box and the fireworks, much appreciated. Mahesh and Marco B. for the free graphic design and data visualisation consultations, my work is much more presentable now. My library buddy; Evelyne for being there during the darkest periods of my thesis write-up in ARU and also dancing with me in the park with a Chatime in hand. Many thanks to my imaginary friend Linda whom, has acted as a statistical voice of reason in the times I've needed it most, you have been a great support throughout the biggest turning points in my life and during this PhD. Shout out to all of my buddies in BIC, Brunel, LSBIC, PI, TWI, NIC and NSIRC that have also contributed to this enterprise and cheered me on throughout, I hope you all enjoyed the consequential memes/stickers/GIFs produced during this period.

The support I have received from my family throughout my life has given me the courage to get to where I am now. I am almost certain that they still don't know what my research is about however, they never fail to believe in my capabilities to achieve whatever I put my focus into.

My ghetto proof-reader, lifelong companion and captain of the cheerleading squad, Shanice, thanks for reading all the scientific jargon and saving me from some very questionable lines getting published, I couldn't have done it without your support and belief, I've truly been blessed to have you in my life since day one.

Abbreviations

2D	2-Dimensional
3D	3-Dimensional
CFD	Computational Fluid Dynamics
CLV	Compact Laser Vibrometer
EDM	Electrical Discharge Machining
FE	Finite Element
FEA	Finite Element Analysis
FFT	Fast Fourier Transform
FSI	Fluid-Solid Interaction
FVM	Finite Volume Method
GA	Genetic Algorithms
GUIGUW	Graphical User Interface for Guided Ultrasonic Wave
HPUT	High Power Ultrasonic Transducer
pH	Potential of Hydrogen
PIG	Pipeline Intervention Gadget
PSV	Polytec Scanning Vibrometer
PZT	Piezoelectric Transducer
RoHS	Restriction of Hazardous Substances
SAFE	Semi Analytical Finite Element
SAW	Surface Acoustic Wave
SBSL	Single-Bubble Sonoluminescence
TDR	Time-Domain Reflectometry
UGW	Ultrasonic Guided Wave
UT	Ultrasonic Testing

Nomenclature

Symbol	Description	Unit
a	radius	M
c	speed of sound	m/s
c_l	group velocity of longitudinal wave	m/s
c_t	group velocity of torsional wave	m/s
c_E	elasticity matrix	Pa
$\mathbf{D}$	electric displacement field	C/m^2
D	Diameter	M
E	young's modulus	Pa
$\mathbf{E}$	electric field	V/m
e	piezoelectric coupling coefficient	-
E_J	Energy	J
ε_S	permittivity matrix.	F/m
f	Frequency	Hz
F_{bw}	frequency bandwidth	Hz
F	Force	N
f_0	central frequency	Hz
h_0	maximum allowed element size	M
k_n	wave number	-
k	taper factor	-
k_i	bandwidth of lobe	-
L	length	M
L_{Horn}	length of the ultrasonic horn	M
l_e	element length	M
n_x	natural number of optimal distance	
N_C	number of cycles	-
N	natural number	-
N	number of elements per wavelength	-
p_a	acoustic pressure	Pa
Pw	power	W
P	pressure within the bubble	Pa
p_∞	external pressure infinitely far from the bubble	Pa

ϱ_L	liquid density	kg/m^3
ϱ_S	solid density	kg/m^3
ϱ	Density	kg/m^3
R	radius of the bubble	M
r	radius of the inner pipe wall	M
S	surface tension of the bubble	N/m
S_A	surface area	m^2
$\bar{\bar{S}}$	strain tensor	-
$\bar{\bar{T}}$	stress tensor	Pa
ts	duration of cleaning	S
$\varDelta t$	observational time step	S
t_x	ratio of mesh size over observation time step	-
t	Time	S
T_t	time of arrival of the torsional wave mode	S
T_l	time of arrival of the longitudinal wave mode	S
U	three-dimensional displacement vector	M
$\boldsymbol{u}$	solid displacement field	M
V	electric potential corresponding to the electric field	V
Vo	modulated input signal	V
v_0	velocity amplitude of the horn tip	m/s
v_L	kinematic viscosity of the surrounding liquid	m^2/s
υ_{gr}	group velocity	m/s
υ_{ph}	phase velocity	m/s
W	amplitude of vibration	m/s
ω_n	angular frequency	Hz
x	distance	M
λ	Wavelength	M
λ_{min}	wavelength of the maximum frequency propagated	M
$\varLambda$	Lamé constants	-
μ	Lamé constants	-
∇	three-dimensional Laplace operator	-
ϕ	compressional scalar potential	-
Φ	equivoluminal vector potential	-
ω	displacement	M

Chapter 1: Introduction

Every journey begins with a single step. We just have to have patience – Milly Thompson

1.1 MOTIVATION

Fouling is a well-known problem in industry as it occurs on various different engineering assets depending on the environmental conditions surrounding the fouled structure. In industry, there are different means in which a liquid substance can be transported, one example being through pipes. As pipes are filled with a liquid, the movement of this fluid can begin to accumulate fouling and/or scaling on the inner wall of the pipe (example is shown in Figure 1.1) and can result in a pipeline blockage. The occurrence of a blockage in a pipeline will immediately affect the pipeline performance to transport liquid and leads to the operating condition being below an acceptable level. The fouling/scaling that is generated also contribute to the contamination of the moving liquid, which can affect the quality of the fluid which passes the contaminated walls.

> *"According to Scottish industry leader Paradigm Flow Solutions,*
> *subsea pipeline blockages cost operators tens of millions of dollars*
> *every year, by using expensive conventional methods such as subsea*
> *interventions by ROVs or saturation divers."* [1]

The accumulation of fouling has a significant effect on pipelines as it increases the likelihood of pipeline failure. More specifically, corrosion fouling accounts for 65% of pipeline failure [2]-[3]. The implications of this includes; danger to surrounding individuals, unscheduled downtime as well as economic impact due to maintenance costs and profit loss (see Table 1.1). The

Figure 1.1: Example of fouling accumulation on inner wall of pipe specimen

decommissioning process of pipelines must abide by regulations to de-contaminate, clean, dispose and recycle material [4], [5]. In some cases, the pipelines must be transported to land to carry out de-fouling, which again has cost implications. For the decommissioning process to achieve a more streamlined approach, various aspects must be maintained to allow decommissioned pipelines to carry less cost implications; one method is to minimise the fouling accumulation of the pipe before decommission and also prolong the pipelines lifespan by the reduction of fouling.

Table 1.1: Costs and implications of scale accumulation [6]

Scale Location	Problems Caused	Costs
Pipelines transferring oil/gas	• Reduced flow capacity. • Increased linear pressure drop.	• Production shut-downs (planned and forced). • Capital costs for increased pump capacity. • Chemical inhibitor costs.
Well bore	• Loss of communication with reservoir. • Loss of reservoir pressure maintenance for injectors. • Loss of water flood pattern injectivity. • Increased potential for watered out production wells (reduced secondary recovery).	• Workover rig costs. • Loss of well and field production potential. • Equipment costs to reduce hydrostatic head (pumps). • Chemical inhibitor costs. • Production shut-down (planned and forced).
Heat transfer equipment on the oil/gas recovery platform	• Reduced process efficiency. • Equipment failure (may be catastrophic).	• Increased thermal energy input costs. • Reduced process capacity. • Chemical inhibitor costs. • Equipment replacement costs. • Production shut-downs (planned and forced).

The removal of fouling can be very costly and has resulted in many attempts to mitigate, monitor and remove fouling accumulation in a cost-effective manner. This growth of fouling is difficult to mitigate and also costly to remove, as mitigating means cannot guarantee 100% anti-fouling of a structure.

1.1.1 FOULING MITIGATION

Methods for mitigation of fouling build-up have been addressed through means of new materials (such as composites) as lining rehabilitation. This includes but is not limited to Teflon, nanocomposites, plastics, fibre-reinforced polymers and alloys. The addition of coatings of the aforementioned materials can assist in preventing the build-up due to the lining on the structures'

walls. Other preventative means can include the design optimisation of the structure to reduce fouling build-up, common in heat-exchangers. Another method of prevention is the assistance of chemicals known as 'acid treatment' or 'pH control' [7], as well as the addition of chemical agents into the processed liquid. Magnetic fields [8] and electric fields [9] have both been used for crystallisation fouling and biological fouling prevention.

1.1.2   FOULING DETECTION

Current detection methods require halts in production to carry out monitoring such as Pipeline Intervention Gadget (PIG), also known as PIGging. New tools in PIGging have been used such as ultrasonic inspection equipment, for not only cleaning, but also for detecting failures and corrosion, or to verify the cleaning efficiency. In recent years, the usage of Ultrasonic Guided Waves (UGW) has been recognised as a potential solution for the detection of fouling accumulation through structural health monitoring but is still in its initial stages of readiness for industrial practice.

1.1.3   FOULING REMOVAL

One of the most used fouling removal techniques that has been applied to pipelines is the use of chemicals as it can achieve up to 100% removal; however, this is achieved with the addition of harsh implications to the environment. Legislation has recently surfaced to demote the use of chemicals, thus other solutions for fouling removal and prevention must be reviewed and carried out in replacement of chemicals. Various techniques on the market require the halt of production and facilities to carry out de-fouling due to its invasive approach. The pause in production can amount to profit losses that can become costly. A non-invasive approach would provide added benefit of removal without the halting of facilities (see Figure 1.2). This thesis investigates the ultrasonic approach to fouling removal of pipelines using a bespoke array of High Power Ultrasonic Transducers (HPUT). With the support of previous work that has shown potential of

| Alternative to chemicals | Reduced downtime | Reduced maintenance | Improved efficiency | Extended service life |
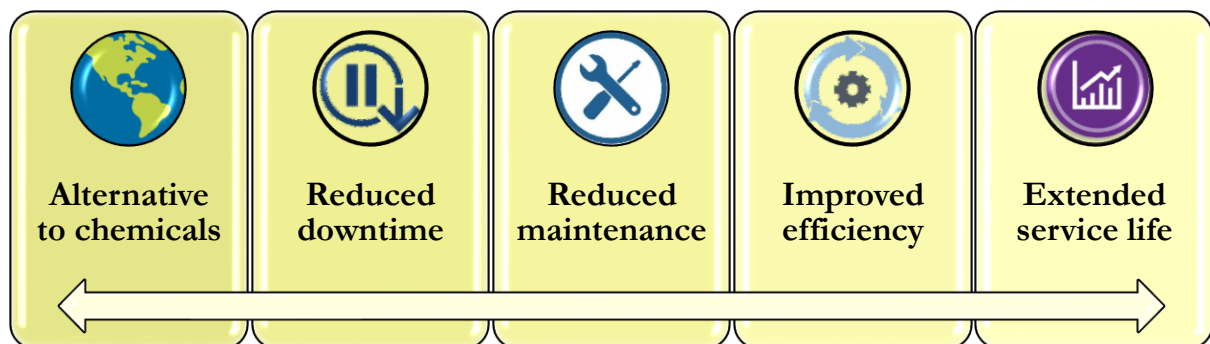
Figure 1.2: Advantages of a non-invasive and in-situ alternative to fouling removal

non-invasive fouling removal of a common crystallisation fouling known as Calcite, the ultrasonic technique is investigated to achieve long distance cleaning. To assist in the optimisation of fouling removal at long distances, UGW are used to non-invasively detect fouling build-up.

Table 1.2: Current fouling removal and mitigation for internal scaling formation [6]

Cleaning method	Intrusiveness (damage risk)	Geometrical constraints	Effectiveness	Cost
Internal scaling				
Flushing	L	L	L	L
Swabbing or PIGging	H	H	M/H	M/H
Non-stop production PIGging	L/M	H	H	H
Abrasive PIGging	H	H	H	M/H
Smart PIGging	M/H	H	H	M/H
Ice PIGging	L/M	L	H	L/M
Air scouring	H	L	H	M/H
Chemical cleaning	M/H	L	H	H
Chelating agents (prevention)	L/M	L	H	H
Chemical inhibitors (ditto)	L/M	L	H	H
Jetting	H	L/M	H	M/H
Explosives	H+	H+	H	H
Lining and rehabilitation	H	M/H	H	H
Abrasive cleaning	H	L	L	H*
Non-toxic protective coatings	H	H	L**	M/H
Proposed ultrasonic method	L	L	H+	L
Note: Cost L = ~ £230k. Cost H+ = costs exceeding ~ £1.5m- £3m per platform per annum (5-10% of total operational expenditure).				

1.2 AIM OF RESEARCH

Current methods for the removal of fouling has shown to be invasive and require a halt in operation of the engineering asset to carry out the procedure. This research intends to improve an alternative in-situ ultrasonic fouling removal technique for the application onto larger diameter, pipeline structures. This is shown through the investigation of ultrasonics to generate acoustic cavitation within the liquid of a filled pipe. Resulting in the implosion of bubbles that dislodge fouling accumulation from the structure. The accumulation is detected using UGW to assist in optimising the ultrasonic fouling removal procedure. Numerical investigation is utilised to develop an HPUT array that is applied to a larger diameter pipeline for achieving long-distance cleaning coverage. The HPUT configuration is adapted for experimental validation in underwater conditions for future industrial applications.

1.3   SPECIFIC OBJECTIVES

To achieve the aim of the research, key objectives are outlined as follows:

- Understanding of different types of fouling and review the current state-of-art UGW detection and ultrasonic fouling removal methods. Define a gap in knowledge that is investigated for the remainder of this research.

- Development of a HPUT Finite Element (FE) model, consider geometric variations which could improve the HPUT for acoustic cavitation generation and cleaning coverage. The model should output wave propagation and impedance results that can be compared to the HPUT characterisation in experimental conditions.

- Adaption of the HPUT FE model for development of an ultrasonic cleaning FE method. Collect supportive literature to understand key features of predicting acoustic cavitation through Finite Element Analysis (FEA).

- Generate crystallisation fouling known as Calcite on pipe samples that can be up-scaled onto a large diameter pipeline. The fouling accumulation will be investigated and monitored by using a UGW collar in pitch-catch configuration and further analysed using FEA.

- Create a fouled sample pipe to undergo validation of the FE method and verify the ultrasonic cleaning concept by measuring the wave propagation across the outer wall of the pipe specimen. The validated FE model will be expanded for larger diameter pipes and investigate HPUT parameters to optimise the cleaning technique to achieve long-distance coverage.

- Laboratory trials of the selected HPUT configuration to be characterised by acquiring vibrational displacement on the outer wall of the structure to determine its long-distance wave propagation. The confirmed configuration will be adapted for underwater demonstration.

1.4   SUMMARY OF RESEARCH METHODOLOGY

The research begins with conducting a literature review of current fouling removal methods using ultrasounds to recognise current strengths and limitations as well as the specific fouling removal mechanisms presented (i.e. vibration and pressure field). A general FE model of the HPUT is created within COMSOL Multiphysics, which is validated using the Agilent 4294A Precision Impedance Analyzer in laboratory conditions. With the validated model, ultrasonic sonotrode enhancements are investigated for improved wave propagation and coverage using the Polytec PSV-400 3D Laser Scanning Vibrometer. To carry out de-fouling, a hard scale crystallisation fouling known as Calcite is generated on the inner walls of a Schedule 40 (168 mm outer diameter

and 7.11 mm wall thickness), 6 inch diameter, 6 meter long carbon steel pipe. This is done by heating the outer wall of the pipe up to 120 °C using Cooper heating and spraying a highly concentrated calcium carbonate solution on the inner wall of the pipe. The fouled pipe specimen undergoes UGW inspection to detect the accumulation of fouling and is compared with FE modelling results using COMSOL Multiphysics. A fouled sample pipe is used to demonstrate the ultrasonic cleaning concept and validate the FE method using the Polytec PSV-400 3D Laser Scanning Vibrometer to measure out-of-plane displacement of the outer wall of the pipe. The displacement locations are matched to the achieved cleaning on the inner wall of the sample pipe. The validated ultrasonic cleaning numerical model is applied to the Schedule 40, 6 inch diameter, 6 meter long carbon steel pipe. COMSOL Multiphysics is used to investigate HPUT parameters for improved coverage and long-distance wave propagation capabilities to promote the generation of acoustic cavitation away from the HPUT location. The selected HPUT configuration is validated in laboratory conditions using the Polytec CLV-3D Laser Vibrometer to monitor fixed points along the length of the pipe. The HPUT configuration undergoes marinisation to characterise its performance for future underwater applications.

Figure 1.3 highlights the research methodology in the form of a flowchart which shows decisions driven by the development of a numerical methodology that achieves experimental validation. The research begins with identifying the fundamental need of an alternative to current fouling removal methods and carrying out a literature survey. Once areas of improvements are identified, the proposed technique can be numerically modelled and validated using experimental trials. The validated model can then be applied for the desired structure to carry out de-fouling.
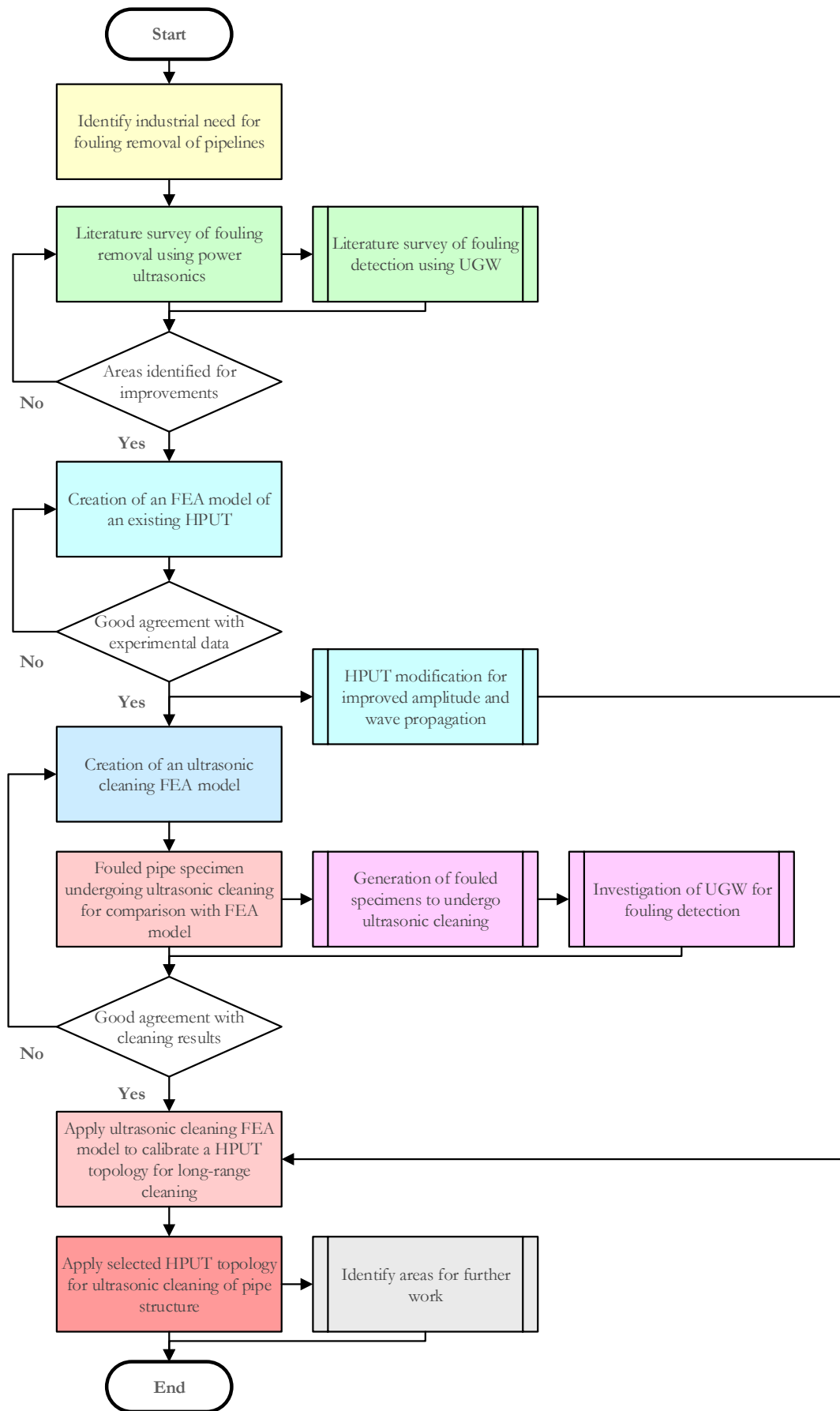
Figure 1.3: Research methodology flowchart of thesis

1.5   THESIS OUTLINE

The thesis framework is summarised in Figure 1.4, presenting the background, methods and applications chapters. The thesis is organised to discuss the fundamentals of fouling accumulation and current methods to mitigate, monitor and remove fouling. This is highlighted in **Chapter 2**, which focuses on non-invasive techniques currently used for the detection and removal of fouling using ultrasonics.

The design, development and application of HPUTs are discussed in **Chapter 3**, portraying the advances of optimisation of the HPUT using FE modelling by the enhancement of ultrasonic sonotrodes. These undergo validation in laboratory conditions and show improvement of wave propagation which, in turn, promotes the generation of acoustic cavitation.
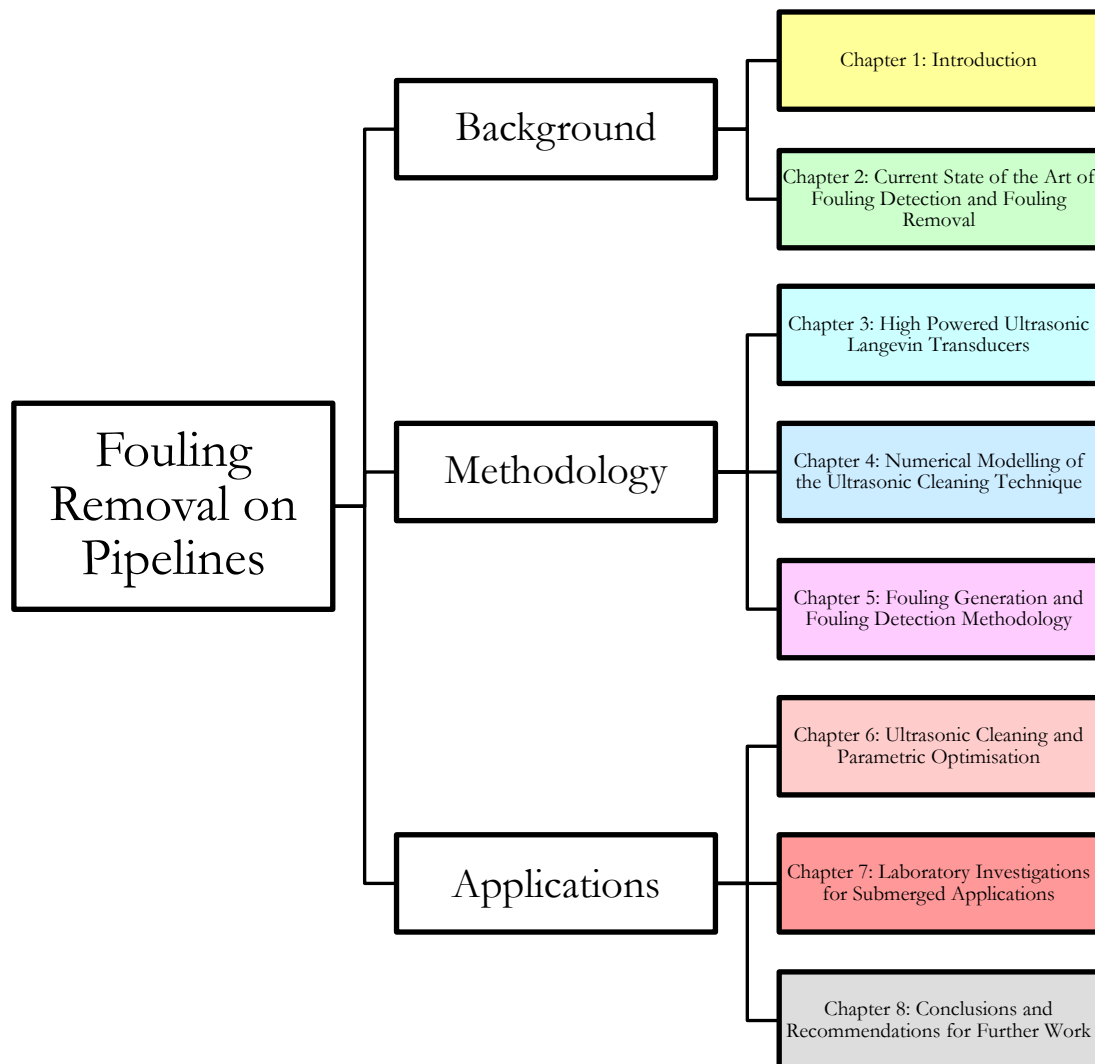
Figure 1.4: Thesis framework

The FE method is extended in **Chapter 4** to firstly understand the current state-of-the-art methodologies used to model ultrasonic cleaning and predict acoustic cavitation. An FE model is then created which discusses the attachment of an HPUT on the outer wall of a cylindrical specimen, to measure the acoustic pressure field determining it has met the threshold to generate acoustic cavitation.

To validate the ultrasonic cleaning method, a hard-scale crystallisation fouling known as Calcite is created on the inner wall of pipe specimens in **Chapter 5** using electrochemistry before trialling a heat deposition methodology for fouling generation on larger diameter, longer pipelines. This chapter uses UGW to detect the accumulation of fouling in laboratory conditions, which is demonstrated by a change in UGW signal in pitch-catch configuration. This characterises fouling detection based on frequency, cycle input and wave mode excitation before investigating further the fouling thickness using FEA.

Chapter 6 utilises the fouled sample pipe to demonstrate the ultrasonic cleaning technique and validate the FE method created in Chapter 4. A laboratory investigation is carried out to determine the capabilities of the numerical method for predicting de-fouling patterns based on out-of-plane displacements. With the verification of the model, this is used to assist in optimising a HPUT configuration for cleaning of a larger cylindrical sample that has been previously produced in Chapter 5. The number of HPUTs in the configuration and parametric wave inputs is studied to select the final configuration.

The selected HPUT configuration undergoes marinisation for characterisation of its performance for potential underwater applications in **Chapter 7**. Opportunities for applications in underwater and de-commissioned pipe specimens has been utilised for investigating the cleaning capabilities in conditions representative of pipeline structures currently operating in industry.

The knowledge developed throughout the thesis is discussed in the conclusions, along with the suggestions of applications for further technical development and scalability (**Chapter 8**).

1.6　CONTRIBUTIONS TO KNOWLEDGE

1.6.1　HPUT SONOTRODE ENHANCEMENT

HPUTs have undergone improvement and optimisation of their amplification properties for various applications in industry. However, this has not been investigated for fouling removal purposes. Common HPUT sonotrode geometries (cylindrical, conical, exponential and stepped)

were designed in COMSOL Multiphysics for a 40 kHz HPUT. Each design was optimised to half a wavelength and manufactured in aluminium for acoustic coupling with the HPUT front mass. The Polytec PSV-400 3D Laser Scanning Vibrometer was used to measure the wave propagation across a carbon steel plate. The results show improvements of the out-of-place displacement by 300% when using a cylindrical sonotrode. This promotes the capability of the HPUT to surpass the minimum threshold for generating acoustic cavitation for ultrasonic cleaning applications.

1.6.2   INSPECTION OF FOULING ACCUMULATION IN PIPELINE USING UGW

UGW has become a common practise in industry for non-invasive, long range inspection of structures. Some work has been done to detect fouling accumulation, particularly for food industry applications but has not utilised the non-dispersive torsional wave mode and has not been applied for long range detection. This technique has been applied within this research in pitch-catch configuration for the inspection of Calcite fouling accumulation of a Schedule 40, 6 inch diameter, 6 meter long carbon steel pipe using the fundamental, non-dispersive torsional wave mode, and has shown a reduction in amplitude in the received signal by 0.5 dB/m with the accumulation of Calcite. Further FEA in COMSOL Multiphysics has shown that, with an increase in Calcite thickness, there is a reduction in amplitude as well as a shift in time-of-arrival of the receiving signal. This gives two variables that can be used for further characterisation of fouling accumulation monitoring.

1.6.3   LONG DISTANCE ULTRASONIC CLEANING

With the proof of concept of the ultrasonic cleaning technique, an FE model was created in COMSOL Multiphysics that has shown the cleaning potential by linking the displacements achieved in experimentations to cleaning patterns in the numerical results. The acoustic pressure has achieved a minimum of 5 Bar pressure within the liquid at the locations of predicted cleaning regions, confirming the possibility of generating acoustic cavitation to carry out the fouling removal mechanism. The numerical method was expanded onto a Schedule 40, 6 inch diameter, 6 meter long carbon steel pipe where the number of HPUTs and cleaning parameters were studied to select a final configuration. Experimental investigations were carried out and show that with an increase in the number of HPUTs, there is an increase in wave propagation across the length of the pipe. The 4-HPUT configuration has shown improved potential for generating acoustic cavitation up to 3 meters away from the HPUT attachment location, resulting in long distance non-invasive cleaning from a single attachment location.

1.6.4 HPUTs FOR UNDERWATER APPLICATIONS

The 4-HPUT configuration undergoes marinisation for underwater applications. This study has shown that the addition of marinised material dampens the vibrational output from the HPUT configuration. This reduction in vibration is most significant when the structure is filled with water due to attenuation, resulting in a marinised HPUT configuration dropping by up to 85% and a non-marinised HPUT configuration dropping by up to 80%.

1.6.5 JOURNAL PUBLICATIONS ARISING FROM THIS PHD

a) Lais, H., Lowe, P.S., Gan, T.-H., and Wrobel, L.C. (2018) 'Numerical Modelling of Acoustic Pressure Fields to Optimize the Ultrasonic Cleaning Technique for Cylinders', Ultrasonics Sonochemistry, Vol. 45, 7-16.

b) Lais, H., Lowe, P.S., Gan, T.-H., Wrobel, L. C. and Kanfoud, J. (2018) 'Characterization of the Use of Low Frequency Ultrasonic Guided Waves to Detect Fouling Deposition in Pipelines', Sensors, Vol. 18, article 2122.

c) Lais, H., Lowe, P.S., Gan, T.-H., and Wrobel, L.C. (2019) 'Numerical Investigation of Design Parameters for Optimization of the In-Situ Ultrasonic Fouling Removal Technique for Pipelines', Ultrasonics Sonochemistry, Vol. 56, 94-104.

d) Lais, H., Lowe, P.S., Wrobel, L.C., and Gan, T.-H. (2019) 'Investigation of Ultrasonic Sonotrode Design to Improve the Performance of Ultrasonic Fouling Removal, IEEE Access, Vol 7, 148897-148912.

e) Lais, H., Lowe, P.S., Wrobel, L.C., and Gan, T.-H. (2019) 'Ultrasonic Transducer Array Performance for Improved Cleaning in Marine and Freshwater Applications', Applied Sciences, Vol. 9, article 4353.

1.6.6 CONFERENCE PUBLICATIONS ARISING FROM THIS PHD

a) Lais, H., Lowe, P.S., Kanfoud, J., and Gan, T.-H. (2017) 'Application of High Power Ultrasonics for Fouling Removal in Submerged Structures', IEEE/MTS OCEANS'17 Conference.

b) Lais, H., Lowe, P.S., Kanfoud, J., and Gan, T.-H. (2017) 'Advancements in Fouling Removal using High Power Ultrasonics for Industrial Applications', IEEE ICIIS'17 Conference.

c) Lais, H., Livadas, M., Lowe, P.S., Kanfoud, J., Wrobel, L.C., and Gan, T.-H. (2017) 'Removal of Fouling in Submerged Structures Using High Power Guided Ultrasonic Waves', NSIRC Annual Conference.

d) Lais, H., Livadas, M., Lowe, P.S., Kanfoud, J., Wrobel, L.C., and Gan, T.-H. (2017) 'Fouling Removal in Submerged Structures Using High Power Ultrasonics', Brunel University Student Research Conference.

e) Lais, H., Livadas, M., Lowe, P.S., Kanfoud, J., Wrobel, L.C., and Gan, T.-H. (2018) 'Fouling Removal in Submerged Structures Using High Power Ultrasonic Transducers', NSIRC Annual Conference.

f) Lais, H., Livadas, M., Wrobel, L.C., and Gan, T.-H. (2019) 'Optimisation of the Non-Invasive Ultrasonic Fouling Removal Technique for Submerged Structures', NSIRC Annual Conference.

g) Lais, H., Livadas, M., Wrobel, L.C., and Gan, T.-H. (2019) 'the Generation of Cavitation for the Removal of Fouling on Submerged Structures Using High Power Ultrasonic Transducers', Brunel University London Mechanical and Aerospace Engineering PGR Symposium.

h) Lais, H., Kanfoud, J., and Gan, T.-H. (2019) 'Numerical Optimization of the Ultrasonic Cleaning Technique for Pipelines', COMSOL Conference.

Chapter 2: Current State of the Art of Fouling Detection and Fouling Removal

Stop looking for reasons and look for a solution – Kang Chul

2.1 TYPES OF FOULING

Fouling can be found in various structures, the majority of cases being related to the transport of a fluid around a structure. The applications of a production line can result in fouling created and affecting the operating capabilities of the production. The majority of structures that suffer from fouling accumulation are commonly found in heat exchangers, pipelines, ship hulls, turbines and reverse osmosis membranes. Heat exchangers carry the most publications of fouling removal due to the high temperature operation creating crystallisation fouling which affect the operation of the heat exchangers. Ship hull biofouling is a major problem as it affects the ship's speed due to the added drag and can also damage the ship's structure. Fouling removal from a ship is very expensive and time consuming and is a requirement for ships that enter American sea. Work has been done internally in companies for dealing with ship hull biofouling and is not widely published due to the undesired announcement of problems within a company to the public. The food and beverage industry requires a fouling removal technique to assist in production lines to ensure that hygiene is being upheld for quality control and assurance. Fouling can be categorised into two types; macro-fouling and micro-fouling. Macro-fouling consists of larger-sized fouling such as rubbish, barnacles, mussels, leaves, etc. whereas micro fouling has seven sub-categories (shown in Figure 2.1), is harder to remove, and causes a lot of problems in industry.

Crystallisation
- Due to supersaturation of a liquid containing salts which attach onto a structure (typically in high temperature conditions)

Corrosion
- Structure is exposed to flowing oxygenated water

Particulate
- Solids existing in a bulk liquid that attach onto a structure

Chemical Reaction
- A chemical reaction taking place and the surrounding structure accumulates fouling during the reaction

Solidification
- Occurs on a cooled surface while the bulk liquid remains unsaturated

Biological
- Layer of fouling on a surface which consists of an organism

Composite
- Combination of two or more types of fouling

Figure 2.1: Types of fouling formation and definitions

2.1.1 CRYSTALLISATION FOULING

This is a type of fouling that is commonly found in boilers and heat exchangers due to the hard water. The growth of this fouling is dependent on temperature, evaporation and degassing. The fouling is achieved when the concentration of salt within the liquid surrounding the structure exceeds saturation, i.e. due to a supersaturated solution. A more scientific definition of how the salts within a supersaturated solution attach onto a structure (shown in Figure 2.2) is due to the ionic elements that are transferred (either by diffusion of bulk transport) to the solid surface. This then attaches the nucleated species by integration into the crystalline deposit [10]. This fouling formation is temperature dependent and requires a degree of supersaturation, as the crystals are formed around a nucleus [11]. This type of fouling is common in heat transfer surfaces due to the temperature allowing the fluid to become supersaturated and attach crystallised solids onto a surface. A softer deposit known as sludge is formed and remains within the bulk liquid [10]. The

process of creating this fouling requires numerous processes that are all occurring simultaneously. The following shows the complex process needed to create this type of fouling naturally [10]-[11]:

1. Bulk diffusion of solvated ions through the diffusion boundary layer
2. Bulk diffusion of solvated ions through an absorption layer
3. Surface diffusion of solvated and unsolvated ions
4. Partial or total desolvation of ions
5. Integration of ions into the crystal lattice
6. Counter diffusion of released water through the absorption layer
7. Counter diffusion of water through the boundary layer
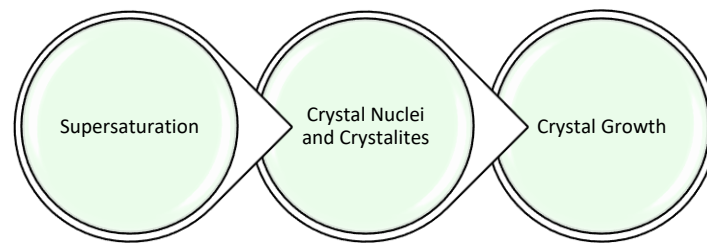
Figure 2.2: Crystallisation fouling build-up process

2.1.2 PARTICULATE FOULING

This type of a fouling is formation of particle solids that are larger in size than crystallisation fouling and exits within a bulk liquid before attaching onto the surface of a structure. The solids within the bulk liquid can be due to the following [10]:

- Pre-existing particulates in the flow
- Generation of particulate matter due to operating conditions
- Generation within a supersaturated solution (contributes towards crystallisation fouling)
- Material deposition from the surface which is released into the bulk liquid/fluid flow
    o Can be due to erosion or sloughing

2.1.3 CORROSION FOULING

Corrosion fouling occurs on a surface which has been exposed to flowing oxygenated water. This type of fouling is a big problem on heat transfer surfaces as this can introduce a resistance to the heat transfer surface. There has been little work done on this type of fouling which means there is room for further development and modelling. This type of fouling was not widely recognised until the 1960s. In a scientific definition, corrosion fouling is created due to the formation of an oxide

layer on a metal surface which is exposed to a high temperature oxygen containing gas [10]. Examples of corrosion fouling include [12]:

- Heat exchangers which carry natural water
  - Usually in combination with other types of fouling
- Water cooled components of electrical components
- Cooling systems of combustion engines (that uses water as cooling)
- Hot water heating systems

2.1.4 BIOLOGICAL FOULING

Biofouling or biological fouling is a layer of fouling on a surface consisting of an organism. This can be micro or macro organisms. Micro and macro fouling can occur on structures or systems that are placed in seawater where larger organisms can appear and micro-organisms can live within the seawater. Micro biofouling is the only biofouling that can occur in heat exchangers due to its size [13]. Micro and macro organisms can be categorised as shown in Figure 2.3.
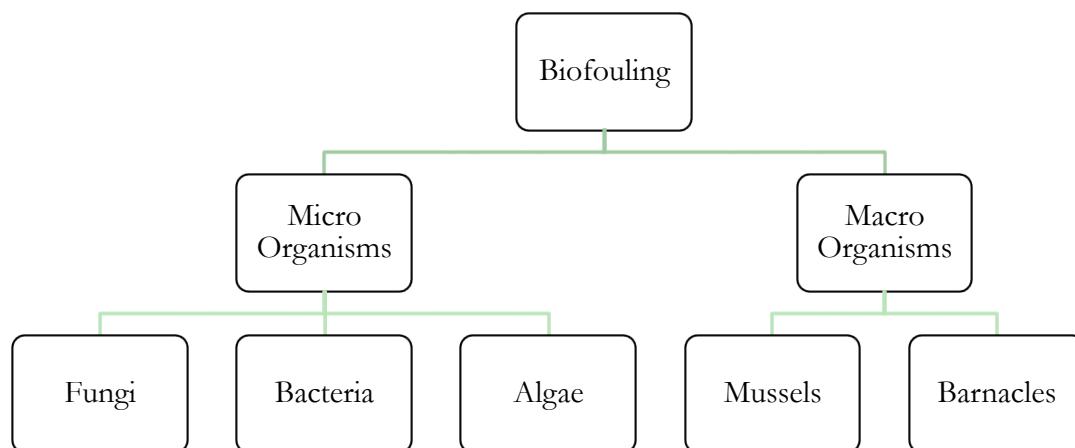
Figure 2.3: Sub-categories of biofouling organisms

For biofouling to occur and attach onto a surface, a biofilm formation must take place. A surface is contaminated with bacteria, resulting in cells to move towards the surface as bacteria prefer to be on a surface rather than be free floating within a liquid. The bacteria or other micro-organism exist within natural water source as they contain the molecules of previously-living organisms. The initial bonding of bacteria onto a surface can be reversible but, with time, the adhesion of these layers becomes greater and reaches an irreversible state. This means that there is a rapid development in the biofilm thickness as it is irreversible and continues to attract organisms. The sequence of the biofilm formation is described as follows:

1. Mass transfer of macromolecules to a surface and formation of an absorbed layer (to attract bacteria)

2. transportation of micro-organisms to the absorbed layer

3. layer reaches irreversible adhesion of cells and/or clusters to the surface

4. at this stage, there is still a possibility to remove cells from the surface (using the flow force over this surface)

5. establishment of a stronger bond between the micro-organisms and the surface layer

6. mass transfer of nutrients towards and after from the surface layer (through the biofilm)

7. cell metabolism – to produce new cells

8. potential sloughing of the biofilm when reaching a critical thickness

Although there is an extensive sequence to form biofouling, pure biofouling cannot be observed as this biofilm encourages other types of fouling to grow such as corrosion (due to the pH) or crystallisation fouling [14].

2.1.5   CHEMICAL REACTION FOULING

Chemical reaction fouling is self-explanatory, as this is a type of fouling formed due to a chemical reaction taking place and the surrounding structure accumulating fouling during the reaction. Chemical reaction fouling is a multi-step process and can be described in Figure 2.4 [15]. The formation of chemical reaction fouling can be identified as follows:

1. Identify reactants and precursors

2. Determine the kinetics of the reactants that form the precursors

3. Determine whether the solid fouling phase is initially created within the bulk

With this example, chemical reaction fouling can be modelled; however, identifying the fouling precursor can be a major task. There are different reaction types such as autoxidation, polymerisation and thermal decomposition. Various industries have stated that chemical reaction fouling increases the chance of corrosion fouling to be produced as well [15].

Reactants → Precursors (Soluble) → Foulant (Insoluble
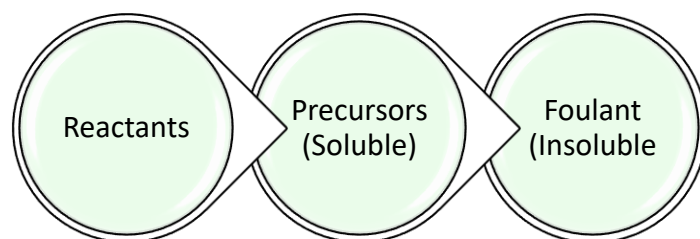
Figure 2.4: Chemical reaction fouling build-up process

2.1.6   SOLIDIFICATION FOULING

The most widely known type of solidification fouling is 'freezing fouling' and is defined as solidification which occurs on a cooled wall while the bulk liquid remains unsaturated and is at a higher temperature than the solidified fouling. The solidification is controlled by heat and mass transfer rates to achieve this type of fouling. Freezing fouling is a layer of deposit on a surface which is cooler than the bulk liquid. This is not always solidification fouling, as this can also be crystallised fouling. Freezing fouling is a type of solidification fouling [16] but can also be classified as crystallisation fouling [11]. This type of fouling is not always undesirable as it can be controlled to isolate a section in a pipe for maintenance and inspection [17]. Freezing fouling can also be created using a novel spinning disk apparatus for a controlled experimental set-up [18].

2.1.7   COMPOSITE FOULING

Commonly, fouling is not found as one type as it is difficult for only one type of micro-fouling to be formed and is instead a combination of another type of fouling(s) which result in a composite fouling. For example, corrosion and biofouling: [19], corrosion and particulate fouling due to binding iron oxide to the surface and corrosion and precipitate fouling [20].

2.2   FOULING DETECTION USING UGW

Monitoring of the fouling accumulation in pipelines allows optimisation of fouling removal procedures and also the detection of fouling which could affect the quality of the fluid being carried past the contaminated walls. Various methods for the detection of fouling have been discussed [21], for example, observing changes in hydrodynamics [22] and detecting changes to heat transfer parameters in the build-up of fouling [23]. Withers [24] also investigated various methods including electrical and optical processes, and discussed acoustic methods covering pulse-echo and transmission techniques. Current acoustic methods have the advantage of detecting fouling accumulation non-invasively and, potentially, over large distances from a single test location [25], [26].

2.2.1   PROPAGATION OF ELASTIC WAVES

Compared to conventional Ultrasonic Testing (UT), UGW is an emerging technique that requires understanding of the elastic wave propagation within the structural boundaries to obtain a reliable assessment of the structural health [27]. Navier's equation of motion for an isotropic elastic unbounded media is as follows:

$$(\Lambda + \mu)\nabla\nabla.u + \mu\nabla^2 u = \rho\left(\frac{\partial^2 u}{\partial t^2}\right) \tag{2.1}$$

where Λ and μ are Lamé constants, u is the three-dimensional displacement vector, ∇ is the three-dimensional Laplace operator and ρ is the material density.

Helmholtz decomposition is used to write u as a sum of the compressional scalar potential ϕ and the equivoluminal vector potential Φ:

$$u = \nabla\phi + \nabla x\Phi \tag{2.2}$$

where $\nabla.\Phi = 0$

When substituting the potentials of Helmholtz deposition (2.2) into Navier's equation (2.1), this produces two equations for unknown potentials that govern longitudinal waves (2.3) and torsional waves (2.4):

$$\left(\frac{\partial^2 \phi}{\partial t^2}\right) = c_l^2\nabla^2\phi \tag{2.3}$$

$$\left(\frac{\partial^2 \Phi}{\partial t^2}\right) = c_t^2\nabla^2\Phi \tag{2.4}$$

Using Helmholtz decomposition, substituting into Navier's equation, gives the following Equations (2.5) and (2.6), where c_l and c_t are the velocities of longitudinal and torsional waves respectively.

$$c_l = \sqrt{\frac{\lambda + 2\mu}{\rho}} \tag{2.5}$$

$$c_t = \sqrt{\frac{\mu}{\rho}} \tag{2.6}$$

2.2.2 NOMENCLATURE OF UGW MODES

There are two types of elastic waves that can propagate in pipes, longitudinal waves and torsional waves. These can travel in any direction. In typical pipeline sizes and test frequencies (20-100 kHz) the three axisymmetric guided wave modes that can be excited as L(0,1), L(0,2) and T(0,1) [28]. Longitudinal axisymmetric wave modes are denoted by L(0,m) and torsional axisymmetric wave modes are denoted by T(0,m). Non-axisymmetric flexural wave modes are denoted by F(n,m).

This nomenclature was suggested by Meitzler [29] and popularized by Silk and Bainton [30]. According to this nomenclature, vibration modes in cylindrical structures are based on the following format:

$$X(n, m) \tag{2.7}$$

where, X represents the character to denote whether the vibration modes are longitudinal and axisymmetric (L), torsional and axisymmetric (T) or non-axisymmetric (flexural) (F). The n is a positive integer giving the identification of harmonic vibrations of displacement around the circumference and m, is a positive integer to indicate the incremental order of the modes of vibration within the wall.

2.2.3   BULK WAVES AND UGW

The application of UGW inspection has been commonly used to inspect large engineering structures such as pipelines. As pipelines are used in various industries to carry oil, gas, chemical and water. These are very difficult to access for inspection; however, the use of UGW inspection can allow large lengths of pipelines to be inspected from one location. The requirement for UGW is for the elongated geometry to consist of a constant cross section which is suitable for pipes.

The behaviour of UGWs can be better understood when compared to bulk waves (conventional UT) and can also contribute to improving the resolution of the UGW inspection (see Table 2.1).

Table 2.1: Comparison of conventional UT and UGW

Bulk Waves (Conventional UT)	Ultrasonic Guided Waves (UGW)
Can only propagate away from a boundary	Travel along with the boundary
Propagation is only dependent on material properties and reflections within the structure	Propagation is dependent on material properties and waves guided by boundaries of the structure
Commonly operated at relatively high frequencies (MHz range)	Commonly operated at relatively low frequencies (kHz range)
Short wavelengths due to high frequencies	Long wavelengths due to low frequencies
High attenuation due to high frequencies	Relatively low attenuation due to low frequencies
High resolution due to high frequencies and short wavelengths	Low resolution due to low frequencies and long wavelengths
Localised inspection	Long distance inspection from one test location (up to tens of meters)

The sound waves generated in these structures are constrained to propagate along the axis of the body but will return back by means of a reflection to the point of transmission when there is a change in impedance due to a discontinuity. Depending on the geometry of the structure, material properties and excitation frequency, various types of wave modes can be produced.

2.2.4 PHASE VELOCITY AND GROUP VELOCITY

Two important variables in wave propagation are the phase velocity and group velocity. Phase velocity is the speed of propagation of a continuous wave. A continuous pulse has a range of phase velocities at different frequencies which causes the pulse to spread out as it propagates.

When inspecting using UGW, the propagating wave modes must be identifiable by exciting them as a distinct wave with a finite number of cycles. The pulse used in this research is a sinusoidal wave controlled by a Hamming function (2.8) and is associated with a bandwidth of frequencies.

$$U(t) = \frac{1}{2} sin(2\pi f t) \left[1 - cos\left(\frac{2\pi f_o t}{N_c}\right) \right]$$ (2.8)

Where U is the output function as respect to time, t is time, f_o is the central frequency and N_c is the number of cycles.

The propagation speed of the envelope of the distinct pulse is the group velocity. The relationship between the phase and group velocity can be described using the following equation:

$$v_{gr} = \frac{v_{ph}}{1 - \frac{f}{v_{ph}} \cdot \frac{dv_{ph}}{df}}$$ (2.9)

where v_{gr} is the group velocity, v_{ph} is the phase velocity and f is the frequency.

2.2.5 DISPERSION AND DISPERSION CURVES

The variation in wave velocity relative to the operating frequency is known as dispersion [27]. This causes spreading of the signal when propagating through a structure, which is an undesirable phenomenon when using UGW inspection as it makes the data interpretation complex. Pavlakovic et al. [31] developed the commercial software DISPERSE which has been used to generate the dispersion curves for the structure under investigation; Schedule 40, 6 inch diameter, carbon steel pipe, (See Figure 2.5). The black dashed lines represent the computed DISPERSE dispersion curves.

Another promising software code for plotting dispersion curves is the open-source core code based on Semi Analytical Finite Element (SAFE) known as Graphical User Interface for Guided

Ultrasonic Waves (GUIGUW) [32]. This code has been developed in MATLAB and is a stand-alone software. Its advantages are enhanced numerical stability, computational efficiency and it allows multiple layers to be investigated. It is useful to investigate the effects of the addition of a fouling layer when generating dispersion curves. Figure 2.5 displays the dispersion curves generated by the GUIGUW software as red dashed lines. As the graph shows reasonable agreement between both dispersion plotting codes, the group velocity dispersion curve is generated using GUIGUW shown in Figure 2.6.
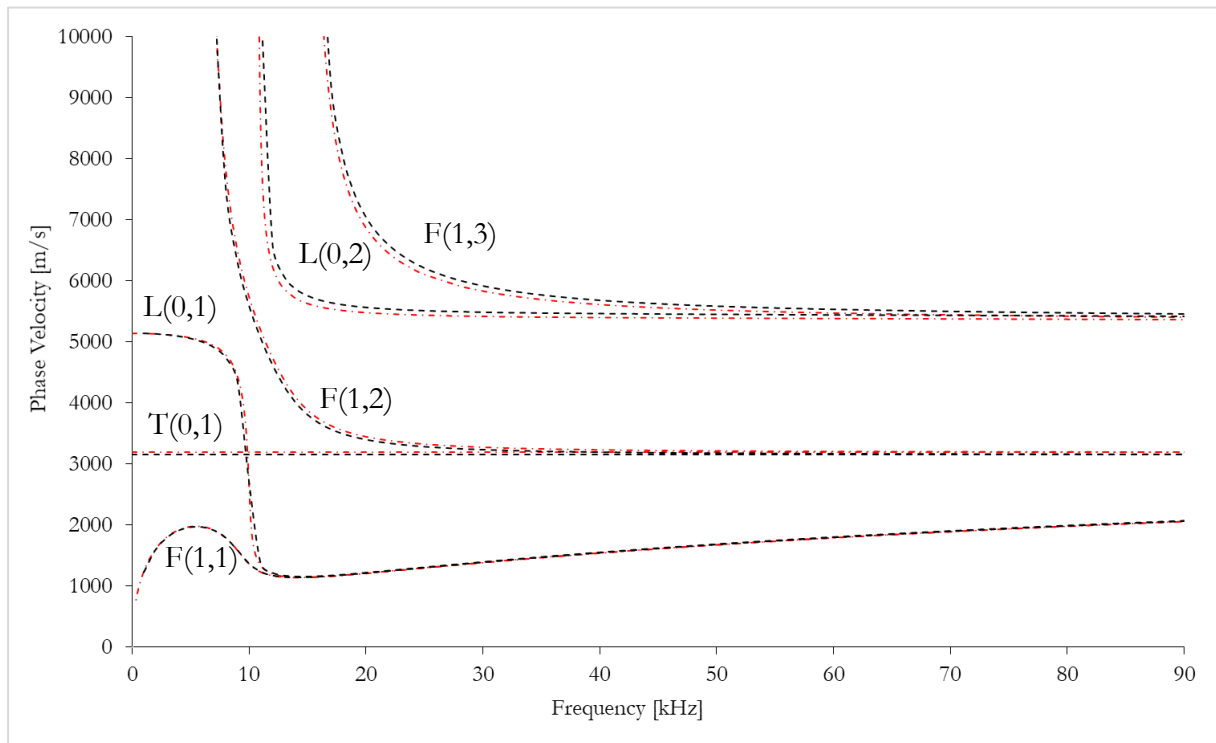
Figure 2.5: Phase velocity dispersion curve for Schedule 40, 6 inch diameter, carbon steel pipe using DISPERSE (black dashed lines) and GUIGUW (red dashed lines)
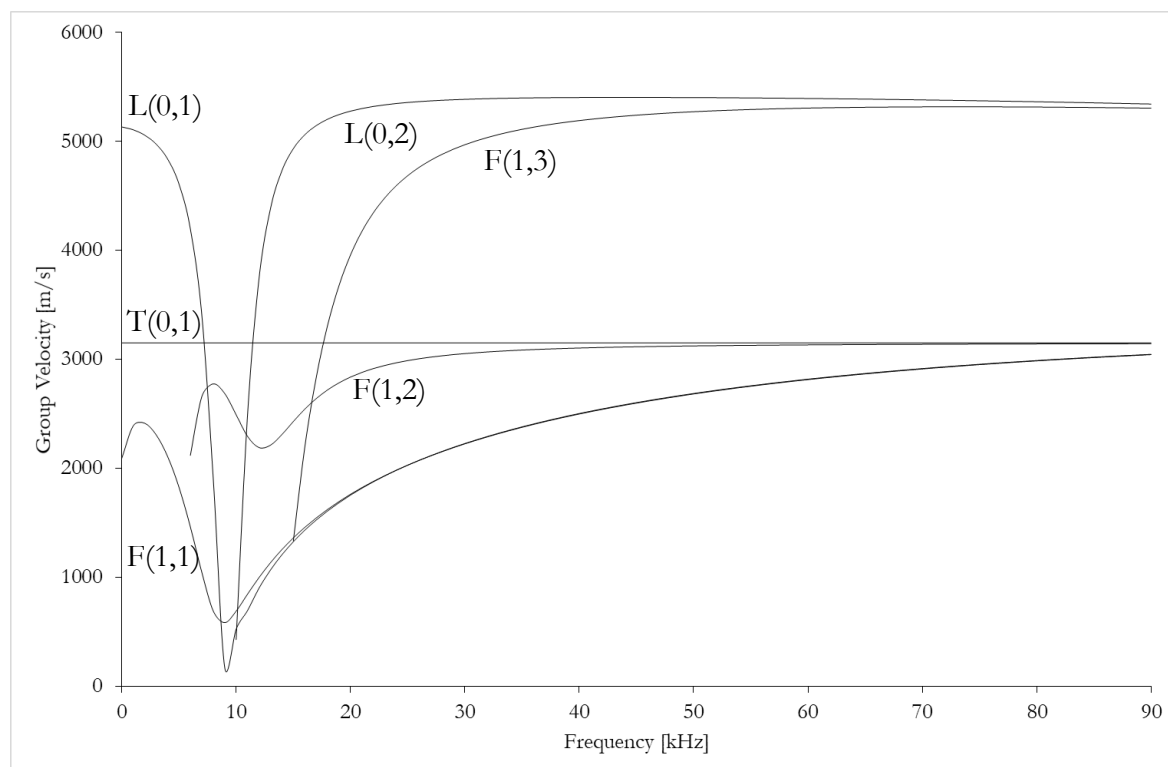
Figure 2.6: Group velocity dispersion curve for Schedule 40, 6 inch diameter, carbon steel pipe using GUIGUW

2.2.6 COMMERCIAL UGW SYSTEMS

The commercialisation of UGW systems began in the late 1990s. Current commercial UGW systems are listed in Table 2.2 [33]. Dependent on the UGW system, the systems can inspect pipelines that are coated, insulated, buried or operating at high temperatures. UGW systems can inspect not only pipelines but also tanks, bridges and offshore structures. Primarily, the method has been used to detect anomalies in engineering assets where they can lead to catastrophic bursts and failures. There has been recent work on applying the UGW technique for fouling detection [21], specifically for food industry applications carrying food/liquids. Lohr and Rose [26] used a 2.62 MHz piezoelectric transducer on an angled Plexiglas wedge to produce the non-leaky longitudinal wave S0 through a stainless steel pipe. The results showed that the amplitude decreases with the addition of the fouling layer (tar) seen in the L(0,5) mode with an increase in fouling thickness. Hay and Rose [25] also investigated the use of UGWs for fouling detection using a comb sensor operating at 2.5 MHz attached to a stainless steel pipe. The longitudinal mode L(0,4) showed high sensitivity to the addition of fouling. Both investigations [25], [26] operated at a higher frequency range (MHz) and also only studied longitudinal waves; this limits the length of fouling detection from one location due to the higher level of attenuation. This thesis focuses on the use

of a lower frequency range (kHz) and torsional wave modes to achieve a prolonged coverage using a single location.

Table 2.2: Comparison of UGW systems on the commercial market.

Supplier	UGW System	Method of Excitation	Operating Frequency	Inspection Range
Plant Integrity Ltd. (EddyFi)	Teletest® Focus+	PZT array	20–100 kHz	60 m
Guided Ultrasonic Ltd.	Wavemaker® G4	PZT array	15–80 kHz	60 m
Structural Integrity Associates Inc.	PowerFocus™	PZT array	20–85 kHz	150 m
Olympus corporation	UltraWave® LRT	PZT array	15–85 kHz	90 m
Innerspec Technologies Inc.	Temate® MRUT	Magnetostrictive coils	0.1–1 MHz	1–5 m
NDT-Consultant Ltd.	MsSR® 3030R	Magnetostrictive coils	2–250 kHz	-

2.2.7 UGW INSPECTION METHODS FOR FOULING ACCUMULATION

UGW has also been used to detect fouling in a duct using the acoustic hammer technique [34]–[36] and an ultrasonic transducer wedge at 500 kHz [35]; however, the research focused on signal processing aspects of the received signal to detect fouling. The application of acoustic hammer is inadvisable for industrial use as the hammer impact may be inconsistent and may vary in amplitude, resulting in difficulties of comparison between the amplitude changes due to the accumulation of fouling and those due to the impact of the hammer itself. The transducer wedge application used was operated at a high frequency and did not specify the wave mode used in the investigation.

The UGW research on fouling detection has shown it to be sensitive to the change in material and thickness of layers [21]. The method itself is non-invasive and can be used whilst fouling removal is being carried out to monitor the cleaning. Another area that has not been investigated is the application of UGW to long range fouling detection. Recent investigations have focused on smaller samples which may justify why longitudinal mode excitation has been used [25], [26] as it is dispersive but it is only being applied to a short specimen due to the excitation at MHz range [27]. The low frequency UGW has been used to inspect tens of meters of pipes for over two decades (commercial system i.e., Teletest [37]) due its low attenuation as an inherent characteristic; furthermore, benefits of using low frequency UGW over conventional UT have been reported in the literature for the inspection of elongated structures [38]. This thesis investigates the use of the fundamental torsional mode T(0,1) for its non-dispersive characteristics over the operating frequency range of UGW (20–100 kHz) for long-range detection.

2.2.8   FEA of UGWs

A review of numerical modelling methods has been discussed in depth by Wallhäußer et al. [21], where various research studies have attempted to model and predict fouling. The benefits of modelling are the ability to predict the amplitude drop, attenuation and other parameters to relate the UGW signal to the presence of fouling. This allows the development of fouling to be predicted and removed before the structure reaches a detrimental condition that results in pipe blockage, bursts and human casualties. More specifically, predictive models can be used for comparison when monitoring real-time data from a structure. This collective data can be cross-referenced with the predictive model to determine the extent of fouling build-up.

The SAFE method is commonly used for generating dispersion curves for different structures. An example of this is the modelling of hollow cylinders with coatings to generate dispersion curves and attenuation characteristics of axisymmetric and flexural modes [39]. 3D hybrid models have also been investigated, combining both SAFE and FEA, to model UGW interaction with non-axisymmetric cracks in elastic cylinders [40], allowing the technique to be used on defects with complex shapes.

FEA methods have been applied to model UGW propagation within a structure for more specific applications. For example, a 2D FE model was used for UGW propagation in complex geometries and proved to be more effective than analytical solutions [41]. UGW propagation in bones has been modelled using FEA of the fracture callus and healing course within a three-stage process [42]. 3D numerical simulations have been carried out on UGW for non-destructive inspection of CFRP rods with delamination [43].

The software code ABAQUS has been used to model UGW propagation for long-range defect detection in rail road tracks [44]. ABAQUS has also been used to model longitudinal and torsional wave propagation on a cylinder [45]. The optimal excitation mode was selected using signal processing algorithms and used the reflection coefficient for defect sizing. Although ABAQUS can successfully model UGW propagation, COMSOL Multiphysics has recently become more popular due to its multiphysics and post-processing capabilities. For example, COMSOL has been used to model UGW propagation in the frequency domain, later converted to the time domain using a Fast-Fourier Transform (FFT) [46] which reduces computational time.

2.3   FOULING REMOVAL USING ULTRASOUND

Current methods that are deployed for fouling removal span over hydraulic, chemical and manual means. Chemical agents for fouling removal have been successful as, for instance, the Ocean Team Group [47] who have a working chemical agent used for fouling removal in pipelines of organic material, showing successful results. There are various other methods under the mechanical and hydraulic category but all of which need to stop the production for maintenance to be achieved. Although chemical agents require production to be halted, the results show the ability to achieve 100% de-fouling but with the costs of using harsh chemicals that can impact the environment. The various types of fouling removal methods are categorised in Figure 2.7.

As chemical means pose a negative impact on the environment, another approach must be investigated and optimised for improved cleaning. The conventional approach typically uses mechanical and hydraulic means to flush out the fouling as a means of removal; however, current conventional technologies have one common disadvantage that is the requirement to put the operation of the structure to a halt in order to commence the fouling removal process.
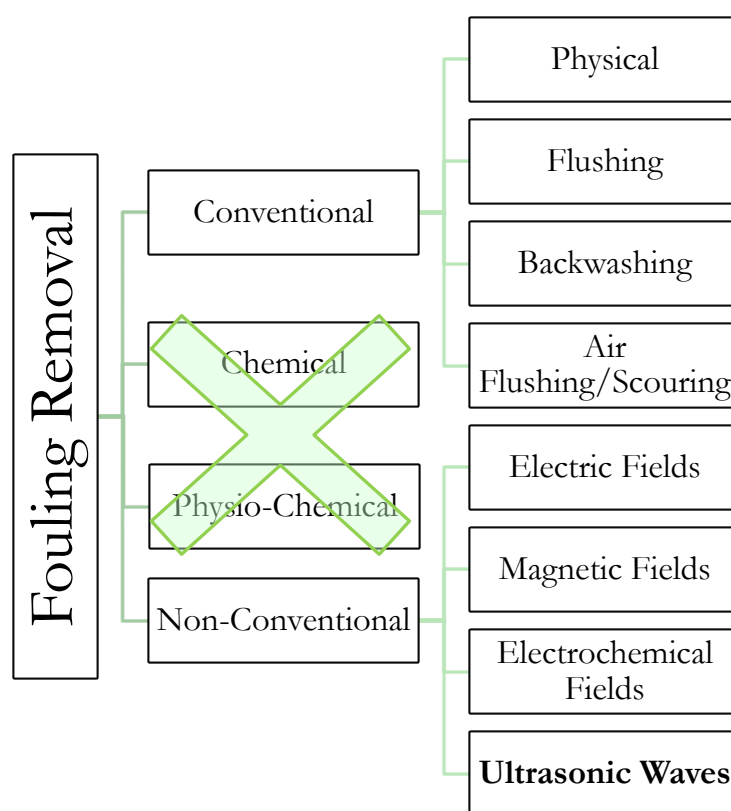
Figure 2.7: Sub-categories of fouling removal approaches and examples of techniques

Ultrasounds provide a non-invasive approach to fouling removal. This technique is considered to be a low cost and efficient cleaning method [48] and can accommodate to complex shapes with internal cavities. The bubbles are typically generated for a uniform distribution [49]. Currently, ultrasonic baths are used for cleaning individual parts of the plant by generating cavitation bubbles which implode on the fouling surface (see Figure 2.8). Applications of cleaning using ultrasonics, specifically, ultrasonic baths, have been used for assisting the cleaning of reverse osmosis applications [50]–[52] and membranes for ultrafiltration. A membrane is immersed into an ultrasonic bath to begin fouling removal as fouling build-up can block pores and affect the purpose of ultrafiltration of a liquid passing through the membranes.

Figure 2.8: Commercially available ultrasonic cleaning baths

An example of a membrane cleaning application is for controlling fouling formation in membrane ultrafiltration of waste water [53]. Membrane fouling is reduced by having ultrasound to assist in cleaning. There is also a relationship between the frequencies applied; when exciting at a low frequency (~35 kHz), this slows down the fouling formation while exciting at a higher frequency (~130 kHz) improves fouling removal. The results showed better cleaning at locations of radicals within the bulk liquid due to having a higher frequency. Radicals also appear at low frequencies but are located around the surface of the transducer. A frequency of 50 kHz is used for cleaning of semiconductors which conforms to health and safety regulations as this frequency is outside of the audible range for humans [54].

Some other novel applications of the ultrasonic cleaning technique have been to clean pesticides on strawberries without damaging the strawberries [55], cleaning 3D printed parts using a dissolution liquid with ultrasonic cavitation [56], using the ultrasonic cleaning device for fish productive studies by separating the oocytes from each other and from the ovarian tissue [57] and

ultrasonically cleaning turbine engines' oil filters [58]. The technique can also be applied to assisting the cleaning of textiles [59], [60]. In boat cleaning, it is very costly for dry docking and commencing cleaning, and ultrasonics has shown potential as an alternative to cleaning underwater but with the requirement of distance and good angle/position [61]. For the production of wine, ultrasonics has shown a better cleaning performance and extended life of oak barrels compared to conventional cleaning means such as high pressure and hot water [62].

2.3.1   ACOUSTIC CAVITATION

The acoustic cavitation phenomenon is used in ultrasonic cleaning applications. Acoustic cavitation bubbles are generated due to the high pressure vibration generated by Langevin bolt clamped HPUTs [63]. These HPUTs generate ultrasonic compressional waves which can travel through a liquid and generate cavitation if the transducer is exciting at its main resonant frequency and achieving the required pressure amplitude to surpass the cavitation threshold. Figure 2.9 shows an example of an HPUT array attached to an ultrasonic cleaning bath, generating high pressure waves into the liquid of the bath.

Direction of compressional wave propagation
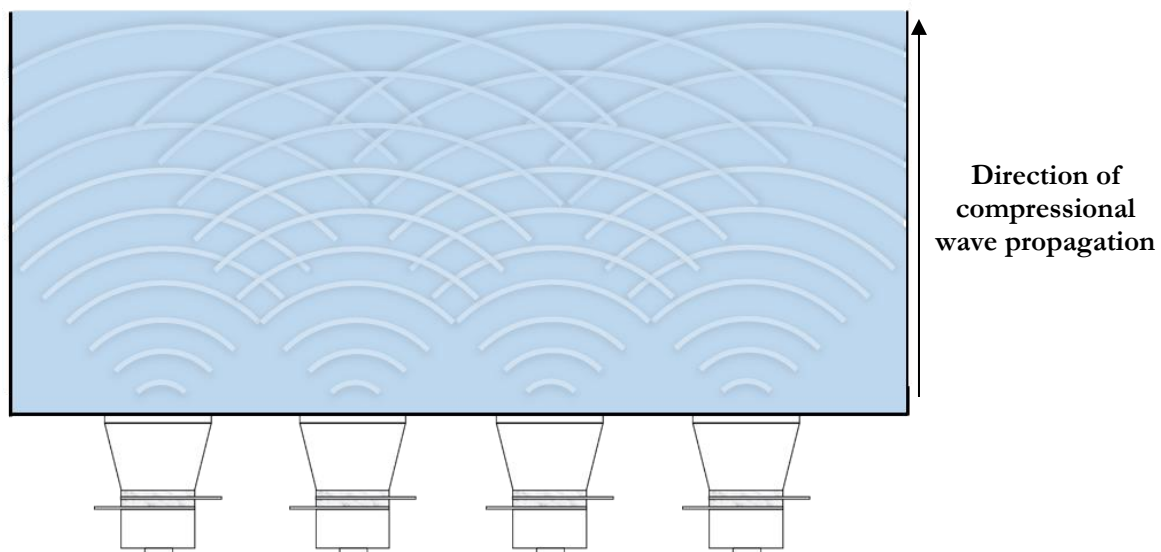
Figure 2.9: Schematic of ultrasonic cleaning bath HPUT array

The development and implosion of acoustic cavitation bubbles can be defined as the formation of vapour bubbles due to a sudden decrease in pressure in a liquid caused by a (de-) compressional wave [64]. A rarefaction instant is thereby introduced and forms a vacuum, where a bubble can appear as shown in Figure 2.10. During the oscillation of the bubble, the radius increases in the rarefaction instants and decreases in the compressional instants. In one of these cycles, the compression can burst the bubble (adiabatically) to produce pressures of up to 500 Bar and temperatures up to 5000 K.
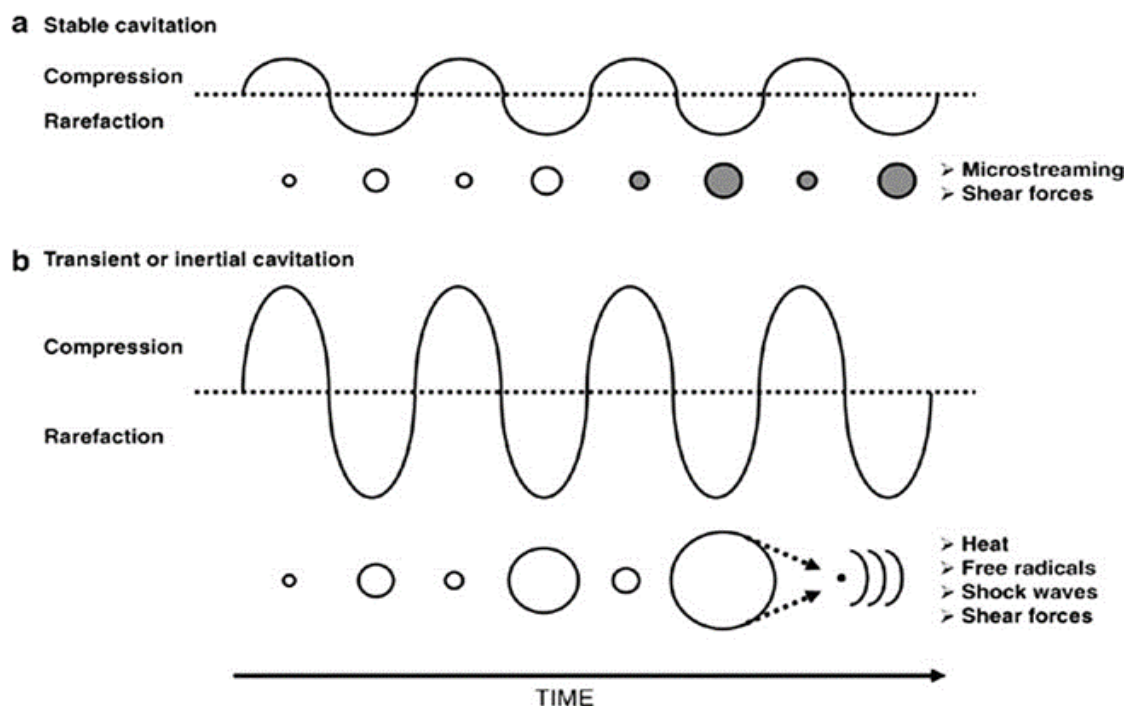
Figure 2.10: Illustraton of cavitation bubbles displaying stable and transient cavitation [65]

There are two types of cavitation bubbles that can form within a liquid; stable cavitation where the bubbles oscillate for a long period of time in a sound field with a large number of cycles, and transient cavitation which lasts for less than one cycle and is violent enough to potentially damage the surface of the body in contact with the liquid [64]. Figure 2.10 [65] illustrates and compares the development of stable and transient cavitation bubbles.

Due to stable cavitation bubbles oscillating for a period of time, they do not produce any light emission or chemical reactions when imploding. However, transient cavitation bubbles implode with a strong collapse, which creates light emissions and/or chemical reactions within the liquid as a result of the implosion [66].

Although two types of cavitation have been defined, cavitation bubbles can also be a combination of both stable and transient cavitation, as discussed in the literature by Yasui [66]. This phenomenon is also known as 'high energy stable' and 'repetitive transient cavitation'. Cavitation bubbles that are a combination of both types of cavitation oscillate for a long period of time similar to stable cavitation; however, they produce small amounts of light emission and chemical reactions. An example of this combination of both stable and transient cavitation can be found in Single-Bubble Sonoluminescence (SBSL) [67].

Stable cavitation oscillates at the excitation frequency of the transducer as well as the harmonics and subharmonics of the cavitation [68]. These harmonics and subharmonics produce acoustic emission which can be detected to indicate the generation of the cavitation. The non-linear nature of a single spherical oscillating cavitation bubble is explained by the Rayleigh-Plesset equation [69]:

$$\frac{p(t) - p_\infty(t)}{\rho_L} = R\frac{d^2R}{dt^2} + \frac{3}{2}\left(\frac{dR}{dt}\right)^2 + \frac{4v_L}{R}\frac{dR}{dt} + \frac{2s}{\rho_L R} \tag{2.10}$$

where, $p(t)$ is the pressure within the bubble, assumed to be uniform, $p_\infty(t)$ is the external pressure infinitely far from the bubble, ρ_L is the density of the surrounding liquid, assumed to be constant, $R(t)$ is the radius of the bubble, v_L is the kinematic viscosity of the surrounding liquid, assumed to be constant. S is the surface tension of the bubble.

For fouling removal applications to be achieved, transient cavitation must be generated to produce forces large enough for dislodging fouling from a surface. The impact and distribution of the cavitation bubbles are also dependent on the frequency applied as a result of the selected HPUT. With lower frequencies (~ 20 kHz), this results in cavitation bubbles of high forces but with a low number of bubbles within a fluid medium. When exciting a fluid medium at higher frequencies (~ 60 kHz), this results in a higher number of bubbles but of lower forces on implosion. Literature has shown that 40 kHz is a favourable frequency to operate the ultrasonic cleaning technique as this achieves a balance between the impact of the forces upon implosion as well as the number of distributed bubbles throughout the fluid.

2.3.2   CAVITATION BUBBLE IMPLOSION

The process of cavitation bubble implosion is affected by the properties of the cavitating liquid such as the temperature and also the properties of the ultrasonic vibration which includes the excitation frequency and the wavelength, these have been investigated [70]. The increase in temperature shows an increase of the energy level of water molecules which in turn affect the cleaning time, concluding a relationship between temperature and cavitation intensity. Equations relating to cavitation, acoustic impedance, transmission coefficient and temperature increase were used to investigate these parameters as an affect on cavitation. The change in temperature resulted in a change in viscosity of the liquid, solubility of the gas in the liquid, diffusion rate of dissolved gasses in the liquid and the vapour pressure. Specifically, when minimising viscosity, this allows maximum cavitation effect to be achieved. As viscous liquids cannot respond quickly enough to form cavitation bubbles for violent implosion, a lower viscosity is required forcavitation bubbles to be formed.

Vaporous cavitation bubbles are filled with vapour of the cavitating liquid, as this is the most effective form of cavitation. During the bubble growth, gas that is dissolved within the liquid is released and prevents buble implosion; however, increasing the liquid temperature reduces the amount of dissolved gasses due to an increase in the diffusion rate of the dissolved gases. The temperature is found to increase the energy level of water molecules, which affects the cleaning time due to the relativity between temperature and cavitation intensity. This means that it is harder to create cavitation at lower temperatures. However, when reaching boiling temperature, the cavitation intensity reduces as the liquid starts to boil at the cavitation sites.

2.3.3   FOULING REMOVAL MECHANISMS

The four fouling mechanisms known as acoustic streaming, micro streaming, micro-jets and micro streamers have been discussed in the literature [71] and are defined as the physical effects of cavitation. Figure 2.11 illustrates the four fouling removal mechanisms produced by ultrasounds
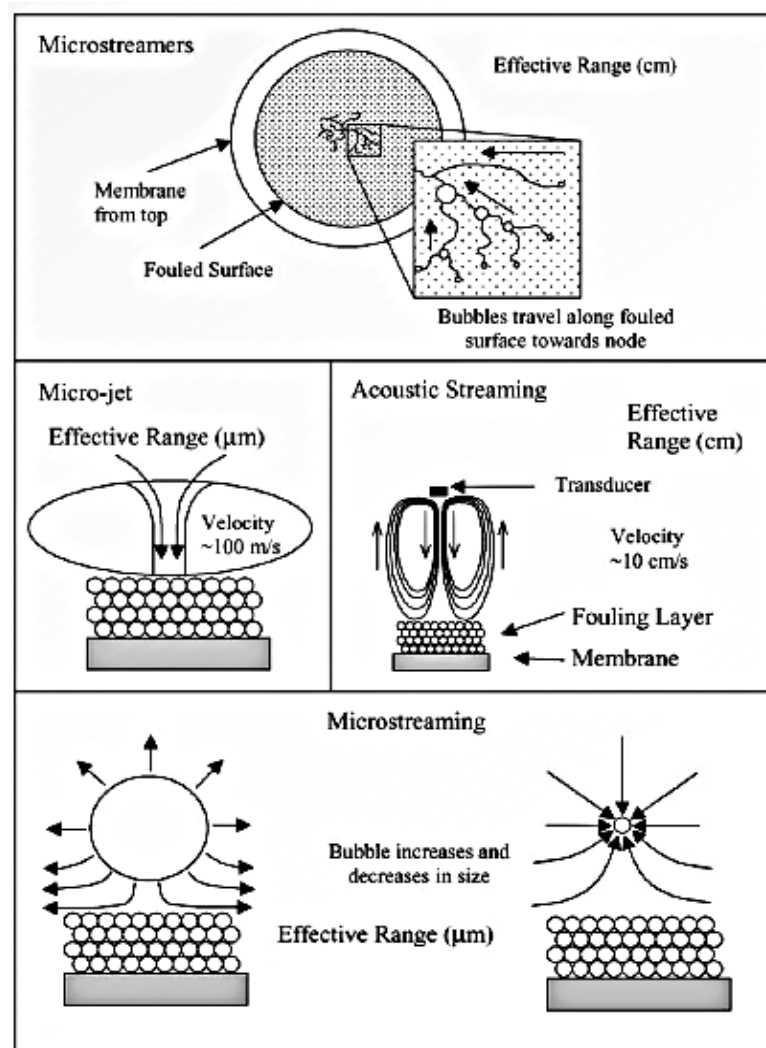
Figure 2.11: Fouling mechanisms produced by ultrasound [72]

[72] and Table 2.3 describes the characteristics of each fouling removal mechanism. The mechanisms formed from cavitation were applied to different applications for cleaning, particularly in the biofouling removal application. Exciting at low ultrasonic frequencies such as 20 kHz created strong shear forces resulting in the four fouling mechanisms to be achieved. The generation of cavitation has been shown not only to remove fouling but also to oxidise water, resulting in purification, deactivation of pathogens and removed of bacteria from fouled surfaces. This displays the application of cleaning to not only be on the surface of a structure, but also on the bulk liquid which results in beneficial chemical effects.

Table 2.3: Fouling removal mechanisms and its physical behaviours

Fouling Removal Mechanism	Characteristics
Acoustic Streaming	• Absorption of acoustic energy resulting in fluid flow [73] • Does not require the collapse of cavitation bubbles • This mechanism is important near surfaces with loosely attached particles or with a readily dissolvable surface [74] • Higher frequency results in higher absorption of energy and in turn produces greater acoustic streaming [75] • High power intensities result in greater acoustic streaming due to higher energy gradients between acoustic and non-acoustic simulated areas • Mechanism creates movement toward and away from fouling and may scour particles from the surface
Microstreaming	• Time dependant circulation of fluid in the vicinity of bubbles set into motion by oscillating sound pressure • Bubble rise oscillation cause sudden fluctuations in magnitude and direction of fluid movement, resulting in significant shear forces [73] • If a cavitation bubble is near fouling, microstreaming results in dynamic velocity profile that will create drag forces on particles and result in fouling removal
Microstreamers	• Cavitation bubbles that form at nucleation sites and are then translated to a mutual location (antinodes) • Bubbles travel in a ribbon shaped manner along tortuous paths at approximately an order of magnitude faster than the average velocity of the liquid • The migration of bubbles is due to Bjerknes force between the pulsating bubbles in the pressure field [76] • Proposed that antinodes on fouled surface may result in bubbles that will scour away particles while translating to antinodes [73]
Micro-Jets	• Formed after a cavitation bubble collapses due to asymmetry • During the collapse, the bubble wall accelerates more on the side opposite to a solid surface, resulting in the formation of strong jet of water [73] • High velocity of the micro-jets could scour particles from the fouled surface but requires further investigation to confirm

Investigation into the different fouling mechanisms [72] has used Scanning Electron Microscopy (SEM) to show the effects of ultrasonic cleaning to identify the different fouling mechanisms. It showed microstreaming to detach particles, acoustic streaming to transport particles away. The SEM showed micro-jet pitting in the fouling and no damage to the membrane itself. Not only are the mechanisms described, but the work also shows the correlation between power and frequency for improved cleaning. For particulate fouling, lower frequencies are more suitable and higher power can promote cleaning mechanisms further. These potential factors of affecting cleaning of a structure of interest are as follows:

- Orientation and position of ultrasonic field
- Ultrasonic power intensity and field
- Membrane material
- Membrane housing
- Operating pressure
- Fouling material

2.3.4 ULTRASONIC FOULING REMOVAL OF BIOFOULING

One application of the ultrasonic technique has been to remove juvenile barnacles [77] at different stages of fouling growth, such as early stages before a hard calcareous structure has been formed and, after this, a hard layer has been formed. The transducer is excited to generate cavitation bubbles within the liquid and aimed towards the barnacles as shown in Figure 2.12. The results
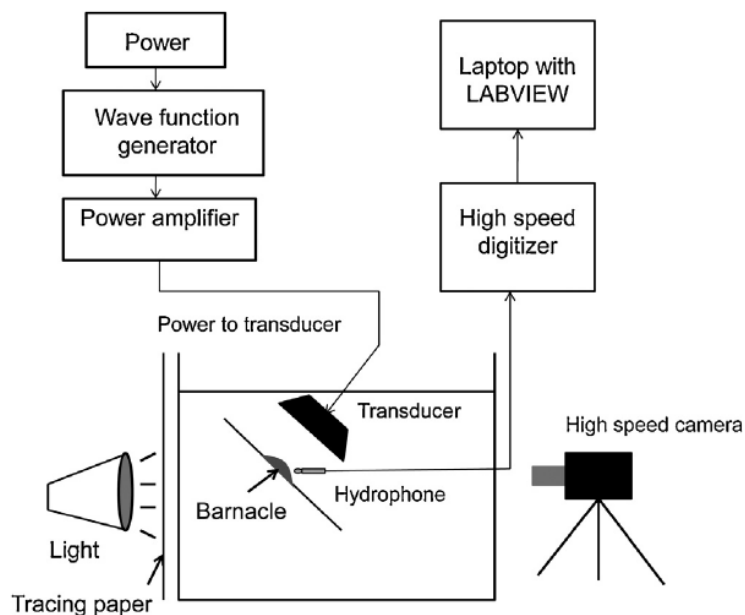
Figure 2.12: Schematic of biofouling removal experiment [77]

showed damages to the barnacles' shells due to the impact of the different fouling mechanisms created by cavitation bubbles. The cavitation itself also produces a liquid jet which impinges on the surface, resulting in the bacteria and biofilm to detach. The age of the barnacles also has an effect on the ability to be removed. The paper concluded that applying the ultrasonic method at an earlier stage provides better results than at a later stage, as calcium carbonate is used by the adult barnacles to make their exoskeletons which results in a much harder layer to remove, resulting in just damage to the shell rather than removal. The optimal time to use this method is at an early stage.

Biofouling build up on structures can be very critical in situations such as a biosensor which is used to pick up on biomarkers [78]. The research shown from biosensor fouling removal was done numerically to discuss the fouling removal mechanisms. The protein molecules attach to the biosensor, resulting in the sensor not being able to operate as it should do. Rather than discussing cavitation as the fouling removal method, it discussed the result of cavitation which creates mechanisms such as acoustic streaming which creates a force large enough for fouling removal to be achieved. The modelling uses Fluid-Solid Interaction (FSI) to model Surface Acoustic Waves (SAWs) as a means of fouling removal. The SAW forces showed to overcome the adhesion layer created from the fouling and the fluid-induced lift and drag forces prevent the re-attachment of the detached fouling particles. The biosensor cleaning was better in fluids with similar properties to that of water, which implies that cleaning is achieved in liquids to create cavitation and result in acoustic streaming from the implosions of bubbles. The results of fouling removal prediction showed good agreement with experimental data, which supports the concept of modelling fouling removal mechanisms such as acoustic streaming rather than cavitation bubbles themselves.

An example of using an ultrasonic bath is shown in [79] where a whey-fouled membrane is immersed into a bath for fouling removal. The ultrasonic method was compared against using a surfactant and later in combination between both cleaning methods, which improved cleaning results and showed no damage to the membrane itself. The analysis of the properties of the different membrane variables during cleaning noted that the main variables to affect cleaning were the fouling time, surfactant concentration, power level of transducer and the sonification time. The paper implied that the requirement of optimal parameters as shown from discussing the sonification time demonstrated that 10 minutes was effective but any longer would not show any advantages. Also, the effectiveness of cleaning showed to increase with the increase of power level to the transducer.

2.3.5   ULTRASONIC FOULING REMOVAL IN CYLINDERS

Heat exchangers are commonly under investigation as the operation of the device results in fouling to accumulate depending on its operating parameters and the liquid it is carrying. An experimental research paper has looked into using a 35 kHz piezoelectric transducer attached directly onto a heat exchanger [80]. When looking at the fouling removal patterns, it showed that the patterns correlate with the locations of nodes and antinodes at the beginning of cleaning and in time, expands onto the vibrating length (see Figure 2.13 and Figure 2.14). The method had more success in removing fouling placed on the outer wall of the samples but had more difficulty on removing fouling from the inner walls. The purpose of achieving cleaning from the technique was to apply this method onto structures with biofouling and calcium carbonate build up; however, the actual samples themselves used paint as a fouling layer as a control measure to replicate it for several cases.
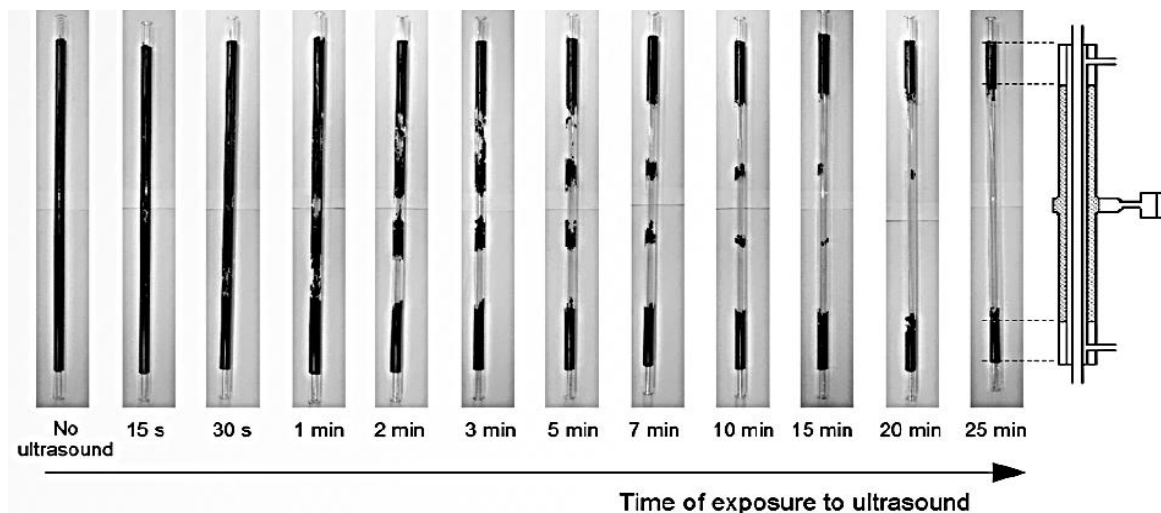
Figure 2.13: Fouling removal of sample over time due to exposure to ultrasonic cleaning transducer [80]
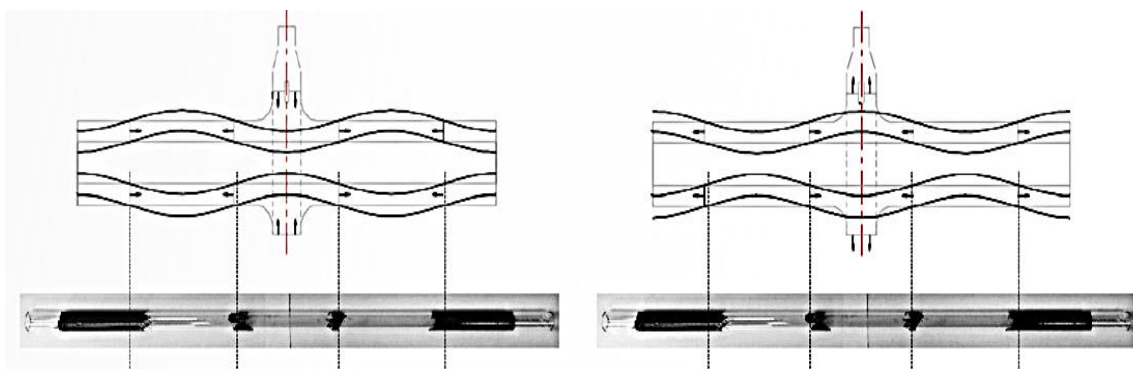
Figure 2.14: Fouling removal patterns at nodes and antinodes [80]

2.4 SUMMARY

The current state-of-the-art has shown a lack of non-invasive solutions for fouling detection and fouling removal in pipelines. UGW has shown its potential in long-distance detection of defects in engineering structures based on thickness variation, which can be used to characterise fouling accumulation. Current work carried out for the detection of fouling using UGW has only focused on short samples and used the dispersive longitudinal wave mode.

Ultrasonic baths are currently used in industry, which requires the fouled component to be submerged into the bath to carry out de-fouling, but is not a viable solution for pipeline cleaning. However, the fouling removal mechanisms produced within an ultrasonic bath as a result of the generation of cavitation, can be utilised by directly attaching HPUTs onto the outer wall of a pipeline structure. This allows the pipe to act as an ultrasonic bath to allow the fluid within the pipe to generate cavitation and promote fouling removal. Similar work to this concept has been shown on heat exchangers where an HPUT is attached to the structure and produces high vibration which dislodges fouling from the structure without the use of liquid but has only been proven on small samples and does not achieve 100% cleaning due to only dislodging fouling at the nodes and anti-nodes.

From identifying the shortcomings of current UGW techniques for fouling detection and Ultrasonic techniques for non-invasive fouling removal, this research will carry out UGW detection using the non-dispersive torsional wave mode on a schedule 40, 6 meter long pipeline. The research will also investigate the application of HPUTs for non-invasive fouling removal by the attachment onto the outer wall of a pipe filled with water to generate cavitation as the mechanism for fouling removal. FEA will be used to assist in investigating the fouling detection and fouling removal research and identify parameters that improve the techniques for its application.

Chapter 3: High Powered Ultrasonic Langevin Transducers

Power is not will, it is the phenomenon of physically making things happen – Madara Uchiha

3.1 INTRODUCTION

In recent years, the use of ultrasounds has shown to be an alternative non-invasive technique for fouling removal. Ultrasonic cleaning is achieved by exciting HPUTs which generate cavitation bubbles within a liquid. Once the cavitation bubble implodes, the force produced can dislodge solids attached to a fouled surface. Conventionally, ultrasound is used in ultrasonic baths to clean a submerged component by the generation and implosion of cavitation bubbles on the fouled surface [81]-[82]; this method is particularly used in reverse osmosis applications [50]-[51]. However, this requires the submersion of the fouled structure and thus may require a halt to production. Large fouled structures such as pipelines could not be accommodated. Table 3.1 lists important cleaning parameters used to improve the ultrasonic cleaning performance in current ultrasonic cleaning applications.

Currently, industrial HPUT-horn attachments/sonotrodes are designed to generate high amplitude vibrations for various applications including welding, cutting and sonochemistry. An in-depth literature review has been carried out in the past to study the various applications of power ultrasounds [83] [84]. The industrial uses of power ultrasonics include sterilisation of medical equipment, welding of thermoplastics and metals due to sheer vibration. The transducers are easily embedded for mass-production automated tools and can be used for composite materials and additive manufacturing. Sonochemistry has benefited from the inclusion of ultrasounds for material science, chemistry, biotechnology, cell activation and oxidation. The food industry utilises ultrasounds for the decontamination of water, sterilisation, tenderisation, freezing, degassing and altering some properties of food.

The development and addition of ultrasonic horns has been used to further the properties of HPUTs to achieve higher amplitude and more precision. This is usually carried out following numerical analysis and theoretical calculation to optimise the design of the horn for its given application. Examples of this include micro-Electrical Discharge Machining (EDM) drilling [85], electro-discharge machining [86], flange making [87], grinding [88], plastic welding [89], ultrasonic machining [90]. Aside from these applications, other purposes of the HPUT enhancement include achieving multi-frequency transduction [91] and improvement of velocity amplification [89]-[92]. Another enhancement is the addition of diagonal slits on horns to promote longitudinal-torsional wave modes [93].

Table 3.1: Cleaning parameters for improved ultrasonic cleaning performance [84]

Parameters	
Cleaning Fluid	• Chlorinated solvents are conventionally used as a cleaning medium. • The addition of an organic liquid can contribute towards the transmitting of the ultrasonic vibration due to the change in liquid properties that enhance wave propagation [94]. • Selected cleaning fluids must have cavitating properties [95]. • There is a recent dismissal of solvents due to adverse environmental effects.
Temperature	• Temperature of a liquid affects the intensity of the cavitation generation as this changes the liquid properties and affects the pressure threshold required to generate cavitation [96]. • 35°C has been shown to be the most optimal temperature for water as higher temperature allows liquid to cavitate. At higher liquid temperatures, this may reach boiling state and gaseous bubbles are produced instead of vapour bubbles (cavitation bubbles) [97]. • With the addition of a cleaning fluid, the optimal temperature can approximate to 60°C as the liquid properties change [97].
Standing Waves	• Standing waves produce active cavitation zones at fixed points. • The active zones correspond to half wavelength distances dependent on the excitation frequency used. • To achieve a more even distribution of energy, industrial cleaning tanks excite a frequency sweep to avoid standing waves.
Power	• An increase in power input results in increase of vibrational amplitude. • However, there is an upper threshold limit which, when surpassed, can result in mechanical fracture of the transducer leading to a reduction in vibration. • If there is a high intensity of cavitation emitting at the surface of the vibration location, this can reduce the transfer of acoustic energy to the bulk of the structure and lead to decoupling [98].
Frequency	• Typically, the cleaning frequency ranges between 20 – 40kHz [99]. • 40 kHz popularised due to health and safety reasons and the audible range of humans. • Higher frequency is used for microscopic cleaning. • Lower frequency is used for larger cleaning. • Higher frequency tends to generate cavitation that resonates and does not lead to collapsing.

Ultrasonic horns are typically designed to a geometrical iteration of half a wavelength in length to achieve maximum amplitude at the contact surface of the horn tip [100]. Horns can be found of simple shapes such as cylindrical, conical, stepped or OF exponential diameter variation [89]-[92], or as a combination of these different shapes [85]. The magnitude of amplification is increased in line with the ratio of the horn diameter to its tip diameter. Each shape contributes TO different amplitude characteristics, such as the filtering of noise, increased amplitude and non-contact performance. Combinations of these shapes have been investigated to further improve the performance for given applications.

Literature shows many attempts to improve amplification through the use of ultrasonic horns, but there is no previous work related to the improvement of fouling removal applications. Research that is most similar to improving fouling removal properties are ultrasonic horns that can generate and enhance cavitation intensity. Cavitation activity from ultrasonic horns has been investigated using COMSOL [101]-[102]. Such as, sonochemistry enhancement by the generation of cavitaton for oxidation [103]. As ultrasonic horns have the potential to generate cavitation for sonochemical applications, this suggests the prospect for improving the non-invasive ultrasonic cleaning technique by increasing its cleaning distance.

This chapter investigates the development of different ultrasonic horn geometries and studies improvements in the wave propagation across a plate structure. This is carried out by designing a half-wavelength ultrasonic horn within COMSOL (with cylindrical, conical, exponential and stepped shapes). The ultrasonic horns are designed with a threaded piece for attachment onto an existing 40 kHz HPUT. The transducer is attached at the center of a carbon steel plate (300 mm x 300 mm x 2 mm), and is excited using a discrete pulse. A PSV-400 3D Laser Scanning Vibrometer is used to measure the displacement across the plate structure over time.

3.2 DESIGN AND CONSTRUCTION

The most common type of piezoelectric transducer is known as the *Langevin transducer*. This HPUT consists of piezoelectric ceramic ring elements that are stacked and sandwiched between electrodes and are pre-stressed using a front and back mass (Figure 3.1). HPUTs are fabricated by bolting the front and back masses, and by placing stacked piezoelectric ceramic rings (1/8th wavelength each) between both masses before bolting. The bolt diameter is less than the inner diameter of the piezoelectric ceramic ring to ensure there is no contact. Insulating tubing may also be used on the bolt for this purpose. The material used for these components varies depending on the desired mechanical properties of the HPUT, and are listed below to create a half-wavelength HPUT:

- Two piezoelectric ceramic rings (compressional) – 1/8 wavelength thickness
- Two contact plates
- Front mass – ½ wavelength length
- Back mass – ¼ wavelength
- Bias bolt with nut – ¼ wavelength length
- Insulating tubing for bolt
- Epoxy resin - as adhesive and acoustic couplant between each component
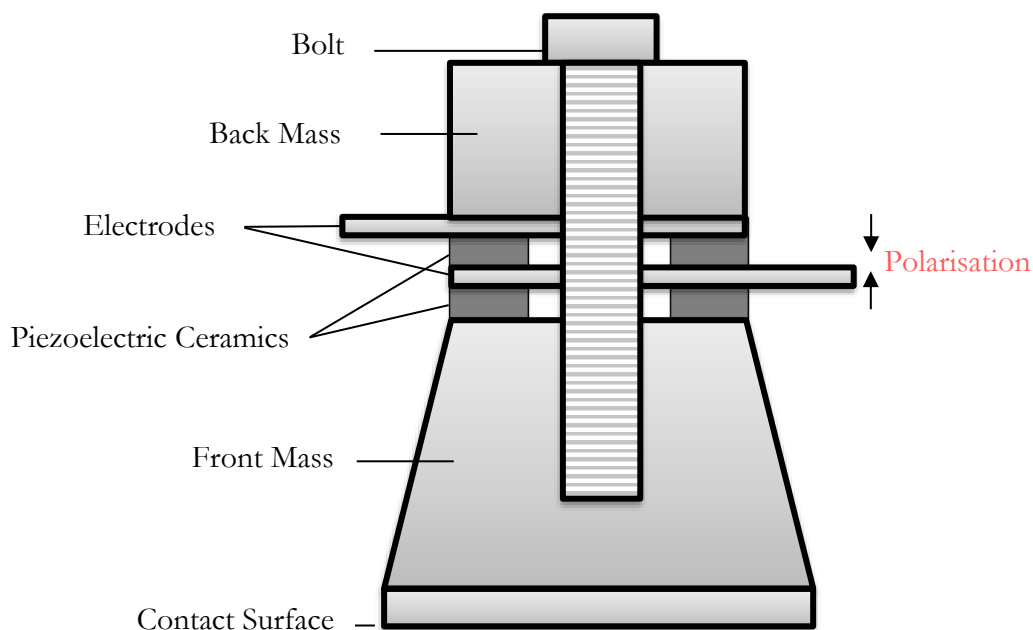
Figure 3.1: Cross-section illustration of main components of HPUT

As the HPUT is asymmetrical, the purpose of the back mass is to boost the vibration of the HPUT towards the front mass, delivering maximum amplitude at the HPUT contact surface. A common method to achieve this is to select an appropriate backing mass geometry and a material that has a higher acoustic impedance.

3.3 THEORETICAL BACKGROUND

3.3.1 LONGITUDINAL VIBRATIONS

To understand the vibration behaviour of a designed mechanical horn, vibration in bars of circular cross-section must first be understood [104]. To calculate the longitudinal vibration in bars, the stress-strain formula can be used, where strain is given by:

$$\epsilon = \frac{\partial \omega}{\partial x} \tag{3.1}$$

The stress is given by

$$\frac{F}{S_A} = -E \cdot \epsilon \tag{3.2}$$

where ω is the displacement along the bar, x is the distance, S_A is the surface area cross-section of the bar, F is the force and E is the Young's modulus.

Using the stress and strain equations, the longitudinal wave equation is as follows:

$$\frac{\partial^2 \omega}{\partial x^2} = \frac{1}{c_L^2} \frac{\partial^2 \omega}{\partial t^2}$$

(3.3)

where c_L is the velocity of the longitudinal vibration, calculated using:

$$c_L = \sqrt{\frac{E}{\rho_S}}$$

(3.4)

where ρ_S is the solid density of the material.

Assuming the cylindrical bar is free at both ends, its mode shape can be calculated as follows:

$$\omega(x, t) = 2W e^{j\omega_n t} \cos(k_n x)$$

(3.5)

where W is the amplitude of the vibration, k_n is the wave number and ω_n is the angular frequency of the nth resonance.

The nth resonant frequency can be calculated as follows [105]:

$$f_n = \frac{n c_L}{2L}$$

(3.6)

where L is the length of the bar.

The first resonance is also known as the half-wavelength resonance and is typically the length used to design the front mass of HPUTs.

3.4 FINITE ELEMENT METHODOLOGY

The HPUT model was implemented in COMSOL 5.4 and neglects the contact plates and epoxy resin within the HPUT. Instead, the voltage is applied directly to the faces of the piezoelectric ceramic rings. The model uses the HPUT dimensions in Figure 3.2 and the material properties in Table 3.2. The piezoelectric ceramic rings are made of PZT-4 and their material properties are selected from the built-in database in COMSOL [106].

Chapter 3: High Powered Ultrasonic Langevin Transducers
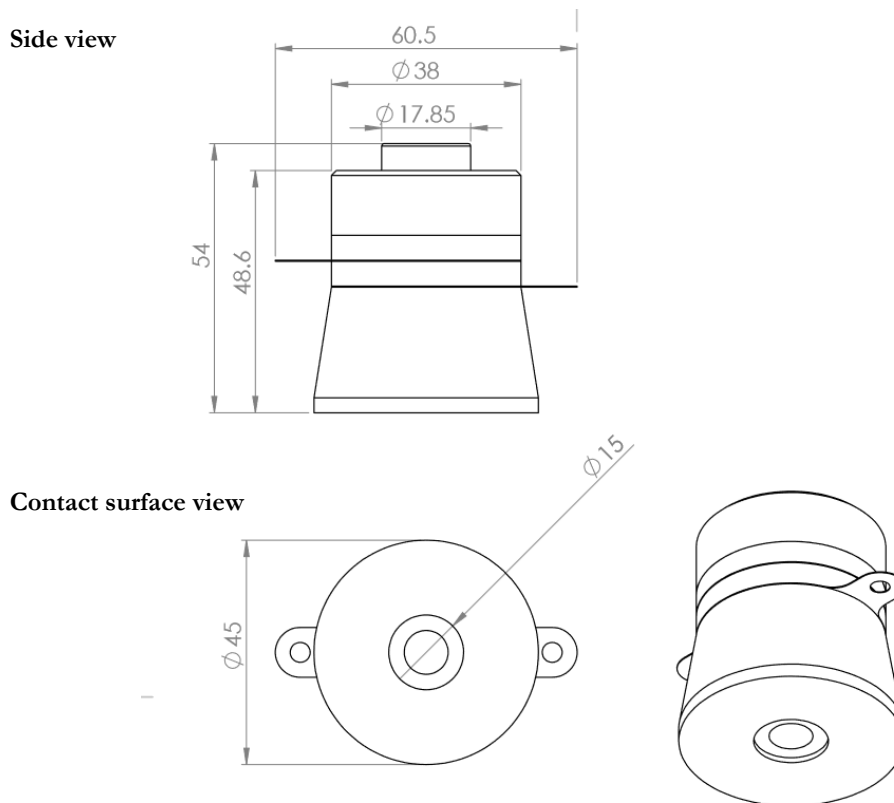
Figure 3.2: Technical drawing of 40 kHz HPUT selected for investigation

Table 3.2: Material properties for metallic components of HPUT

Material Property	Aluminium	Stainless Steel
Density	2700 kg/m³	7830 kg/m³
Young's Modulus	70 x 10⁹ Pa	207 x 10⁹ Pa
Poisson's Ratio	0.35	0.3

The geometry is created in COMSOL by creating shapes using polygon for the front mass and rectangles for the other components (Table 3.3). The geometry created on an xz-axis is then revolved to create a solid HPUT.

The HPUT is modelled to excludes the electrode plates as the terminal and ground are assigned to the face of the piezoelectric ceramic to make up for the input signal.

Table 3.3: COMSOL definition selections of HPUT components

Definitions	HPUT Component	Selection
Explicit – used to define a domain or surface by a specific name	+z poled piezoelectric ceramic ring	Domain
	-z poled piezoelectric ceramic ring	
	Bolt	
	Front mass	
	Back mass	
	Ground Terminal	Boundary
	Voltage Terminal	
Union – combine two or more explicit components	+z poled piezoelectric ceramic ring -z poled piezoelectric ceramic ring	Domains

3.4.1   ROTARY SYSTEM

The poling of +Z of piezoelectric elements is in the direction of the +Z axis as default. This allows modelling piezoelectric ceramics in COMSOL without having to rotate the poling axis of the element; however; the polarisation of the HPUT requires the piezoelectric ceramic ring in contact with the back mass to have +Z facing downwards. This means that the explicit domain marked as –Z poled must be rotated to have its +Z axis going in the opposite direction to default. The material is selected for each component as defined in Table 3.4.
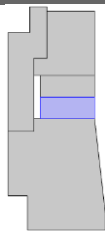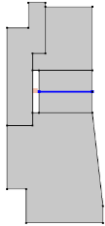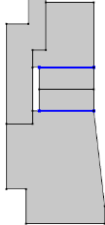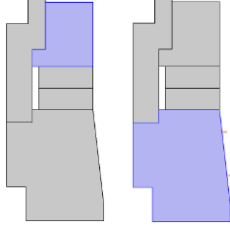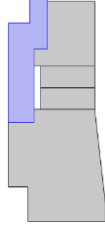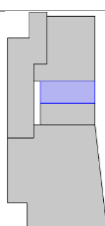
Table 3.4: Selection of material for HPUT components

Material	HPUT Component
Stainless Steel	Bolt and back mass
Aluminium	Front mass
PZT-4	Piezoelectric ceramic rings

3.4.2   PHYSICS OF THE FE MODEL

The FEA consists of solid mechanics and electrostatics which is coupled by the piezoelectric effect multiphysics. The physics used in the FE model are listed in Table 3.5 and displays each component of the HPUT selected per physics.

Table 3.5: Physics assigned to HPUT domains and boundaries

Physics	Domain/Boundary Selected	Explanation
Piezoelectric Material 1 +Z Poled		Piezoelectric element of the device – not grouped with other piezoelectric rings
Terminal 1		Selected faces of the piezoelectric rings to have a positive voltage applied
Ground 1		Selected face with ground
Linear Elastic Material 1		Front and back mass are not piezoelectric and will need to be defined as linear elastic material
Linear Elastic Material 2		Bolt is not piezoelectric and is defined as linear elastic material
Fixed Constraint 2		Bolt is fixed as this holds the transducer together from the top surface of the back mass
Piezoelectric Material 2 -Z poled		Separate from default as this ring will include a rotary system to rotate its positive poling

Linear elastic behaviour is assumed for all solid parts of the model, excluding the piezoelectric ceramic rings. The application of Newton's law yields the following equation:

$$\rho_S \frac{\partial^2 \boldsymbol{u}}{\partial t^2} = \nabla . \bar{\bar{\mathbf{T}}}$$

(3.7)

where, $\boldsymbol{u}$ is the solid displacement field, $\bar{\bar{\mathbf{T}}}$ is the stress tensor, and ϱ_S is the density of the solid.

A piezoelectric material is assigned to the piezoelectric ceramic rings which obey the solid mechanics governing equations and, additionally, the PZT- linearised constitutive equations in stress-charge form:

$$\bar{\bar{T}} = c_E \cdot \bar{\bar{S}} - e^t \cdot E \tag{3.8}$$

$$D = e \cdot \bar{\bar{S}} + \varepsilon_S \cdot E \tag{3.9}$$

where $\bar{\bar{T}}$ is the stress tensor, $\bar{\bar{S}}$ is the strain tensor, E is the electric field, D is the electric displacement field, c_E is the elasticity matrix, e is the piezoelectric coupling coefficient for the stress-charge form and ε_S is the permittivity matrix.

Electrostatic behaviours are assigned to the piezoelectric ceramic rings with the signal applied as follows:

$$\nabla \cdot D = 0 \tag{3.10}$$

$$E = -\nabla V \tag{3.11}$$

where V is the electric potential corresponding to the electric field E.

The terminal and ground equipotentials are applied to the boundaries explicitly as in previous work [107]. The ground boundary is set to 0 V and the terminal boundary is set to:

$$V = V_0 \tag{3.12}$$

where V_0 is the modulated input signal. The correct polarisation is achieved by assigning a rotated global co-ordinate system to one of the two piezoelectric ceramic rings and rotating its polarisation towards the second piezoelectric ceramic ring.

3.4.3   GEOMETRY MESH

A dynamic transient simulation to map out the wave propagation requires the calculated mesh to be optimal. The wave equation requires the time stepping within the solver to complement the meshing itself to yield an accurate solution. The meshing size uses ten 2nd-order elements per wavelength. The equation used to calculate the maximum allowed mesh element size (h_o) is given by [108]:

$$h_o = \frac{\upsilon_{gr}}{N f_o} \tag{3.13}$$

where υ_{gr} is the group velocity, N is the number of elements per wavelength and f_o is the centre frequency.

3.4.4   IMPEDANCE VALIDATION OF FEA

For validation, the model is computed in the frequency domain to produce an impedance plot for comparison with laboratory data. This is carried out in the frequency domain and allows a selected range of frequencies with an incremental value to be used when computing the model; this will be the frequency range that will be plotted within the impedance analysis obtained from the results. Experimental data of the 40 kHz HPUT is collected using the Agilent 4294A Precision Impedance Analyzer [109].

Figure 3.3 shows an experimental impedance of 18.51 Ω at 39.98 kHz and a numerical impedance of 9.72 Ω at 39.60 kHz. The HPUTs are procured from Beijing Ultrasonics [110] which states the HPUT to be 40 kHz ± 1 kHz, this means that the numerical model is in good agreement to the resonating frequency. The variation in impedance is due to neglecting the electrode contact plates within the numerical methodology.
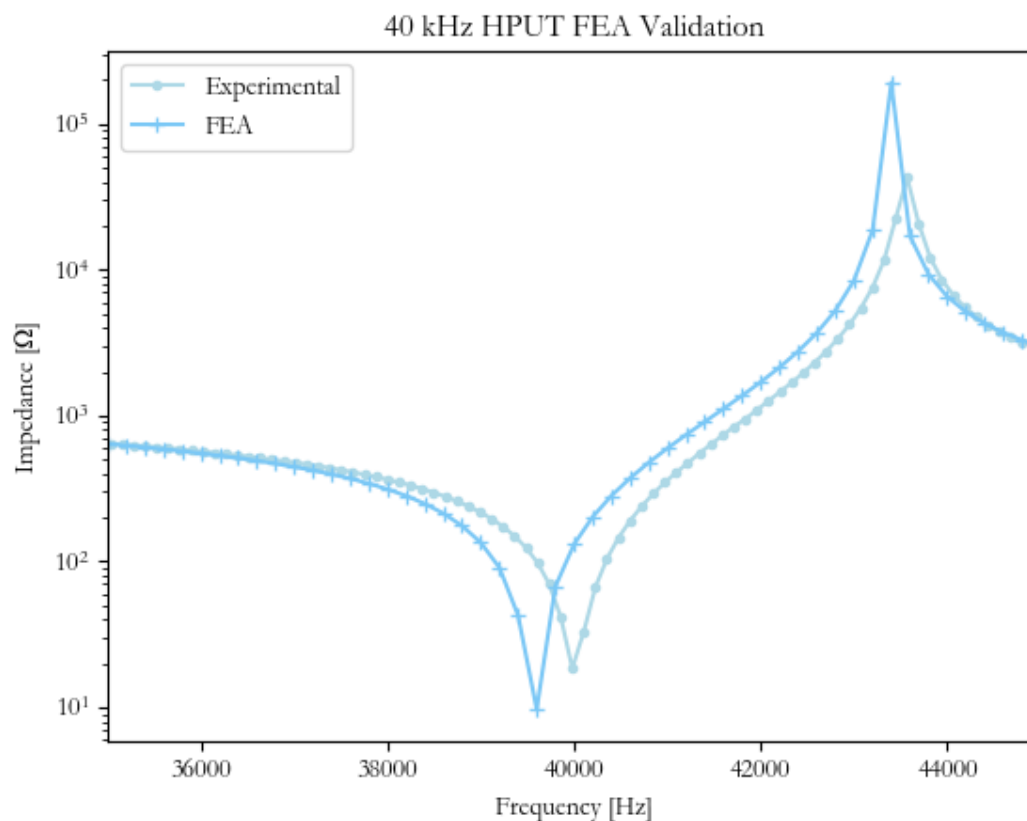
Figure 3.3: Impedance comparison of numerical results and experimental values for the 40 kHz HPUT

3.4.5 EIGENFREQUENCY ANALYSIS

The validated HPUT model is simulated in 2D axisymmetric and undergoes eigenfrequency analysis for ease of computation. The maximum displacement achieved across the HPUT is localised at the HPUT contact surface (see Figure 3.4).
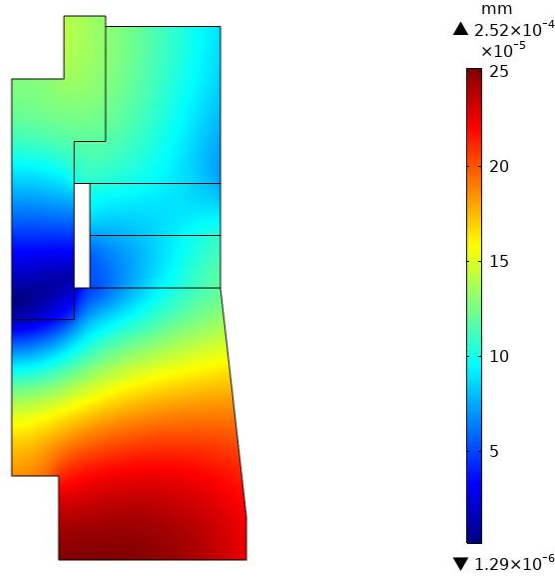
Figure 3.4: Displacement distribution of 40 kHz at resonant frequency

3.5 TRANSDUCER SONOTRODE DESIGN

The sonotrodes are designed to have a total length equivalent to half a wavelength, calculated by using the fundamental equations below and the material properties of the desired sonotrode. These are designed in aluminium to match the material of the front mass of the HPUT. Using the equations below, the length of the ultrasonic horn is calculated as 0.0636 m:

$$L_{Horn} = \frac{\lambda}{2} \tag{3.14}$$

$$\lambda = \frac{c_L}{f} \tag{3.15}$$

$$L_{Horn} = \frac{\lambda}{2} = \frac{c_L}{2f} = \frac{\sqrt{\frac{E}{\rho}}}{2f} = \frac{\sqrt{\frac{70 \times 10^9}{2700}}}{2 \times 40000} = 0.0636m$$

where L_{Horn} is the length of the ultrasonic horn and λ is the wavelength.

Excluding the cylindrical horn, which has a constant diameter throughout its length, the sonotrodes are designed to have a *magnitude* of 2 at the horn tip. This means that the diameter at

the tip of the horn is half the diameter in contact with the HPUT surface. The conical horn has a linearly varying diameter along its length. The stepped horn comprises two quarter-wavelength cylinders, the first quarter matching the diameter of the HPUT contact surface and the second part is half the diameter of the HPUT contact surface, resulting in a *magnitude* of 2. The diameter of the exponential horn varies along its length according to the equation:

$$S_A(x) = S_{A1}e^{-kx} \tag{3.16}$$

$$k = \frac{-ln\left(\frac{D_2}{D_1}\right)}{L} \tag{3.17}$$

where S_A is the surface area, k is the taper factor, D is the diameter, L is the length. Subscript 1 refers to the input/wider part of the ultrasonic horn and subscript 2 refers to output/narrower part of the ultrasonic horn.

3.5.1   NUMERICAL INVESTIGATION

Each horn is designed in COMSOL using the equations appropriate to each ultrasonic horn geometry. A parametric study was conducted on the length of the ultrasonic horn to adjust the geometry to achieve an eigenfrequency close to 40 kHz. The numerical analysis of each ultrasonic horn is shown in Figure 3.5. The cylindrical horn shows high displacement at the original HPUT contact surface and at the tip of the ultrasonic horn, dsplaying that the addition of the half-wavelength horn achieves approximately double the displacement of the HPUT in Figure 3.4.
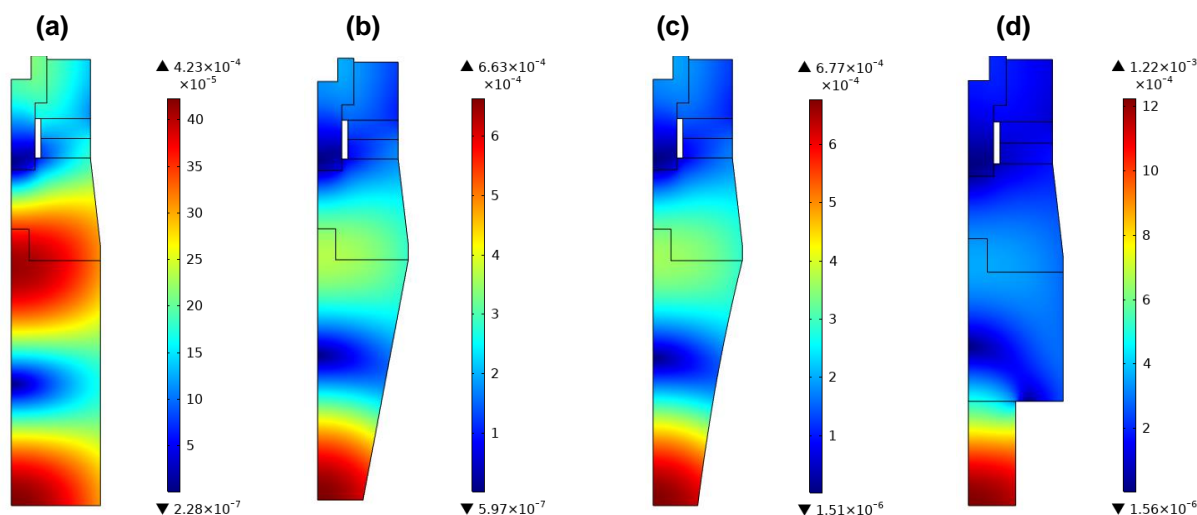
Figure 3.5: Displacement distribution across 40 kHz HPUT with (a) cylindrical, (b) conical, (c) exponential and (d) stepped ultrasonic horns attached

The conical horn shows much higher displacement at the horn tip compared to the original contact surface, and is higher than for the cylindrical horn, showing that the *magnitude* at the horn

51

tip improves the amplitude. The exponential horn gives a similar result to the cylindrical horn but shows minor increases in the displacement. This can be due to having a similar diameter variation along the length of the horn as a result of the selection of horn magnitude. The stepped horn shows the largest increase in displacement at the horn tip, possibly due to the geometry achieving optimal filtering and focusing of the HPUT vibration.

3.5.2   EXPERIMENTAL INVESTIGATION

The final ultrasonic horn geometries are shown in Figure 3.6 and have been manufactured with a threaded component for interchangeability (shown in Figure 3.7). Each ultrasonic horn is attached to the 40 kHz HPUT and undergoes analysis using the Agilent 4294A Precision Impedance Analyzer [109] as shown in Figure 3.8, with the results shown in Figure 3.9. The 40 kHz HPUT (flat) achieves the lowest impedance at its resonant frequency. With the addition of an ultrasonic
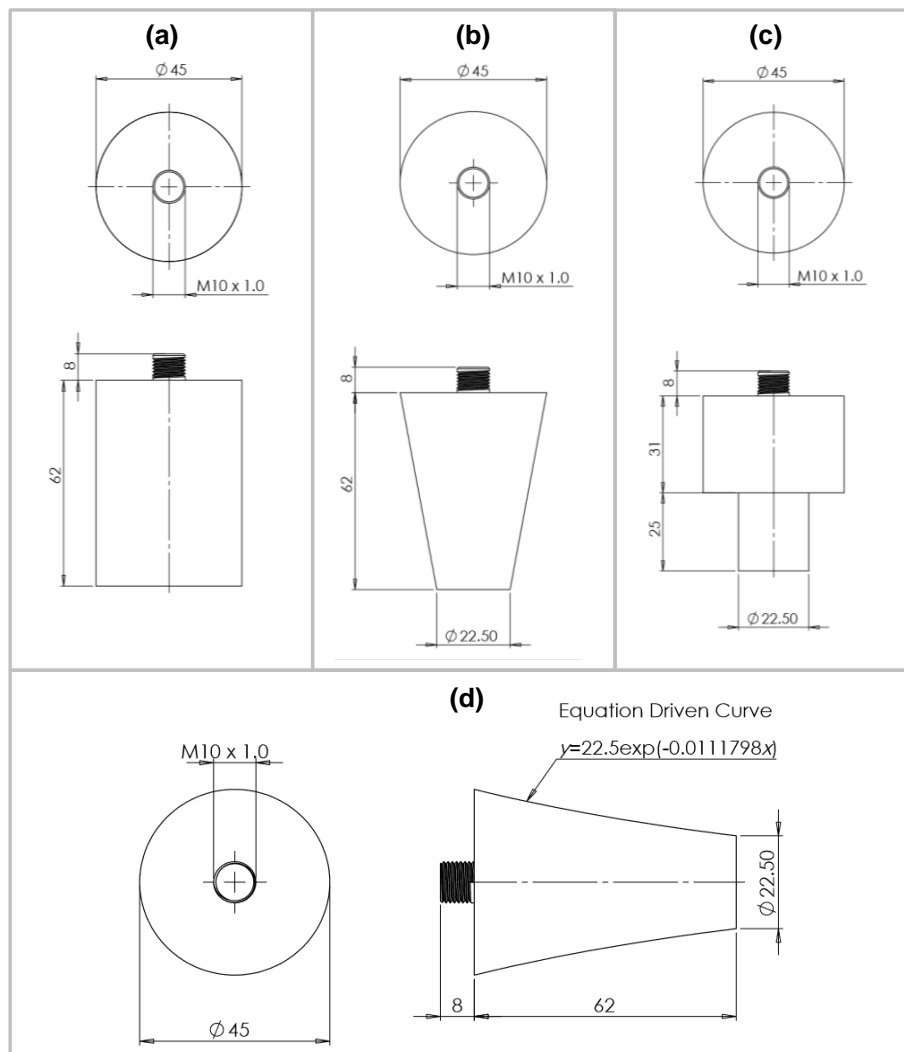
Figure 3.6: Technical drawings of final ultrasonic horn shapes (a) cylindrical, (b) conical, (c) stepped and (d) exponential
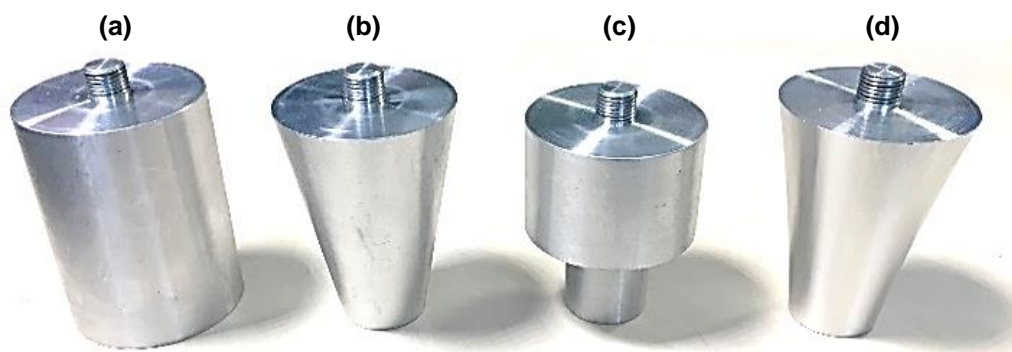
Figure 3.7: Manufactured (a) cylindrical, (b) conical, (c) stepped and (d) exponential ultrasonic horn

horn, the added mass results in an increase in impedance as well as additional resonant and anti-resonant response for the stepped horn. The horns also shift the natural frequency, thus numerical analysis and parametric optimisation were used to maintain a resonant frequency close to 40 kHz. When comparing the impedance achieved from the manufactured sonotrodes to the numerical impedance calculated in Figure 3.10, this shows a good agreement aside for each of the sonotrodes excluding the stepped horn. This may be due to the extreme change in diameter of the horn at the stepped section and also due to this horn being shorter than the other three sonotrodes under investigation which may produce an additional resonant and anti-resonant response. Figure 3.9 is used to tune the excitation frequency of the HPUT when each horn is attached onto a plate structure for wave propagation analysis.
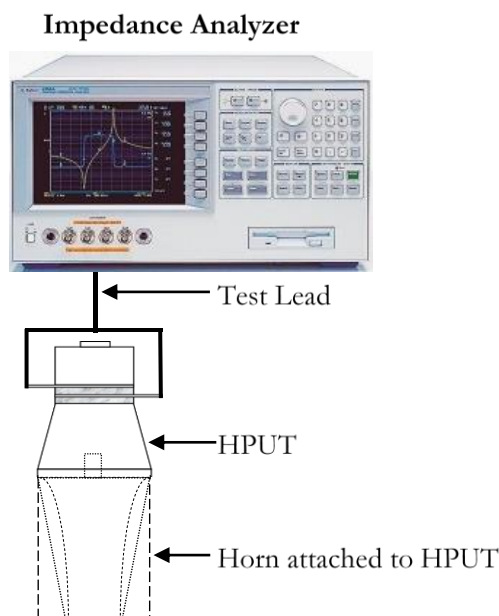
Figure 3.8: Experimental set-up to collect impedance of HPUT and ultrasonic sonotrode attachments
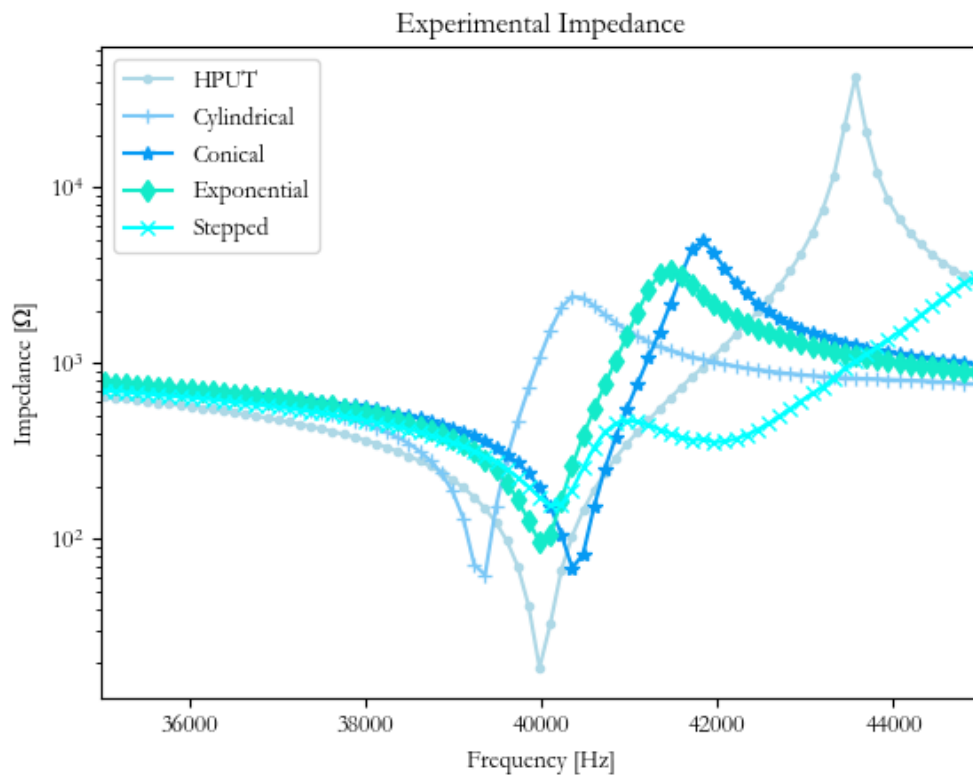
Figure 3.9: Experimental impedance of HPUT and ultrasonic sonotrodes
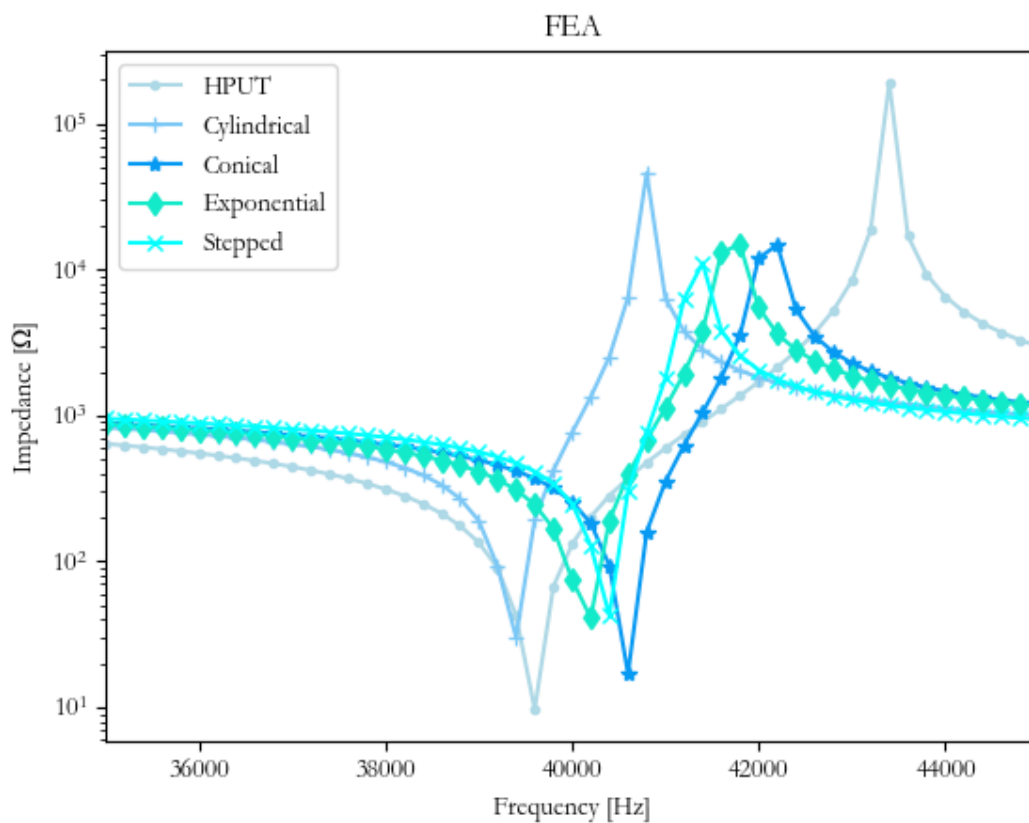
Figure 3.10: Numerical impedance of HPUT and ultrasonic sonotrodes

3.5.3 WAVE PROPAGATION STUDY

A 300 mm x 300 mm x 2 mm carbon steel plate is placed within an upright frame as shown in Figure 3.11. The frame holds the 40 kHz HPUT and pressurises the HPUT against the center of the plate. A Polytec PSV-400 3D Laser Scanning Vibrometer [111] is used to scan the outer surface
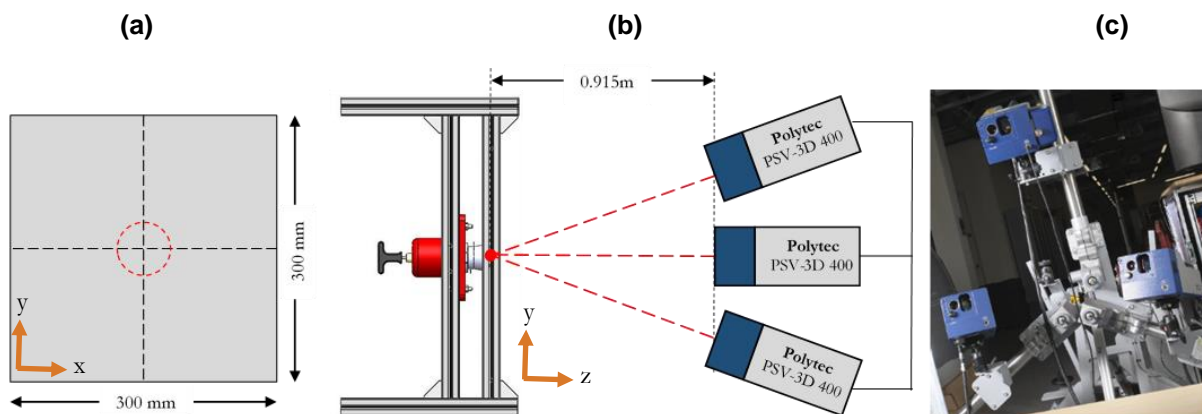
Figure 3.11: (a) dimensions of 2 mm thick carbon steel plate and location of HPUT attachment, (b) experimental set-up for vibrometry analysis and (c) Polytec PSV-400 3D Laser Scanning Vibrometer

of the plate structure. For this to be achieved, the plate is placed at an optimal distance using the equation:

$$Distance = 0.099 + (n_x \times 0.204) \tag{3.18}$$

where n_x is the iteration of the optimal distance between the PSV-400 and the test specimen.

The PSV-400 was calibrated to scan the plate where surface preparation is applied. The HPUT is excited using a discrete pulse, which is a 5-cycle sinusoidal wave modulated using the Hamming function using equation (2.8).

Figure 3.12 shows a high amplitude displacement propagating from the HPUT location. For comparison between the horns, the maximum value at the HPUT location as annotated in Figure 3.12 is used. To compare the wave propagation across the plate, the edge point is taken as the maximum value from the furthest ripple from the HPUT pulse. At each of these points, the x (displacement along the height of the plate), y (displacement along the width of the plate) and z (out-of-plane displacement, perpendicular to the plate) components are monitored. The component axis is annotated in Figure 3.11.

Monitored edge point

HPUT location

mm/s
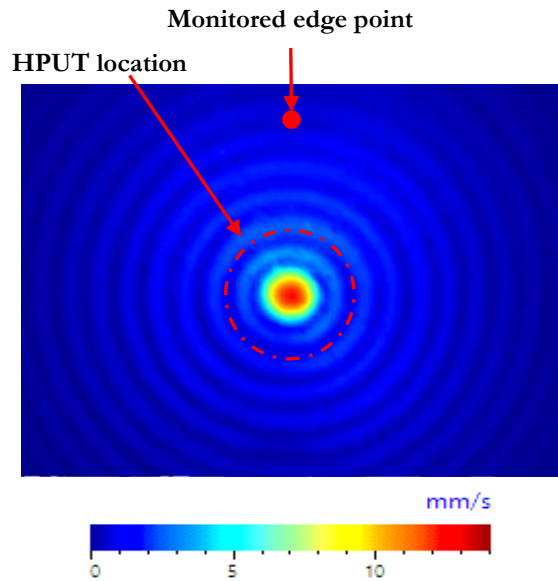
Figure 3.12: HPUT with conical ultrasonic horn attached to center of plate undergoing data collection using 3D Laser Scanning Vibrometer. Displaying high amplitude at the HPUT location

When exciting the HPUT, a compressional vibration is generated across the piezoelectric ceramic rings, resulting in vibration perpendicular to the HPUT front mass. The discrete pulse generates vibration in both directions from the piezoelectric ceramic rings. This is shown in Figure 3.13. The vibration will follow a path of propagation in the form of a wave packet. Wave packet 1 describes the first pulse to be received at the HPUT contact surface. Depending on the efficiency of the HPUT, some double reflection from the HPUT contact surface and back mass will occur and result in a second wave packet 2, returning to the HPUT, where it is expected to have reduced amplitude compared to wave packet 1. Wave packet 3 is the backwards propagating vibration from

Propagation path of wave packet 1

Propagation path of wave packet 2

Propagation path of wave packet 3
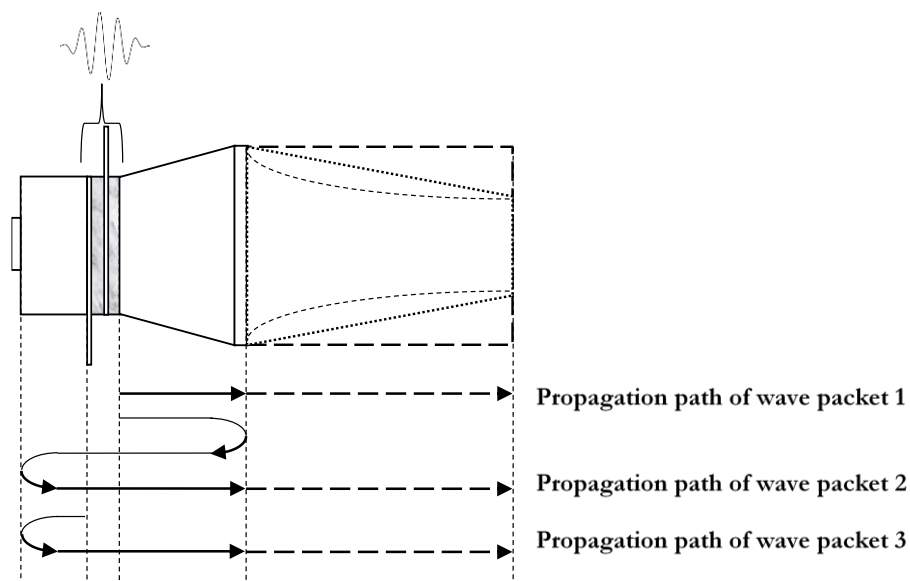
Figure 3.13: Diagram of HPUT propagation paths when excited by a discrete pulse

the initial pulse, reflected at the back mass, and resulting in some reduced signal on arrival at the HPUT contact surface. Further wave packets are produced as results of multiple signal reflections across the HPUT, with reduced amplitude after each reflection. Each wave packet can be identified by the delay of the signal.

3.5.4   HPUT

At the HPUT location, Figure 3.14 shows a high out-of-plane (z-direction) velocity. The annotated section A relates to wave packet 1 as described in Figure 3.12. Section B shows a combination of two reflections overlapping, related to wave packets 2 and 3. Over time, the discrete pulse is reflected from the plate edge and is annotated in Figure 3.13. The x and y components of the signal follow a similar amplitude pattern and result from a compressional excitation of the plate structure.
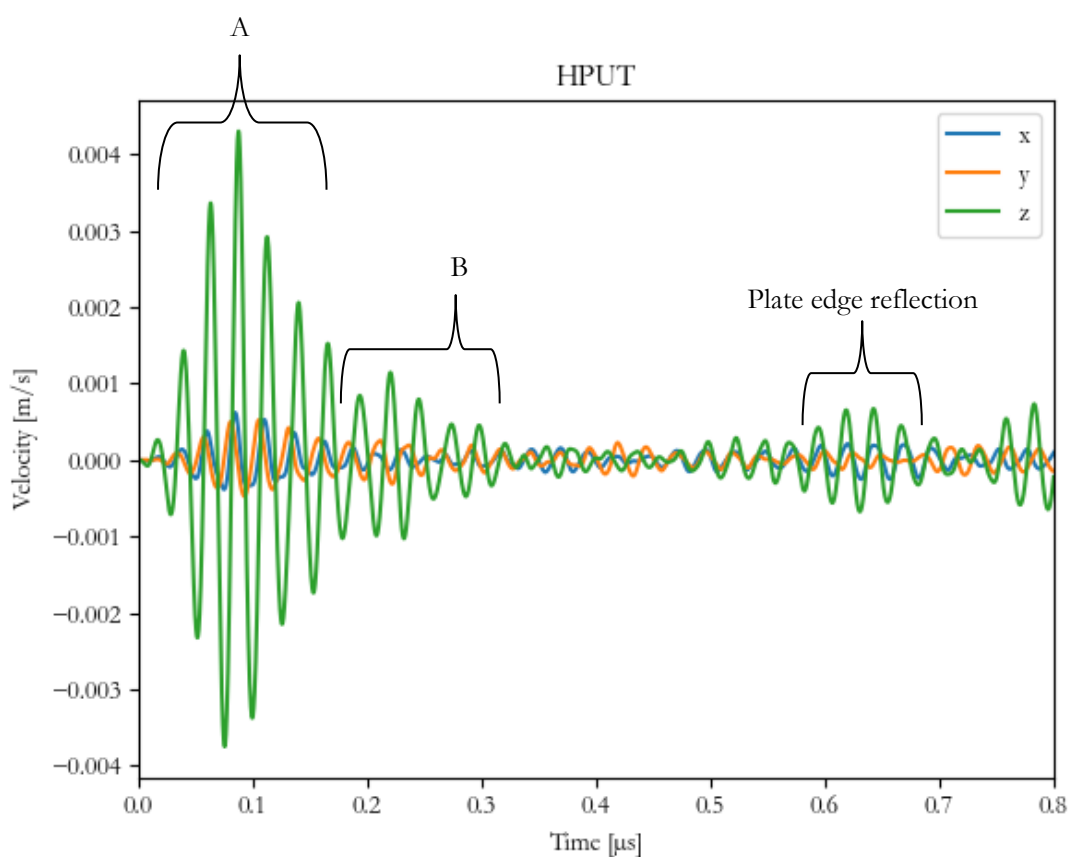
Figure 3.14: Velocity at the HPUT location for HPUT without ultrasonic horn

3.5.5   CYLINDRICAL

The cylindrical horn (shown in Figure 3.15) achieves 30% higher amplitude in the z-direction at section B compared to the HPUT. Although the HPUT is excited using a discrete pulse, the signal is oscillating through the structure due to multiple structure reflections and the lack of filtering of
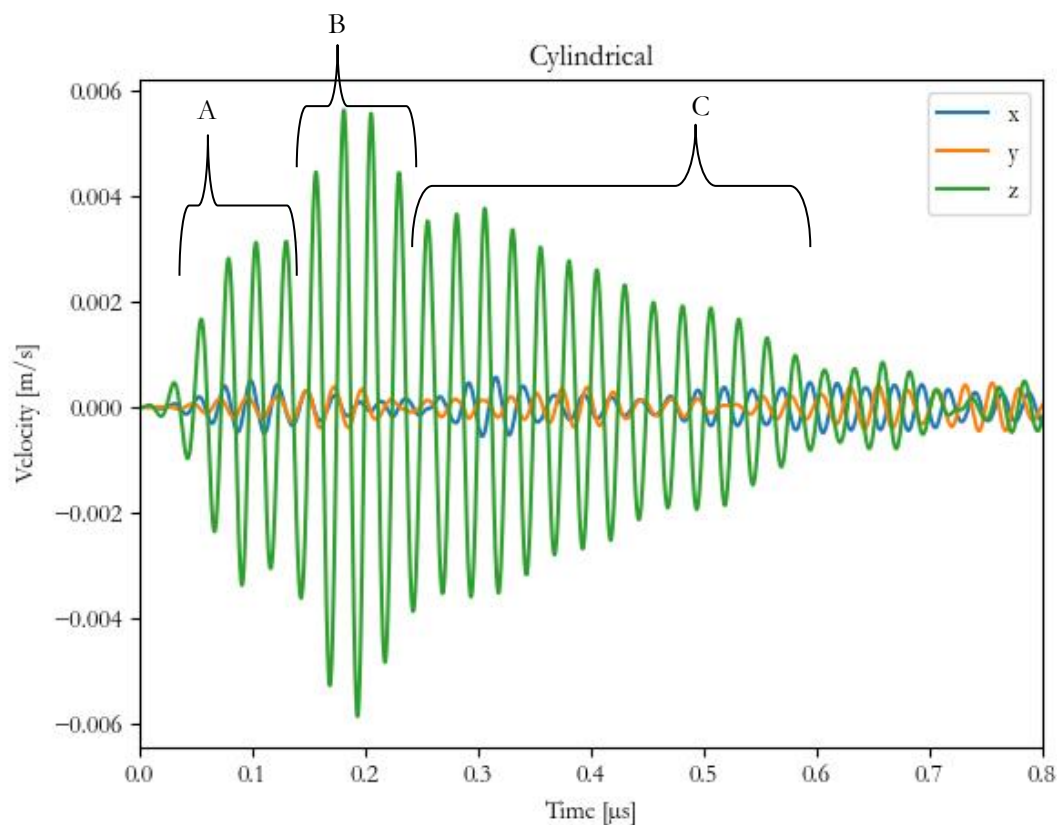
Figure 3.15: Velocity at the HPUT location for HPUT with cylindrical sonotrode

the signal due to the horn geometry. Wave packet 1 (section A) is overlapped by section B, which is a combination of multiple reflections including wave packets 2 and 3. The remainder of the signal (for example; section C) shows a reduction in oscillation as the discrete pulse propagates away from its source. This configuration improves the amplitude of the HPUT only due to the addition of wave packets at section B.

3.5.6   CONICAL

Figure 3.16 shows an increase in amplitude (three times the HPUT) of wave packet 1 (section A), which means that the geometry has improved the initial wave packet pulses. Section B is again a combination of wave packets 2 and 3. Section C is a result of an additional reflection generated by the horn geometry. The plate edge reflection can be seen in the figure; however, this is oscillating which may be due to the increased amplitude and additional wave packet reflections.

3.5.7   EXPONENTIAL

The amplitude of wave packet 1 is shown in Figure 3.17, where section A is increased by 50% compared to the HPUT. However, this is not as high as achieved using the conical horn. Again,
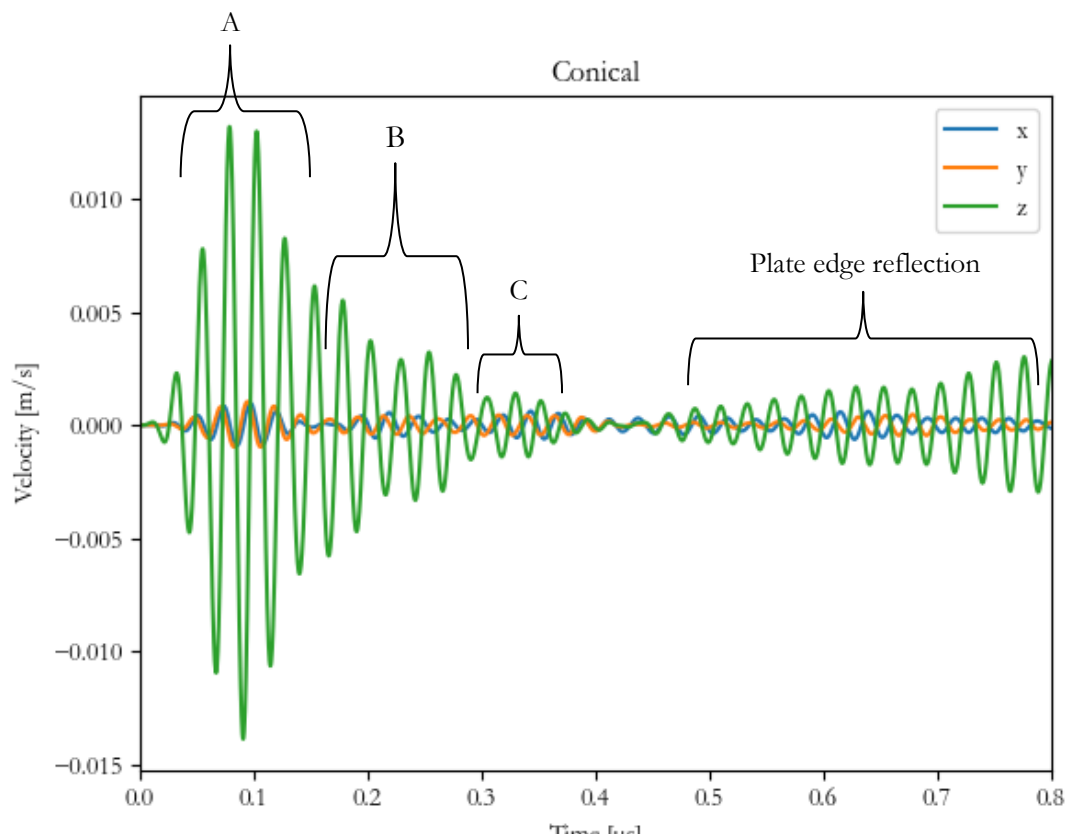
Figure 3.16: Velocity at the HPUT location for HPUT with conical sonotrode

in the figure, section B is a combination of wave packets 2 and 3. Section C is a result of reflections from the addition of the exponential horn which oscillates for a longer period of time compared to the conical horn. There is very little reflection from the plate edge, possibly due to the lower amplitude achieved using this horn shape.

Exponential horns typically have improved amplitude due to filtering of the signal. However, this may be due to the horn tip *magnitude*, known to improve the amplitude in other applications. The attachment to the plate can also attenuate the signal.

3.5.8   STEPPED

The stepped horn shows a 30% reduction in the displacement (Figure 3.18) but an improvement of the signal delivery as wave packet 1 (section A) and wave packet 2 (section B) are now separated. The removal of wave packet 3 is due to the geometry of the horn which filters reflected signals.
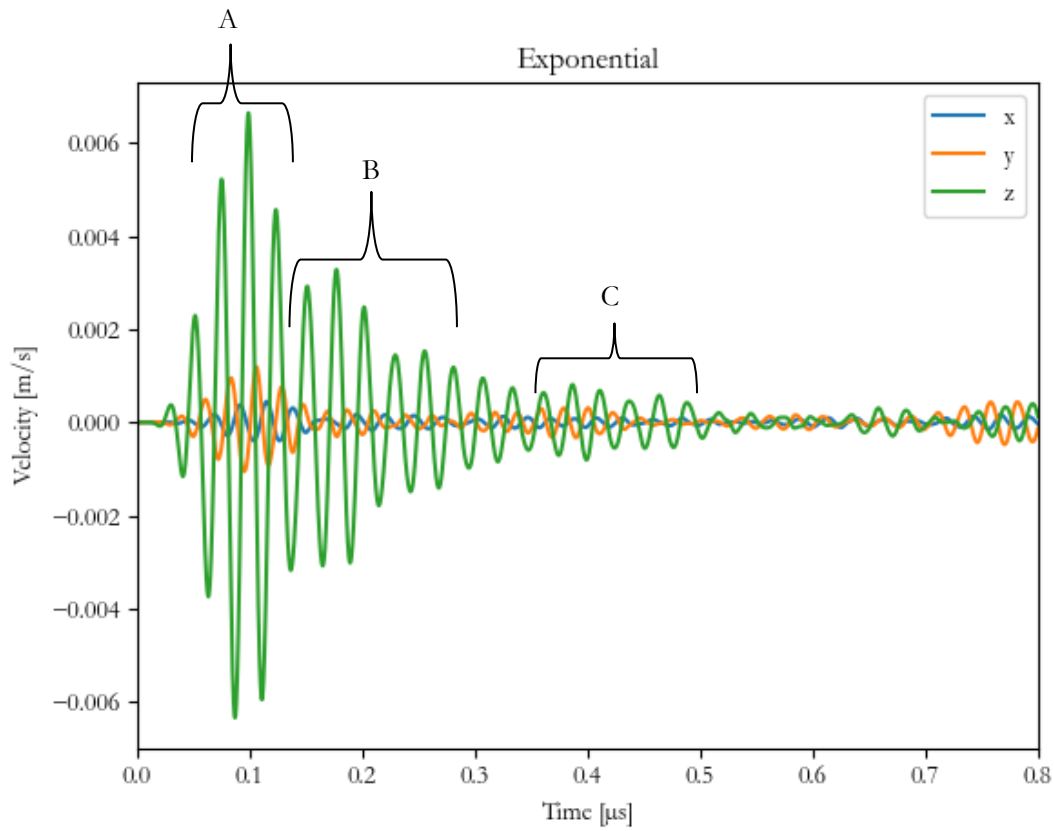
Figure 3.17: Velocity at the HPUT location for HPUT with exponential
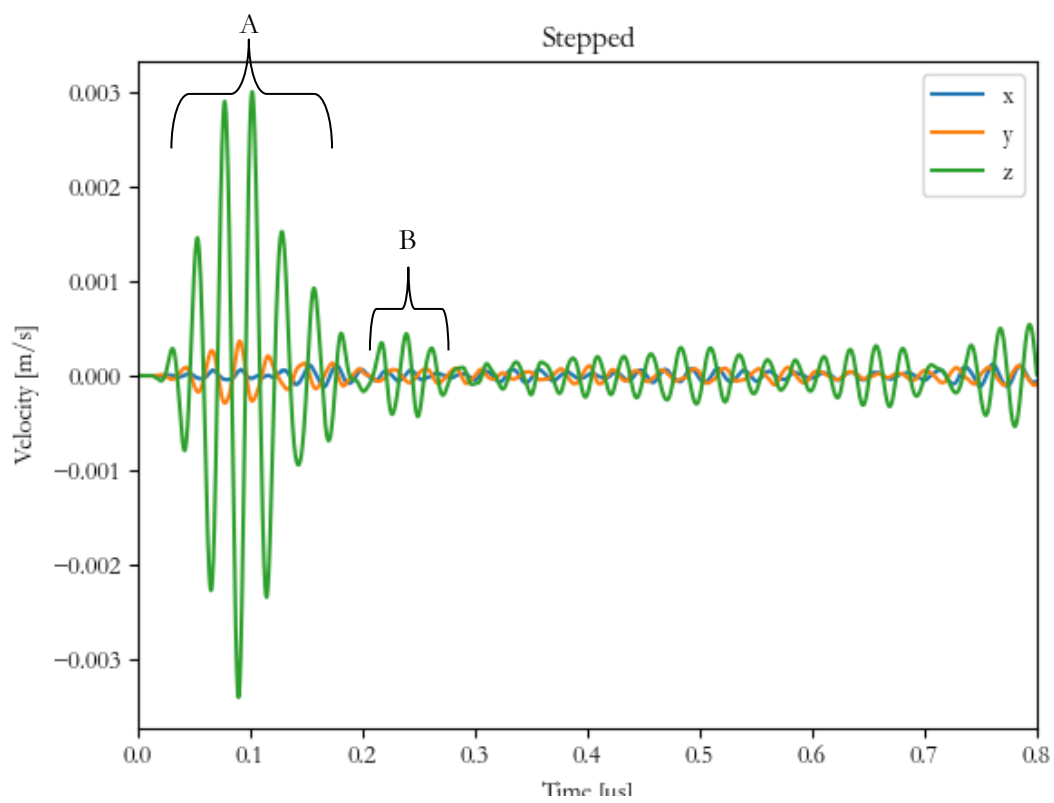
Figure 3.18: Velocity at transducer location for HPUT with stepped sonotrode

Separation of these signals is beneficial for some applications. However, for ultrasonic cleaning, the HPUT would be driven at a continuous sinusoidal waveform so they will not be separable.

The numerical results show the stepped horn should achieve the highest displacement but this was not experimentally achieved in the laboratory investigation. This may be due to the attachment of the plate which attenuated the delivery of the signal and also dampened the vibration of the ultrasonic horn.

3.5.9   COMPARISON OF ULTRASONIC HORNS

The conical horn achieved the highest increase in amplitude at the HPUT location (Figure 3.19), and the cylindrical and exponential horns improved the performance compared to the HPUT. The stepped horn showed a reduction of 30% compared to the HPUT. The velocity achieved at the edge monitored point (refer to Figure 3.12) follows a similar trend of improvements and reductions.

Another factor that can improve or reduce the amplitude across the plate is the x and y components generated from the horn. As the HPUT has a conical shape, x and y vibrations are generated across the plate, whereas the filtering of the signal with the exponential and stepped horns minimises the x and y components and reduces their propagation once the horns are attached onto the plate.
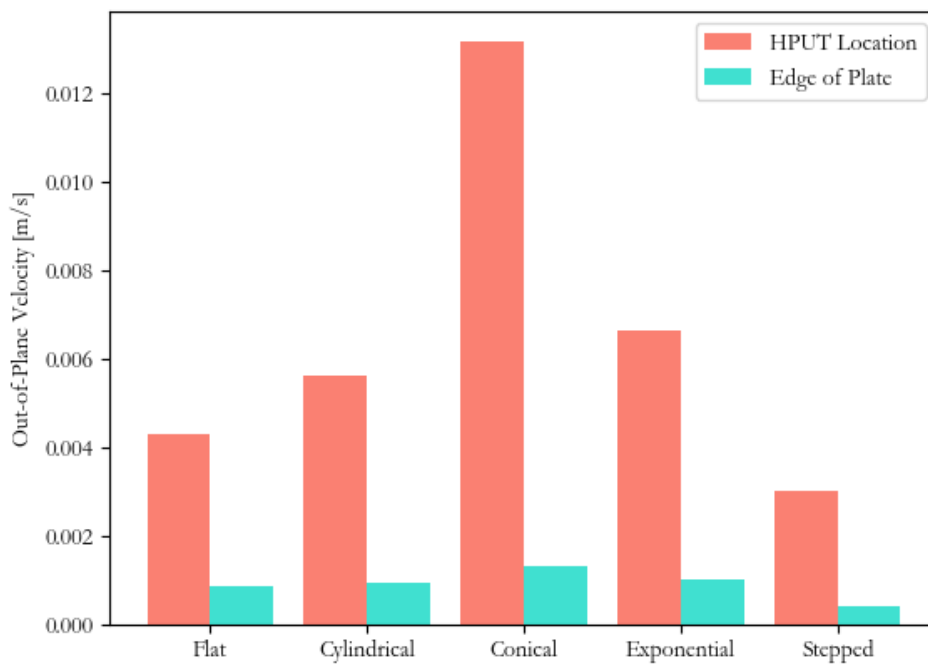
Figure 3.19: Comparison of maximum out-of-plane velocity of sonotrodes
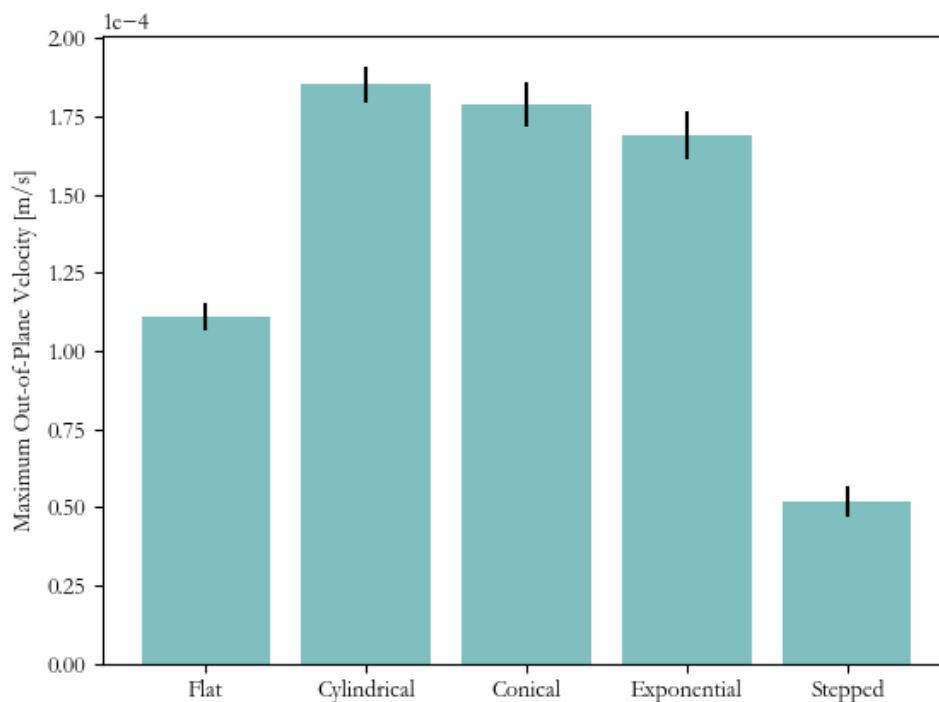
Figure 3.20: Comparison of converted FFT spectrum and standard deviation of sonotrodes

The data at the HPUT location is converted to FFT spectrum (Figure 3.20) showing highest amplitudes for the cylindrical horn. This is a result of the multiple reflections produced by this horn attachment. The stepped horn has achieved the lowest amplitude due to the filtering of the signal shown in Figure 3.18.

3.6 SUMMARY

This chapter investigated four ultrasonic horn designs (cylindrical, conical, exponential and stepped) tailored to a 40 kHz HPUT to study the potential wave propagation across a 300 mm x 300 mm x 2 mm carbon steel plate. This has shown that, with the attachment of the ultrasonic horn, there is an increase in out of plane displacement at the HPUT location. This feature is important for designing and optimising ultrasonic cleaning applications as it can enhance the generation of acoustic cavitation bubbles. A factor that must be accounted for at the HPUT location is the displacement in the x and y directions, which will contribute to the wave travelling along the plate structure. From the study, the conical horn has shown the most improvement of the wave propagation (300%) while the stepped horn shows a 30% reduction in wave propagation. Although improvements have been shown, the size of the HPUT with the addition of an ultrasonic horn will directly affected the HPUT collar, increasing the materials and costs for its manufacturing process. As the propagation away from the HPUT with the conical horn shows partial

improvement, another approach without the attachment of an ultrasonic horn should be investigated.

Chapter 4: Numerical Modelling of the Ultrasonic Cleaning Technique

Repeated failures lead to success – Japanese Proverb

4.1 INTRODUCTION

Chapter 3 discusses the development of a HPUT FE model which has been validated against impedance characteristics in experimental conditions. This model is used as the foundation to develop an ultrasonic cleaning FE model to predict cleaning patterns. To create an FE model that can represent the cleaning capabilities of the ultrasonic cleaning technique, relative FEA literature is reviewed to identify the pressure threshold required to generate cavitation for fouling removal. This will support the development of the ultrasonic cleaning FE model and determine whether the ultrasonic cleaning configuration is generating cavitation for comparison with laboratory investigation in later chapters.

4.2 FEA LITERATURE REVIEW

4.2.1 CAVITATION GENERATION FOR MATERIAL REMOVAL

An example of modelling ultrasonic cleaning has been done numerically using governing equations related to generating cavitation bubbles and the pressure field created [112]. The model aimed to map the bubble dynamics, dirt particle motion and the fluid-material interaction, and was done by creating three different models to produce different cases including potential fluid flow, viscous flow and compressional flow. Different cleaning parameters were considered during the development of the model which included:

- Relative size between bubble at its maximum volume and particle size
- Bubble stand-off distance from the particle and from the material wall
- Excitation pressure field driving the bubble dynamics

The approach to modelling was different depending on the model case. The potential flow model used the Helmholtz equation, the viscous model used incompressional Navier-Stokes equations and the compressional model used a multi-material fluid domain and shockwave capturing. Finally, the boundary element model used the Laplace equation and a boundary integral equation based on Green's theorem. The paper explains in depth the different parameters and methods used to create the different models, resulting in the ability to create a small cluster of cavitation bubbles shown in Figure 4.1. The researchers then create a model of the removal of material and focused on a single particle, modelling the pressure field to move this particle without creating imploding cavitation bubbles to move the particle from a surface as shown in Figure 4.2.
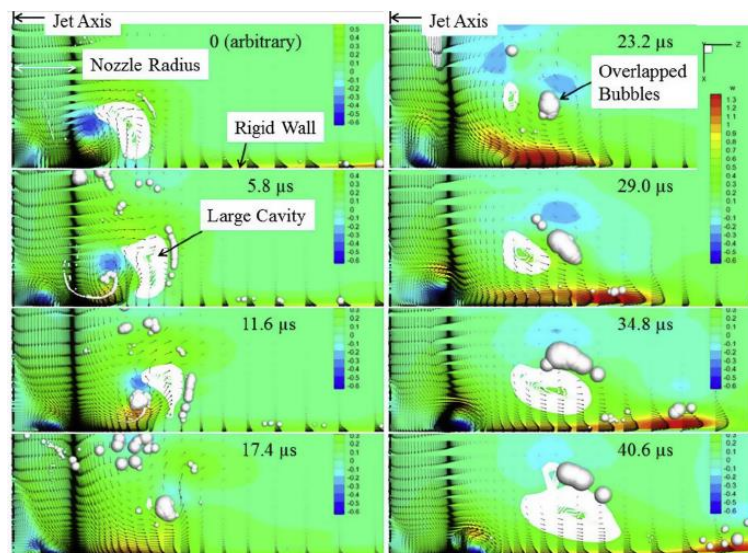
Figure 4.1: Example of cavitation bubbles being formed within the model [117]
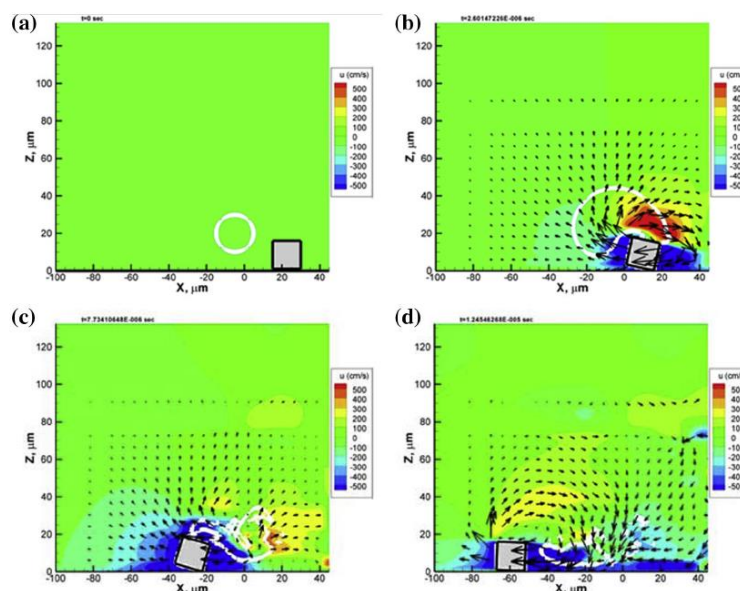
Figure 4.2: Images of model using pressure field to move a particle [117]

4.2.2   MATERIAL PITTING FROM BUBBLE COLLAPSE

FSI has been used to model the material pitting from bubble collapse [113]. The pitting in the material is formed when the pressure created from the bubble implosion is large enough to equal the stress exceeding the material yield stress. The bubble dynamics considered in this model included the following:

- Bubble size

- Maximum volume

- Bubble stand-off distance from material wall

- Pressure during bubble collapse

Another factor that results in material removal is due to fatigue of the material over time. The general numerical simulation begins with a spherical bubble at its maximum radius which is followed by collapsing as a response to high pressure; this method is valid for bubbles in a bulk liquid and does not work for cavitation generated near a wall.

4.2.3   PRESSURE DISTRIBUTION PREDICTION

There have been many attempts at modelling cavitation generation in several papers but the scope of the generation of bubbles was of a very small number of cavitation bubbles, as this generation is a very complex phenomenon to model [112]-[114]. Another approach to model ultrasonic cleaning is to map the pressure distribution and link this to the potential generation of cavitation by reaching the pressure threshold required for cavitation to be generated. Various papers have attempted to create this prediction method.

A study which modelled the prediction of ultrasonic cleaning was conducted by Lewis et al. [115] by linking the cavitation pressure threshold found from experimentation to the models pressure distribution results, to predict if cavitation will appear in the locations of pressure above the threshold within the model. The work stated that the minimum pressure required for cavitation to occur in water was 5 Bar [116], but this requires a pressure amplitude large enough to overcome the tensile strength bonds [117].

The model was meshed for wave propagation using the following equation:

$$l_e = \frac{\lambda_{min}}{20} \tag{4.1}$$

where l_e is the element length and λ_{min} is the wavelength of the maximum frequency propagated through the system.

The equation used for pressure through the medium is the wave equation:

$$\frac{1}{\rho c^2}\frac{\partial^2 p_t}{\partial t^2} + \nabla \cdot \left(-\frac{1}{\rho}(\nabla p_t - q_d) \right) = 0 \tag{4.2}$$

The pressure output (p) from the transducer as a timed harmonic is as follows:

$$p = p_0 e^{i\omega t} \tag{4.3}$$

The pressure variation from the transducer allows the wave equation to be approximated by the Helmholtz equation for time harmonic analysis [10]. The time stepping procedure to solve the model in a time-dependent study requires a minimum of 20 points per cycle, which results in the following time step size:

$$\Delta t = \frac{1}{20 f_{max}} \qquad (4.4)$$

The results of this model showed discrepancies; however, it gives the idea of modelling the prediction of cavitation rather than creating complex models to generate actual cavitation bubbles. By neglecting the generation of cavitation and instead focusing on the pressure distribution, this can be applied to the modelling of much larger structures, which would potentially create large numbers of cavitation bubbles which cannot be done simply in FEA.

Effective extensions of linear acoustics have been proposed in Caflisch *et al.* [118]. The effective equations have been applied [119] where they are most suitable for low amplitude waves or weakly nonlinear conditions [120]. Similar methods have been applied for waves of reasonable amplitude [121], [122] but their use is restricted for inertial cavitation due to the amplitude of waves ranging below the Blake threshold. Some attempts have been made to extend the Caflisch model with the purpose of simulating larger wave amplitudes; however, this is limited to small spatial regions [123].

4.2.4   MODELLING USING COMSOL

In recent years, the use of the COMSOL Multiphysics package has become popular for modelling cavitation bubbles and for mapping the pressure distribution [124]. COMSOL allows the incorporation of different physical effects related to cavitation generation and ultrasonic cleaning. The approach can be adopted to neglect the development of cavitation bubbles and focus solely on the pressure distribution, to assist in designing ultrasonic cleaning systems [124], [125].

COMSOL has also been used to generate a model based on the Caflisch model, producing reasonably good estimates of the acoustic pressure field and approximate cavitation zones [126], [127], [127]–[129]; however, these results have not been able to justify unfitting calculations.

From the various linear and non-linear modelling methods, the prediction of cavitation is a phenomenon which is not close to being solved numerically. However, FEA does provide insight into the potential wave propagation and can assist as a useful design tool, but this cannot completely avoid experimental investigation and validation.

Mettin *et al.* [130] investigated the modelling of a single acoustic cavitation bubble and its change over time using both COMSOL and an analytical method, resulting in a hybrid model to achieve the task. The model aimed to calculate the sound field and the cavitation bubble redistribution, which required modelling the acoustic wave propagation using a linearized bubble liquid wave equation, bubble motion by discrete particle approach and using Bjerknes forces using spatial pressure distribution of the sound field. As the model couples the wave propagation and bubble

redistribution, this complex interaction is decoupled for short time intervals to create a 2 step model for the bubble redistribution to be achieved.

2 step calculation:

1. Pressure distribution calculated using the linearized bubbly liquid wave equation. This is a linearized approximation of the bubble oscillations the modified Helmholtz equation.

This step keeps a fixed continuous bubble density function in space and uses FEM to solve the modified wave equations.

2. Nucleation, translation, rectified diffusion and merging/splitting of cavitation bubbles is calculated using the particle model approach, as this will represent the bubble motion trajectories.

This step keeps a fixed pressure field which has been calculated in step 1. Once calculating the new local speed of sound from the bubble density, this value is passed back to the FEM in step 1 to repeat the cycle once more. Steps 1 and 2 are repeated to model the movement and redistribution of cavitation bubbles over time.

This work achieved results that are comparable to the images of cavitation bubbles as shown in Figure 4.3; however, the models focused on a location where the authors knew a bubble would appear due to prior experiments.
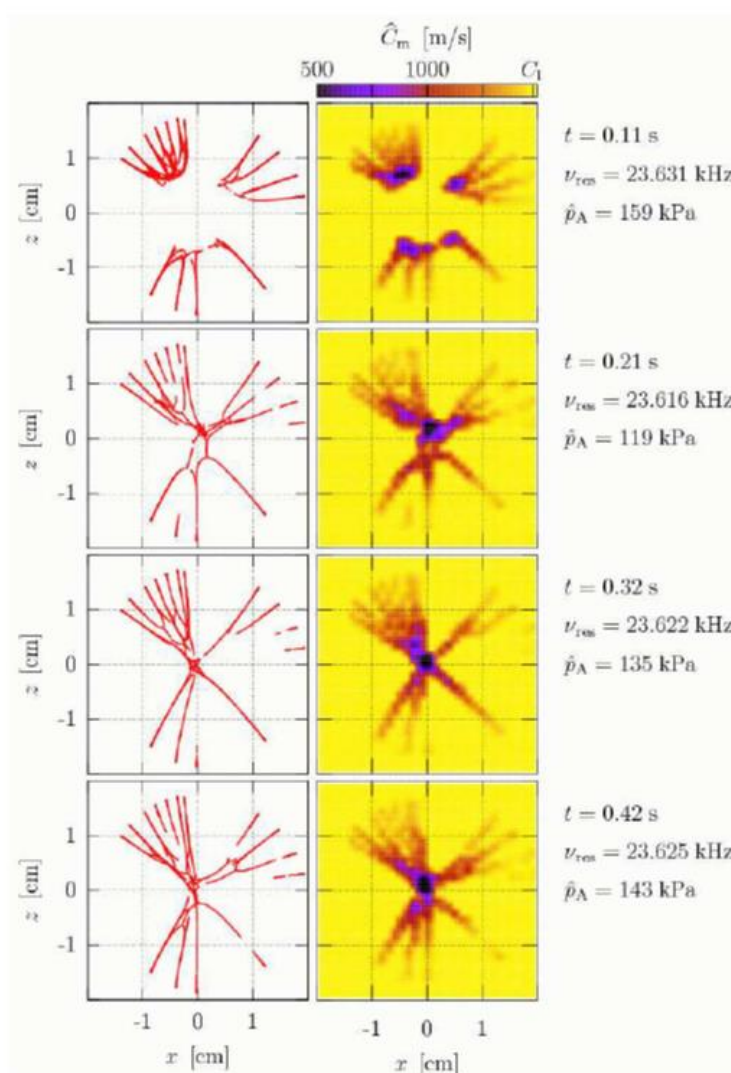
Figure 4.3: Cavitation redistribution plots from model [135]

As this a conference paper, there is no depth of analysis to fully explain how the model was created, and there is also a lack of full validation as the model displays the redistribution on a selected location and not on a bulk liquid full of cavitation bubbles. What is interesting from this paper is the application of Bjerknes forces which are associated with the fouling removal mechanisms created from cavitation generation.

Another paper discusses the link between OPENFOAM, an open source Computational Fluid Dynamics (CFD) program written in C++ and based on the Finite Volume Method (FVM), combined with COMSOL [131]. The numerical simulation aimed to model bubble interactions in 3 stages:

- Stage 1: in-phase (symmetric)
- Stage 2: out-of-phase (second bubble is introduced before first bubble reaches its maximum radius)

- Stage 3: anti-phase (second bubble is introduced when first bubble has reached its maximum radius)

The paper did produce bubbles within the modelling technique; however, this was not compared with experimental results and there were no in-depth steps into creating the numerical simulation.

The COMSOL package has also been used to assist in designing a sono-reactor by mapping the acoustic pressure [124]. The model made assumptions and neglected some variables for a relatively simple model to be created. The model aimed to identify locations in which cavitation would appear, which is linked to the pressure distribution. The model uses governing equations that are predefined in the relative physics in COMSOL. This includes PZT- linearized constitutive equations, linear elastic behaviour governed by Newton's second law, acoustic wave equation and equations to take into account the structure-acoustic interface.

The model was validated by using a hydrophone in an experimental set up to map the pressure and cavitation intensities of the sono-reactor under investigation. Figure 4.4 shows the locations of cavitation intensities to match with the pressure in those locations within the model to determine if the pressure value exceeds the cavitation threshold for cavitation to be assumed to be formed.
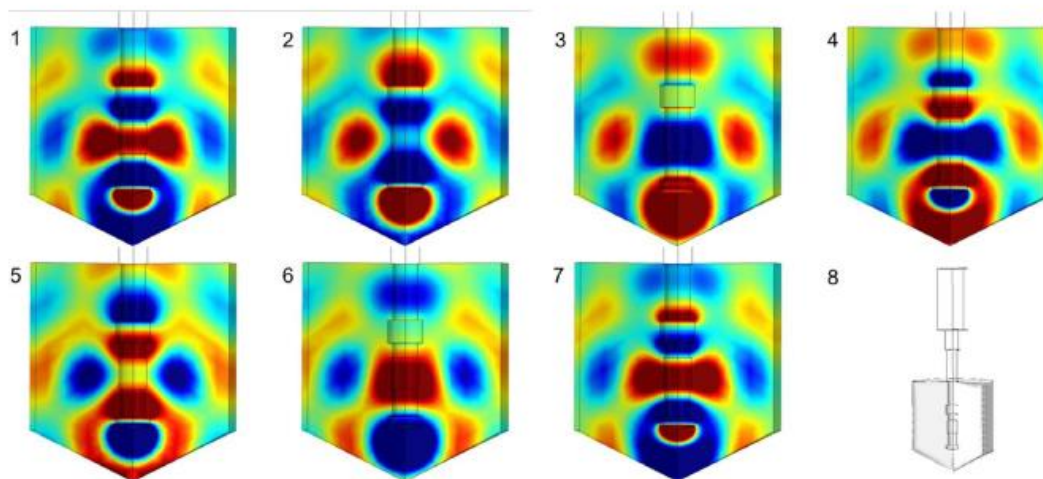
Figure 4.4: Simulation of acoustic pressure propagation in the proposed reactor configuration [124]

The model showed that, with the exclusion of cavitation, the model does not recreate the four fouling mechanisms which in fact, change the pressure distribution. The model is shown as a simplistic guide to design the sono-reactor to reach the pressure threshold required for cavitation to be achieved but does not model the actual cleaning or cavitation processes.

A simulation of ultrasonic energy in a cleaning tank also presented [125] to map the time varying pressure field due to the wave propagation. The model aimed to find the optimal ultrasonic energy

level and to allow the model to contribute towards designing future tanks. The COMSOL model uses governing equations for pressure acoustic module. This was carried out in the frequency domain to map pressure and displacement.

4.3   CAVITATION APPROXIMATION

The literature shows various methods to model the generation of cavitation. However, each method is limited to modelling a small number of cavitation bubbles due to the complexity of this phenomenon [112], [114], [130]. Another approach to model ultrasonic cleaning is to map the pressure distribution and correlate this to the potential for reaching the pressure threshold required for cavitation to be generated.

A study which modelled the prediction of ultrasonic cleaning was the previously discussed work conducted by Lewis *et al.* [115], which shows the potential to create a simplified model for predicting cleaning from the pressure distribution.

Although the initial pressure required for generating cavitation can be modelled, this neglects the effect from cavitation generation which can in fact change the pressure distribution across the fluid medium [132]. The equation used to calculate the dotted line in Figure 4.5 [117] is the spatial distribution of the pressure amplitude:

$$p_a(x) = \rho_L c v_0 \left| 2 \sin\left(\frac{\pi}{\lambda}\sqrt{x^2 + a^2} - x\right)\right| \qquad (4.5)$$

where $p_a(x)$ is the acoustic pressure amplitude at position x, x is the distance from the circular piston to the symmetry axis, ρ_L is the liquid density, c is the sound velocity in the liquid, v_0 is the velocity amplitude of the horn tip, λ is the wavelength of ultrasound within the liquid, a is the radius of the circular piston.

Yasui *et al.* [132] discusses the change in acoustic amplitude when cavitation is being generated to be a third of the pressure produced in a fluid medium with no cavitation. When applying this ratio to an FEA model which neglects cavitation generation, the pressure distribution will over estimate values to be 3 times larger.

 Moholkar *et al.* [133] stated a minimum of 5 Bar to generate cavitation but as this model neglected cavitation, they also did not consider that the presence of cavitation will affect the pressure distribution. Also, the minimum pressure required to generate cavitation is uncertain as the recent
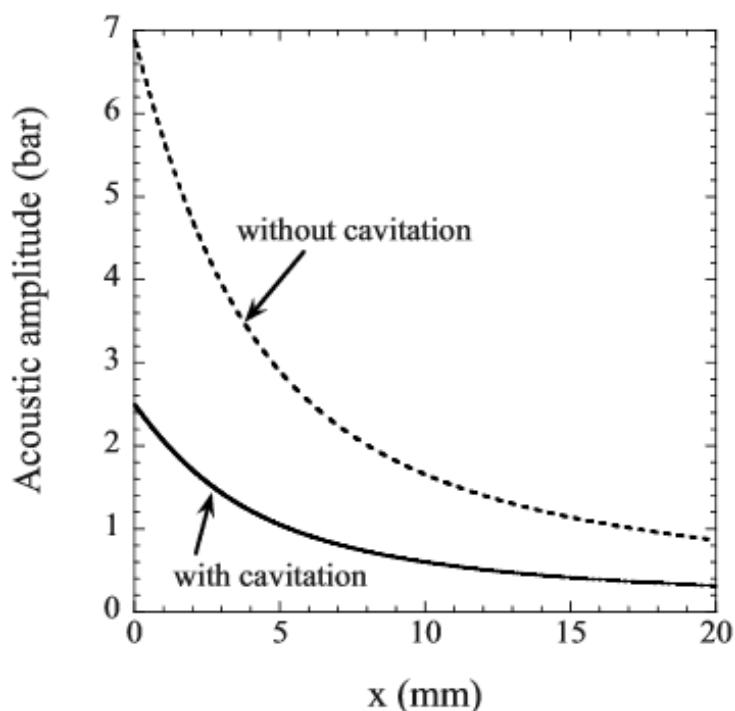
Figure 4.5: Calculated acoustic amplitude under an ultrasonic horn as a function of the distance from the horn tip on the symmetry axis. The dotted curve is the calculated result by equation (4.5). The solid curve is the estimated one by the comparison of the numerical simulation and the experimental observation [121]

work by Yasui [66] stated that a 40 kHz resonant transducer required approximately 1-2 Bar of pressure as the minimum cavitation threshold.

The generation of cavitation within a fluid reduces the pressure amplitude within the acoustic field, attenuating the acoustic wave into the surrounding liquid [134]. Due to the ultrasonic wave being applied onto the wall of a structure, this vibrates the wall due to the pressure oscillation. The strong vibration of the wall radiates strong acoustic waves. The acoustic field depends on the material of the wall and the attenuation coefficient of the ultrasound (which increases with the addition of cavitation bubbles). The increase in attenuation decreases the wall vibration. Another effect on the acoustic field which requires further research is the degassing of bubbles within the fluid [134].

Yasui *et al.* [135] describe the importance of coupling the radiation of the reactors wall within the sonochemical reactor. They have described previous work where the vibration of the wall has been neglected in several pieces of research; however, they also discussed previous research papers that have included the effects of the vibration of the wall by coupling this interface with the fluid domain but neglected the effects of cavitation bubbles within the sonochemical reactor. Yasui *et al.* [132] implemented numerical simulations which couple the vibration of the wall of the sonochemical reactor but also take cavitation bubbles into account by changing the attenuation

coefficient of the model, due to the relationship between attenuation and cavitation bubbles. Cavitation bubbles not only affect the attenuation on the vibration wall but also the speed of sound within the fluid domain, but this effect was neglected in Yasui *et al.* [132] and the speed of sound of the liquid was kept constant.

4.4   ULTRASONIC CLEANING FINITE ELEMENT METHOD

Using the HPUT model created in Chapter 3, the modelled pipe specimen is a stainless steel 315L pipe which is 300 mm in length, 1.5 mm in wall thickness and 50.08 mm in outer diameter. The HPUT is modified with a concave contact surface and attached at the mid-length of the pipe. The model assumes two lines of symmetry as shown in Figure 4.6. A single quadrant of the pipe is modelled to reduce the computation size.
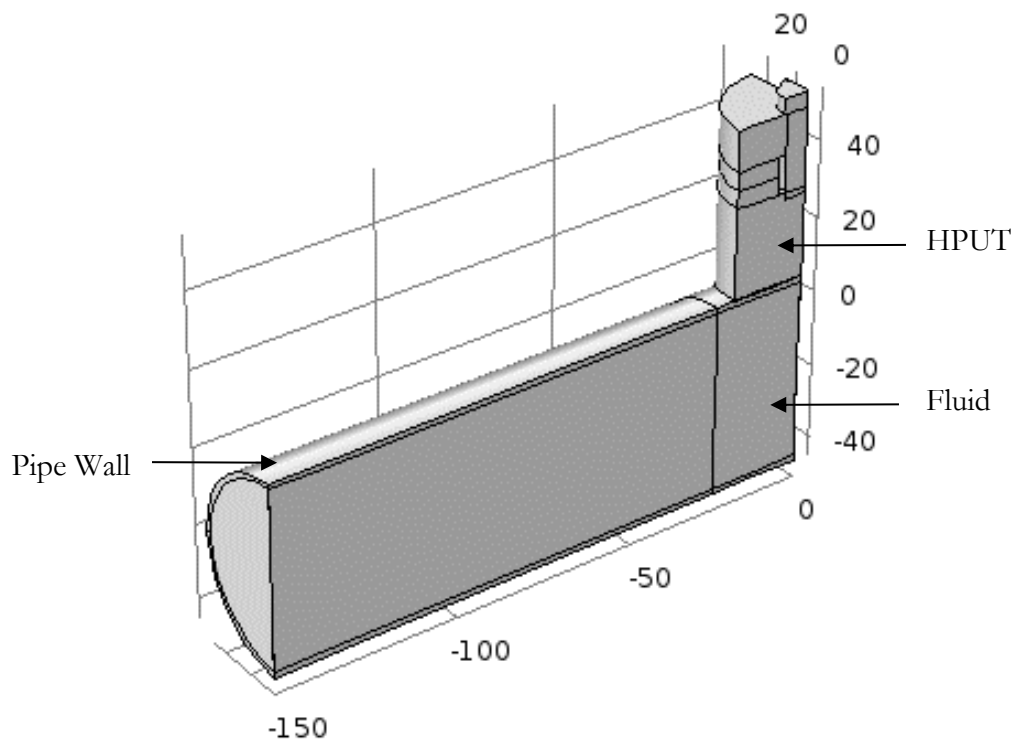
Figure 4.6: geometry of FE model displaying cut planes at lines of symmetry for computation efficiency

Physics are assigned within the FE model to account for the HPUT, solid pipe and fluid domain within the pipe. The fluid surrounding the outer pipe is considered to be atmospheric air, which is not modelled, instead, the walls in contact with the air are assumed as 'free'. The assigned physics are listed below:

- Pressure Acoustics, Transient – fluid domain

- Electrostatics – piezoelectric ceramic components of the HPUT

- Solid Mechanics – elastic components of the HPUT and pipe

- Piezoelectric Effect – coupling of the piezoelectric components with elastic components

- Acoustic-Structure Boundary – coupling of the interface between the inner pipe wall and fluid domain

The Pressure Acoustics model uses the wave equation:

$$\frac{1}{c^2}\frac{\partial^2 p_a}{\partial t^2} + \nabla^2 p_a = 0 \tag{4.6}$$

where p_a is the acoustic pressure and c is the speed of sound in the liquid, which is assumed constant.

The linear elastic behaviour is used for the solid parts of the model. All solid parts excluding the piezoelectric ceramic rings will obey their material properties and are considered to be of linear elastic material. The application of Newton's law yields the following equation:

$$\rho_S \frac{\partial^2 u}{\partial t^2} = \nabla . \overline{\overline{\mathbf{T}}} \tag{4.7}$$

where u is the solid displacement field, $\overline{\overline{\mathbf{T}}}$ is the stress tensor, and ρ_S is the density of the solid.

The terminal is selected to voltage where V0 can be written as a single value in volts or be written as a function of time which define a function created by using the modulation function. The ground boundary assumes V= 0 on this surface. V_0 is the modulating 40 kHz, 500 Vpk-pk sinusoidal waveform.

Multiphysics modules are assigned to couple the pressure acoustics and solid mechanics physics across the acoustic-structure interface between the fluid and solid domains. This allows the radiation of the wall due to transducer excitation to be taken into account and create high and low pressures to propagate into the fluid domain [135]. For this reason, COMSOL is used to incorporate the required physics to simulate the experimental configuration.

In experimental conditions, the coupling of the HPUT contact surface to the pipe surface is done by applying acoustic couplant gel between the contact surface of the HPUT and pipe to remove any air bubbles which can affect the ultrasonication performance. The COMSOL model mimics this attachment by using integration along the boundary between the HPUTs contact surface and the pipe surface. A fixed constraint is placed on the top of the HPUT and the HPUT holder is ignored within the model. As this model neglects the presence of cavitation bubbles, the resulting

attenuation and acoustic radiation effects are not considered [134]; however, some attenuation has been applied to his model by altering the bulk viscosity of the fluid domain.

The effects of decreased radiation from the presence of cavitation [132] have not been taken into account in the model methodology, as this model does not consider the effects of cavitation which decreases the sound velocity and acoustic field.

The model is meshed using equation 3.13 as *Free Tetrahedral* elements for a high density around the transducer location, while the remainder of the geometry is swept as follows:

$$sweep\ density = \frac{2800mm}{h_o} \tag{4.9}$$

The selected study for this model is *Transient*, so that the simulation can generate results as the modulated wave propagates from the HPUT.

The increments are based on the maximum allowed mesh size. The time steps are chosen to resolve the wave equally over time whilst the meshing is placed to resolve the wave propagation over the model itself. Time steps must be optimiSed relative to the mesh, and this is supported with the relationship between mesh size h_0 and observation time step (Δt):

$$t_x = \frac{c\Delta t}{h_o} \tag{4.10}$$

The t_x ratio is given as 0.2 as this value is suggested to be near optimal [108]. By rearranging equation (4.10), the time steps are calculated using equation (4.11):

$$\Delta t = \frac{t_x h_o}{v_{gr}} = \frac{0.2 h_o}{v_{gr}} \tag{4.11}$$

The simulation duration is selected based on the time of arrival, which is calculated using the group velocity of the longitudinal mode found for the 6 inch schedule 40 carbon steel seamless tube with 168 mm outer diameter, 7.11 mm wall thickness (see Figure 4.6). The Time of Arrival can be calculated as follows:

$$T_l = \frac{x}{c_l} \tag{4.12}$$

Where T_l is the time of arrival of the longitudinal mode, x is the distance between the HPUT location and the end of the pipe, and c_l is the group velocity of the longitudinal wave mode at the excitation frequency.

4.4.1   FEA RESULTS

The total displacement is shown on the outer (see Figure 4.7) and inner pipe wall (see Figure 4.8). This shows the propagation of the HPUT vibration resulting in high amplitudes of displacement

around the circumference of the pipe. When comparing the displacement patterns, there is a reduction of propagation distance achieved at the same time instant on the inner pipe wall. This can be due to the pipe wall thickness attenuating the vibration delivery through the structure.

The total acoustic pressure on the outer wall of the pipe is shown in Figure 4.9 for the same time instant as in Figure 4.7 and 4.8. As stated previously, a minimum of 1-2 Bar must be applied by the HPUT to create acoustic cavitation [66]. The results show the surface of the HPUT to have achieved a pressure value above 4 Bar, thus meeting the requirement for producing acoustic cavitation at the HPUT attachment location. There is a pressure drop across the circumference but is achieving 1-2 Bar of pressure in a similar location to the displacement patterns shown in Figure 4.7.
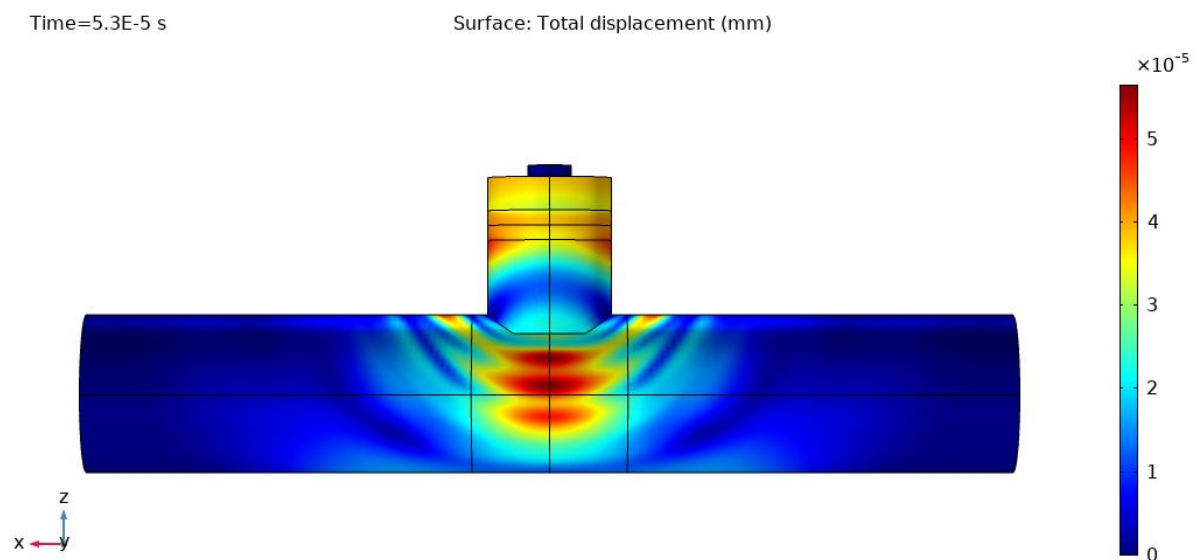
Figure 4.7: Outer pipe wall solid displacement
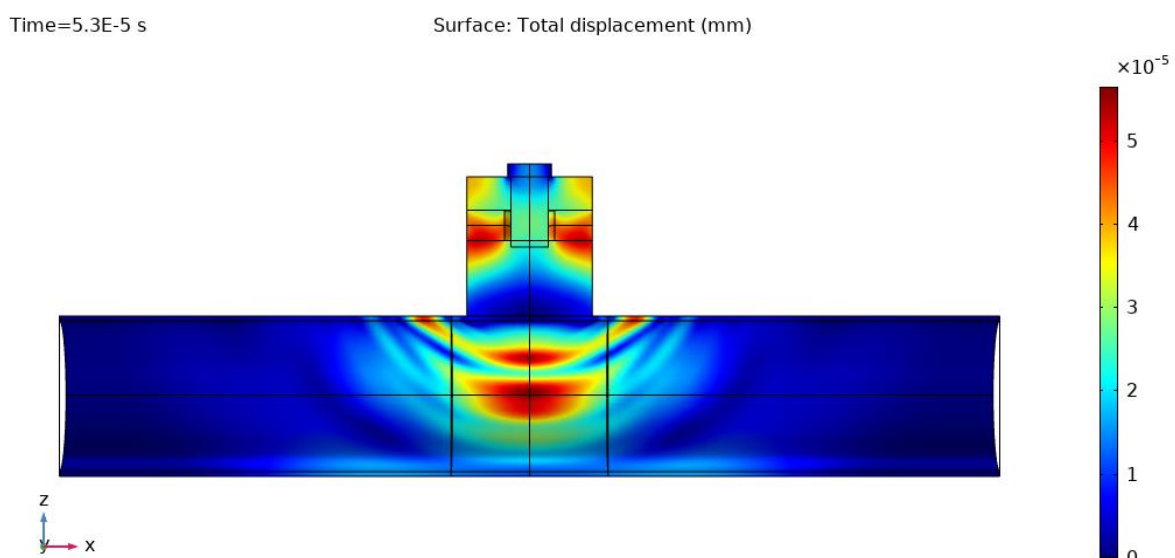
Figure 4.8: Inner pipe wall solid displacement

A cross-section view of the pipe in Figure 4.10 shows the isosurface of the total acoustic pressure of the fluid domain. The HPUT location shows a pressure above 4 Bar which assumes that a compressional instant of high pressure wave is being produced. As this travels through the liquid, a pressure drop to 4 Bar is shown which represents a rarefaction instant where cavitation bubbles appear. This shows a high intensity of pressure at the centre of the liquid and suggests that the HPUT vibration is delivering the minimum required pressure into the liquid.
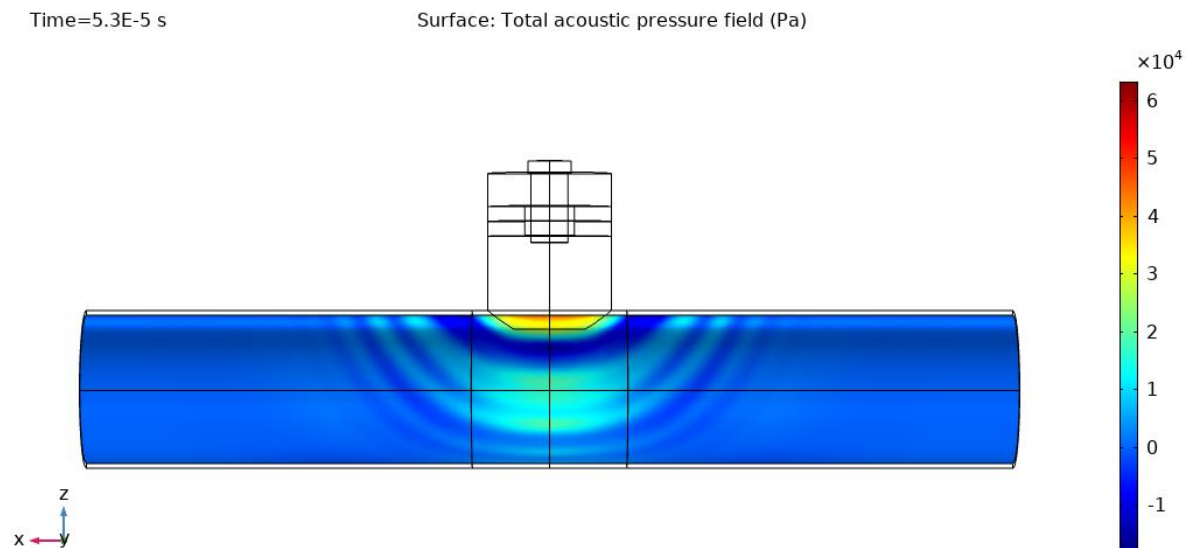
Figure 4.9: Total acoustic pressure of fluid at pipe wall
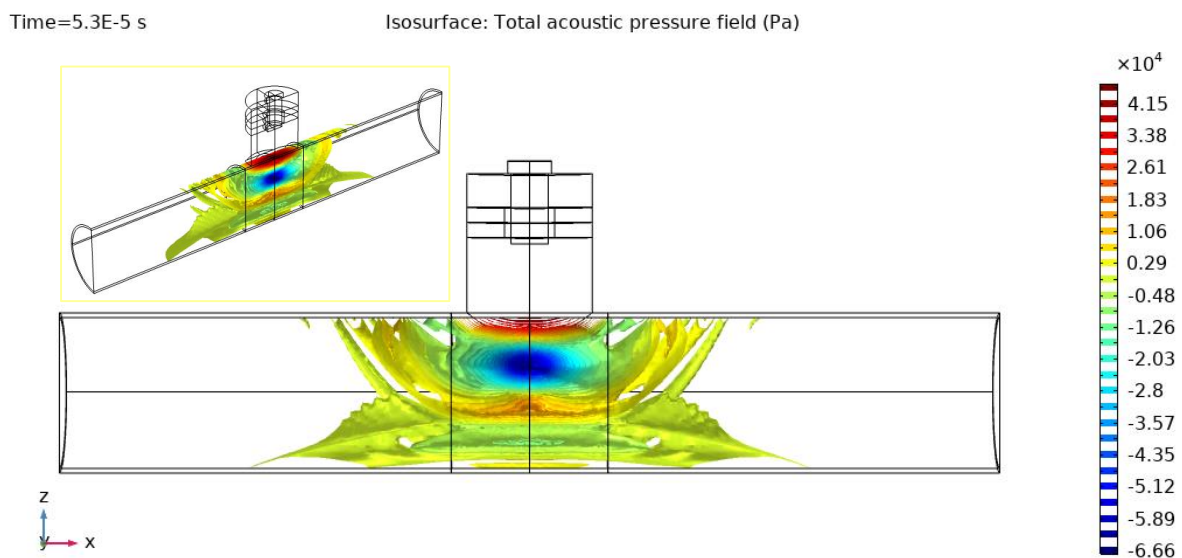
Figure 4.10: Cross-section of fluid displaying isosurface of total acoustic pressure

The simulated results are converted to FFT spectrum for further analysis of the vibration across the frequency spectrum. A single point is selected on the outer wall of the pipe to display the

average out-of-plane velocity (see Figure 4.11). This shows the resonating frequency to be approximately 40 kHz, similar to the excitation frequency applied to the HPUT.
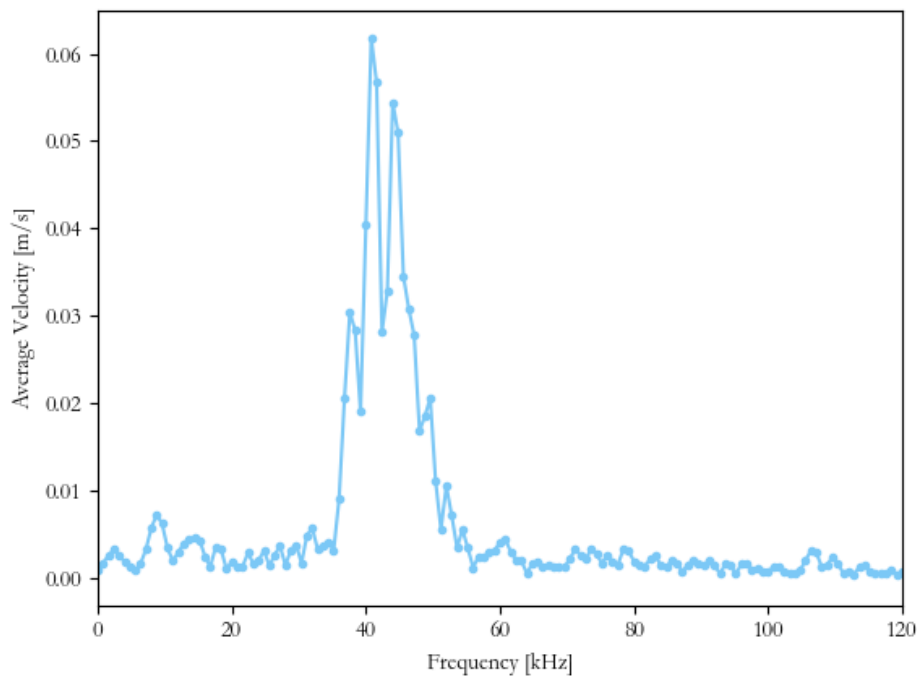
Figure 4.11: FFT of numerical results obtained from single point on outer pipe surface, displaying the average velocity

4.5 SUMMARY

This chapter presented an FEA methodology which models ultrasonic cleaning patterns based on outer wall displacement and acoustic pressure within the fluid as the acoustic pressure reaches past the cavitation threshold [117]. This is a simplified model which neglects the generation of cavitation and gives a baseline reference when designing and optimising the HPUT for cleaning on different structures, while minimising the time and costs from optimisation through purely experimental means. The FE model has shown an example of a single HPUT attached to a 2 inch diameter pipe, displaying the cavitation threshold to be achieved locally at the HPUT location and along the circumference. This model requires validation of the predicted cleaning patterns as a result of the pressure fields and displacement.

Chapter 5: Fouling Generation and Fouling Detection Methodology

Research is creating new knowledge – Neil Armstrong

5.1 INTRODUCTION

Chapter 4 presents the development of an ultrasonic cleaning FE model, this requires comparison with a fouled pipe specimen undergoing ultrasonic fouling removal in laboratory conditions. This chapter investigates the development of calcite, a known crystallisation fouling, commonly found in pipelines carrying high-temperature fluid. Smaller samples are investigated using the electrochemistry approach by immersion into a vessel filled with a calcium carbonate solution. Due to geometrical limitations, to generate fouling on the inner wall of the schedule 40, 6 inch diameter carbon steel pipe specimen, a new method must be investigated to up-scale a crystallisation fouling generation technique onto larger diameter, larger length pipelines.

5.2 CRYSTALLISATION GENERATION: ELECTROCHEMISTRY

Calcite is formed from a calcium carbonate solution, obtained by adding calcium chloride and sodium hydrogen carbonate in equal amounts to deionised water. Each chemical reacts to the water as follows:

Calcium chloride:

$$CaCl_2 \xrightarrow{water} Ca^{2+} + 2Cl^- \tag{5.1}$$

Sodium hydrogen carbonate:

$$NaHCO_3 \xrightarrow{water} Na^+ + HCO_3^- \tag{5.2}$$
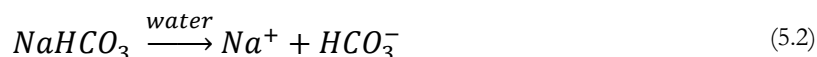
The components from (5.1) and (5.2) that are important from these reactions in the creation of calcium carbonate are:

$$Ca^{2+} \text{ and } HCO_3^- \tag{5.3}$$

The calcium carbonate solution has the potential to form calcite in the mixture; however, to ensure that calcite formation occurs, two key electrochemical reactions known as electrolysis are needed to produce calcite in this method of fouling creation.

One of the electrolysis reactions is known as hydrolysis, and is the breakdown of water molecules through a potential energy as follows:

$$H_2O \xrightarrow{{}^oE} \frac{1}{2}H_{2(gas)} + OH^- \tag{5.4}$$
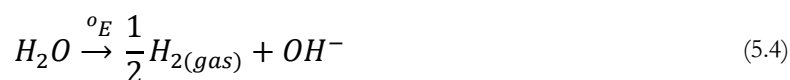
The breakdown of water molecules will increase the concentration of OH^- (5.4) on the surface of the sample. Another electrolysis reaction that takes place is due to the air supplier which is used to supply oxygen to the solution. As there is water in the solution already, the added oxygen will result in the following:

$$\frac{1}{2}O_2 + H_2O \xrightarrow{^oE} 2OH^-$$ (5.5)

As it can be seen in (5.5) that the electrolysis reaction to the air supplier also increases the OH^- concentration, this will therefore increase the pH in the middle of the sample, which will allow the chemical reaction for fouling creation to happen faster and result in fouling to be produced and attach to the inner walls of the sample in less time.

The important factor resulting from the reactions in equations (5.4) and (5.5) is the OH^- production. The reason why the increase of OH^- will increase the reaction for fouling creation is due to the requirement of OH^- to form calcite in the solution with the reactants (5.3) as shown:

$$Ca^{2+} + HCO_3^- + OH^- \rightarrow CaCO_{3(solid)} + H_2O$$ (5.6)
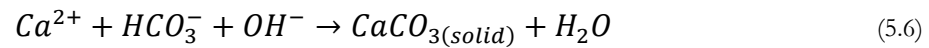
By taking the key components from the calcium carbonate solution (5.3) and adding OH^-, which is produced from electrolysis in (5.4) and (5.5), a solid known as calcite will then form on the inner walls of the sample.

5.2.1 METHODOLOGY

The equipment required for the creation of fouling is listed below and shown in Figure 5.1:

- Glass vessel: to hold 20 litres of solution
- Magnetic stirrer and hotplate
- Air supplier
- Diffuser
- Condenser
- Salt bridge: reference electrode
- Potentiostat
- Multimeter
- Sample pipe: working electrode
- Copper wire: counter electrode
- Calcium carbonate solution
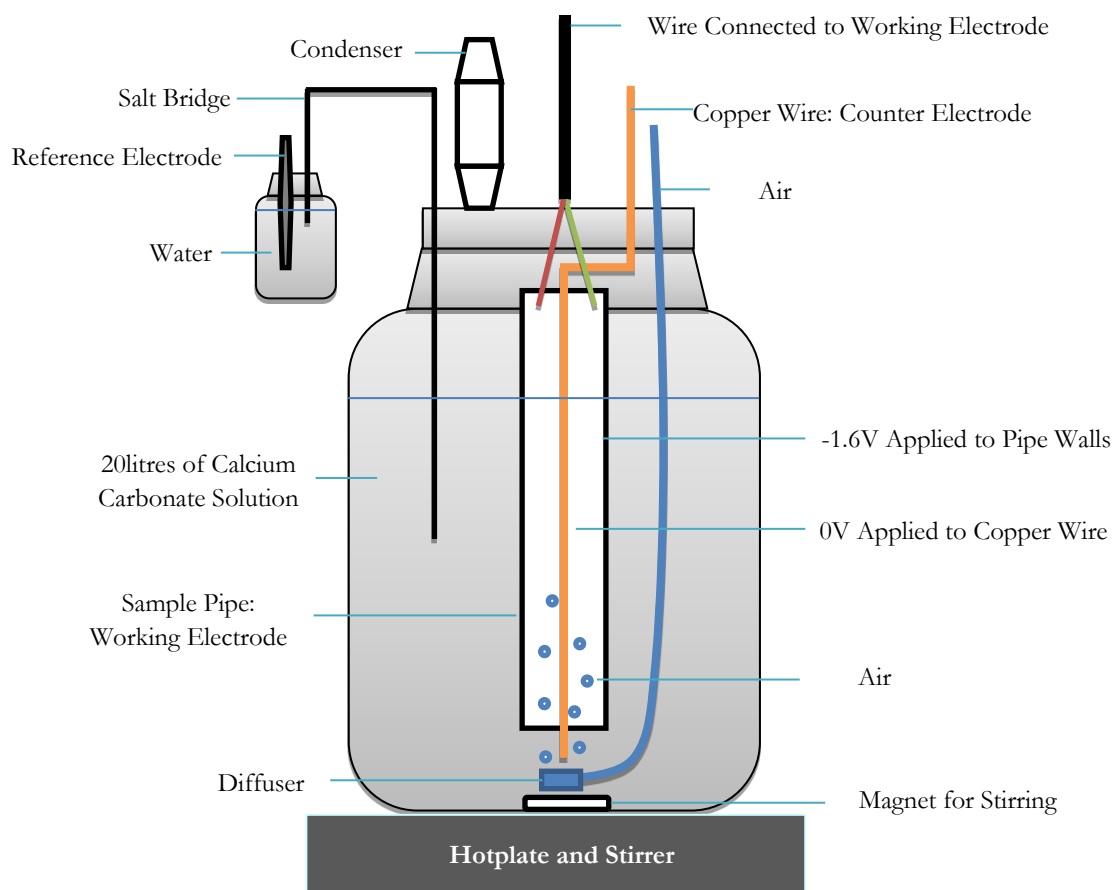
Figure 5.1: Diagram of fouling creation of calcite using electrochemical set-up

Calcium carbonate is a chemical compound which can exist in different allotropic forms in the solution such as calcite, aragonite and vaterite. Each solid is formed if certain conditions are met; as calcite is the desired fouling in this case, the following conditions must be met:

- Temperature of solution: 40-50°C
- Voltage applied to working electrode: -1.6V

The sample pipe is prepared for fouling creation by protecting the outer walls using a black film to ensure that fouling is only created on inner walls. This is suspended into the calcium carbonate solution as shown in Figure 5.2. Wires are attached to the pipe to make this the working electrode; a negative voltage will be applied to this. A copper wire is placed through the centre of the sample whilst ensuring that there is no contact with the working electrode, as this would short circuit the set-up and not allow a voltage distribution across the entire sample. This wire will have a potential applied and is known as the counter electrode. A multimeter is used to measure the voltage applied to the working electrode to ensure that voltage conditions are met for the formation of calcite on the inner pipe walls.
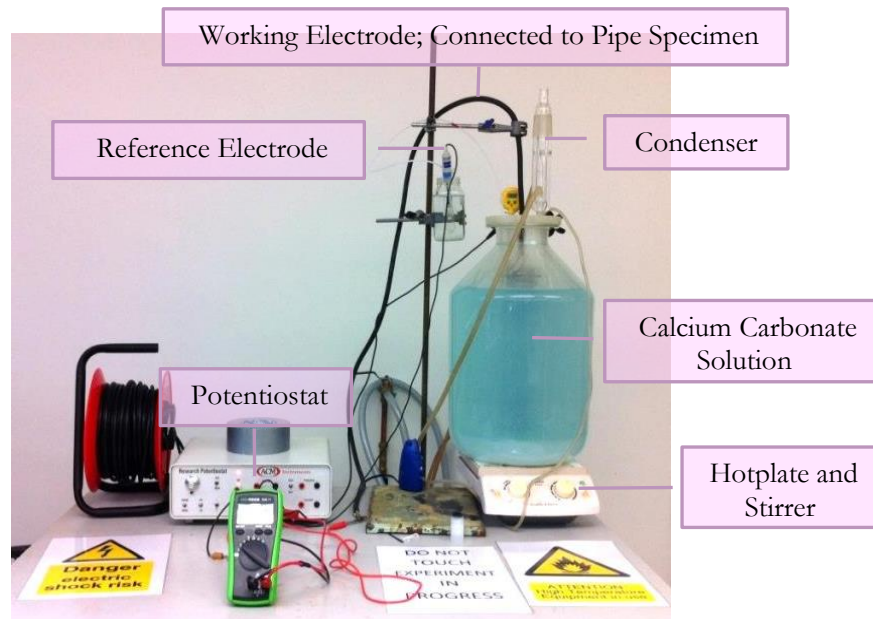
Figure 5.2: Preparation of fouled sample (Calcite) in laboratory conditions, illustrating the fundamental equipment used to generate electrochemical reactions. This sample is used for experimental validation.

During the process of fouling creation, the calcium carbonate solution is cloudy after being mixed and added to the glass jar, but once calcite is formed within the solution the copper will start to lose electrons and decompose, resulting in a blue colour in the solution as seen in Figure 5.2. The calcite will later attach onto the inner pipe walls. An example of this is shown in Figure 5.3, displaying a pipe with Calcite and corrosion fouling attached on the inner wall of the pipe.

Figure 5.3: Example of pipe with Calcite and corrosion fouling attached to inner wall

5.3 CRYSTALLISATION GENERATION: SPRAY DEPOSITION

As the electrochemical set-up is only suitable for short pipe samples, another method of fouling creation must be carried out that is suitable for long pipe samples. One method previously discussed [136] is spray deposition on heated plates. This is done by heating a plate and spraying a calcium carbonate solution onto its surface, resulting in the sprayed solution dissolving into a solid onto the plate. By heating the plate, the solution can precipitate.

The method to create fouling in long pipes is shown by using heating mats to heat the pipe before introducing the solution. The pipe must reach 120 °C to allow the solution to boil when reaching the pipe walls. The solution has a higher concentration of calcium carbonate of 6g/litre, to require less additions of solution to the pipe during the experiment.

5.3.1 FOULING GENERATION TRIALS

Prior to creating fouling on longer pipes, trials were carried out on shorter pipes to validate a suitable method to up-scale to a larger diameter, longer pipe. A summary of the findings from each trialled heating method is shown in Figure 5.4.

Emulsification — Pipe filled with calcium carbonate solution, heating element immersed in liquid
- Did not heat liquid fast enough
- Did not reach 100 °C
- Corrosion formed

Rubber Element — Pipe filled with calcium carbonate solution, rubber element wrapped around outer pipe wall
- Did not heat pipe fast enough
  Did not maintain 120 °C once solution is added
  Corrosion formed with some crystallisation

Heating Mat (Vertical) — Pipe filled with calcium carbonate solution, heating mat wrapped around outer pipe wall
- Reached 120 °C
- Temperature did not drop due to addition of liquid
- Water remained at the bottom of the pipe, producing corrosion and crystallisation

Heating Mat (Horizontal) — Heating mat wrapped around outer pipe wall, small amout of calcium carbonate solution is poured into pipe and rotated
- Reached 120 °C
- Fast saturation of liquid due to small amounts of fluid being poured onto the pipe wall
- Crystallisation fouling is produced with minimal corrosion fouling in sight

Figure 5.4: Heat deposition methods trialed for generating calcite on inner pipe wall

From the different heating methods (as shown in Figure 5.5), the heating mat in the horizontal configuration was selected for carrying out fouling generation on longer pipe samples. The initial set-up was done by placing the pipe horizontally which is wrapped by a heating mat. Small amounts of calcium carbonate solution is poured into the pipe whilst rotating the pipe manually. The heating unit and mats allow the solution to dissolve instantly compared to filling a pipe specimen with the solution. As small amounts of calcium carbonate are poured into the pipe, this allows it to dissolve instantly.

(a)　　　　　　**(b)**　　　　　　**(c)**　　　　　　　　**(d)**
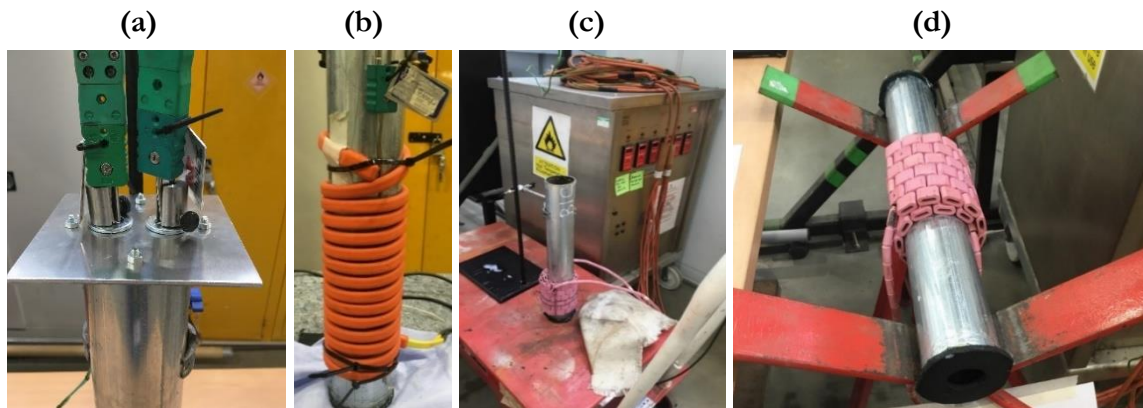
Figure 5.5: (a) emulsification, (b) rubber element, (c) vertical heating mat and (d) horizontal heating mat set-ups

5.3.2　SPRAY DEPOSITION FOR LARGER PIPELINE SAMPLES

Using the selected method, fouling was generated on the inner wall of a 6.2 m long, Schedule 40, 6 inch diameter, carbon steel pipe by heating the outer wall of the pipe up to 120 °C whilst spraying a highly concentrated calcium carbonate solution on the inner wall as illustrated in Figure 5.6. A Cooper heating system [137] was used to heat four heating mats wrapped around the pipe, and further wrapped with carbon fibre insulation as shown in Figure 5.6. Three thermocouples were placed between each mat to monitor the temperature and to allow the Cooper heating system to reach and maintain the target temperature. The highly concentrated mixture was placed into a manual pressure sprayer connected to a 3.2-m telescopic pressure sprayer lance.
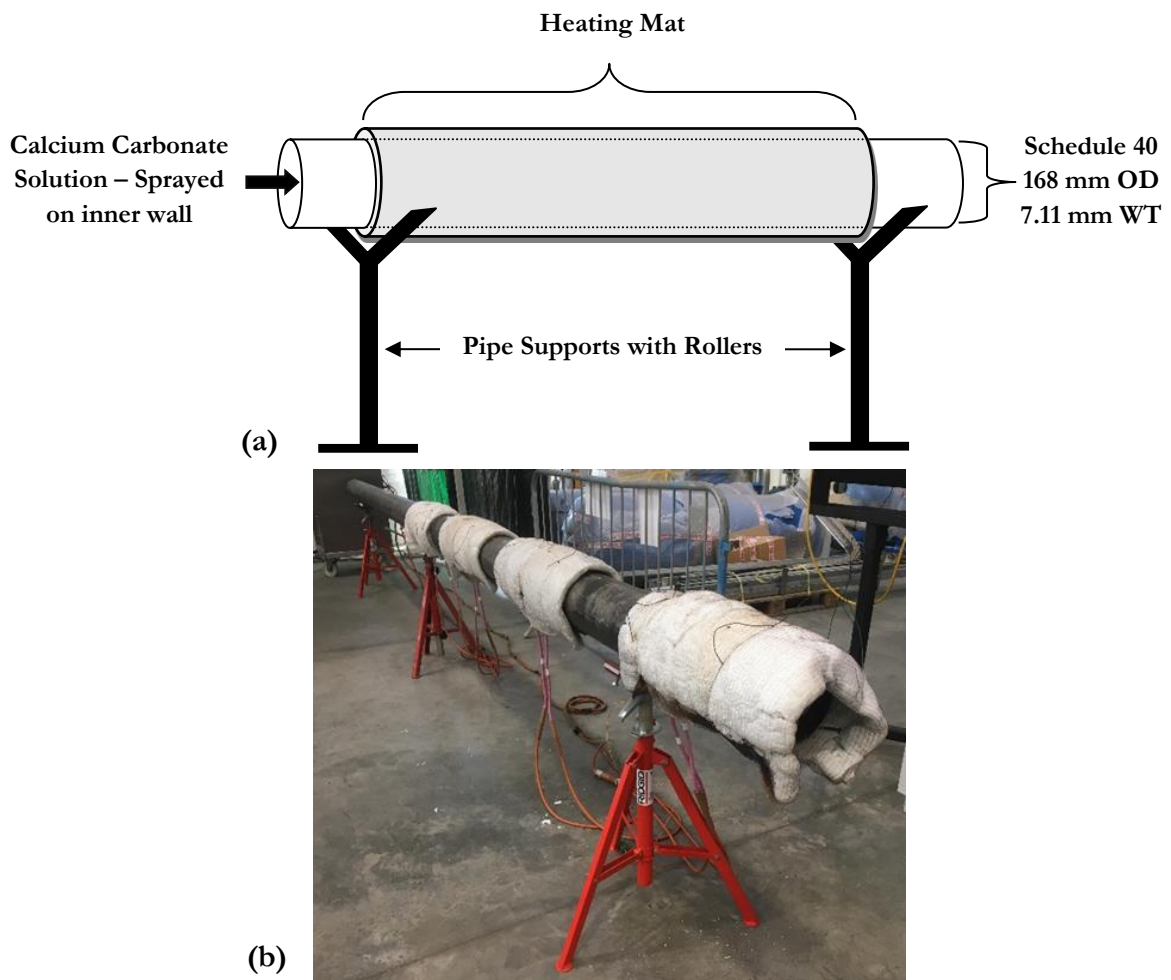
Figure 5.6: Fouling generation of 6.2 m long, Schedule 40, 6 inch diameter, carbon steel pipe (a) schematic and (b) experimental set-up.

Figure 5.7 displays the inner pipe wall before undergoing fouling and shows the successful generation of hard-scale fouling. There is some corrosion on the inner walls. The fouling generation is carried out and achieves a layer of Calcite on the inner pipe wall. After creating a layer of fouling on the inner pipe wall, the UGW Teletest collars were placed at their original locations to collect further data for analysis.
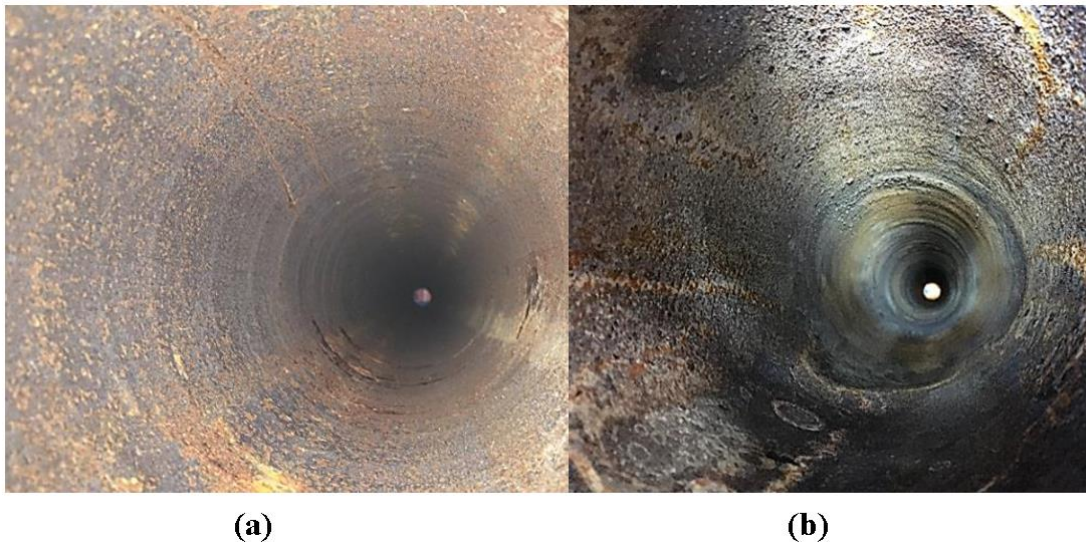
Figure 5.7: Image of the inner wall of the 6.2 m long, Schedule 40, 6 inch diameter, carbon steel pipe (a) displaying some corrosion before commencing fouling generation procedure and (b) after generating a layer of Calcite.

5.4   FOULING DETECTION USING UGW

Laboratory experiments were conducted to investigate the UGW propagation within a 6.2-m long, schedule 40, 6 inch diameter, carbon steel pipe. This study was conducted to characterise the change in UGW propagation as an effect of the presence of fouling within the pipe wall. Two Teletest® UGW collars were used to collect data in pitch-catch configuration to ease the data interpretation. Each collar consists of 24 transducers evenly spaced around the circumference of the 6-inch schedule 40 carbon steel pipe. The transmission collar is placed 1 m away from the pipe end and the receiving collar is placed 4 m away from the transmission collar as shown in Figure 5.8. A tool lead is connected to both collars to synchronize the data collection. The data is collected using the Teletest® software in time-domain for each transducer per collar and is exported for further analysis. Baseline data was collected from the clean pipe before generating hard-scale fouling on the inner wall of the pipe. Data collection is implemented by transmitting a torsional mode or a longitudinal mode wave from the transmission collar and monitoring the transmitted signal at the receiving collar. The data collection was performed over a frequency range of 30–80 kHz in 1 kHz increments. This is due to the frequency having an effect on the length of the discrete excitation pulse which results in a shift in the time-of-arrival. Furthermore, different numbers of cycles for the input signal were also considered to state the optimum number to use in order to detect fouling with higher sensitivity.
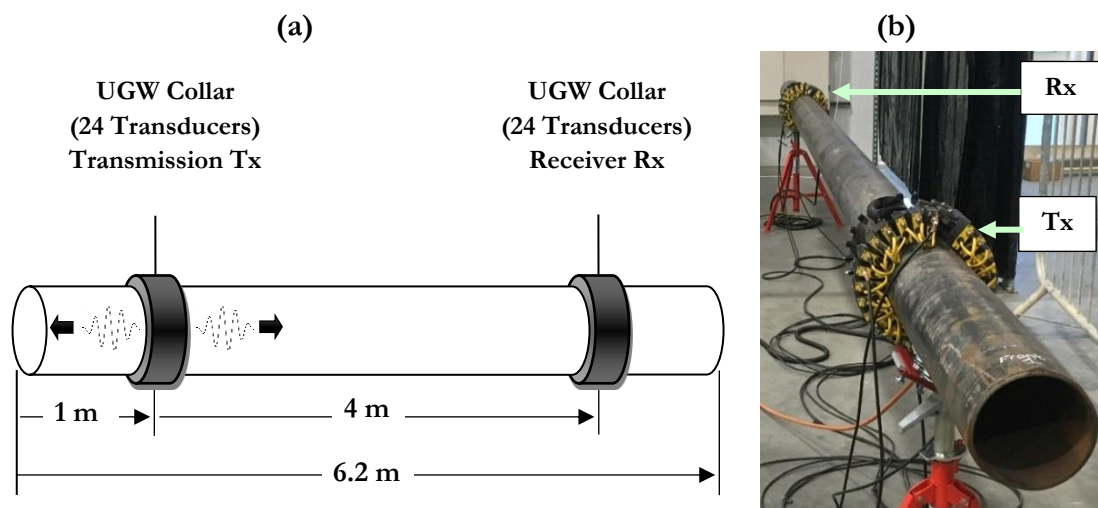
Figure 5.8: (a) Schematic and (b) set-up of the UGW collar arrangement for the current investigation on a 6.2 m long, Schedule 40, 6 inch diameter, carbon steel pipe for data collection using pitch-catch configuration.

5.4.1 FOULING DETECTION RESULTS

The laboratory experiment was conducted over a frequency range of 30–80 kHz for 5, 10 and 15 cycles. This is displayed in Figure 5.9. The longitudinal wave mode generates higher amplitude compared to the torsional wave mode; however, the longitudinal wave mode is more dispersive, especially with an increase in the number of cycles.

Figure 5.10 shows the torsional wave mode to have a lower amplitude but is less dispersive. For both wave modes, the signal amplitude is higher at lower frequencies, therefore the frequency range above 50 kHz is neglected for future analysis.
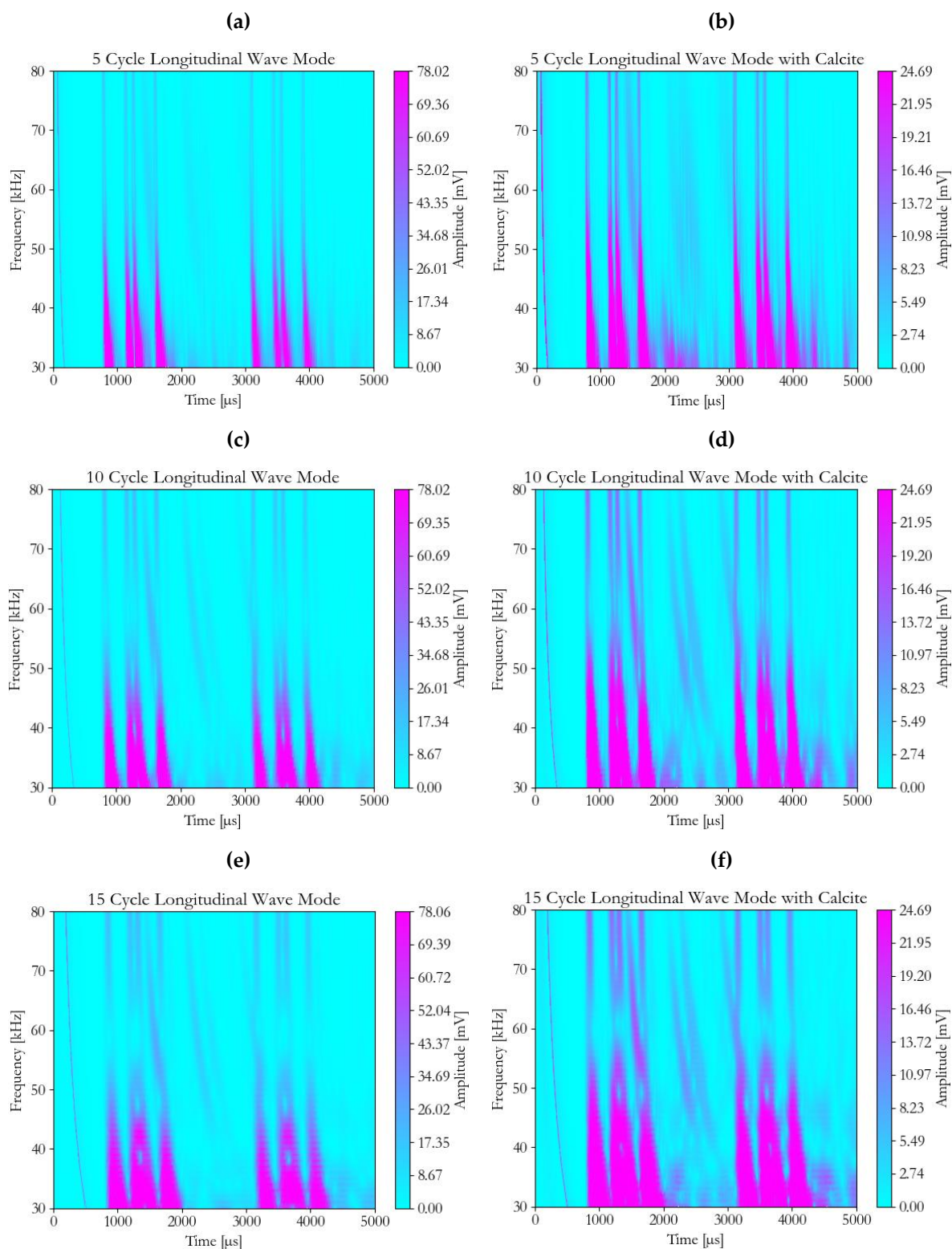
Figure 5.9: Longitudinal pitch-catch data for 5 cycle input (a) baseline and (b) calcite, 10 cycle input (c) baseline and (d) calcite and 15 cycle input (e) baseline and (f) calcite
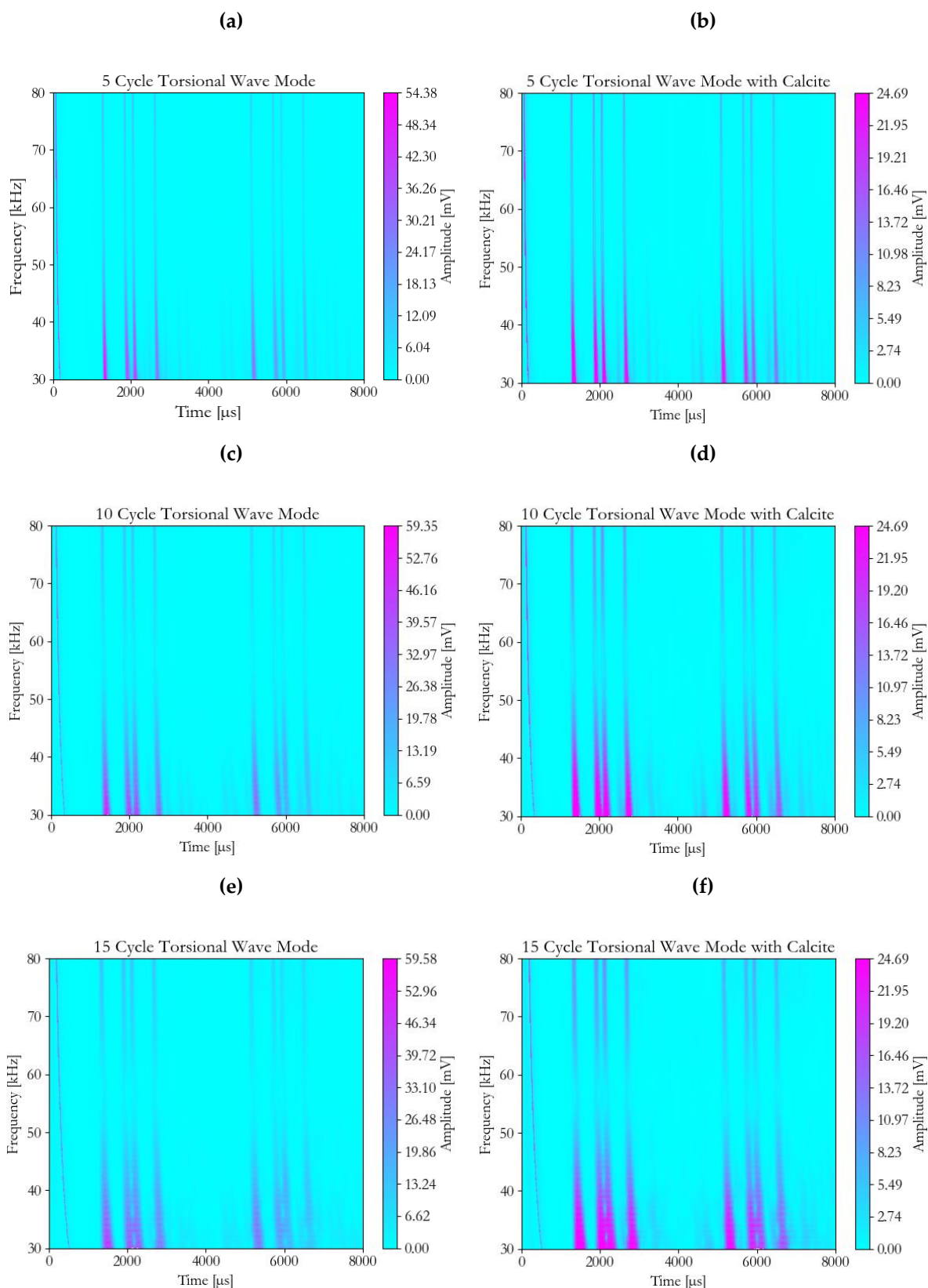
Figure 5.10: Torsional pitch-catch data for 5 cycle input (a) baseline and (b) calcite, 10 cycle input (c) baseline and (d) calcite and 15 cycle input (e) baseline and (f) calcite

Based on the results, the 45 kHz frequency is selected for further analysis as the lower frequencies display some spreading of the signal due to having a larger wavelength. The data is extracted and normalised for each wave mode excited, where the longitudinal baseline and calcite data is normalised to the amplitude of the longitudinal baseline data at 5 cycles, this normalisation method is the repeated for the torsional data, where it is normalised to the amplitude of the torsional baseline data at 5 cycles. The longitudinal wave mode shows a decrease in signal with an increase in the number of cycles for the baseline signal. For the calcite signal, there is no variation in signal amplitude due to the number of cycle inputs. The drop in amplitude is between 40-60%.

For the torsional wave mode, the number of cycles is also compared in Figure 5.11, which shows a drop of approximately 20% in signal amplitude at 5, 10 and 15 cycles. The signal amplitude also drops due to the increase in the number of cycles, similar to the longitudinal mode.

Figure 5.11: Experimental result comparison of maximum amplitude for baseline and calcite signal at different number of signal cycles

The frequency bandwidth of the input signal can be calculated as follows:

$$F_{bw} = f \pm \frac{(k_i + 2)f}{N_c} \tag{5.7}$$

where F_{bw} is the frequency bandwidth, k_i is the bandwidth of the desired lobe (where $k_i = 0$ for the main lobe and $k_i = 1$ is for the first side lobe).

92

At a particular frequency, the bandwidth of the excited pulse is dependent on the number of cycles [138]. The frequency bandwidth (main lobe) of the 5-cycle input signal is in the range of 27-63 kHz whereas the frequency bandwidth (main lobe) of the 15-cycle input signal is 39–51 kHz. As shown in Figure 5.9 and Figure 5.10, there is a higher amplitude response when the frequency is lower due to having a larger wavelength. This behaviour is asymptotic but the amplitude variation over different number cycles is low and can be neglected due to the low attenuation and non-dispersive characteristics of the T(0,1) mode. However, this behaviour can be detrimental for the excitation of longitudinal modes as shown by the drop in signal for the baseline data and a 40-60% drop in signal due to the calcite layer.

5.4.2   NUMERICAL INVESTIGATION

To aid the understanding of the wave propagation over a pipeline with and without fouling accumulation, an FEA model was created in COMSOL Multiphysics 5.4. The model followed the geometry of the 6.2 m long, Schedule 40, 6 inch diameter, carbon steel pipe and replicates the geometry and placement of the transmission and receiving transducers for pitch-catch configuration for transmitting and receiving the signal data, as shown in Figure 5.8.

Transmission points were placed at 1 m from one end of the pipe to simulate the 24 transducers in the Teletest UGW collar. For ease of computation, symmetry was invoked to analyse $1/48^{th}$ of the complete model permitting just one point load to be applied. The point load was applied in a direction dependent on the wave mode being excited for a torsional mode, this is applied perpendicular to the length of pipe and for a longitudinal mode, and this is applied along the length of the pipe. The pressure point load is a 5-cycle sine wave modulated using the Hamming function using equation (2.8). The receiving point is placed 4 m away from the transmission point.

The solid mechanics physics is applied to the model where the linear elastic behaviour is governed by Newton's second law. The mesh is optimised using equation (3.13). The fouling model was created in the same manner. However, a 1-mm solid layer was modelled on the inner wall of the pipe to represent the expected thickness of fouling to attach to the pipe during experimentation. The properties of this layer can be found in Table 5.1.

Table 5.1: Assumed material property of steel and Calcite for FE model

Material Property	Carbon Steel	Calcite
Density	7830 kg/m³	2700 kg/m³
Young's Modulus	207 GPa	70 GPa
Poisons ratio	0.33	0.3

The FE model investigates the torsional mode over 30–45 kHz in 5 kHz steps. After selecting a frequency, this model was used to investigate the addition of a Calcite layer at 1 mm, 3 mm and 5 mm thickness. To validate the model, the time of arrival was calculated using the group velocity of the torsional mode found in Figure 2.6. The time of arrival can be calculated as follows [28]:

$$T_t = \frac{x}{c_t} \tag{5.8}$$

$$T_l = \frac{x}{c_l} \tag{5.9}$$

where T_t is the time of arrival of the torsional wave mode, T_l is the time of arrival of the longitudinal wave mode, x is the distance from transmitter to receiver, c_t is the group velocity of the torsional wave mode at the operating frequency and c_l is the group velocity of the longitudinal wave mode at the operating frequency.

5.4.3   NUMERICAL RESULTS AND DISCUSSIONS

The fouling detection experiment was conducted using the Teletest® on a 6.2-m long, Schedule 40, 6 inch diameter, carbon steel pipe (baseline and fouled). Experimental results were compared to the FEA results to achieve a good correlation with the effects of the additional fouling layer.

The FE model investigated 30–45 kHz signals at 5 kHz increments. A frequency of 45 kHz was selected due to the signal having a shorter pulse length as shown in Figure 5.9 and Figure 5.10. At this frequency, the addition of the Calcite layer was investigated with 1-, 3- and 5-mm of fouling thickness on the inner pipe wall. Compared to the torsional baseline model in Figure 5.12, the receiving pulse shows a drop in amplitude with the increase of the Calcite layer thickness.

There is a shift in time of arrival in Figure 5.12 with the incremental thickness of the Calcite layer. With the increase in Calcite thickness, the pulse of interest arrives faster, which is possibly due to the change in the velocity of the T(0,1) mode with the incremental Calcite thickness. The GUIGUW [32] code was used to plot the dispersion curves against the incremental fouling layer. Adding a fouling layer to the pipe increases the velocity of the torsional mode. Although the increase is small, this finding can be concluded as the cause of the shift in the time of arrival. Using the velocity found for each thickness of Calcite, the time of arrival can be calculated using the peak-to-peak values of the signal (Table 5.2). There is a 1% error in the comparison of theoretical and numerical time of arrival. A comparison of the difference between the time of arrival for each case is immaterial due to the small thicknesses of Calcite which would make the data harder to use for interpreting the fouling thickness in comparison to the amplitude drop.
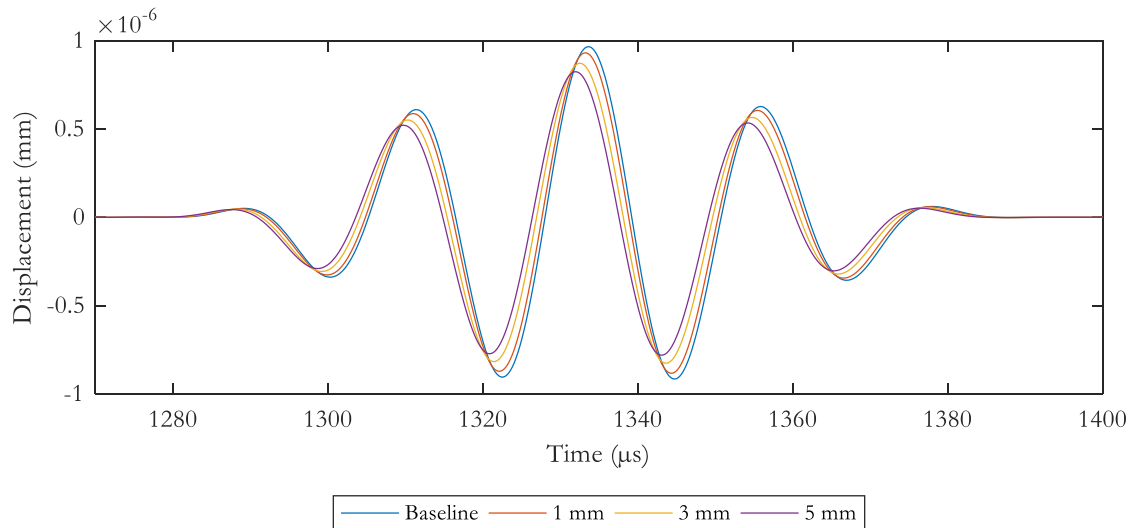
Figure 5.12: Comparison of FEA pitch-catch signal at different fouling thicknesses

Table 5.2: Comparison of theoretical and FEA time of arrival.

	Torsional Group Velocity	Theoretical Time of Arrival at 4 m (μs)	COMSOL Pk-Pk Time of Arrival (μs)	Error %
Baseline	3152.6	1268.8	1282.6	1.1
1 mm	3152.8	1268.7	1282.0	1.1
3 mm	3153.1	1268.6	1281.8	1.0
5 mm	3153.4	1268.5	1281.2	1.0

Compared to the torsional wave mode, the longitudinal wave mode also shows a reduction in signal due to the increase in calcite thickness as shown in Figure 5.13. There is very little identifiable shift in the time of arrival and could be due to the dispersive nature of the longitudinal wave mode. This makes it harder to characterise fouling accumulation based on signal reduction alone.
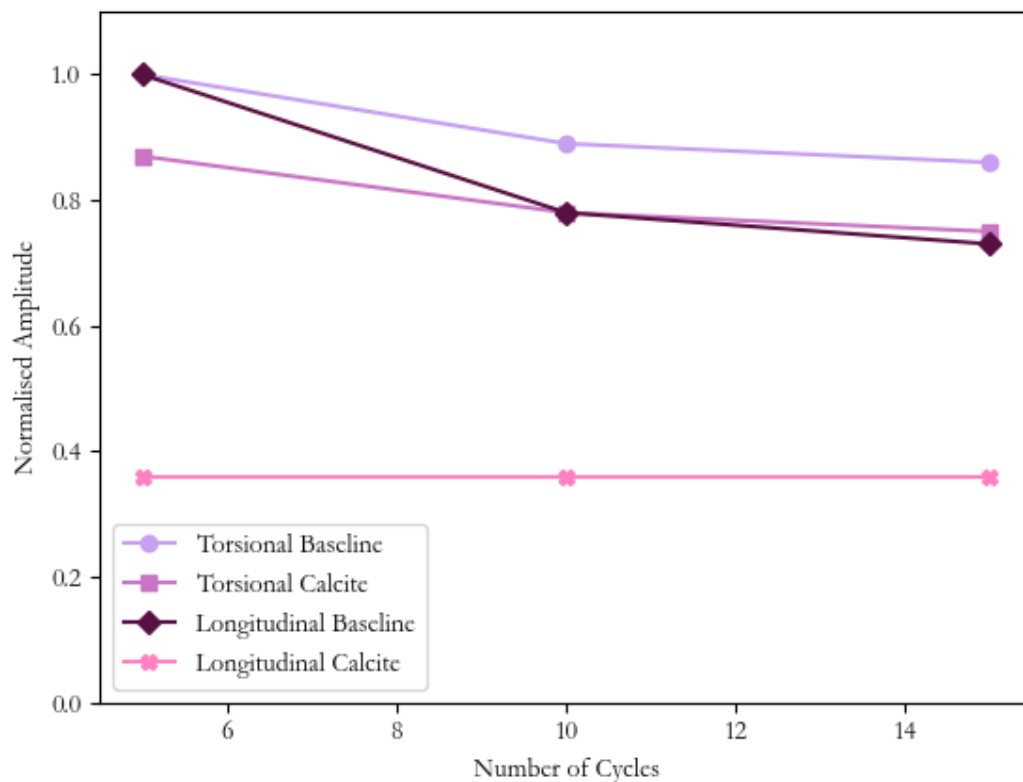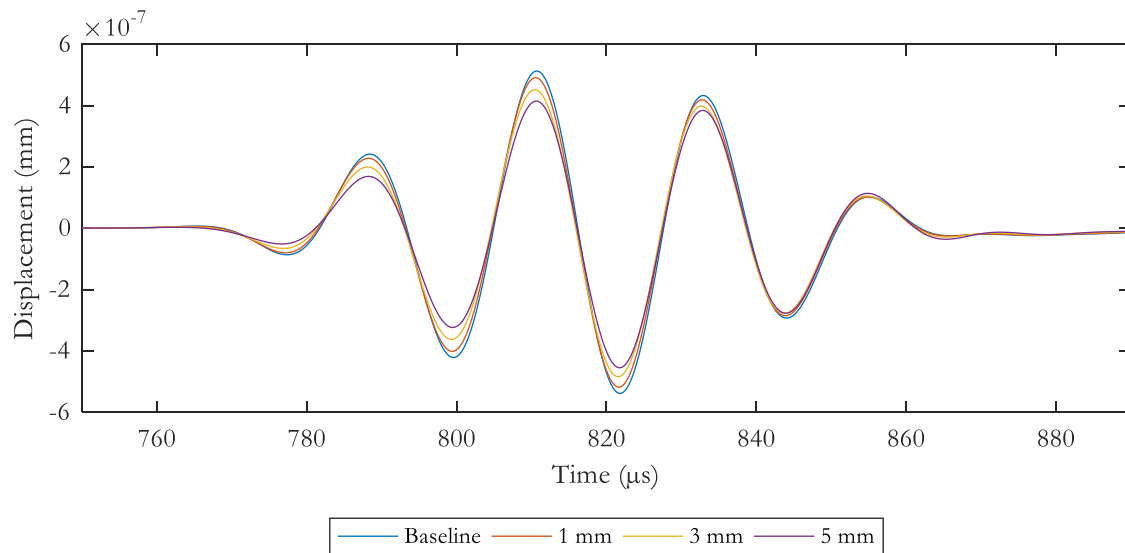
Figure 5.13: Experimental comparison of maximum amplitude for baseline and Calcite signal at different number of signal cycles

5.5 SUMMARY

This chapter has discussed the trial and error tests conducted in order to achieve a fouling generation method that can produce Calcite at an increased rate for larger diameter, longer pipe samples. After this, the detection of fouling accumulation is investigated using UGW by investigating frequency, number of cycles and wave mode excitation. The torsional wave mode has shown to have two characteristics than can be used to identify fouling accumulation through the reduction in amplitude and shift in time of arrival. This can be a result of the non-dispersive characteristics of the torsional wave mode.

Chapter 6: Ultrasonic Cleaning and Parametric Calibration

The greater danger for most of us lies not in setting our aim too high and falling short; but in setting our aim too low, and achieving our mark – Michaelangelo

6.1 INTRODUCTION

This chapter utilises the fouled 2-inch diameter pipe sample generated in Chapter 5. A single HPUT is attached to the outer wall of the water-filled pipe sample to undergo a cycle of fouling removal. During this, vibration analysis is carried out on the outer wall of the pipe sample for comparison with the results produced in Chapter 4 of the ultrasonic cleaning FE model. The experimental and numerical results are compared before applying the ultrasonic cleaning FE method onto calibrating an HPUT configuration to carry out ultrasonic cleaning on the fouled schedule 40, carbon steel pipe sample produced in Chapter 5.

6.2 ULTRASONIC CLEANING EXPERIMENTATION

The experimental set-up includes a signal generator and power amplifier for HPUT excitation. The PSV-400 3D Laser Scanning Vibrometer (PSV-400) is used for data acquisition (Figure 6.1). The fouling removal experiment includes the following list of equipment (Figure 6.2):

- Concave 40 kHz Langevin HPUT
- Polytec PSV-400 3D Laser Scanning Vibrometer
- 1040L Power Amplifier
- DSO-X 2012A Oscilloscope
- Stainless Steel 315L Pipe – 300 mm length, 1.5 mm wall thickness, 50.08 mm outer wall diameter with calcite on inner wall

The sinusoidal wave input signal is pulsed by a DSO-X 2012A Oscilloscope. The frequency is adjusted to the resonant frequency of the 40 kHz HPUT and remains constant throughout the experiment. The amplitude is adjusted to 1 V and is delivered to the 1040 L Power Amplifier.

The 1040 L Power Amplifier, covering the frequency spectrum of 10 kHz - 5 MHz at 55 dB gain, sends the amplified signal to the HPUT. The 40 kHz HPUT is placed on a stainless steel 315L pipe which is 300 mm in length, 1.5 mm in wall thickness and 50.08 mm in outer diameter with a thin layer of Calcite on the inner pipe wall. The HPUT is attached using an HPUT holder and is coupled to the specimen using acoustic coupling gel.
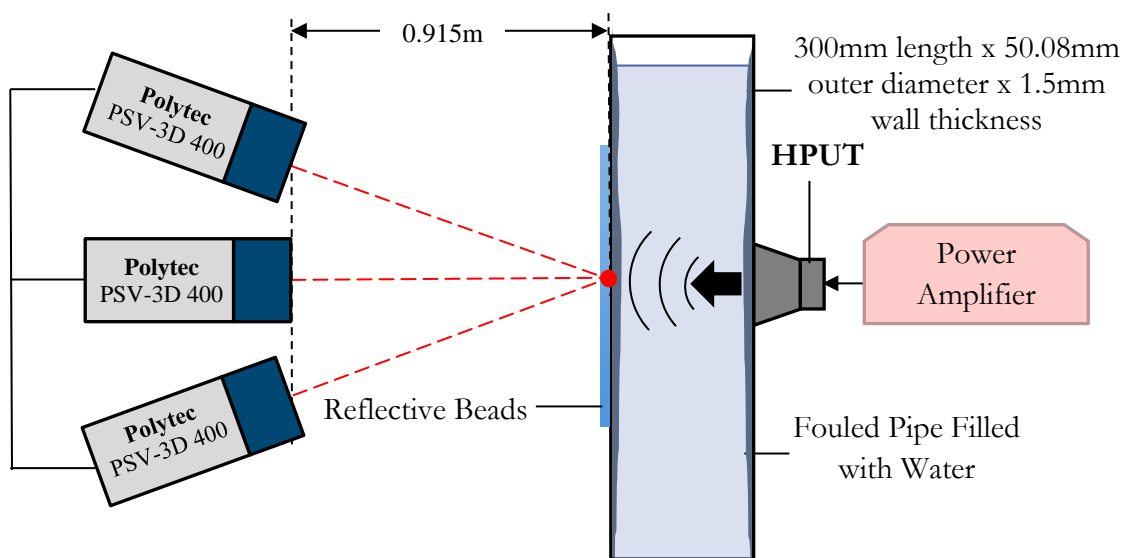
Figure 6.1: Diagram of fouling removal experiment set-up with transducer excitation equipment and 3D Laser Scanning Vibrometer
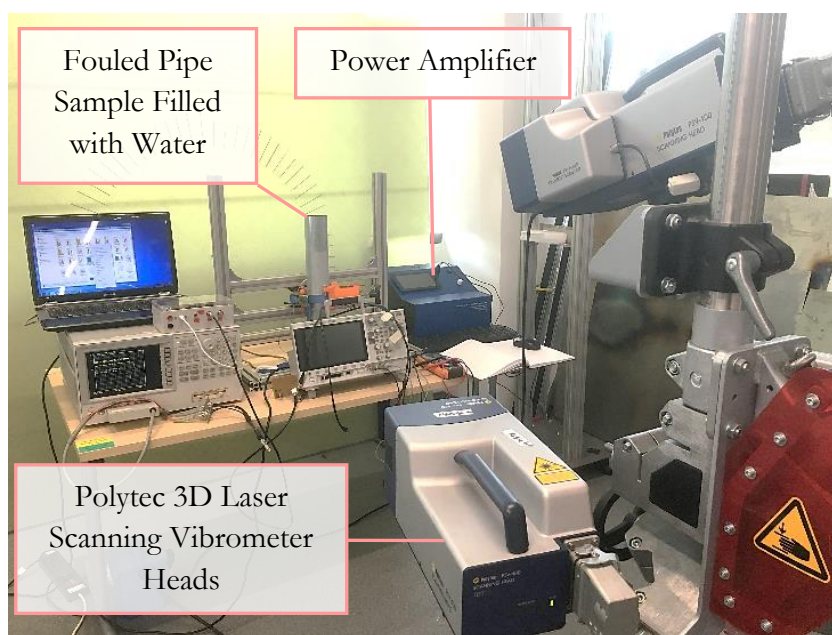
Figure 6.2: Experimental set-up of HPUT excitation equipment and 3D Laser Scanning Vibrometer

During the fouling removal trials the PSV-400 is used to measure the vibrations of the structure undergoing wave propagation from the HPUT. The PSV-400 was used in previous studies to investigate the ultrasonic stress distribution on a pipe surface [139]. The displacement on the outer surface can be compared with cleaning patterns to match the nodes and antinodes on the outer surface with the cleaning patches found on the inner wall.

During a cycle of cleaning, the PSV-400 measures the displacement of the samples outer wall surface to later compare with the cleaning results. Figure 6.2 shows a diagram of the set-up of all the equipment used during the fouling removal process.

6.3 RESULTS AND ANALYSIS

The fouling removal experiment examines a stainless steel pipe with a thin layer of calcite on the inner wall. The excitation from a HPUT was used to clean an area of the calcite from the inner pipe wall whilst measuring outer wall displacements using the PSV-400. Vibrometry analysis shows high displacement at the locations of fouling removal of the pipe sample.

The parameters of the experiment and achieved displacements according to the Vibrometry data are summarised in Table 6.1. These experimental values are replicated in the FE model.

Table 6.1: HPUT parametric inputs for fouling removal experiment

HPUT Parameter	Value
Power	40 W
Resonant Frequency	40 kHz
Material	Stainless Steel
Power Input	65 W
Excitation Frequency	40.46 Hz

6.3.1 PIPE DISPLACEMENT CONTOURS

To validate the model, the predicted pipe displacement is compared with the Vibrometry results. Figure 6.3 shows the comparison of the cleaned area with Vibrometry scan and FE model. Each set of results show an overlap of high displacement where cleaning results were achieved. With the variables from Table 6.1, the developed model shows a good agreement between high displacements and cleaning patterns. The model results in Figure 6.3 shows high displacements propagating from the HPUT and localised at the circumference of the pipe perpendicular to the HPUT attachment. The direction of propagation is due to the HPUT producing compressional waves.

6.3.2 ACOUSTIC PRESSURE CONTOURS

As the model validates the cleaning patterns, the next step is to validate whether an arbitrary experimental set-up is generating cavitation bubbles prior to undergoing experiments using the

pressure threshold. Since this set-up has shown to achieve cavitation generation for the cleaning results to be obtained, the FE model is assumed to be generating cavitation.
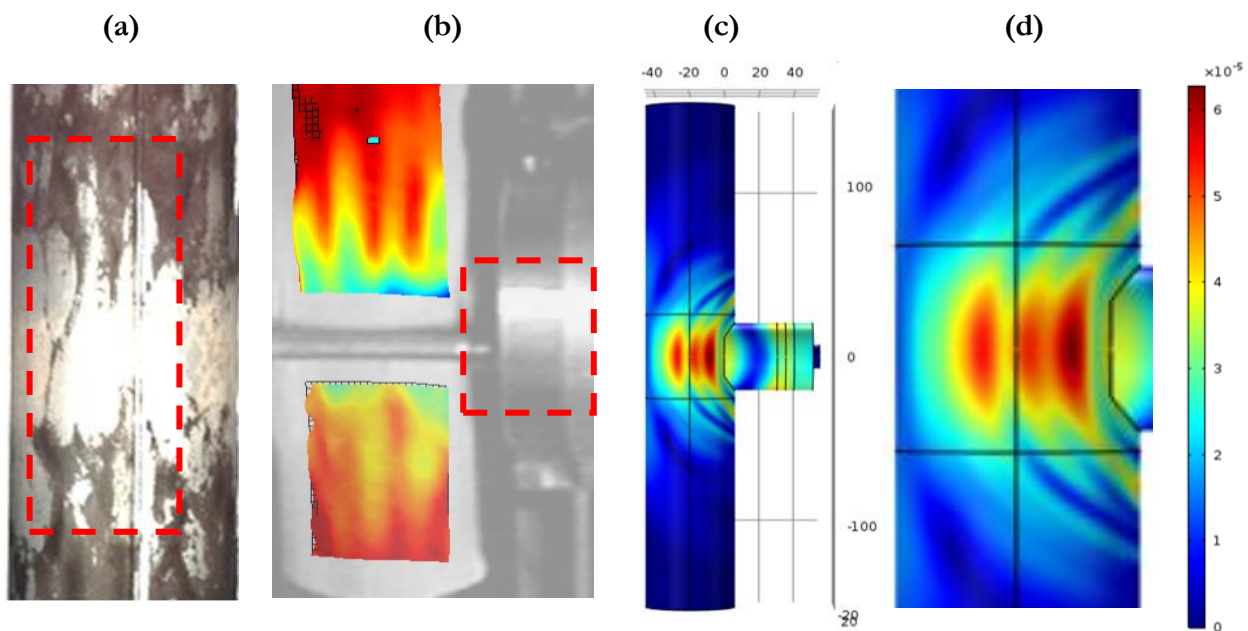
Figure 6.3: Comparison of results (a) experimentally obtained localized cleaning after one cycle of ultrasonic cleaning, (b) 3D displacement measured during ultrasonic cleaning using PSV-400, (c) numerical simulation results and (d) zoomed version of (c) displaying high displacement achieved at same location of cleaning and PSV-400 results

As the pressure continues propagating throughout the liquid, instants of high positive and negative pressure are in-line with the cleaning pattern. The negative pressure instants can be linked to the rarefactions within the liquid where cavitation bubbles are generated and the positive pressure instants relate to the compressional locations in which the generated bubbles implode.

6.3.3 FAST FOURIER TRANSFORM

A Fast Fourier Transform (FFT) is carried out on the PSV-400 results. Figure 6.4 shows the average velocity magnitude across the scanned points at different frequencies. The FFT displays a similar correlation between the average magnitude of velocity in the x, y and z directions. There is a significant peak in velocity at 40 kHz due to the resonance of the HPUT and excitation frequency. This peak is followed by a harmonic at 80 kHz.
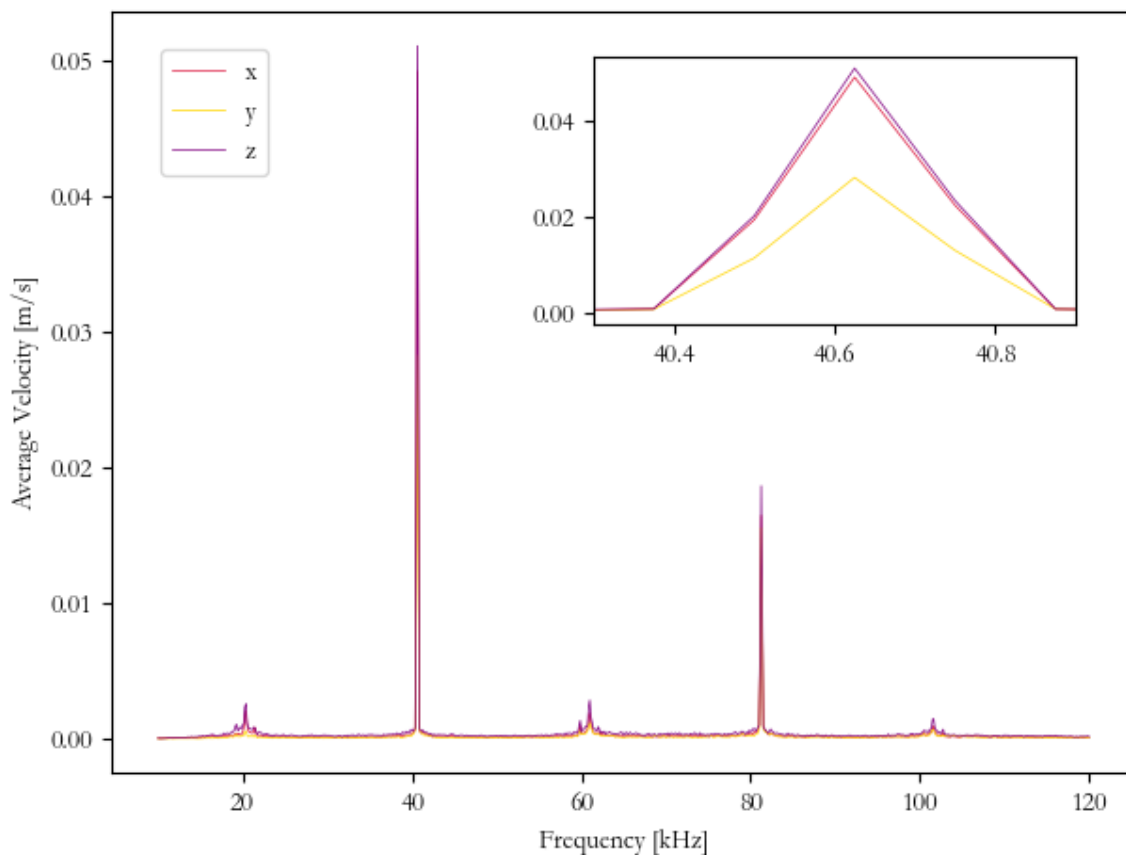
Figure 6.4: FFT of average velocity of scanned area using PSV-400 measurements taken of 40 kHz HPUT attached to pipe

Peak values in the FFT graph from the Vibrometry results are due to the shockwaves emitted from the violent collapse of the cavitation bubbles generated within the fluid of the pipe specimen [140]. Each peak can be calculated based on the operating frequency, f_o.

$$f_o = 40 \ kHz \tag{6.1}$$

$$Harmonics = \ nf_o \tag{6.2}$$

where, n is the natural number. For example, if n equals 1, 2, 3, 4, then the harmonics would be at 40, 80, 120 and 160 kHz respectively.

$$half \ order \ subharmonic = \frac{f_o}{2} = 20 \ kHz \tag{6.3}$$

$$ultraharmonics = \frac{(2n + 1)f_o}{2} \qquad (6.4)$$

$$\therefore \quad if \ n = 1 \ \rightarrow \frac{3f_o}{2} = 60 \ kHz$$

The calculated peaks produced from shockwave emissions have a good agreement with the peaks found in Figure 6.4. When zooming into the 40 kHz peak, there is a large velocity peak in the z-direction due to the high out-of-plane vibration, which is the vibration mechanism required for cleaning results to be achieved.

The FEA FFT graph (Figure 4.11) shows a significant peak at 40 kHz, matching the vibrometry results illustrated in Figure 6.4. Overall there is a good agreement between numerical and experimental results of the consonant frequency for the investigated conditions.

Another clear comparison made from both Figure 6.4 and Figure 4.11 is between the various peaks that follow the resonant harmonic in the acquired vibrometry results that do not appear in the FE model results. This is explained by the vibrometry analysis obtaining data from a specimen which is undergoing cavitation generation within the liquid. The cavitation bubbles emit shockwaves which resulted in the vibration of the pipe wall at frequencies other than the operating frequency. The FE model neglects the generation of cavitation bubbles, which means that there are no shockwaves being generated due to cavitation and, therefore, no frequency peaks other than at the resonance frequency.

6.3.4   POWER REQUIREMENTS

The energy requirement depends on the application. For intense cleaning applications it is in the range of 70 – 100 W and the application in the current study requires 40 – 70 W to achieve an adequate level of cleaning. The HPUT used in this experiment operates at 40 W and the input power of 65 W was required to compensate for power loss. The power requirement can be calculated as follows:

$$Average \ Watts \ Power = \frac{\pi r^2 L}{231} 100 \qquad (6.5)$$

where r is the radius of the inner pipe wall and L is the length of the pipe.

When attaching an HPUT onto a structure, this affects the initial impedance of the HPUT which shifts to a higher impedance value. The change in impedance will affect the required input power to achieve 250V AC.

The cleaning cycle time used for the experimental validation was 30 minutes. The calculation of the energy required for cleaning uses the following equation:

$$E_J = P_W \times t_s \qquad (6.6)$$

where E_J is the energy, Pw is the power and ts is the duration of cleaning.

6.4 PARAMETRIC INVESTIGATION OF ULTRASONIC CLEANING – REVIEW

Research into improving the ultrasonic fouling removal technique has focused on calibrating the cleaning parameters such as cleaning time, frequency and cleaning agent. Different methods have been used to investigate the parameters describing optimisation of cleaning, transducers and applications for the specific problem, this includes experimental testing and modelling.

6.4.1 EXPERIMENTAL TESTING – STATE-OF-THE-ART

Examples of research for improving the ultrasonic technique include boat cleaning [61] where the system uses ultrasonic as a preventative method of fouling. The efficiency of the transducers has been determined through testing on experimentally contaminated samples, which is a costly and time-consuming approach to determining the effectiveness of the selected ultrasonic device and its parameters. The effectiveness of ultrasonic defouling based on pH level, ionic strength and particle size has also been studied [141]. The study found various empirical trends such as both low and high pH solutions being more effective compared to neutral solutions. The effects of frequency (28, 45 and 100 kHz) on ultrafiltration and membrane cleaning [142] concluded that 28 kHz was the most effective frequency whereas 100 kHz had little effect. The use of low frequencies to enhance permeating flux was studied and found that low power enabled at these frequencies can minimize damage to the membrane surface [143].

Nguyen *et al.* [58] focused on a green technology for cleaning turbine engine oil filters on ships with ultrasonics. The study used a 25 kHz multi-transducer system. Under experimental conditions, various parameters were explored including power (300W and 600W), temperature effect, ultrasonic defouling times, and pressure losses through oil filters and solvent for washing. The cleaning efficiency was compared for three cases: hand washing, preliminary washing and ultrasonic washing. The experimental data were correlated using a statistical analysis method and it was concluded that ultrasonic washing was the most effective and time efficient.

Experimental work has been carried out to ultrasonically remove contaminants on plastic parts [144]. The study investigated different cleaning agents and temperatures, and also suggested an optimal operation time and frequency for cleaning. After selecting the optimal parameters, a field trial was implemented to demonstrate the practical effectiveness and time-efficiency of the method. Further work has been carried out on optimising the ultrasonic defouling technique for membrane fouling removal using time-domain reflectometry (TDR) [145]. TDR was shown capable of detecting membrane fouling in real time and also detected the removal of the fouling during ultrasonication. This method can optimise the cleaning runtime.

Generally, experimental investigation of optimisation of the ultrasonic fouling removal technique is very time-consuming and costly. Very few parameters can be investigated as it can be hard to obtain transducers of various frequencies and power. Also, creating an experiment that can control different structural variables such as fluid temperature, fouling thickness can also be difficult to achieve.

6.4.2 NUMERICAL SIMULATION – STATE-OF-THE-ART

In contrast to experimental parameter studies, numerical simulations allow studies with lower cost and time implications. FEA has been used in 2D conditions to calculate the sound field distribution within a water tank to optimise the parameters governing effective cleaning [146]. FEA has also been used to design and test the flow through a separator [147]. Hill and Wood investigated three models; a separation model (particle fluid mixture), a flow model (CFD flow profile) and a transducer model (electroacoustic model of the cell). Overall, the models contributed towards fine tuning the performance of the cell.

Another approach that has been investigated combines numerical simulation and automated optimisation differentiation to design ultrasonic Langevin transducers [148]. This work focused only on the modelling aspects without any experimentation to prove the method works for designing ultrasonic horn attachments.

An in-depth review has been carried out on modelling the acoustic pressure within a sonochemical reactor [120]. Various models were discussed, including linear and non-linear modelling; of the two, non-linear modelling was able to account for the attenuation caused by cavitation bubbles within the sonochemical reactor. The ultrasonic transducer has also been discussed. This is a relatively easy model to create using electromechanical physics. Overall, numerical simulations of sonochemical reactors can model the vibration of the walls and the acoustic pressure field. The

effect of cavitation on wave propagation is significant and can only be taken into account within a non-linear model.

Numerical modelling has also been used to improve the ultrasonic fouling removal technique by correlating the high intensity sound field with the generation of cavitation [149]. The modelling investigated the wave propagation into a cavitating liquid (two-phase continuum model). The results show qualitative agreement with the pressure antinodes and locations of cavitation generation in the experimental validation. In recent work, the use of multiple transducers at moderate power levels has shown to be more effective than using a single transducer at higher power levels [150], which promises improvement of the ultrasonic defouling coverage using a transducer array. The use of FEA for advancing the design and upscaling of the ultrasonic defouling technique for reactors is promising, as reported by Jordens *et al.* [150].

6.5   NUMERICAL PARAMETRIC STUDY

The validated numerical methodology is applied to a 6 meter long, Schedule 40, 6 inch diameter, carbon steel pipe. This thesis conducts a parametric study to investigate the optimal HPUT array (see Figure 6.5) with water filled within the pipe (static), fouling, signal input and fluid temperature. The model focuses on a 40 kHz Langevin bolt-clamped HPUT due to its successful cleaning in
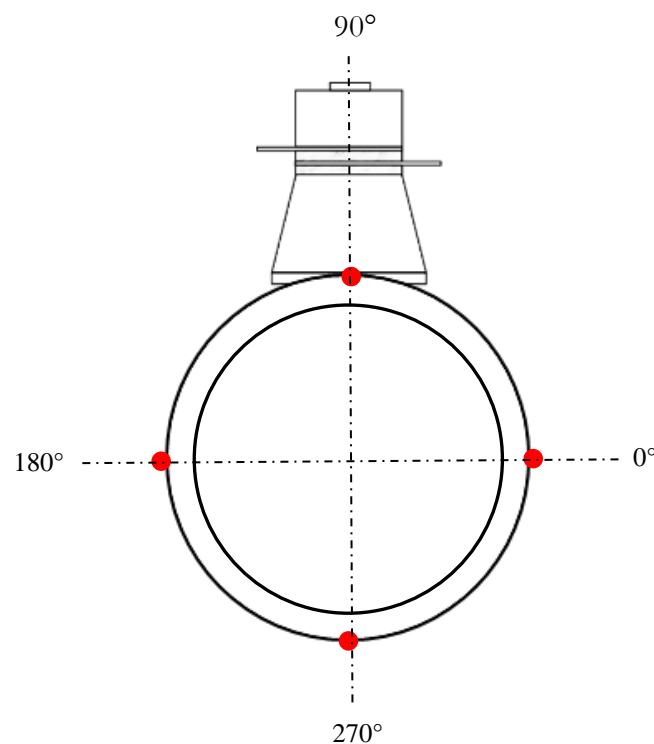
Figure 6.5: illustration of HPUT configurations for FEA analysis
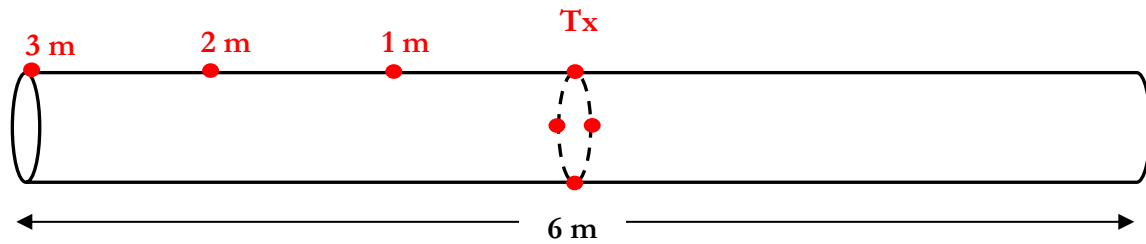
Figure 6.6: Schematic of excitation of and monitored points of the 6 meter long, Schedule 40, 6 inch diameter, carbon steel pipe

prior experiments. The pipe is monitored at different locations along its length to compare the various parameters as shown in Figure 6.6. The points are placed at 1 m distances on the inner and outer walls of the pipe to monitor the acoustic pressure within the liquid and the solid displacement on the outer wall of the pipe.

The geometry is designed assuming symmetry to reduce the computational time of the model as shown in Figure 6.7 and Figure 6.8. The number of planes of symmetry is dependent on the number of HPUTs under investigation.

The end time-step is selected based on the time of arrival which is calculated using the group velocity of the longitudinal mode found in Figure 2.6. The time of arrival of the longitudinal mode can be calculated using equation (5.9).

To ensure that standing waves are achieved, the time of arrival must be calculated based on the signal arriving at the end of the pipe and travelling back to the excitation location, totalling 6 meters
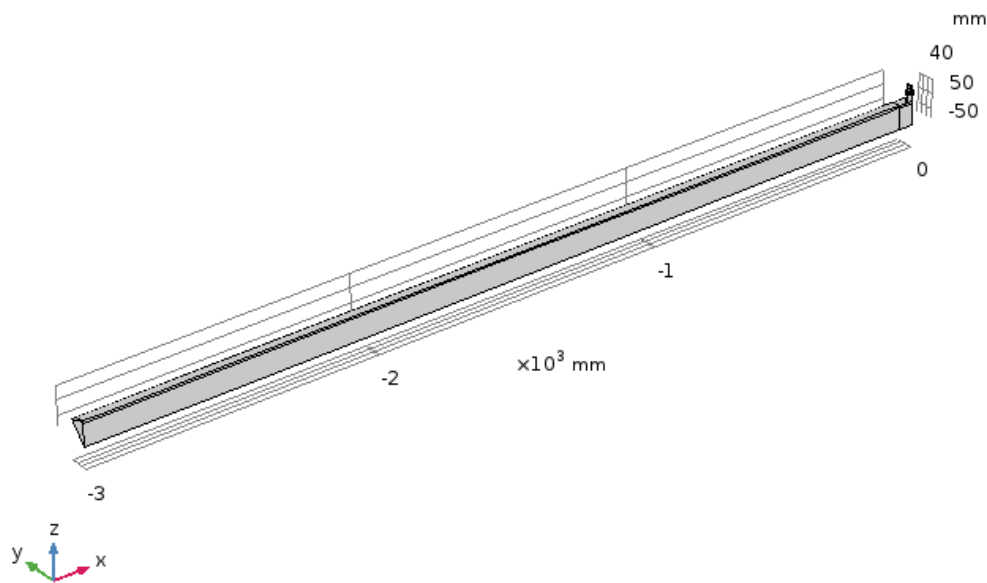
Figure 6.7: Geometry of 4-HPUT configuration on a 6 meter long, Schedule 40, 6 inch diameter, carbon steel pipe
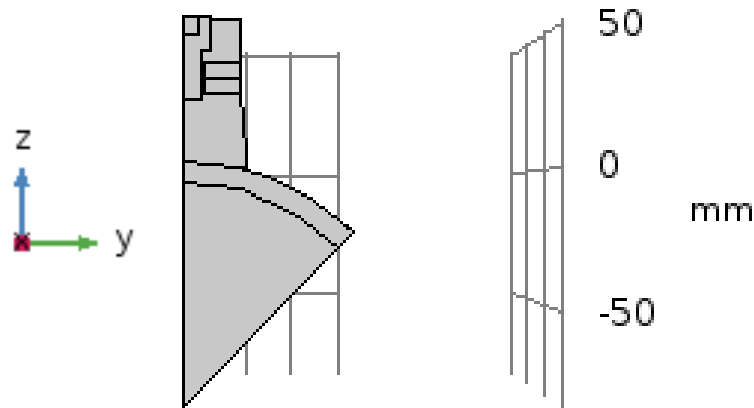
Figure 6.8: Cross sectional view of geometry of 4-HPUT configuration on a 6 meter long, Schedule 40, 6 inch diameter, carbon steel pipe

in travelling distance. Extra time must also be taken into account to accommodate multi-modal responses (higher order flexural modes).

6.5.1   TRANSDUCER ARRAY

The number of HPUTs within a configuration is investigated, as a single HPUT may not develop high enough values of pressure within the fluid to generate cavitation, depending on the diameter of the pipe, wall thickness and pipe length. For the pipe sample of interest, the diameter allows multiple HPUT to be placed around the circumference to potentially increase the acoustic pressure within the fluid and the outer wall displacement. The numbers of transducers being investigated are 1 (90°), 2 (90° and 270°) and 4 (0°, 90°, 180° and 270°) as described in Figure 6.5.

The configuration is placed at the mid-length of the 6 m pipe. Symmetry is applied to each configuration to reduce computation time.

The selected optimal HPUT array for long-range cleaning is utilised for further investigation of the following removal parameters:

- temperature of fluid (20°C, 50°C and 100°C)
- input signal (sinusoidal and square)
- layer of fouling (calcite)
- Number of cycles (10 and 20)

The data obtained will primarily focus on the pressure acoustics and solid displacement at the monitored points.

6.5.2   RESULTS AND ANALYSIS

The results of the FEA parametric study were compiled to compare the solid displacement and total acoustic pressure at monitored points along the length of the pipe (0, 1, 2, 3 m).

To compare the coverage and amplitude achieved from each configuration, the maximum amplitude of solid displacement and total acoustic pressure are measured from the monitored points along the length of the pipe. Polar plots are created for each configuration at the maximum amplitude at different locations to analyse the coverage over the cross-section of the pipe wall.

Comparing the amplitude at the monitored points for the different configurations in Figure 6.9, the trend shows that the 1-HPUT achieves its maximum displacement and acoustic pressure amplitude at the transducer location; along the length of the pipe, the 1-HPUT case reduces in amplitude, resulting in an average acoustic pressure of 3 KPa.
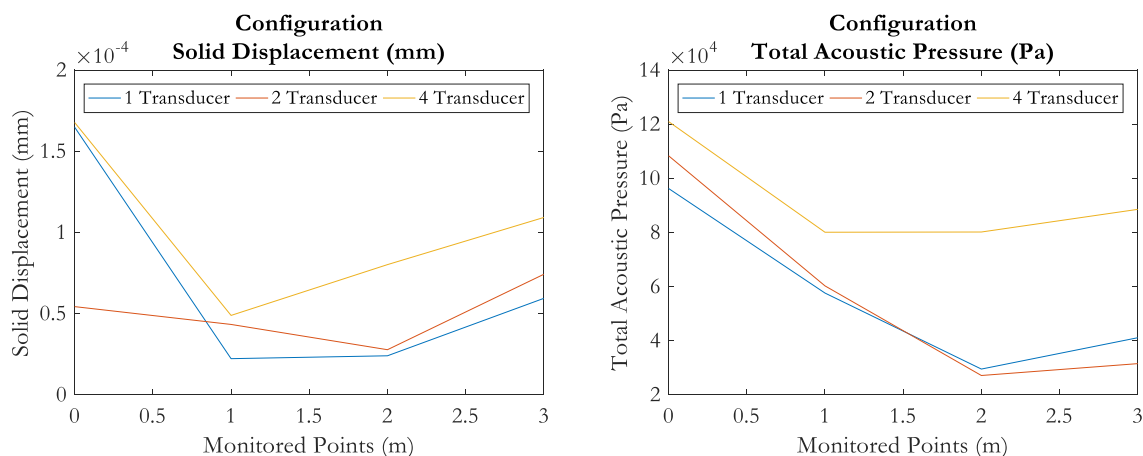
Figure 6.9: Maximum solid displacement and total acoustic pressure at monitored points for each investigated transducer configuration

Comparing each configuration at the excitation location, the 2-HPUT case achieved the lowest displacement, due to the configuration resulting in superposition of the signals. The remainder of the 2-HPUT results follows a similar trend to the displacement amplitude achieved for the 1-HPUT case.

For the total acoustic pressure, with the increase of HPUT, the achieved amplitude at the transducer location also increases. For the remainder of the pipe length, the 1- HPUT and 2-HPUT case follow a similar trend with an average of 3 KPa.

The 4- HPUT case has shown to achieve the highest displacement and total acoustic pressure at each monitored point, averaging 8 KPa for the remainder of the pipe length.

The polar plots in Figure 6.10 for the 1- HPUT case show high amplitude at the HPUT location for both the displacement and total acoustic pressure. For the remainder of the circumference, the displacement averages below 0.5 x 10^{-4} mm. The acoustic pressure shows some peaks reaching 4 KPa at 0° and 180°. The remainder of the circumference has an average of 2 KPa of pressure being achieved. This coverage is not ideal for long distance due to the drop in amplitude and the lack of uniform coverage being achieved.
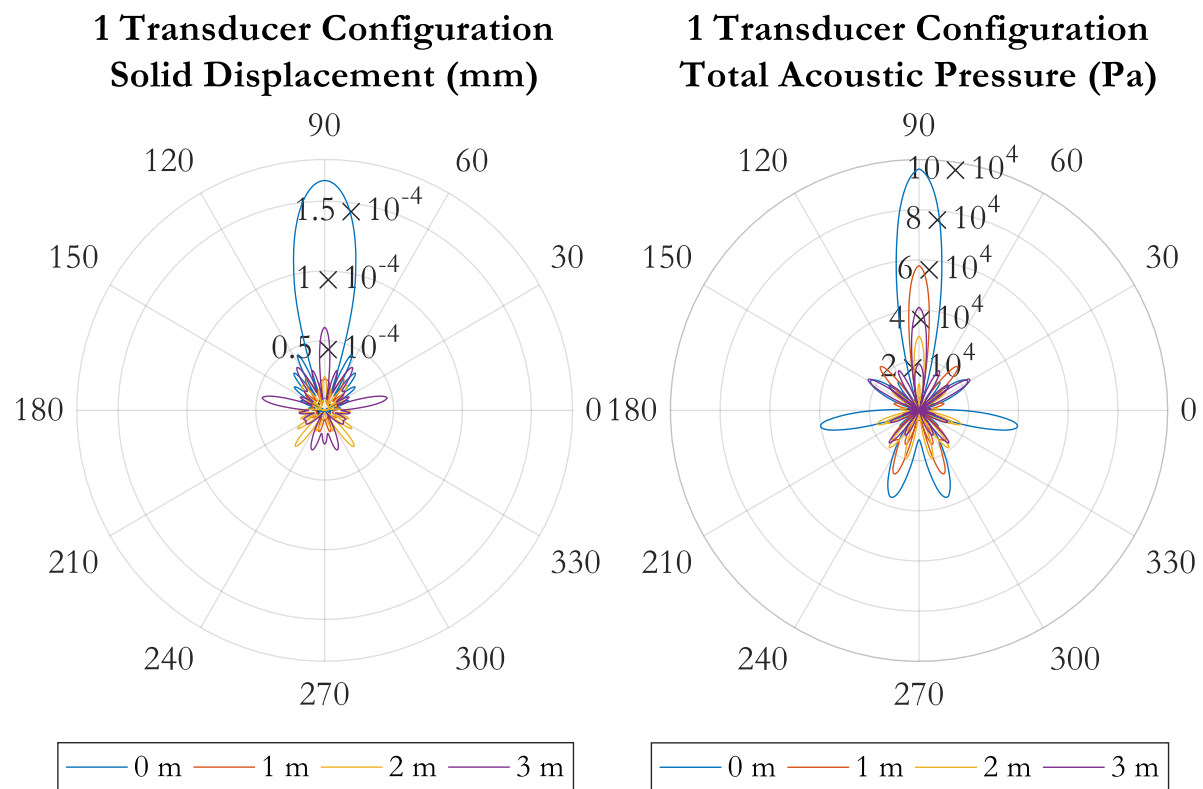
Figure 6.10: Solid displacement and total acoustic pressure polar plots for 1 HPUT case, displaying the maximum amplitude at each monitored point

The 2- HPUT case achieves its highest amplitude at the HPUT locations (90° and 270°) as shown in Figure 6.11. Over the length of the pipe, the amplitude of these peaks drop. The remainder of the circumference averages below 0.5 x 10^{-4} mm and 5 KPa. At 0° and 180°, the peak achieved in the total acoustic pressure shows a blunt feature, which could be due to superposition related to the HPUT spacing.

2 Transducer Configuration Solid Displacement (mm)

2 Transducer Configuration Total Acoustic Pressure (Pa)
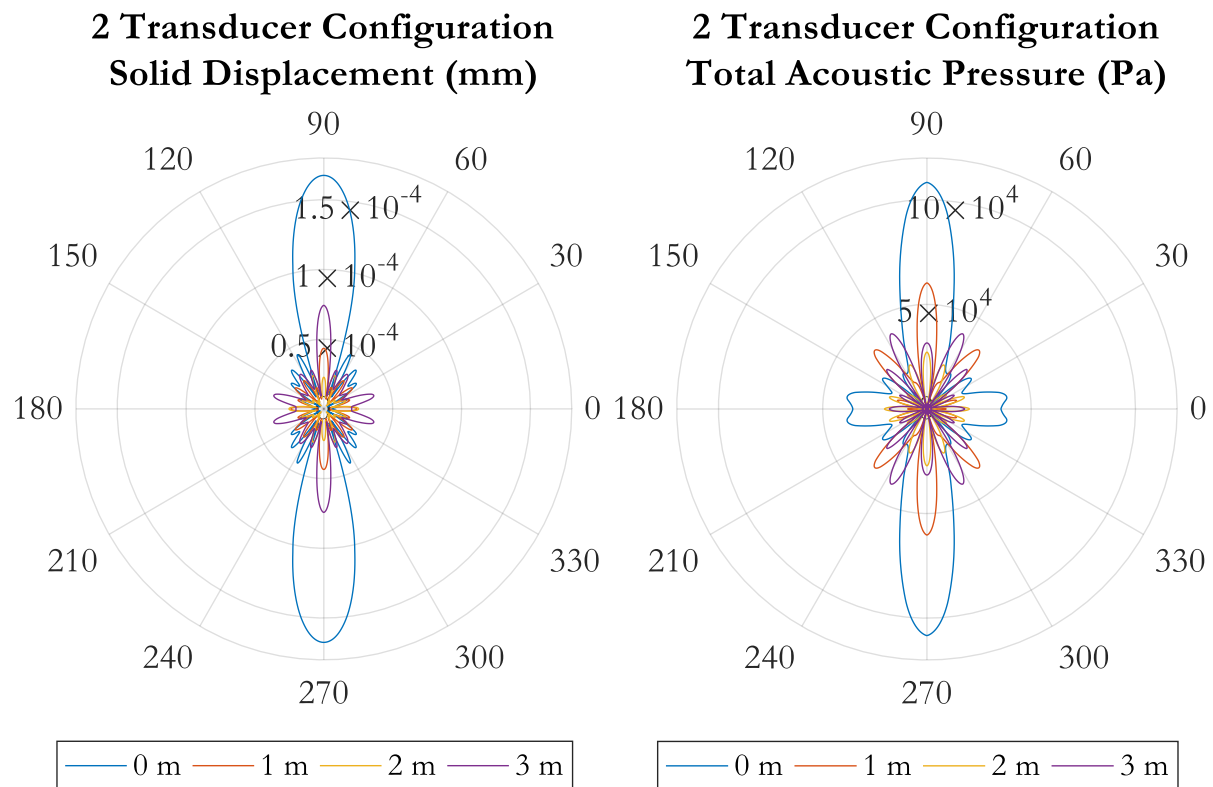
Figure 6.11: Solid displacement and total acoustic pressure polar plots for 2 HPUT case, displaying the maximum amplitude at each monitored point

The highest amplitude for the displacement and total acoustical pressure is achieved in the 4-HPUT configuration at 0°, 90°, 180° and 270° as shown in Figure 6.12. The configuration achieved a more uniform coverage as well as higher averaging coverage for the displacement (1×10^{-4} mm), doubling the average shown in the 1- HPUT and 2- HPUT cases. The acoustic pressure averages approximately 7 KPa.

**4 Transducer Configuration
Solid Displacement (mm)**

**4 Transducer Configuration
Total Acoustic Pressure (Pa)**
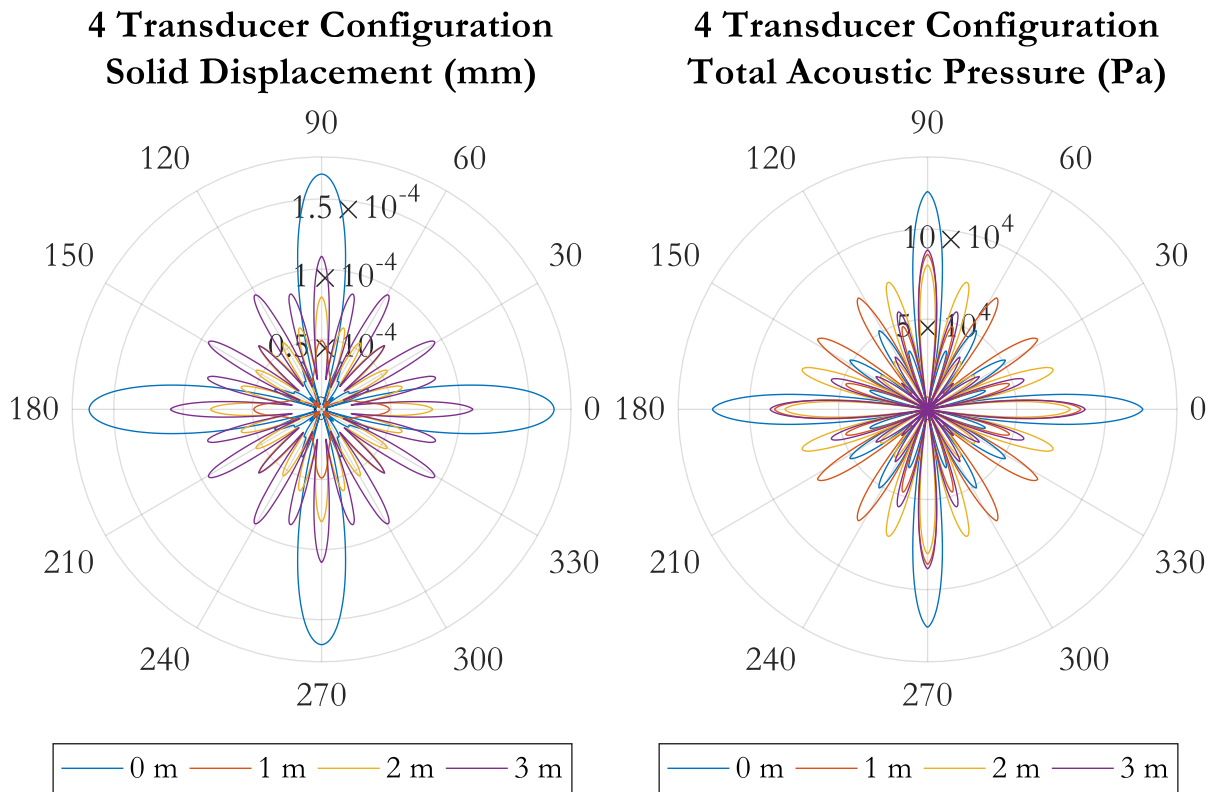
Figure 6.12: Solid displacement and total acoustic pressure polar plots for 4 HPUT case, displaying the maximum amplitude at each monitored point

The study of the HPUT array has shown that the HPUT location should typically achieve the same displacement due to the vibration of the HPUT but the 2- HPUT case has a reduction as mentioned previously due to superposition. The increase in the number of HPUT improves the coverage achieved at the HPUT location and has increased the acoustic pressure within the fluid domain. The 4- HPUT case has also shown to achieve high amplitudes at further distances compared to the 1-HPUT and 2- HPUT cases showing its promise for achieving long distance cleaning coverage.

The 4- HPUT configuration was selected for further parametric analysis of the cycle input, fluid temperature, addition of fouling and signal input. The number of cycles of the sinusoidal input signal is investigated and displayed in Figure 6.13. For the displacement, the increase in cycles has an increase in the displacement being achieved on the outer wall of the pipe; however, for the acoustic pressure, this does not have an effect. This implies that the number of cycles does not improve the delivery of the signal through the pipe wall thickness, into the fluid domain.
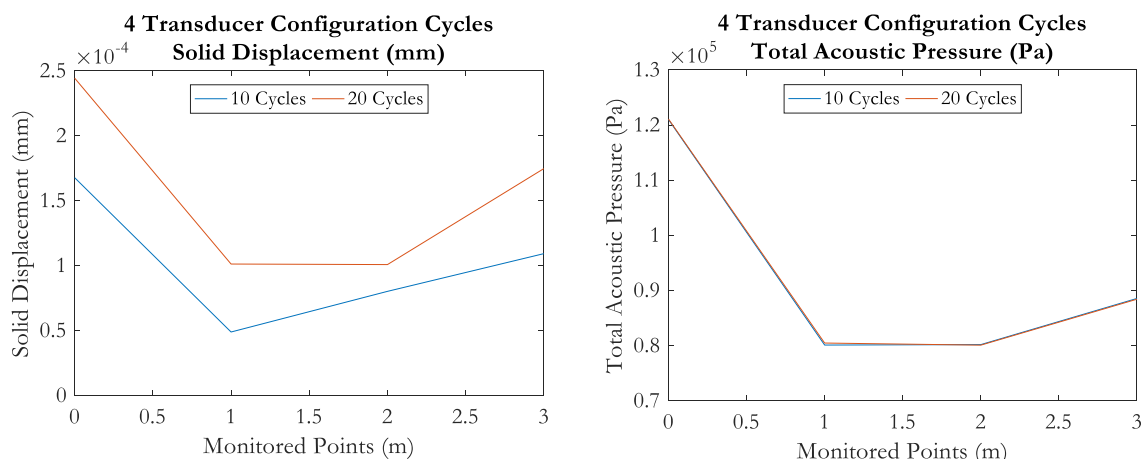
Figure 6.13: Maximum solid displacement and total acoustic pressure at monitored points for each investigated number of cycles

The effects of temperature of the fluid domain is investigated and displayed in Figure 6.14. At the HPUT location, the displacement increases at 50 °C whereas the 20 °C and 100 °C remain the same. Along the length of the pipe, the displacement amplitude increases for 50 °C and 100 °C compared to 20 °C. This suggests that the increase in temperature improved the propagation of the vibration from the HPUT for longer distances.
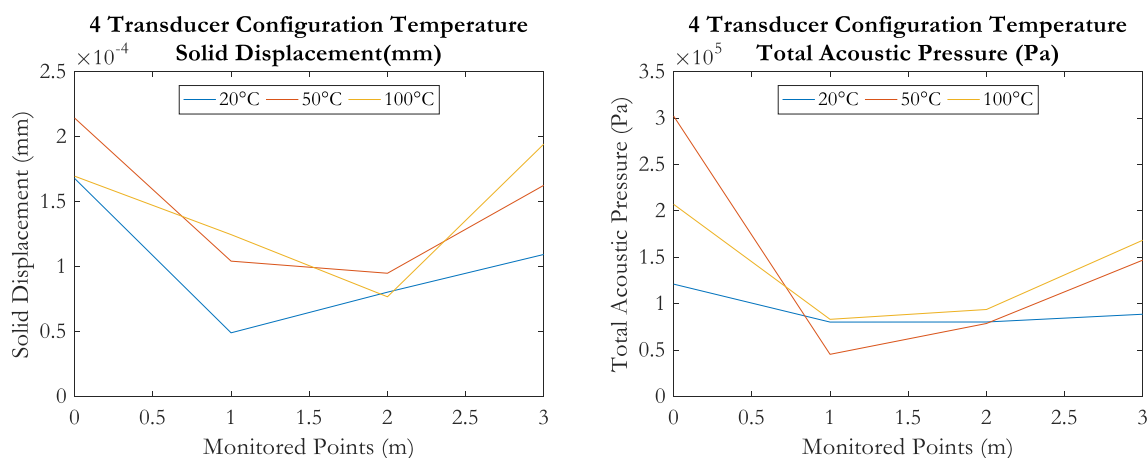
Figure 6.14: Maximum solid displacement and total acoustic pressure at monitored points for each investigated fluid temperature

The 50°C case increases the total acoustic pressure of 3 Bar at the HPUT location whereas the 100 °C achieves 2 Bar, this could be due to the temperature being at the boiling point of water, the fluid used in this model. This can suggest that the increase of temperature can increase the acoustic pressure; however, when reaching boiling temperature, this will decrease. Overall, the acoustic pressure achieved along the length of the pipe does not fluctuate compared to the 20 °C case.

The addition of a 3 mm thick calcite layer on the inner wall of the pipe is then investigated (see Figure 6.15). The displacement shows to have a small variation at the excitation location; however, along the length of the pipe, the amplitude fluctuates between high and low amplitudes. This could suggest that the addition of the calcite has affected the wave propagation across the structure, resulting in a shift in the nodes and antinodes at the monitored points.
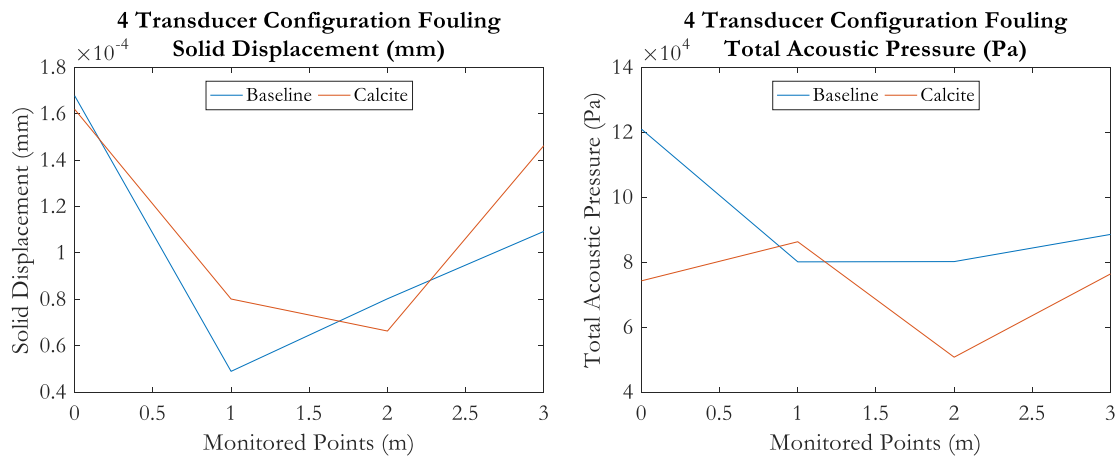
Figure 6.15: Maximum solid displacement and total acoustic pressure at monitored points for each investigated non fouling and fouling case

The acoustic pressure shows a reduction due to the addition of calcite at the HPUT location, which could be explained by the calcite layer attenuating the vibration through the pipe thickness into the liquid domain. At 1 m, there is an increase in acoustic pressure which matches to the high displacement. The remainder of the acoustic pressure of the calcite matches similarly to the increase and decrease in displacement. This shows that the calcite layer attenuates the wave propagation as has been discussed in Chapter 5.

When investigating an alternative waveform to the sinusoidal input in Figure 6.16, it is shown that the square wave input has increased the displacement and the acoustic pressure across all monitored points. The acoustic pressure achieves the minimum 1 – 2 Bar of pressure which is the known threshold to generate cavitation for a 40 kHz HPUT [66]. This provides more evidence that the 4- HPUT case can potentially achieve long-range cleaning by creating pressure amplitudes above the cavitation threshold.
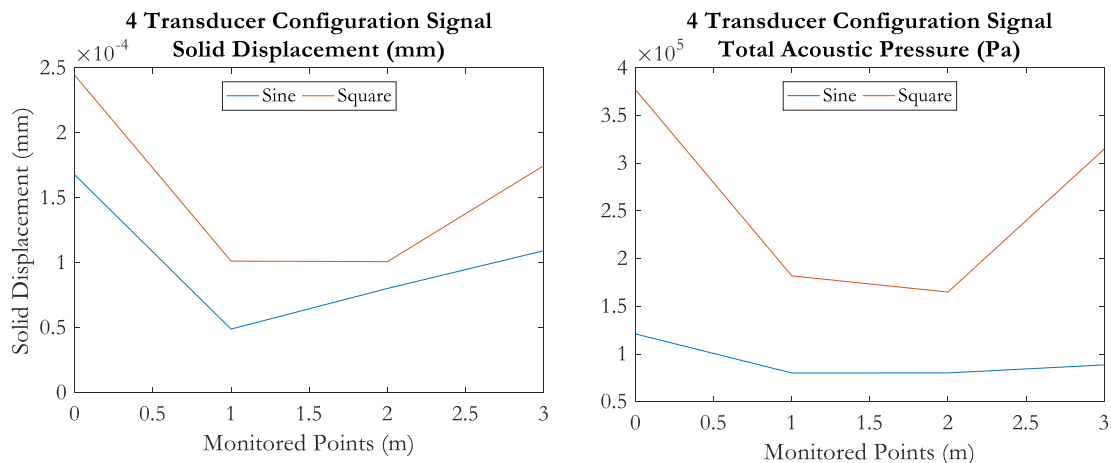
Figure 6.16: Maximum solid displacement and total acoustic pressure at monitored points for each investigated signal input

6.6 SUMMARY

This chapter has validated the FEA methodology developed in Chapter 4 and has utilised a fouling pipe sample generated in Chapter 5. The ultrasonic cleaning technique is carried out by using tailored bespoke HPUTs attached directly to the outer wall of the structure (the inner wall of pipe is filled with liquid). The excitation of the HPUT occurs at its natural resonant frequency and results in cavitation bubbles within the liquid. The implosion of these bubbles occurs in regions of high pressure, favourably on the fouled surface, results in forces large enough to remove the fouling. The experimental validation uses a PSV-400 to acquire the out-of-plane displacements of the fouled pipe sample under investigation and is compared with displacement findings in Chapter 4. The results show a promising comparison of the displacement of the pipe between the FE model and the Vibrometry results. These high nodal displacements are concentrated in the same areas of the cleaning pattern. The acoustic pressure field plotted in the FE model is compared with the pressure threshold reference of 5 Bar to determine whether the model can confirm if exceeding the cavitation pressure threshold of 5 Bar is possible. The model showed both pressure increases (compressional instants) and decreases (rarefaction instants) as large as 5 Bar.

The FE methodology is used to investigate the effects of different parameters and to optimise the HPUT configuration and input variables for cleaning a 6 m long, Schedule 40, 6 inch diameter, carbon steel pipe. A 4-HPUT configuration is selected for further laboratory trials.

Chapter 7: Laboratory Investigations for Submerged Applications

Don't analyse everything, just do it – Alex Karev

7.1   INTRODUCTION

Fouling removal trials were carried out on the fouled 6.2 meter long, Schedule 40, 6 inch diameter, carbon steel pipe created in Chapter 5. Using the optimised HPUT configuration selected in Chapter 6 the HPUTs are integrated into a user-friendly system for laboratory trials. Future applications are also studied where the HPUTs undergo marinisation.

7.2   HPUT MARINISATION

7.2.1   MARINISATION METHODOLOGY

HPUTs are typically bolted onto the outer wall of an ultrasonic bath, resulting in no contact with water, which means that this is not a requirement for a marinisation technique. The marinisation is sub-contracted to STS Defence [151]. This is done by housing the HPUT within a Restriction of Hazardous Substances (RoHS) compliant and Mercury free Polyurethane 3D printed enclosure (see Table 7.1 for material properties). This allows a marinised cable to run through the housing, which is then soldered onto the contact plates of the HPUT. Once the cable is attached to the HPUT electrodes (similarly to Figure 7.1), a RoHS compliant and Mercury free Polyurethane potting is injected into the housing, and then filled to the opening of the housing to ensure that the contact plates and PZT are sealed from any water contact. The design of the 3D printed enclosure is shown in Figure 7.2.

Figure 7.1: Example of cable connection to HPUT using a male BNC test lead cable
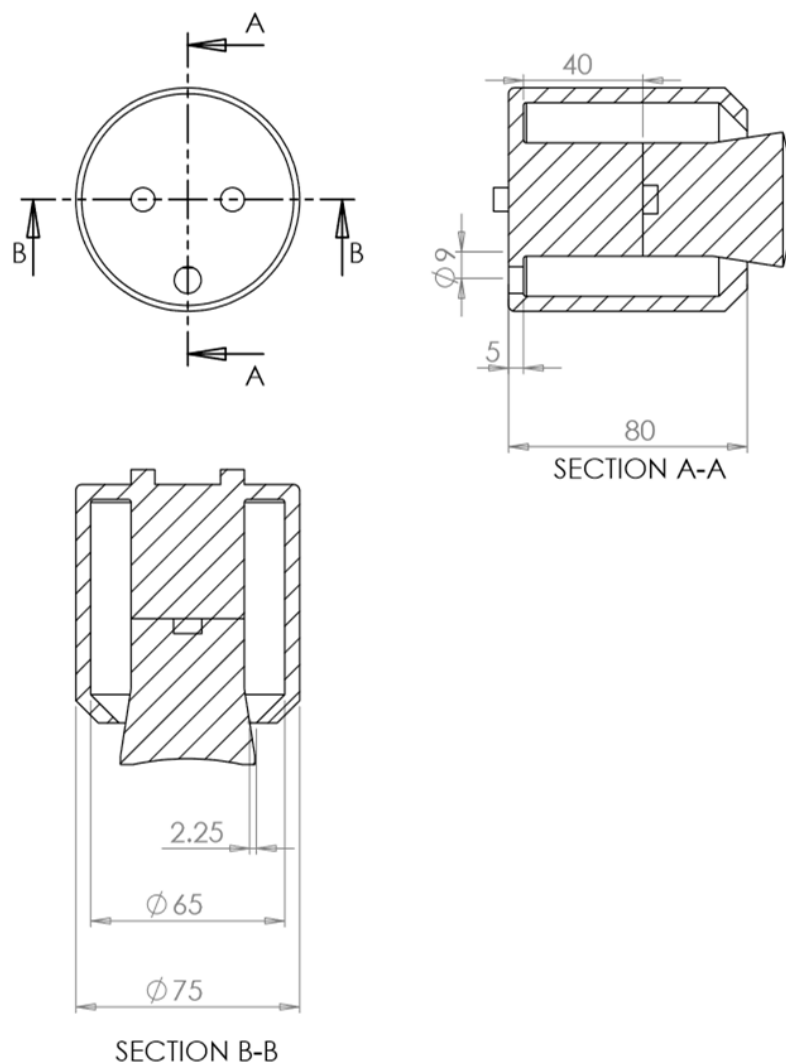
Figure 7.2: Technical drawing of 3D printed housing to encapsulate the 40 kHz HPUT

Table 7.1: Material properties of Polyurethane used for marinisation of the HPUT

Polyurethane	
Test	Result
Flammability	Not flame retardant
Volume Resistivity	13 - 1510 ohm.cm
Surface Resistivity	12.5 – 14.510 ohm.cm
Di-electric Constant	3.1
Breakdown Voltage	20 KV/mm
Hardness	70 Shore A
Tensile Strength	3-4 MPa
Operating Temperature	-55 to 130 °C (application & geometry dependent)
Elongation at Break	200%

Each HPUT is connected to a flame retardant, halogen free, 6.4mm diameter, marinised RG58 cable. A cross section of the cable along with material descriptions are found in Figure 7.3 and Table 7.2.
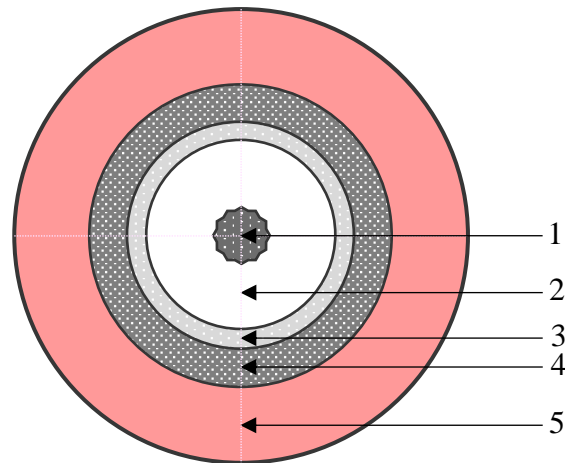
Figure 7.3: Cross section of marinised RG58 cable

Table 7.2: Component and material description of marinised RG58 cable

#	Component	Material
1	Central Conductor	Tinned Copper
2	Dielectric	Solid Polyethylene
3	Outer Conductor	Tinned Copper Wire Braid
4	Inner Jacket	PVC TM2
5	Outer Jacket	Polyurethane

The confirmed number of HPUTs found in Chapter 6 underwent marinisation with a 10 meter long marinised cabling with a BNC connection, a summary of the marinisation requirements is found in Table 7.3.

Table 7.3: HPUT marinisation requirements

Specimen	Quantity	Cabling	HPUT Marinisation	3D Printed Housing
40 kHz HPUT	4	Connection from electrode plates to male BNC (cable to be marinised). Length of 10 meters	Putty to cover electrodes and cabling – metal front mass of HPUT does not require marinisation	HPUT housing to surround putty to be 80 mm in outer diameter

Chapter 7: Laboratory Investigations for Submerged Applications

7.2.2 HPUT MARINISATION CHARACTERISATION

To characterise any changes of power delivery to the HPUTs by the addition of the marinisation material, the Agilent 4294A Precision Impedance Analyzer [109] was used to measure the 40 kHz HPUTs before and after marinisation.

Figure 7.4 shows the addition of the marinisation material has increased the impedance of the HPUTs resonant frequency which also contributes to a partial shift in the resonant frequency. The anti-resonant frequency has reduced in impedance, implying that the marinisation technique is dampening the HPUT components. This causes the HPUT to become more broadband.
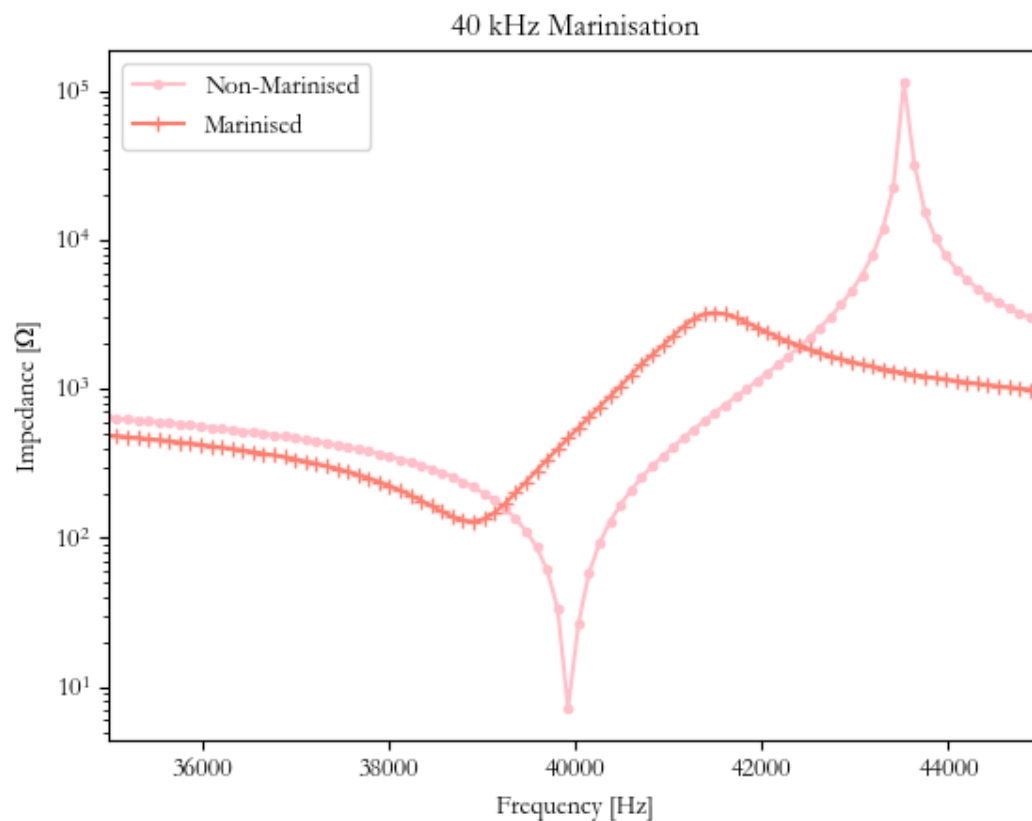
Figure 7.4: Impedance characterisation of 40 kHz HPUT before and after marinisation

7.3 LABORATORY TRIALS

Although the impedance characterisation has shown potential power loss due to the marinisation technique, the HPUTs undergo initial fouling removal trials on the fouled 6.2 meter long, Schedule 40, 6 inch diameter, carbon steel pipe created in Chapter 5. The hardware and software developed by the Brunel Innovation Centre [152] is described to drive the 4-HPUT configuration.

7.3.1 POWER ELECTRONICS

The power amplifier box includes a signal generator that splits into two channels, where each channel is connected to two amplifiers and each amplifier is connected to a load box providing two outputs. Overall, this results in 8 outputs as shown in Figure 7.5.
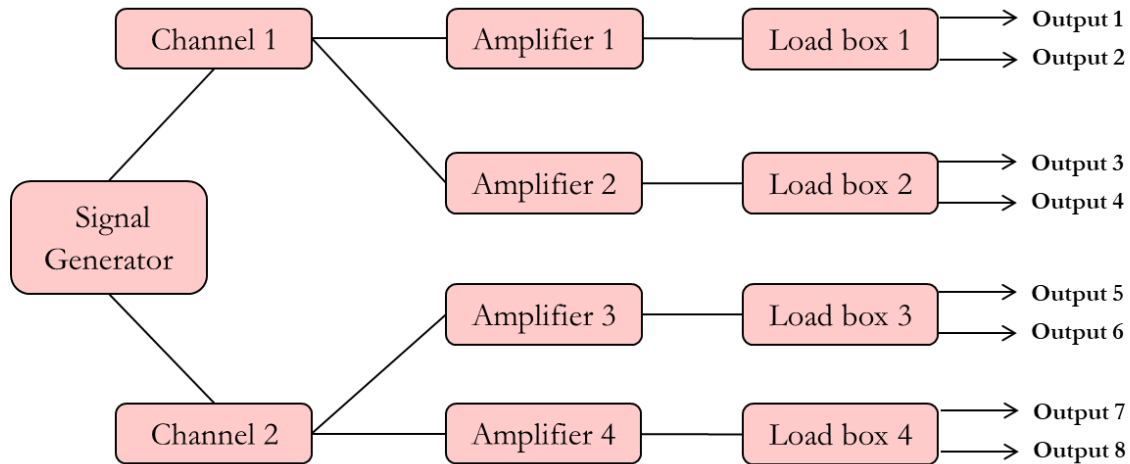
Figure 7.5: Power electronics system schematic

Power amplifier specification:

- Power 4 x 100 W RMS, High Voltage Amplifier
- Power Supply control 100-300 V, adjustable voltage via dimmer & QT_Sendwave
- Maximum current output 5 A RMS
- Operating Frequency 10-300 kHz
- Load Box with current protection, allowing off resonance voltages up to 1000 V
- Programmable 2 channel output signal generator
- 2 channel signal generator – two different outputs simultaneously
- Each signal generator drives 2 amplifiers
- 8 continuous wave output channels (2 per channel 4 per output)
- Single sinusoids and chirp functions
- Arbitrary function generator possible with software upgrade
- Power monitoring functions
- Power supply monitoring functions
- Logging, auto restart and parameter persistence functions
- Raspberry pi with touch screen interface
- 2 USB ports
- Fan cooled
- Isolated transformer

Table 7.4 displays the final system features, this shows that each channel is driven by a signal generator that can be controlled by the user using the Rasberry Pi touchscreen interface, allowing the user to change the signal wave, frequency, power and sampling. The final hardware is developed and shown in Figure 7.6.

Figure 7.6: Bespoke High Power Amplifier

Table 7.4: Final system features

Hardware requirements		
	Specification	Prototype
Powered by	Mains	Mains
Voltage, V	240	100-300 V
Dimensions (L x W x H), cm	50 x 30 x 20	37 x 36 x 23
Weight of the system, Kg	<10 Kgs	1.5 Kgs
Number of channels	4	8
Inputs signal generators	4	2 individual signal generators
Pulsed or continuous excitation	Continuous	Continuous and pulsed
Controlled by laptop?	Yes	Raspberry Pi
Description about the encapsulation	Standard casing	Standard casing

7.3.2 POWER ULTRASONIC SOFTWARE

The software requirement to control the wave parameters to input into driving the HPUTs are listed in Table 7.5.

Table 7.5: Software requirements

Power Ultrasonic Software Requirements	
Capabilities of the software. *i.e.* change the parameters based on the modelling results	1. Insert the input signal limits, *i.e.* frequency limits and number of samples. 2. Control the power. 3. Display the input signal. 4. Display the power outage from the transducer.
Capability of driving the hardware	Yes
Level of user-friendliness	Basic (knowledge of ultrasonic cleaning process is important)
Data acquisition capabilities	Yes
Data storage	Yes – laptop
Reporting capabilities	Desirable

Software Architecture

- High voltage and high frequency operation achieved via dedicated high power OP (PA90) and current boosting power MOSFETs

- Maximum operating voltage 300 V and up to 5 AMPS

- Operation safety controlled by Load Box and power supply variation using Dimmer

- High Voltage supply used directly from mains supply and the use of isolation transformer to avoid shock hazards when operating the unit

- Load Box also used to match impedance of cleaning HPUTs

The software is operated via a touch screen display by following the steps shown in Figure 7.7**.**
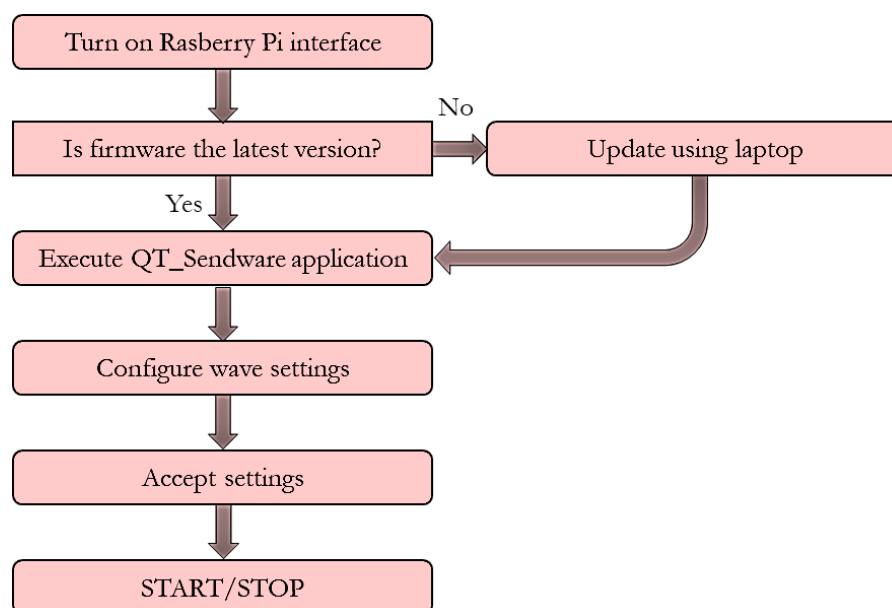
Figure 7.7: Flowchart of the software operation

Functionality

Signal generator and power monitor:

- Centred on STM32F407 chip using evaluation board providing a very cost effective solution for the supported functions needed in this design

- Single board can handle 2 channels working simultaneously

- Board has 2 DAC which can be programmed by software to generate arbitrary function

- System is designed for cleaning, so signals generated are sinusoidal and chirp signals

- 6 ADC channels used for sequential monitoring functions

- Maximum operation signal generated are 100 kHz limited by internal analogue circuitry, but extended to 300 kHz by add on circuitry

- Boards operate dedicated custom firmware that enables DAC and ADC programming functions together with communications with control software via USB

Control Computer:

- Centred on Raspberry PI 3 and 7" touch screen monitor

- Runs Raspbian Linux operation system with full GUI interface

- Dedicated application for controlling signal generation, monitoring, logging and persistence functions

- 2 Port USB interface available on the box for I/O operation

- Wi-Fi support for internet and/or remote access

The GUI interface allows to set the channel and waveform configurations. Figure 7.8 shows the screen for channel settings.
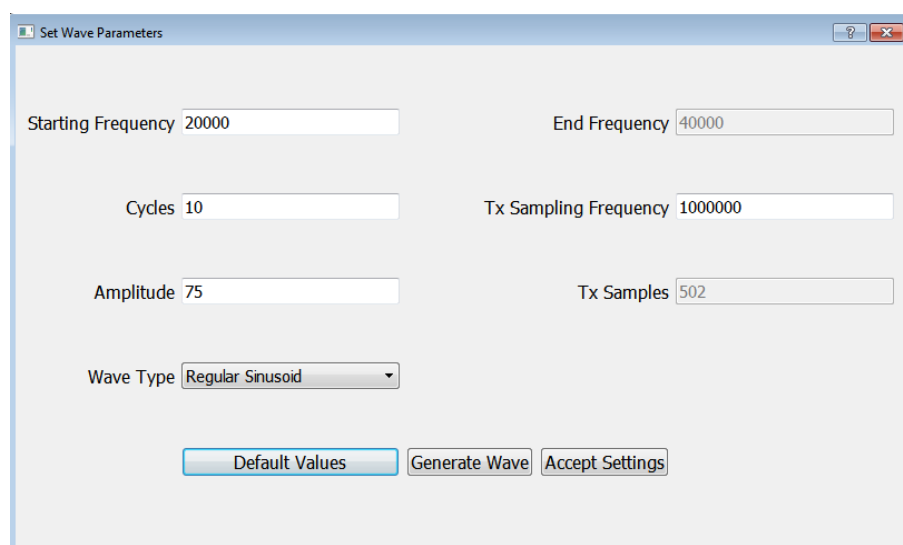
Figure 7.8: Wave generator GUI

7.3.3 HPUT COLLAR

The attachment and detachment of the HPUTs from a structure is crucial for ease of use for future commercial applications. Chapter 6 uses a ratchet strap to attach a single HPUT up to 5 Bar of pressure. For commercial use, a universal and user-friendly method to allow the HPUT configuration to be placed evenly across the circumference of a pipe with sufficient pressure (between 5-10 Bar) was designed and manufactured by InnoTecUK [153] and shown in Figure 7.9.
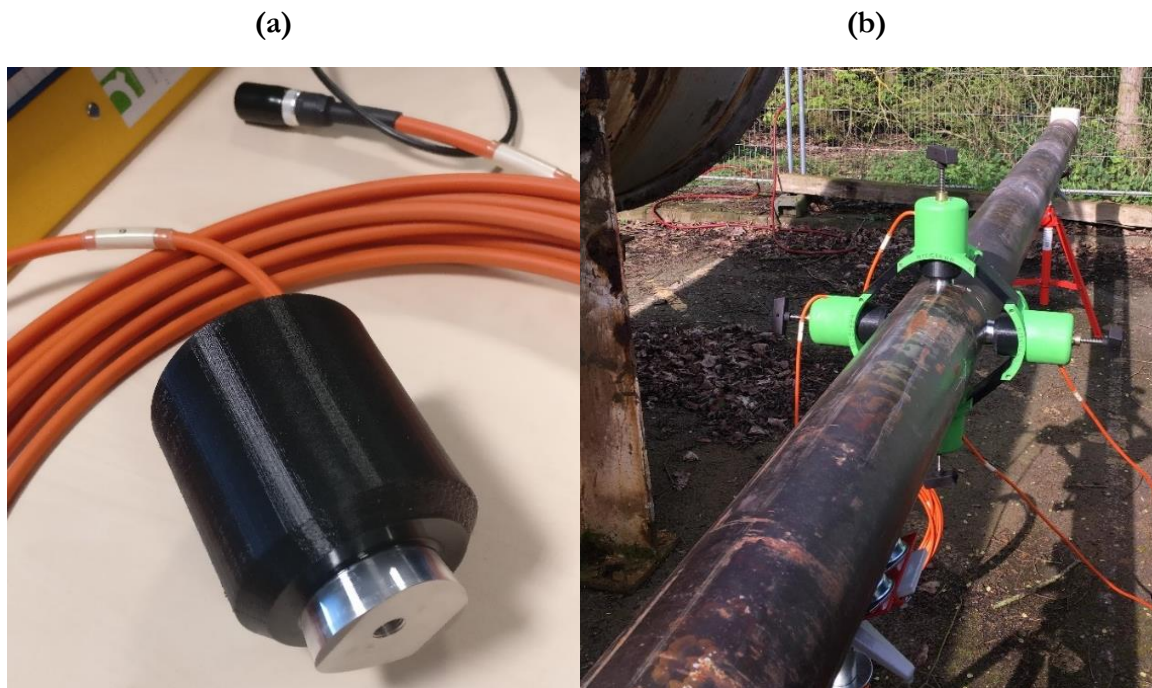
Figure 7.9: (a) marinised HPUT with marinised cabling and (b) marinised HPUTs placed into prototype HPUT collar to commence laboratory investigations

An initial HPUT collar was trialed using the marinised HPUT configuration. The pipe is filled with water and the HPUT collar is attached at the mid-length of the pipe. The high power amplifier is used to drive the HPUT configuration using a continuous 40 kHz sinusoidal waveform. The results show that the liquid within the pipe has discolored after a cycle of cleaning, due to the detachment of fouling from the inner wall.

The HPUT are investigated with the initial HPUT prototype collar. The initial trials have shown that when exciting the transducer configuration at its resonance frequency, the fluid within the pipe darkens and more solids can be seen, which can be due to the dislodging of fouling from the inner wall of the pipe, as shown in Figure 7.10.
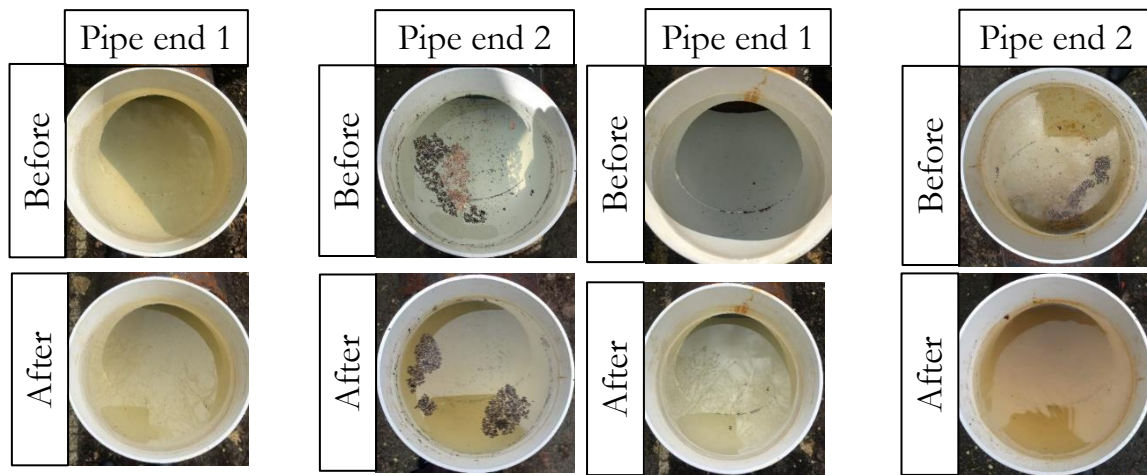
Figure 7.10: Examples of fouling removal results displaying increase in material dislodged into water after one cycle of cleaning

7.4 TRANSDUCER ARRAY VALIDATION

The final HPUT collar was designed and manufactured (Figure 7.11), and then used to further analyse the HPUTs to compare the HPUT array, marinisation effects and maximum out-of-plane displacement across the monitored points. This is carried out by using the Polytec CLV-3D Laser Vibrometer to scan point data along the length of the pipe as shown in Figure 7.12. Similar to the work carried out in Chapter 6, the HPUTs are excited in 1, 2 and 4 HPUT configurations to compare these findings with the trends shown from the FE model.
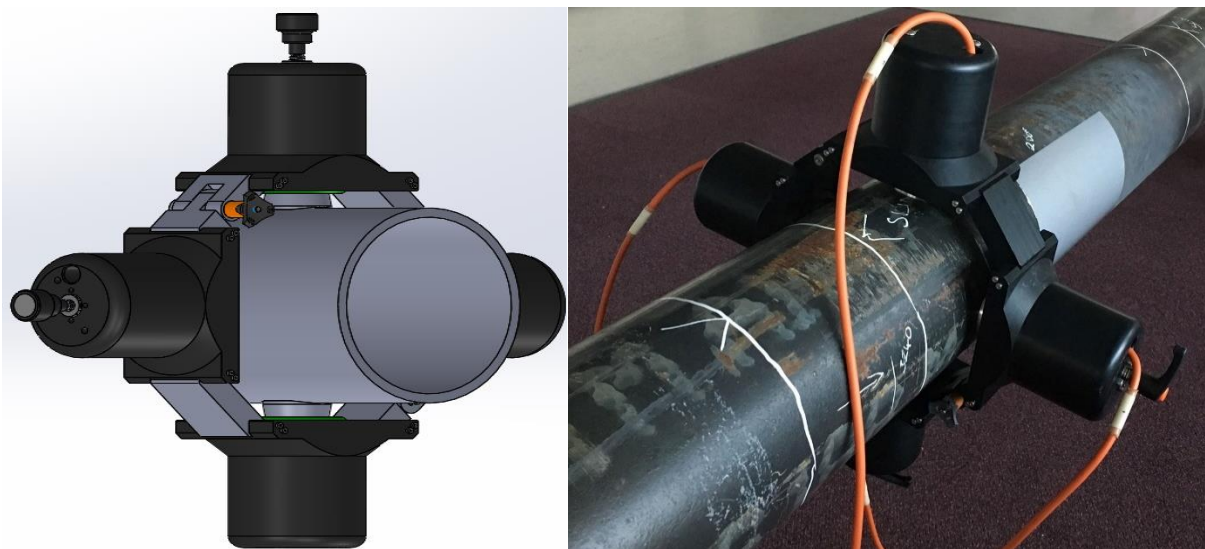
Figure 7.11: HPUT Collar CAD (left) and placed onto 6 inch pipe (right)
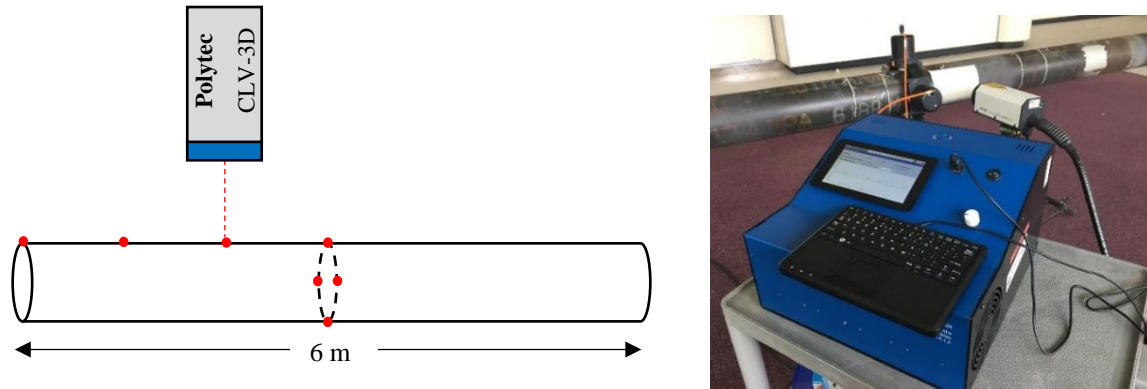
Figure 7.12: Point data along length of pipe using Polytec CLV-3D Laser Vibrometer

7.4.1 RESULTS

For the 0 meter case, results are taken 20 centimeters away from the HPUT configuration (Figure 7.13). From comparing the HPUT configurations, there is a clear trend of an increase in achieved amplitude with an increase in number of HPUTs within the array. Over the length of the pipe, the displacement achieved at the monitored point reduces (Figures 7.14-7.16). The addition of water contributes to the reduction in amplitude due to the attenuation of the ultrasonics into the liquid medium. However, at 0 m, the non-marinised 4-HPUT configuration increases with water and can be due to generating high pressure fields within the liquid.
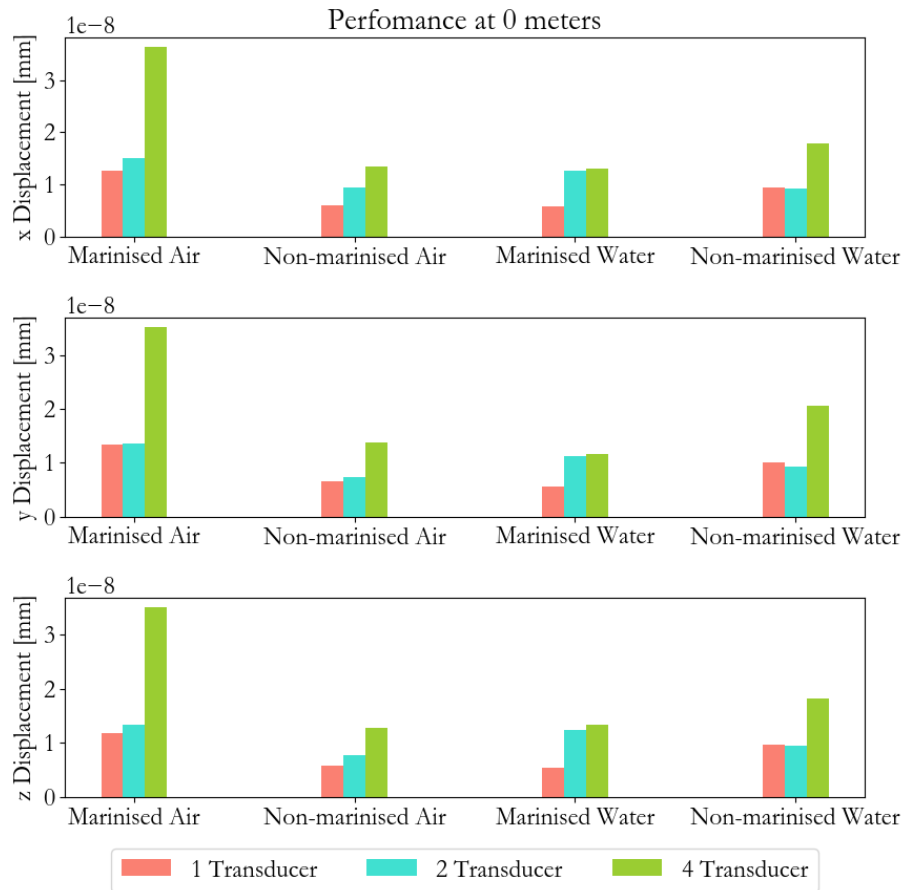
Figure 7.13: HPUT configurations under air and water conditions at 0 meters

There is not a clear conclusion on whether there is a reduction in displacement as a result of the addition of the marinisation material. This is due to having fixed monitored points that may not represent the maximum displacement achieved as there may be a shift in the distribution of standing waves across the structure due to the marinisation. Overall, for both cases, there is a similar trend of a reduction in amplitude across the length of the structure.
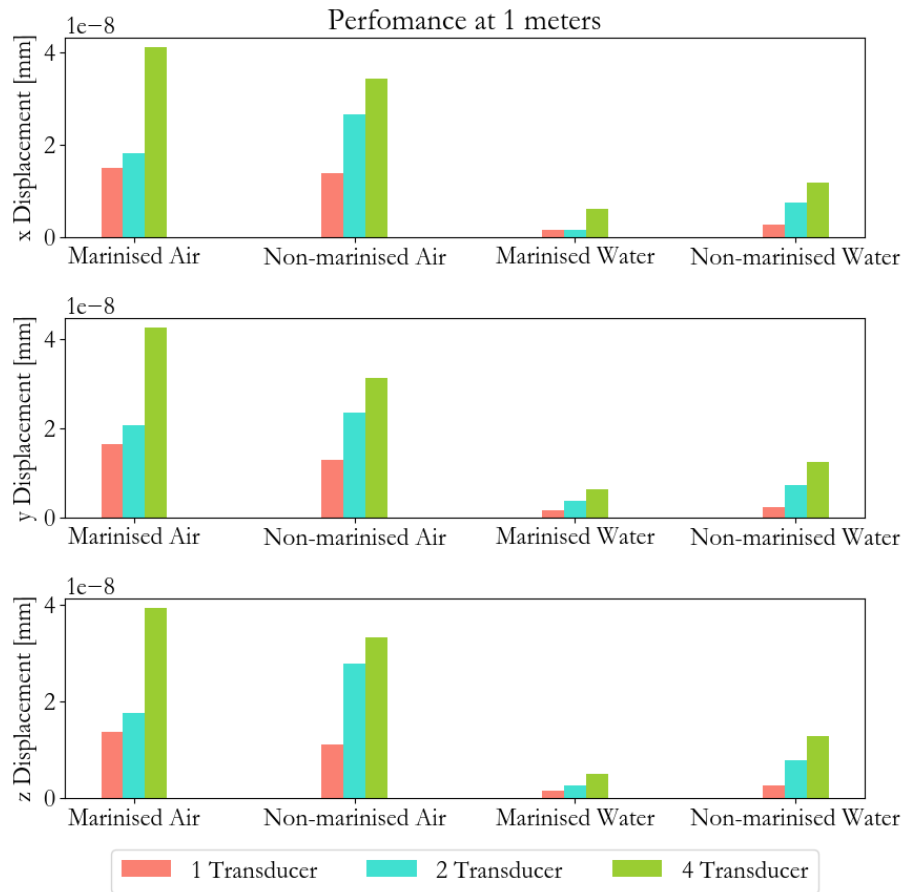
Figure 7.14: HPUT configurations under air and water conditions 1 meters
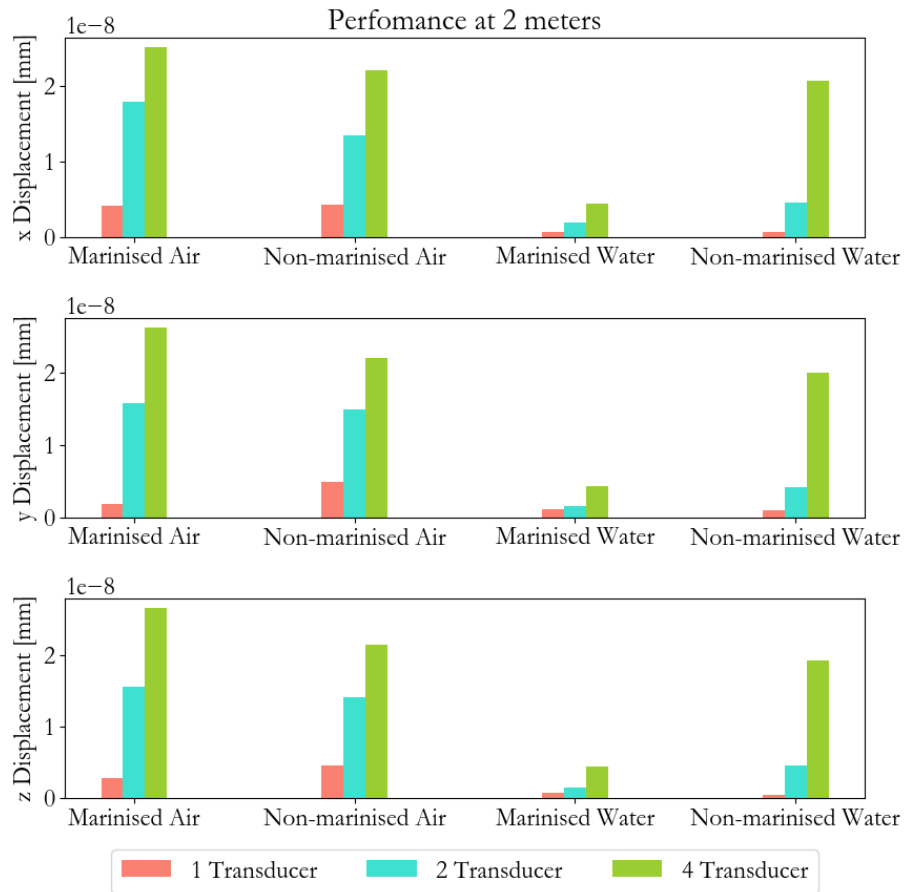
Figure 7.15: HPUT configurations under air and water conditions at 2 meters
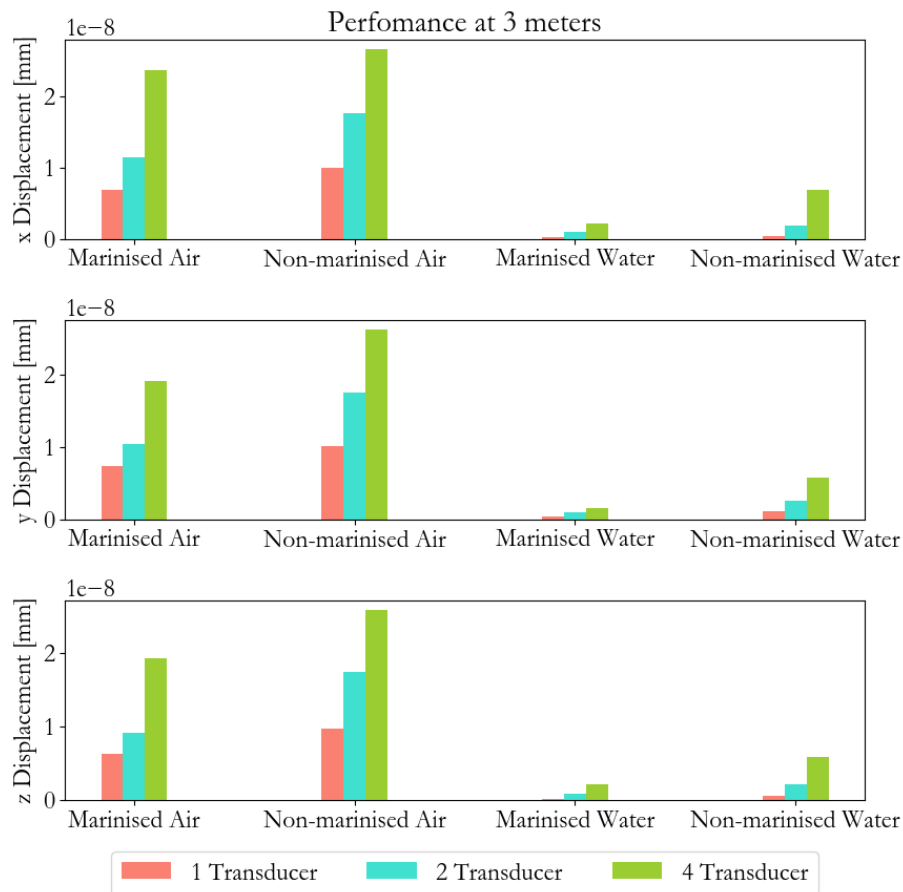
Figure 7.16: HPUT configurations under air and water conditions at 3 meters

7.5 COMPLETE SYSTEM FOR OFF-SHORE APPLICATIONS

The system consists of two technologies, the fouling removal system and the fouling detection system (discussed in Chapter 5). Both systems work together to detect fouling before carrying out fouling removal, which can then be monitored to determine the fouling removal effectivity. The architecture of the system is shown in Figure 7.17.

The UGW collars are configured for pitch-catch where one collar excites a discrete pulse and the second collar receives the signal. This signal is monitored where the variation in signal amplitude varies with the increase of fouling accumulation and reduction in fouling due to cleaning. The UGW collars are placed on each side of the HPUT collar as shown in Figure 7.18.
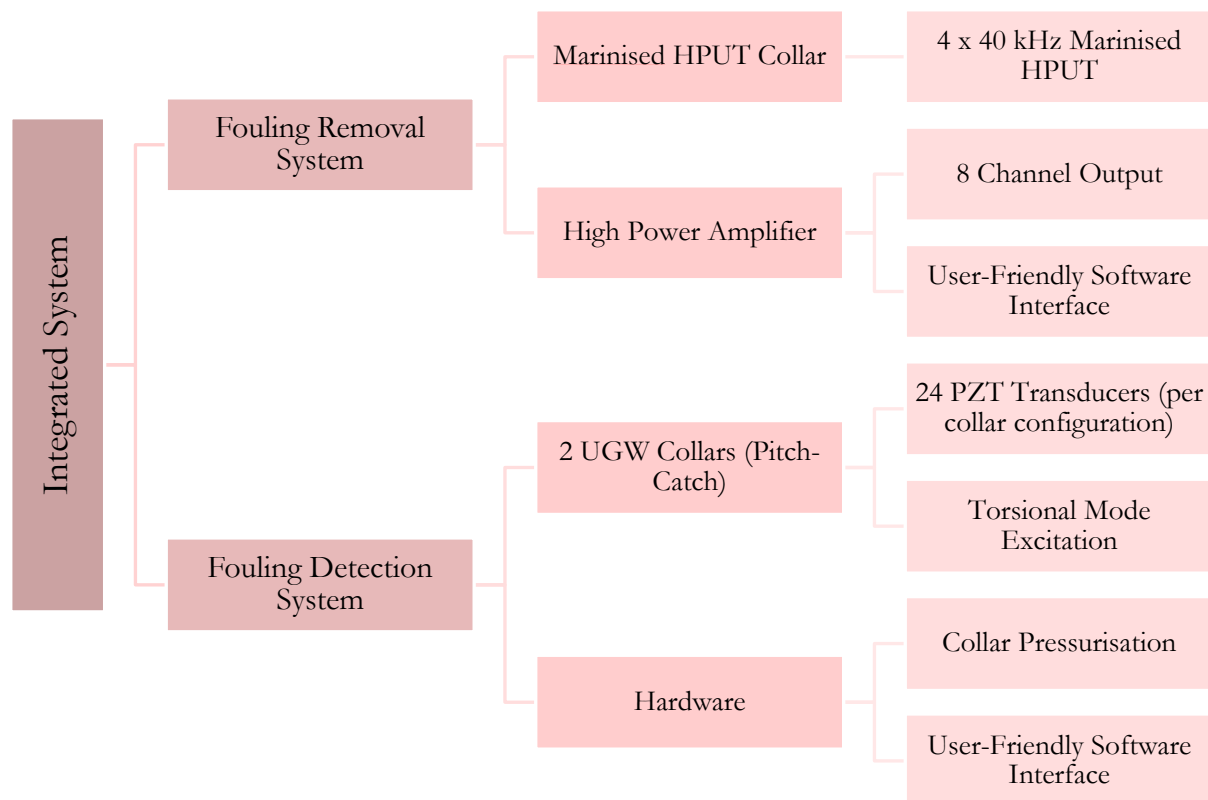
Figure 7.17: Integrated System Architecture
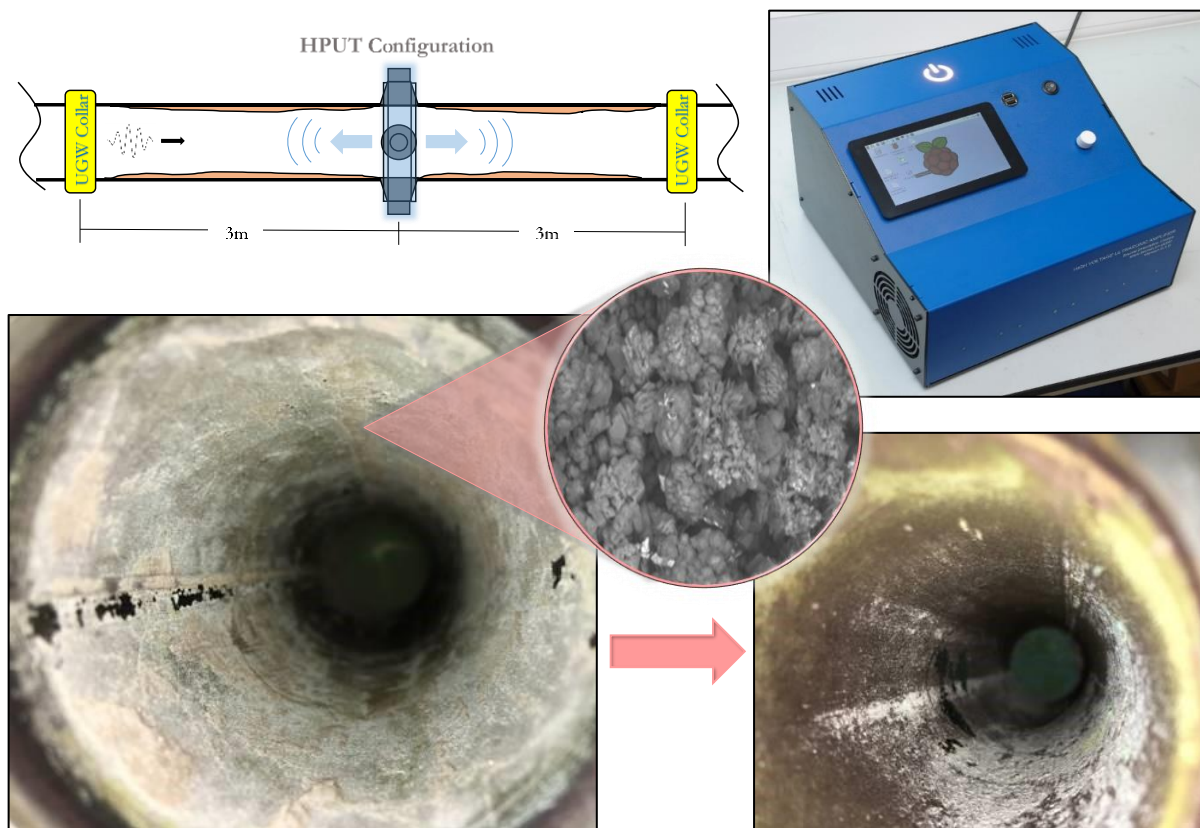
Figure 7.18: Integrated system schematic, displaying cleaning results after a cycle of fouling removal

7.5.1 UNDERWATER DEMONSTRATION

The demonstration tank consists of a sample 2.5 meter long, Schedule 40, 6 inch diameter carbon steel pipe which is placed through a tank enclosure as shown in Figure 7.19. The tank is supported by a steel frame and the pipe is supported by two pipe supports. The section of the pipe which is encapsulated by the tank is sealed using O rings and vacuum lubrication. The pipe ends are closed using flanges where one end includes a valve to allow water to be filled within the pipe. The tank consists of a tap at the bottom panel to allow the water to be drained out. With the completion of the tank assembly, the HPUT collar is placed underwater as shown in Figure 20. Due to the length of the pipe, a single UGW collar is placed at a pipe end outside of the tank for pulse-echo configuration. The power amplifier hardware is used to drive the marinised HPUTs and the Teletest unit [154] is used to pressurise the UGW collar and monitor the pipe.

Figure 7.19: Assembly of the integrated system demonstration tank
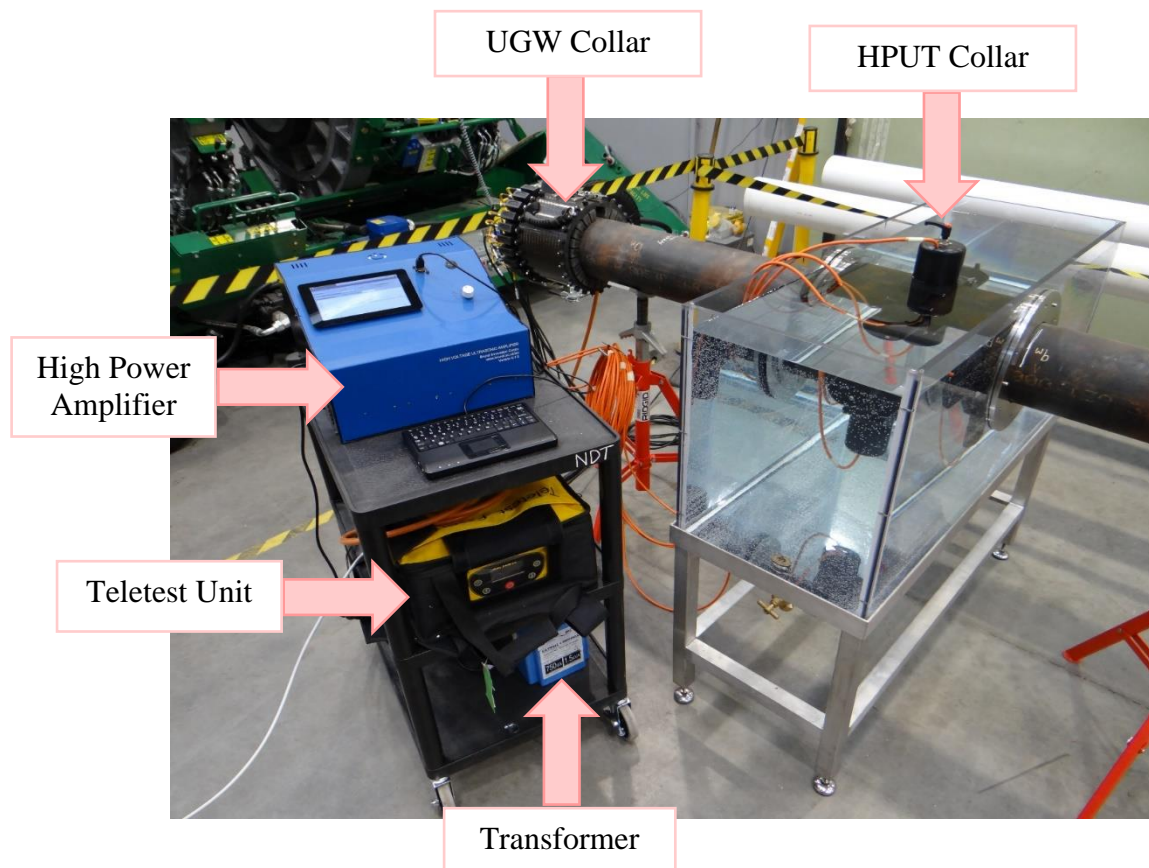
Figure 7.20: Final set-up of ultrasonic cleaning and UGW detection demonstration tank

7.6 FIELD TRIAL

A sample Schedule 40, 6 inch diameter u-bend pipe was received from ESSAR [155]. The specimen is placed upright and is filled with water. The non-marinised HPUT collar is attached approximately 200 mm below the flange as illustrated in Figure 7.21 and shown in Figure 7.22. This is left to excite the pipe for a 30 minute cleaning cycle.
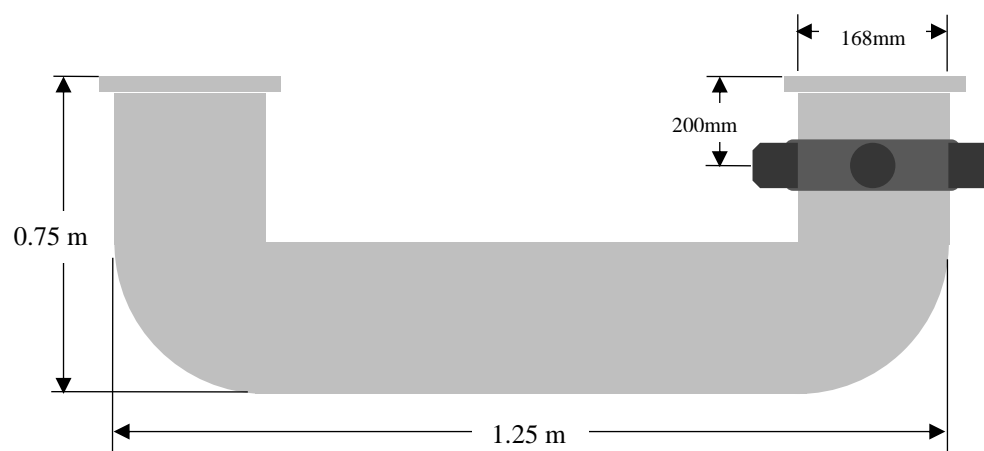
Figure 7.21: Schematic of U-shape pipe specimen
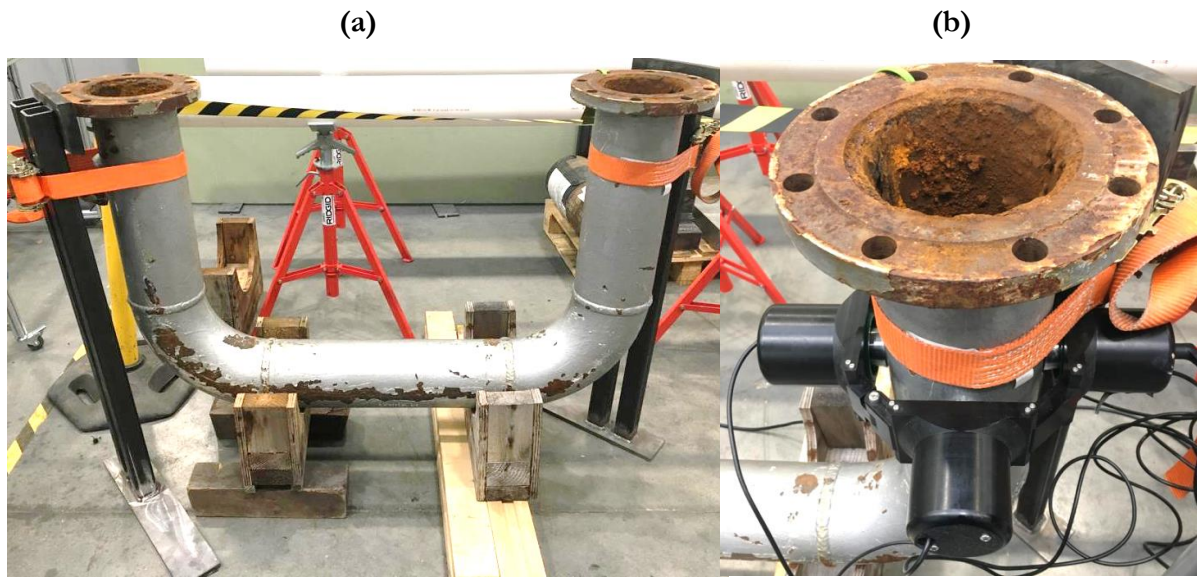
Figure 7.22: (a) u-shape pipe set-up for fouling removal and (b) attachment of HPUT
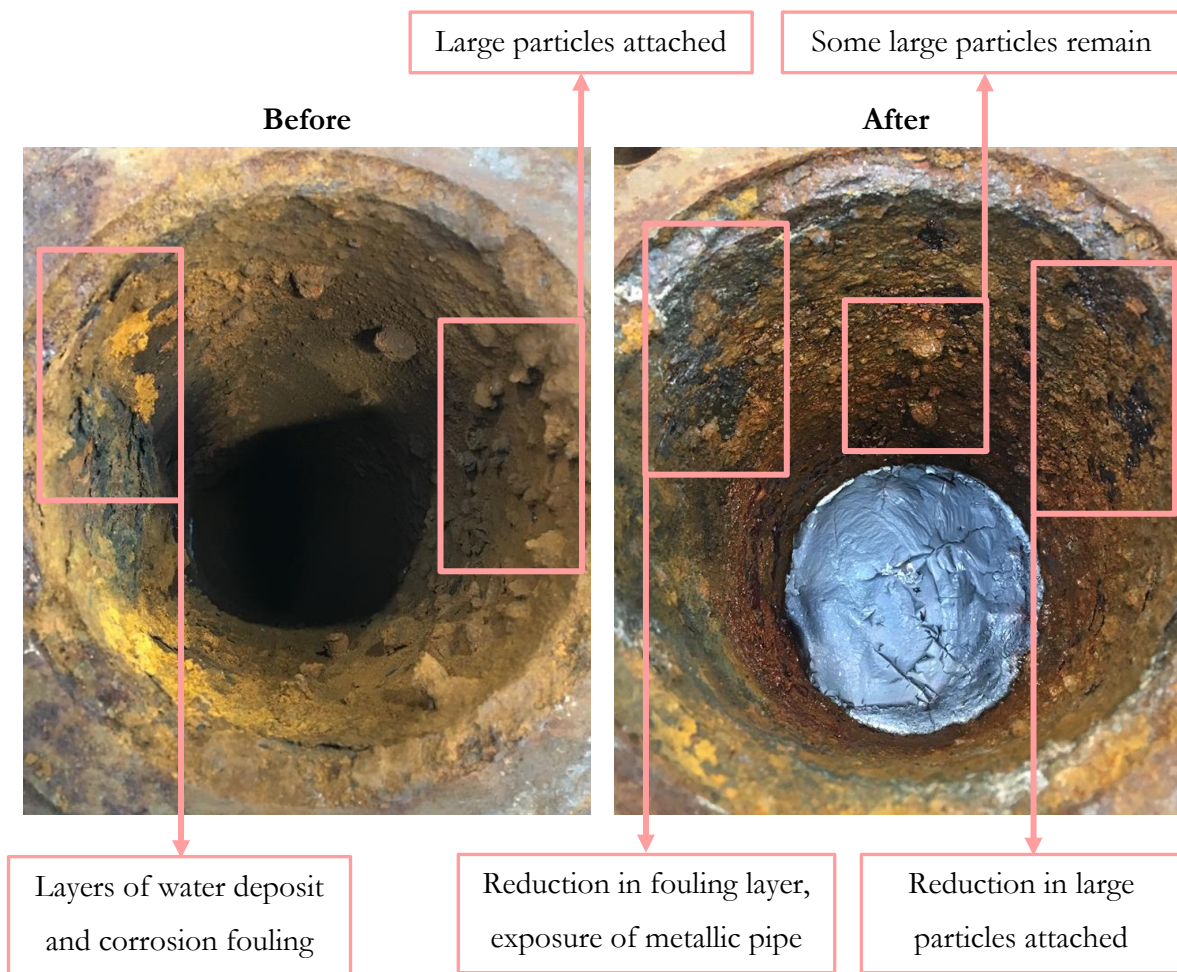
Figure 7.23: Before and after image of the inner wall of the U-shape pipe

Due to the thickness of the fouling, there is only a partial reduction of fouling of the larger deposits. Various parameters have an influence on the achieved performance, as discussed in Table 7.6.

Table 7.6: Ultrasonic cleaning limiting parameters and further suggestions for optimisation

Parameter	Limitation	Performance Optimisation
Fouling Thickness	Takes longer to breakdown fouling layer	Optimise cleaning time to account structural constraints. This will increase the cleaning time duration and may require wave input optimisation to account for attenuation.
Pipe Wall Thickness	Reduction of delivery of power into liquid	
Structural Coating	Attenuation power delivery from HPUT into metallic structure	
High Power Amplifier Hardware	Power delivery into HPUT to compensate for power loss due to pipe thickness and coating	Improve power output and optimise wave generation *i.e.* square wave

This show key parameters that can attenuate the delivery of the ultrasonic vibrations into the fluid medium to generate cavitation. With the thickness of the pipe wall and fouling, as well as the structural coating, these factors can be investigated further within the FE model to develop solutions to counterattack these parameters. The hardware for driving the HPUTs can also contribute to overcoming the attenuation of the vibration due to the aforementioned parameters by supplying more power to compensate for the power losses of the attenuation.

7.7   ULTRASONIC SONOTRODE FOR FOULING REMOVAL

To further improve the ultrasonic cleaning technique, Chapter 3 demonstrated the potential of the conical sonotrode for ultrasonic cleaning improvements. A feasibility trial is carried out on an 85 mm length, 50.08 mm outer diameter and 1.5 mm wall thickness, stainless steel pipe. The pipe has undergone Calcite fouling generation using electrochemistry as discussed in Chapter 5. Figure 7.24 shows both pipe specimens before undergoing fouling removal.

(a)　　　　　　　　　　　　　　**(b)**
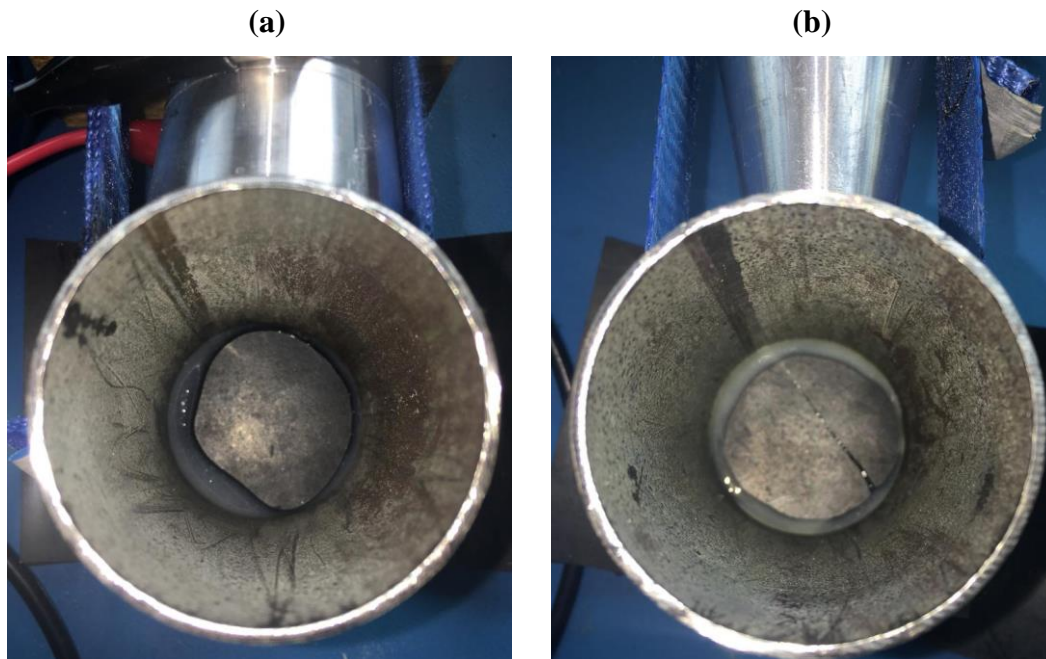
Figure 7.24: Before images of pipe specimen with 40 kHz HPUT attached (left) and conical sonotrode attached (right)

Each configuration undergoes fouling removal for 20 minutes for comparison of cleaning coverage over time. Each HPUT is excited using bespoke hardware developed by Brunel Innovation Centre [152] which inputs a 40 kHz square waveform at 2 amps of current and 200 V.

1 minute　　　　　　**10 minutes**　　　　　　**20 minutes**

Ultrasound over time
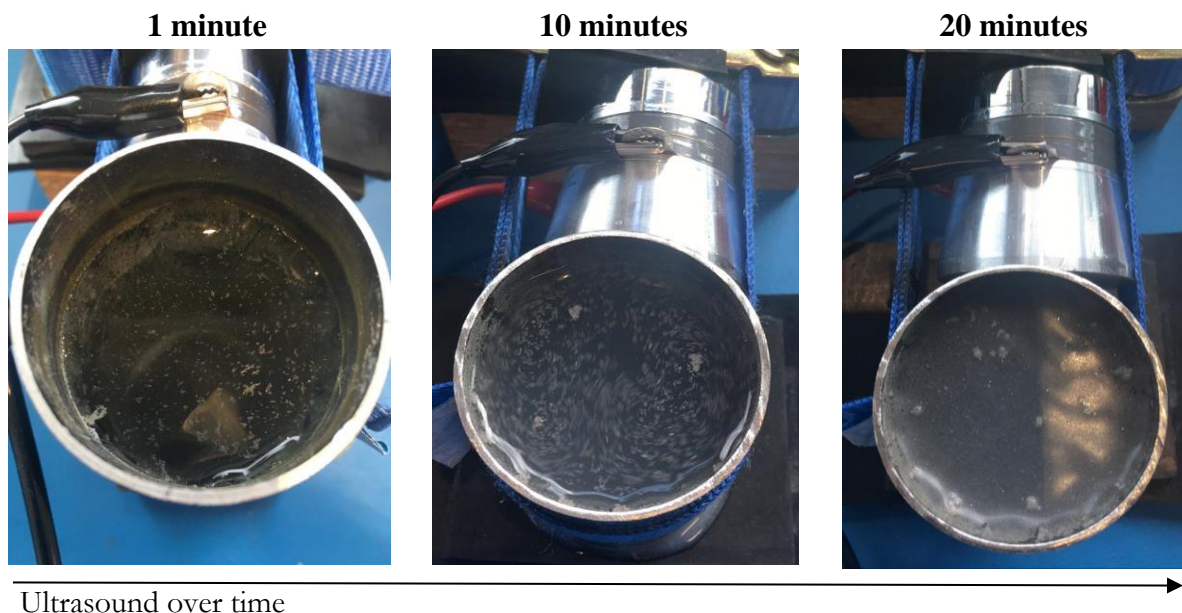
Figure 7.25: HPUT carrying out de-fouling over time

When exciting the HPUT, cavitation bubbles are generated and over time, the fouling is dislodged into the liquid as shown in Figure 7.25. For the conical sonotrode, as well as cavitation, high vibration within the liquid can be seen in Figure 7.26 across the circumference of the inner pipe wall. Figure 7.27 illustrates the angle of photography to be taken of the pipe specimens for comparison of cleaning coverage.

1 minute   **20 minutes**

Ultrasound over time
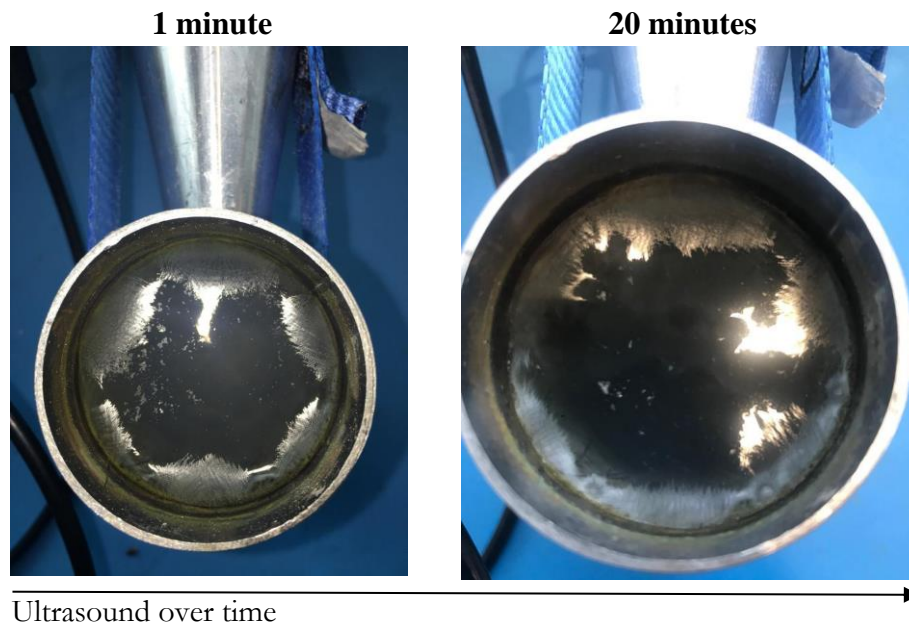
Figure 7.26: Conical sonotrode carrying out de-fouling over time

Annotation for post-fouling removal images

A – HPUT attachment location

B – Left of HPUT

C – Section furthest from HPUT

D – Right of HPUT
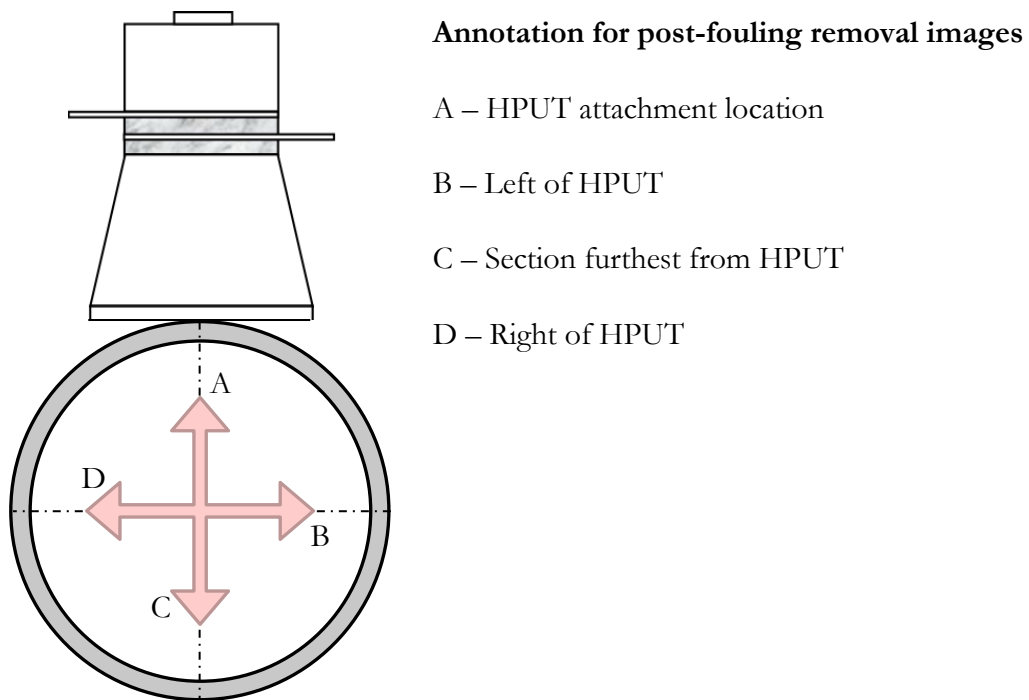
Figure 7.27: Illustration of sectional images for de-fouling analysis

Figure 7.28 compares the fouling removal on the inner wall of the pipe specimen at the HPUT attachment location. This is where highest fouling removal is expected, as the HPUT has a larger front mass diameter which allows more contact with the pipe whereas the diameter of the conical sonotrode is half the size of the HPUT. The conical sonotrode has shown to achieve a larger surface of cleaning compared to the HPUT even with a smaller diameter contact surface, due to the half wavelength sonotrode design amplifying the HPUT vibration and delivery into the pipe structure.

View A: HPUT attachment

(a)   **(b)**

Conical sonotrode attachment   HPUT attachment
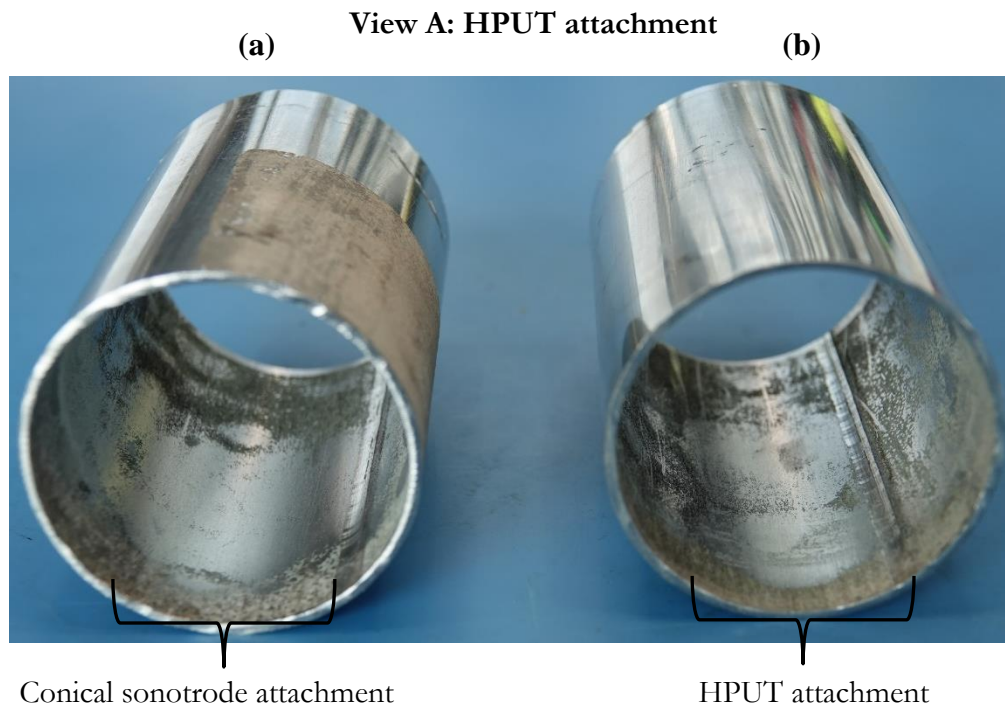
Figure 7.28: View A - HPUT attachment location for (a) conical sonotrode and (b) HPUT

From rotating the pipe specimens, Figure 7.29 displays a propagation of cleaning away from the HPUT location. The conical sonotrode achieves cleaning that is elongated along the length of the pipe whereas the HPUT has shown cleaning along the length of the pipe but consisting of nodal cleaning with remaining patches of fouling.

View B

(a)   **(b)**

Conical sonotrode attachment   HPUT attachment

(a)   **(b)**
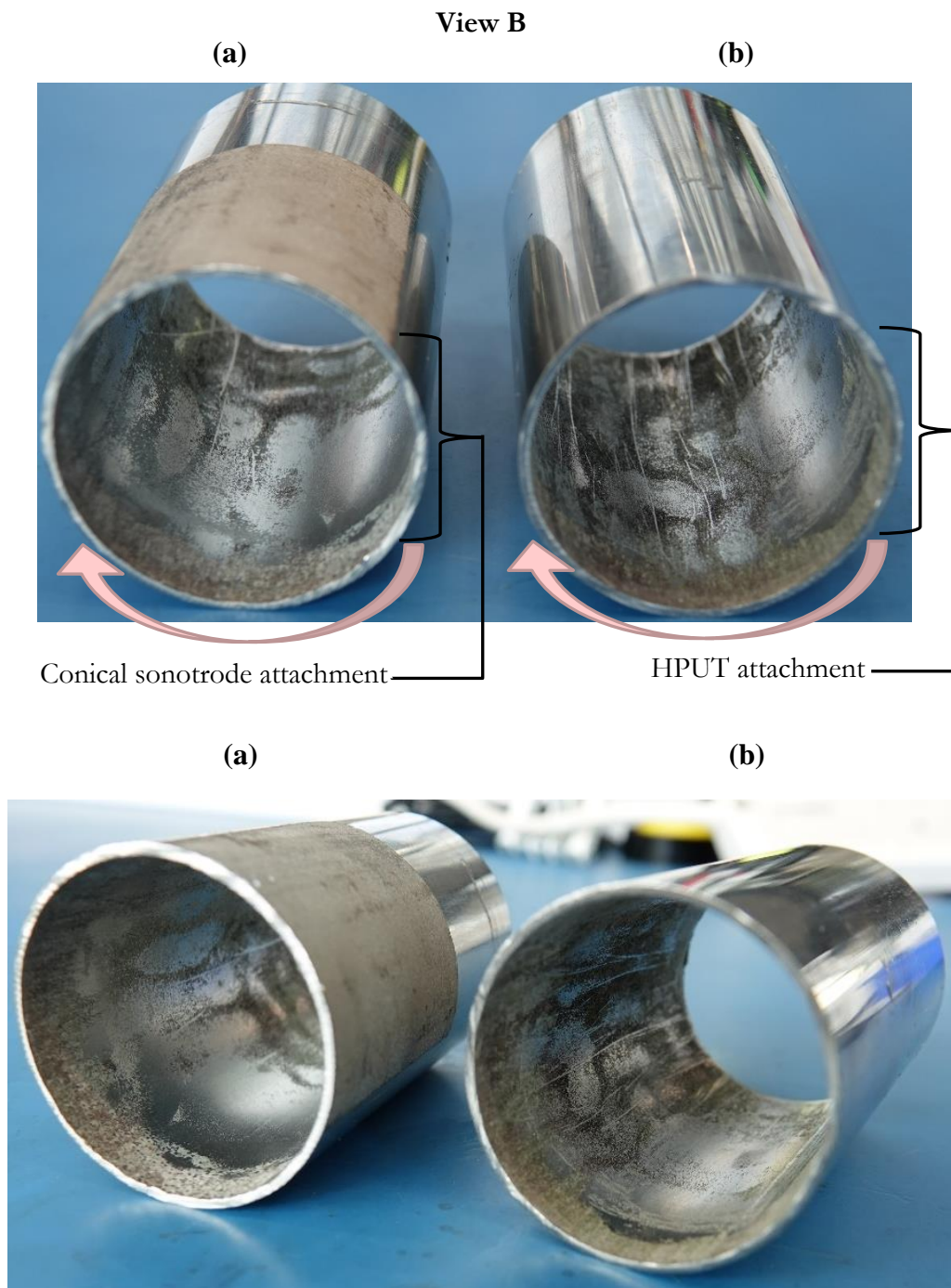
Figure 7.29: View B section for (a) conical sonotrode and (b) HPUT

The section of the pipe specimens furthest from the HPUT location is shown in Figure 7.30. Similar to the pipe walls near the HPUT location, there is cleaning along the length of the pipe. The conical sonotrode shows nodes of cleaning but with some locations of fouling remaining in between the nodes, which can be explained by a reduction in vibration across the circumference of the pipe. The HPUT shows the propagation of three nodes of cleaning along the length of the

pipe but has a larger spacing compared to Figure 7.30, which is also due to a reduction of vibration delivery to this section of the pipe.

View C: Section furthest from HPUT attachment

(a)
Conical sonotrode attachment

(b)
HPUT attachment

(a) **(b)**

Figure 7.30: View C – section of pipe furthest from HPUT excitation for (a) conical sonotrode and (b) HPUT

Figure 7.31 shows the final section of the pipe near the HPUT location, displaying a propagation of cleaning nodes along the circumference and length.

View D

(a)   **(b)**

Conical sonotrode attachment   HPUT attachment

(a)   **(b)**
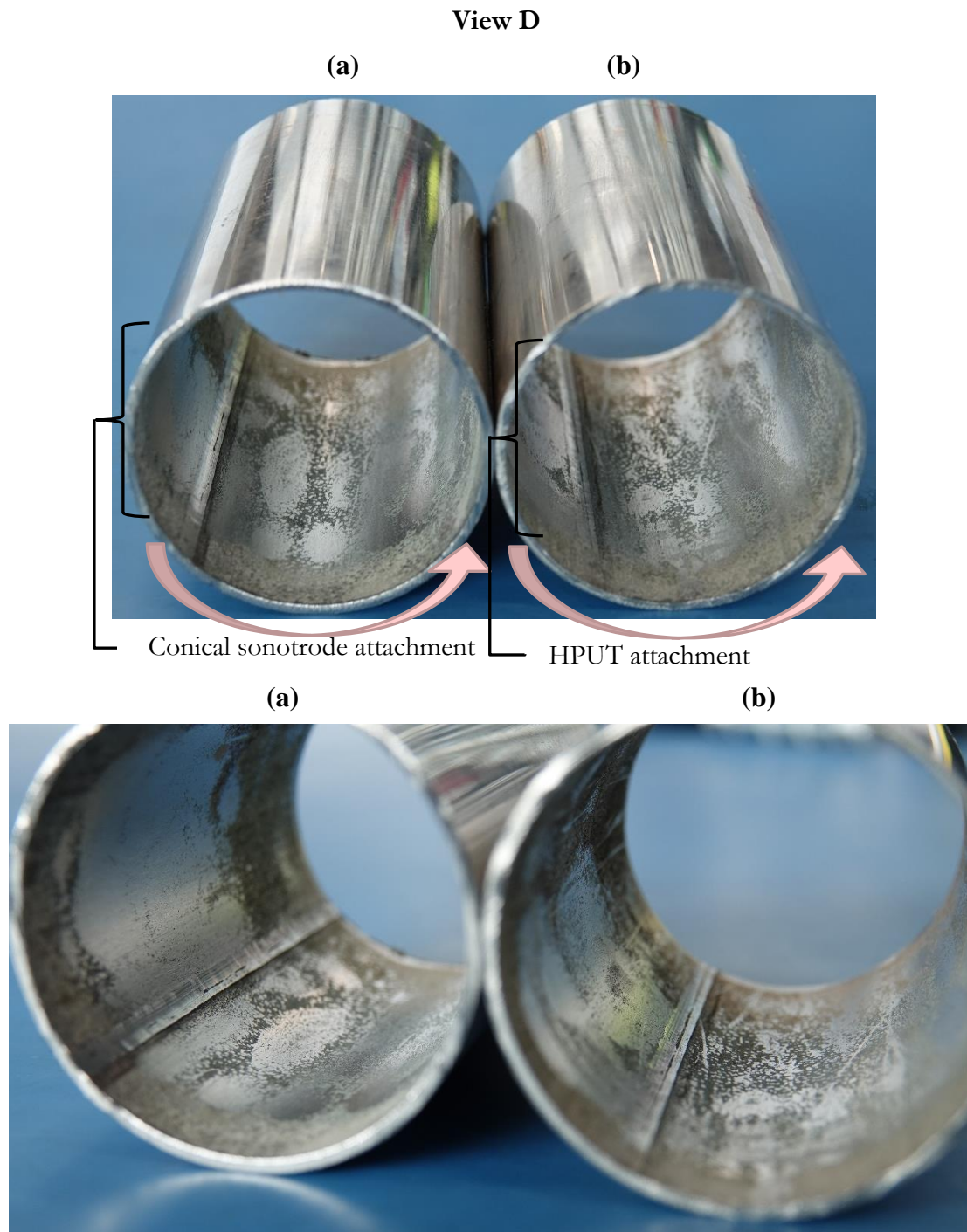
Figure 7.31: View C for (a) conical sonotrode and (b) HPUT

7.7.1   FEA Validation

Utilising the ultrasonic cleaning FEA methodology discussed in Chapter 4, the HPUT and conical sonotrode are investigated on the pipe specimen to display cleaning patterns and compare the pressure being achieved across the structure. The results are displayed for the HPUT case in Figure 7.32 and the conical sonotrode case in Figure 7.33.
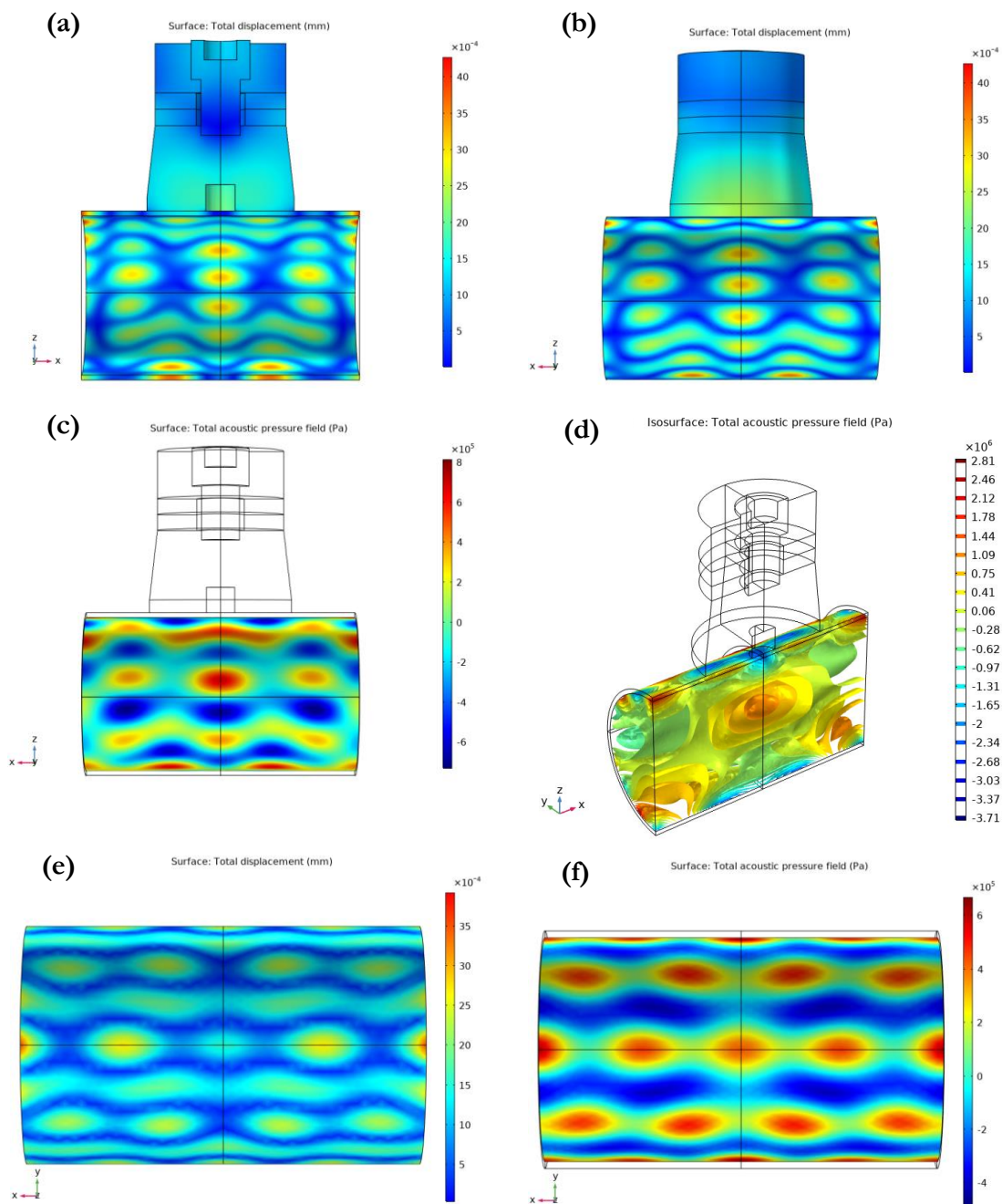
Figure 7.32: FEA results of HPUT on pipe specimen for fouling removal displaying (a) solid displacement on inner pipe wall, (a) solid displacement on outer pipe wall, (c) total acoustic pressure of fluid at inner pipe wall, (d) cross-sectional isosurface view of total acoustic pressure at center of fluid, (e) total displacement of outer pipe wall furthest from HPUT attachment location and (f) total acoustic pressure of fluid at the inner pipe wall furthest from HPUT attachment location
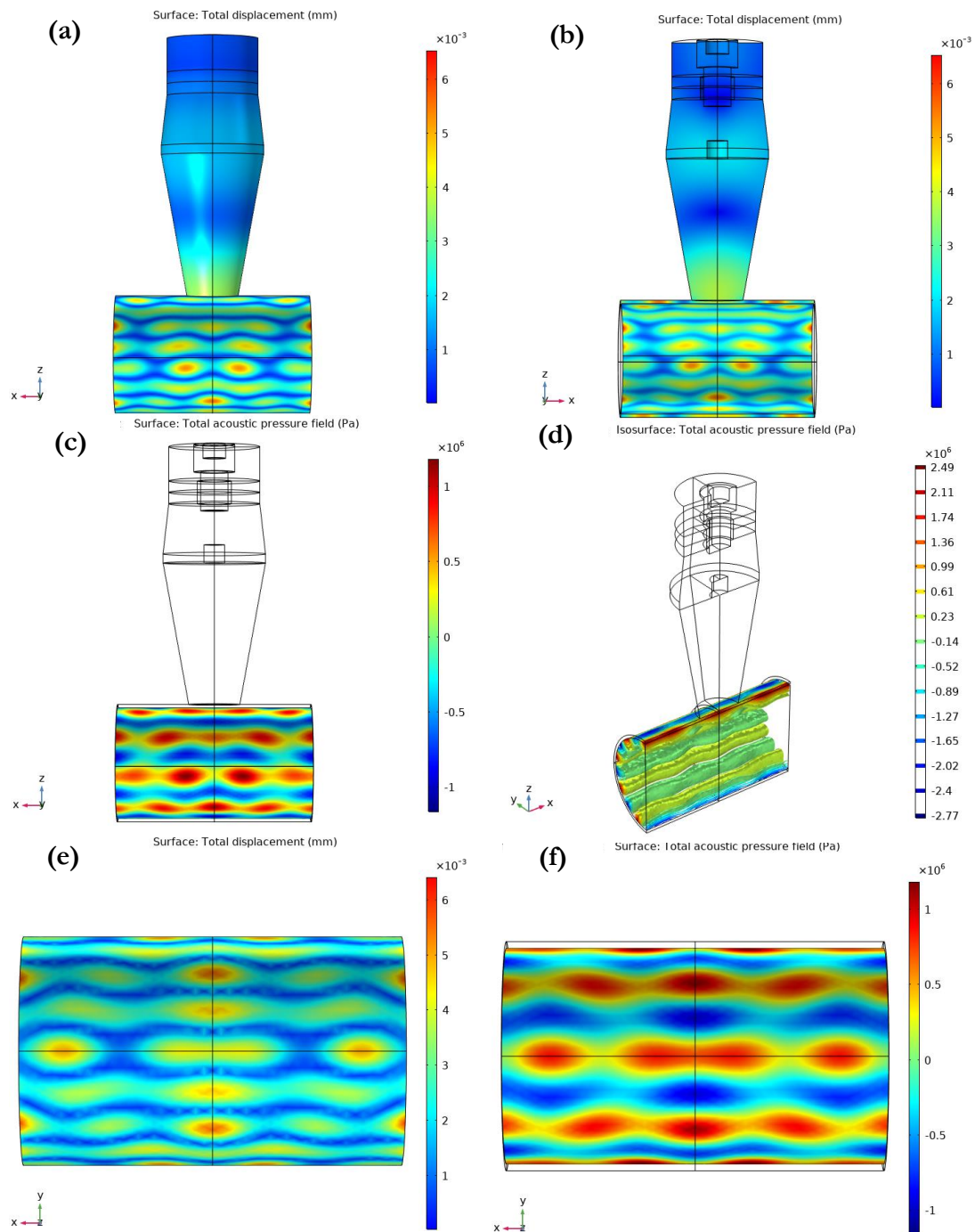
Figure 7.33: FEA results of conical sonotrode on pipe specimen for fouling removal displaying (a) solid displacement on inner pipe wall, (a) solid displacement on outer pipe wall, (c) total acoustic pressure of fluid at inner pipe wall, (d) cross-sectional isosurface view of total acoustic pressure at center of fluid, (e) total displacement of outer pipe wall furthest from conical sonotrode attachment location and (f) total acoustic pressure of fluid at the inner pipe wall furthest from conical sonotrode attachment location

A comparison with the experimental cleaning results for the HPUT attachment shows sets of three nodes propagating before developing into a nodal set of four at the furthest section of the pipe (Figure 7.32). This shows a good agreement of fouling removal patterns whilst also achieving the minimum pressure required to surpass the cavitation threshold.

Similar to the FEA and cleaning results of the HPUT case, Figure 7.33 shows that the conical sonotrode also has good agreement of the cleaning patterns with the experimental cleaning results whilst also surpassing the cavitation threshold. When comparing the FEA results for both cases, the conical sonotrodes achieve higher displacement across the pipe and higher total acoustic pressure at the interface of the inner pipe wall, which supports the improved cleaning found from the experimental investigation. When analysing the isosurface of the total acoustic pressure, the HPUT generates pressure fields into the liquid medium whereas the conical sonotrode produces a distribution of pressure field along the inner wall of the pipe. As the experiments had shown the HPUT to generate cavitation, this can be due to the HPUT delivering high pressure into the liquid medium from the attachment location. The conical sonotrode has also produced cavitation during the fouling removal cycle but more distinctively, had generated higher vibrations along the circumference of the inner pipe wall. This could be explained by the delivery of vibration from the horn which does not only focus at the attachment point, and instead, allows the vibration to propagate across the structure which then delivers high pressure into the liquid. This gives an insight into focusing the cavitation generation at the solid-fluid interface without requiring the entire fluid domain to generate cavitation.

7.8 SUMMARY

This chapter has demonstrated the improvement of wave propagation across the 6 meter long pipe with the increase of number of HPUTs. The effects of marinisation are shown to overall have minimal attenuation of amplitude and instead, a shift in nodes and antinodes across the pipe, which can be a result of the geometry of the marinisation enclosure producing reflections that shift the displacement coverage. A cleaning cycle trialled on a U-shaped sample pipe has shown some promise for fouling removal as the larger deposits have been dislodged from the inner wall. This operation does require further cleaning cycles to remove the thick fouling layer accumulated in the pipe, and proposed methods to improve cleaning efficiency have been discussed in Table 7.6. An example of further improvements to the fouling removal technique had been suggested in Chapter 3, where the conical sonotrode is selected for potential improvements of ultrasonic cleaning results and coverage. This had been investigated both numerically and experimentally and shows the

potential to achieve faster cleaning compared to an individual HPUT. Further investigation is required to determine the improvement of cleaning time with the addition of the ultrasonic horn. This could be combined with the use of UGW to monitor the fouling removal during a cleaning cycle.

Chapter 8: Conclusions and Recommendations for Further Work

I'll leave tomorrow's problems to tomorrow's me – Saitama

8.1 CONCLUSIONS

The generation of cavitation and the wave propagation of HPUTs are the major factors that contribute towards the achievement of non-invasive fouling removal of pipelines. **The research presented within this thesis has made significant advances towards achieving long-distance fouling removal by improving the wave propagation across the structure using an optimised HPUT array. Initial work has been done for further improvements by the addition of a half wavelength sonotrode attachment.** From the objectives listed in Chapter 1, these are reviewed and the main achievements are discussed.

Identification of different types of fouling found in industry which was followed by a review of the current state-of-art has shown limitations of research for long-distance UGW detection. A literature survey of ultrasounds for fouling removal has shown invasive approaches however, recent research has shown a non-invasive application by the attachment of a single transducer on the outer wall of a structure which uses purely vibration for fouling removal. This has shown a gap in the knowledge where long-distance fouling detection and non-invasive fouling removal by the generation of ultrasonic cavitation bubbles can be investigated.

The development of a HPUT model has been created using COMSOL Multiphysics which utilises solid mechanics, electrostatics and the piezoelectric effect. The FE model has been validated using experimental analysis of the impedance characteristics using the Agilent Impedance Analyzer. The validated HPUT FE model has been used to investigate the attachment of ultrasonic horns for improved vibrational output. The optimised ultrasonic horns of varying shapes has undergone vibrational analysis of its wave propagation properties across a carbon steel plate structure using the Polytec PSV-400 3D Laser Scanning Vibrometer.

The validated HPUT FE model is applied onto a water-filled pipe structure within COMSOL Multiphysics by modelling the HPUT attached to the outer wall of the specimen. As this model neglects cavitation generation, a literature review was carried out to identify the minimum pressure threshold to generate cavitation. Literature has shown that for a 40 kHz excitation frequency, 1-2 Bar is pressure is required to generate cavitation. Further literature has shown that numerical modelling represents the pressure produced before cavitation is generated, where the pressure of the liquid drops to a third once cavitation bubbles are apparent. Using this knowledge, an FE model is created, showing locations of 6 Bar of pressure being achieved, these locations would be assumed to be the areas in which cavitation is generated and fouling removal is achieved.

To determine whether the ultrasonic cleaning FE model can predict cleaning patterns, fouled samples are required. This is carried out by generating a crystallisation fouling commonly found in industry known as Calcite, this is typically found on pipelines carrying high temperature fluids. The sample generation is carried out on 2 inch diameter stainless steel samples using electrochemistry. The method was adapted to generate fouling onto larger diameter, longer pipe samples, resulting in a heat-deposition method, where the outer wall of the schedule 40, 6.2 meter long pipe is heated to the required temperature to generate calcite whilst spraying a highly concentrated calcium carbonate solution on the inner wall of the pipe. In parallel to preparing the schedule 40 pipe with fouling, fouling detection was carried out on the pipeline using UGW in pitch-catch configuration. This showed a reduction in signal amplitude received with the addition of fouling within the pipeline. Fouling detection was further investigated in COMSOL Multiphysics which identified two parameters that are affected with the addition of Calcite on the inner pipe wall, the amplitude of the signal and shift in time-of-arrival of the signal.

The 2 inch fouled sample undergoes a cycle of fouling removal with a single HPUT attached to the outer wall of the pipe. During this cleaning cycle, the Polytec 3D Laser Scanning Vibrometer is used to measure the outer wall displacement for comparison with the FE model results. This showed good agreement between the cleaning patterns achieved, the outer wall displacement measured and the FE results. The FE model is adapted to investigate a HPUT configuration to achieve cleaning coverage across the schedule 40, 6.2 meter long pipe. The numerical investigation concluded the 4-HPUT configuration to achieve cleaning coverage up to 3 meters away from the HPUT location.

The 4-HPUT configuration is considered marinised and non-marinised and undergoes laboratory trials to investigate the wave propagation across the schedule 40 pipe sample. The experimental findings has shown with the increase of number of HPUTs excited, this increases the displacement achieved along the length of the pipe specimen. The marinisation technique has shown to dampen the HPUT performance. Field trials were carried out using the 4-HPUT collar displaying potential for industrial applications. Further studies were carried out to investigate, experimentally and numerically, the potential of using ultrasonic sonotrode attachments for which has shown promise for improved cleaning over time and coverage achieved.

8.2   RECOMMENDATIONS FOR FUTURE WORK

This research has shown potential for achieving long-distance coverage on pipelines. However, there are various aspects of the technique that can be improved further. This includes HPUT modifications and power electronics improvements.

8.2.1   ULTRASONIC SONOTRODE ATTACHMENT

As investigated in Chapter 3 and Chapter 7, the addition of a half-wavelength sonotrode has shown to not only remove fouling from a pipe specimen, but to also achieve more coverage compared to a single HPUT. Further work must be carried out to apply the sonotrode attachment for long-distance cleaning whilst also ensuring the vibration being produced at the sonotrode tip is not damaging the fouled structure. Techniques such as Genetic Algorithms (GA) can be used for the purpose of design optimisation (material selection and geometry refinement) by utilising the validated ultrasonic cleaning FEA.

8.2.2   POWER ELECTRONICS IMPROVEMENTS

The hardware electronics and software that is used to drive these HPUTs can also be optimised to improve the signal input, specifically self-adjusting the HPUT to excite at its known resonant frequency for maximum power and to avoid the generation of standing waves by inputting a frequency sweep. With the improvement of the software, the HPUTs can potentially achieve ultrasonic focusing, which can ensure that specific areas within a fouled structure can be specifically targeted and cleaned. Initial investigation of the square wave input has shown to improve cleaning performance, this would require further hardware development to control the temperature of the HPUT and the hardware itself as a result of driving the HPUTs at high amplitudes for longer periods of time in comparison to a sinusoidal wave input. The hardware to drive the HPUTs must also undergo testing for long-term use, CE marking and cable management to minimise power loss across large cable lengths.

8.2.3   COST-EFFECTIVE MARINISATION TECHNIQUE

For scalability of this technology for larger structures in underwater or harsh environments, a more cost-effective solution for marinisation should be developed to account for the number of HPUTs that a large structure may require. A conceptual design is proposed in Figure 8.1, which displays an HPUT encapsulated within a cylindrical enclosure. This would require the use of minimisation techniques such as Genetic Algorithms (GA) to optimise the dimensioning of the enclosure to be

watertight and withstand harsh conditions and to ensure that maximum amplitude is being achieved at the contact surface. For experimental investigations, the back plate and front plate should be detachable to allow access to the HPUT within the enclosure, allowing modifications and maintenance. The HPUT would be soldered to an IP69 rated marinised connector which is attached to the back plate, a marinised cabling can then connect to the connector before deployment.
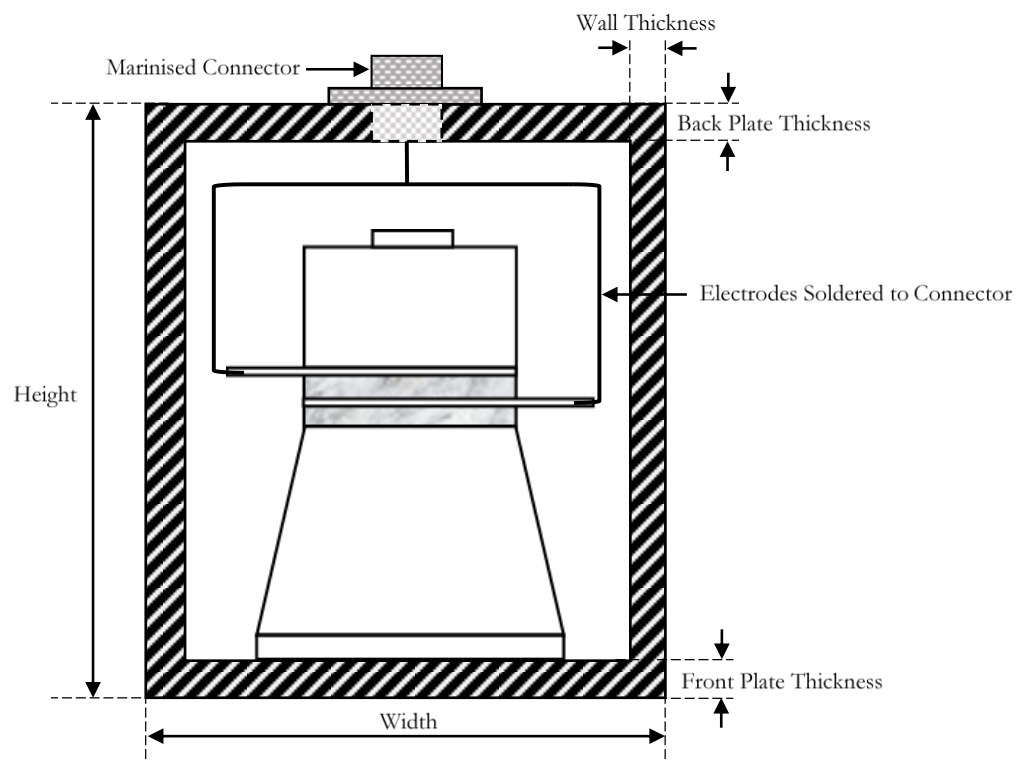
Figure 8.1: Conceptual schematic of cyndrical enclosure for future marinisation of HPUTs to undergo GA for geometry optimisation

8.2.4 FUTURE APPLICATIONS

The application of the fouling detection and removal techniques to cylindrical structures (pipelines) can be expanded onto larger cylindrical structures such as monopoles, see Figure 8.2 for more examples. The HPUTs in this case will need to be designed to conform to curved surfaces, as they may be attached to ship hulls and rotor blades. There is also strong interest in the offshore industry for biofouling removal and prevention due to the high costs of travelling to the offshore facility to carry out cleaning/maintenance. Some examples of offshore structures include wind turbine ladders, floating platforms, tidal generators and hydrogen generators. For offshore applications to be achieved, the marinisation methodology of HPUTs must be further investigated. The nuclear de-commissioning sector requires methods of fouling removal and de-contamination of radio-active material within pipelines. Each industrial application would require further study to

understand the interaction for fouling removal of the desired fouling to be removed, the geometric constraints such as coatings/material and the fluid medium that surrounds the structure.
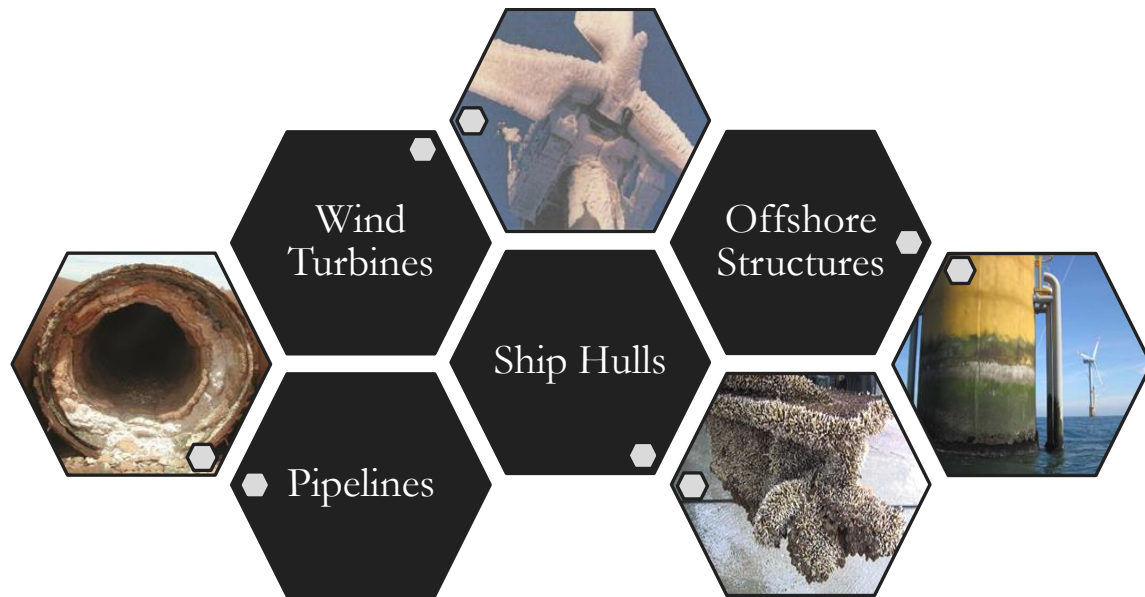
Figure 8.2: Examples of structures with fouling accumulation

REFERENCES

[1]   "Smart solutions for subsea pipeline blockages." [Online]. Available: https://www.offshore-technology.com/features/featuresmart-solutions-for-subsea-pipeline-blockages/ . [Accessed: 06-Feb-2019]

[2]   "Creation of stable and transient cavitation bubbles." [Online]. Available: https://www.hielscher.com/wp-content/uploads/stable-transient-cavitation-Santos-et-al.-2009-opt.png. [Accessed: 25-Jan-2018]

[3]   A. van der W. B. N. B.V., "The Importance of Pipeline Cleaning: Risks, Gains, Benefits, Peace of Mind," in *Pipeline Technology 2006 Conference* , 2006 [Online]. Available: https://www.pipeline-conference.com/sites/default/files/papers/224%20van%20der%20Werff.pdf

[4]   "Standard Decommissioning Programme(s) Template." [Online]. Available: https://assets.publishing.service.gov.uk/government/uploads/system/uploads/attachment_data/file/760561/Non_Derogation_Decommissioning_Programme_Template_-_November_2018.pdf

[5]   "UKCS Decommissioning 2018 Cost Estimate ." [Online]. Available: https://www.ogauthority.co.uk/media/4999/decommissioning-a5-2018-pdf-version.pdf. [Accessed: 06-Feb-2019]

[6]   M. Bourton, "HiTClean Report: D6.1 Dissemination and Exploitation Activities Report," 2019.

[7]   J. Glater, J. L. York, and K. S. Campbell, *Scale formation and prevention*, vol. 627. Academic Press, 1980.

[8]   C. Y. Tai, M.-C. Chang, R.-J. Shieh, and T. G. Chen, "Magnetic effects on crystal growth rate of calcite in a constant-composition environment," *Journal of Crystal Growth*, vol. 310, no. 15, pp. 3690–3697, 2008.

[9]   K. H. Schoenbach, R. W. Alden, and T. J. Fox, "Biofouling prevention with pulsed electric fields," in *Proceedings of 1996 International Power Modulator Symposium*, 1996, pp. 75–78.

[10]   A. P. W. R. Sheikholeslami, "Composite Fouling, Fundamentals and Mechanisms ," in *Encyclopedia of Desalination and Water Resources (DESWARE)*, 2012.

[11]   T. R. Bott, "Aspects of crystallization fouling," *Experimental Thermal and Fluid Science*, vol. 14, no. 4, pp. 356–360, 1997.

[12]   E. F. Somerscales, "Fundamentals of corrosion fouling," *British Corrosion Journal*, vol. 34, no. 2, pp. 109–124, 1999.

[13]   L. Melo and T. Bott, "Biofouling in water systems," *Experimental Thermal and Fluid Science*, vol. 14, no. 4, pp. 375–381, 1997.

References

[14]   T. Bott, "Biofouling control with ultrasound," *Heat Transfer Engineering*, vol. 21, no. 3, pp. 43–49, 2000.

[15]   A. Watkinson and D. Wilson, "Chemical reaction fouling: A review," *Experimental Thermal and Fluid Science*, vol. 14, no. 4, pp. 361–374, 1997.

[16]   M. Fernandez-Torres, A. Fitzgerald, W. Paterson, and D. Wilson, "A theoretical study of freezing fouling: limiting behaviour based on a heat and mass transfer analysis," *Chemical Engineering and Processing: Process Intensification*, vol. 40, no. 4, pp. 335–344, 2001.

[17]   A. Keary and R. Bowen, "On the prediction of local ice formation in pipes in the presence of natural convection," *Journal of heat transfer*, vol. 121, no. 4, pp. 934–944, 1999.

[18]   R. Nigo, Y. M. J. Chew, N. Houghton, W. Paterson, and D. Wilson, "Experimental studies of freezing fouling of model food fat solutions using a novel spinning disc apparatus," *Energy & Fuels*, vol. 23, no. 12, pp. 6131–6145, 2009.

[19]   K. Efird, "Inter-relation of corrosion and fouling for metals in sea water," *Mater. Performance;(United States)*, vol. 15, 1976.

[20]   D. Troup and J. Richardson, "The Link Between the Corrosion and calcium carbonate scaling susceptibilities of heat transfer surfaces," *Materials and Corrosion*, vol. 29, no. 5, pp. 312–320, 1978.

[21]   E. Wallhäußer, M. Hussein, and T. Becker, "Detection methods of fouling in heat exchangers in the food industry," *Food Control*, vol. 27, no. 1, pp. 1–10, 2012.

[22]   B. Espinasse, P. Bacchin, and P. Aimar, "On an experimental method to measure critical flux in ultrafiltration," *Desalination*, vol. 146, no. 1–3, pp. 91–96, 2002.

[23]   T. Davies, S. Henstridge, C. Gillham, and D. Wilson, "Investigation of whey protein deposit properties using heat flux sensors," *Food and Bioproducts processing*, vol. 75, no. 2, pp. 106–110, 1997.

[24]   P. M. Withers, "Ultrasonic, acoustic and optical techniques for the non-invasive detection of fouling in food processing equipment," *Trends in food science & technology*, vol. 7, no. 9, pp. 293–298, 1996.

[25]   T. R. Hay and J. L. Rose, "Fouling detection in the food industry using ultrasonic guided waves," *Food Control*, vol. 14, no. 7, pp. 481–488, 2003.

[26]   K. R. Lohr and J. L. Rose, "Ultrasonic guided wave and acoustic impact methods for pipe fouling detection," *Journal of Food Engineering*, vol. 56, no. 4, pp. 315–324, 2003.

[27]   J. L. Rose and P. B. Nagy, "Ultrasonic waves in solid media," *The Journal of the Acoustical Society of America*, vol. 107, no. 4, pp. 1807–1808, 2000.

[28]   P. S. Lowe, R. M. Sanderson, N. V. Boulgouris, A. G. Haig, and W. Balachandran, "Inspection of cylindrical structures using the first longitudinal guided wave mode in isolation for higher flaw sensitivity," *IEEE Sensors Journal*, vol. 16, no. 3, pp. 706–714, 2016.

References

[29]   A. H. Meitzler, "Mode coupling occurring in the propagation of elastic pulses in wires," *The Journal of the Acoustical Society of America*, vol. 33, no. 4, pp. 435–445, 1961.

[30]   M. Silk and K. Bainton, "The propagation in metal tubing of ultrasonic wave modes equivalent to Lamb waves," *Ultrasonics*, vol. 17, no. 1, pp. 11–19, 1979.

[31]   B. Pavlakovic, M. Lowe, D. Alleyne, and P. Cawley, "Disperse: a general purpose program for creating dispersion curves," in *Review of Progress in Quantitative Nondestructive Evaluation*, Springer, 1997, pp. 185–192.

[32]   P. Bocchini, A. Marzani, and E. Viola, "Graphical user interface for guided acoustic waves," *Journal of Computing in Civil Engineering*, vol. 25, no. 3, pp. 202–210, 2010.

[33]   W. Lowe, "Advances in resolution and sensitivity of ultrasonic guided waves for quantitative inspection of pipelines," *Brunel University London*, 2016.

[34]   J. Silva, I. Queiroz, A. Lima, F. Neff, and J. R. Neto, "Vibration analysis for fouling detection using hammer impact test and finite element simulation," in *Instrumentation and Measurement Technology Conference Proceedings, 2008. IMTC 2008. IEEE*, 2008, pp. 636–640.

[35]   J. Silva, K. Silva, A. Lima, and J. R. Neto, "Fouling detection based on analysis of ultrasonic guided waves using wavelet transform," in *Industrial Electronics, 2008. ISIE 2008. IEEE International Symposium on*, 2008, pp. 1187–1191.

[36]   J. Silva, A. M. Lima, H. Neff, and J. S. R. Neto, "Vibration analysis based on hammer impact for fouling detection using microphone and accelerometer as sensors," *Sensors \& Transducers*, vol. 112, no. 1, p. 10, 2010.

[37]   "Teletest Focus+." [Online]. Available: https://www.teletestndt.com/. [Accessed: 11-Nov-2018]

[38]   J. L. Rose, "Standing on the shoulders of giants: An example of guided wave inspection," *Mater. Eval*, vol. 60, no. 1, pp. 53–59, 2002.

[39]   J. Mu and J. L. Rose, "Guided wave propagation and mode differentiation in hollow cylinders with viscoelastic coatings," *The Journal of the Acoustical Society of America*, vol. 124, no. 2, pp. 866–874, 2008.

[40]   F. Benmeddour, F. Treyssède, and L. Laguerre, "Numerical modeling of guided wave interaction with non-axisymmetric cracks in elastic cylinders," *International journal of Solids and Structures*, vol. 48, no. 5, pp. 764–774, 2011.

[41]   F. Moser, L. J. Jacobs, and J. Qu, "Modeling elastic wave propagation in waveguides with the finite element method," *NDT & E International*, vol. 32, no. 4, pp. 225–234, 1999.

[42]   V. C. Protopappas, I. C. Kourtis, L. C. Kourtis, K. N. Malizos, C. V. Massalas, and D. I. Fotiadis, "Three-dimensional finite element modeling of guided ultrasound wave propagation in intact and healing long bones.," *J. Acoust. Soc. Am.*, vol. 121, no. 6, pp. 3907–21, 2007.

[43]   R. Raišutis, R. Kažys, E. Žukauskas, L. Mažeika, and A. Vladišauskas, "Application of ultrasonic guided waves for non-destructive testing of defective CFRP rods with multiple

delaminations," *NDT \& E International*, vol. 43, no. 5, pp. 416–424, 2010.

[44]   I. Bartoli, F. Lanza di Scalea, M. Fateh, and E. Viola, "Modeling guided wave propagation with application to the long-range defect detection in railroad tracks," *NDT & E International*, vol. 38, no. 5, pp. 325–334, 2005.

[45]   M. Zheng, C. Lu, G. Chen, and P. Men, "Modeling three-dimensional ultrasonic guided wave propagation and scattering in circular cylindrical structures using finite element approach," *Physics Procedia*, vol. 22, pp. 112–118, 2011.

[46]   B. Ghose and K. Balasubramaniam, "Finite Element Modeling and Simulation of Ultrasonic Guided Wave Propagation using Frequency Response Analysis," in *Proceedings of the 14th Asia-Pacific Conference on NDT*, 2013.

[47]   "Ocean Team Group as." [Online]. Available: http://www.oceanteam.eu/. [Accessed: 14-Mar-2017]

[48]   A. Shoh, "Industrial applications of ultrasound-A review I. High-power ultrasound," *IEEE transactions on sonics and ultrasonics*, vol. 22, no. 2, pp. 60–70, 1975.

[49]   K.-V. Jenderka and C. Koch, "Investigation of spatial distribution of sound field parameters in ultrasound cleaning baths under the influence of cavitation.," *Ultrasonics*, vol. 44 Suppl 1, pp. e401–6, 2006.

[50]   H.-C. Flemming, "Reverse osmosis membrane biofouling," *Thermal and Fluid Science*, vol. 14, no. 4, pp. 382–391, 1997.

[51]   H. Maddah and A. Chogle, "Biofouling in reverse osmosis: phenomena, monitoring, controlling and remediation," *Applied Water Science*, pp. 1–15, 2016.

[52]   M. O. Lamminen, "Ultrasonic cleaning of latex particle fouled membranes," *PhD Thesis, Ohio State University, USA*, 2004.

[53]   V. Naddeo, L. Borea, and V. Belgiorno, "Sonochemical control of fouling formation in membrane ultrafiltration of wastewater: Effect of ultrasonic frequency," *Journal of Water Process Engineering*, vol. 8, pp. e92–e97, 2015.

[54]   T. Mason and F. E. Sonochemistry, "Oxford Science Publications," *New York, USA*, 1999.

[55]   B. Lozowicka, M. Jankowska, I. Hrynko, and P. Kaczynski, "Removal of 16 pesticide residues from strawberries by washing with tap and ozone water, ultrasonic cleaning and boiling," *Environmental Monitoring and Assessment*, vol. 188, no. 1, pp. 1–19, 2016.

[56]   B. Verhaagen, T. Zanderink, and D. F. Rivas, "Ultrasonic cleaning of 3D printed objects and Cleaning Challenge Devices," *Applied Acoustics*, vol. 103, pp. 172–181, 2016.

[57]   L. Barnes, D. van der Meulen, B. Orchard, and C. Gray, "Novel use of an ultrasonic cleaning device for fish reproductive studies," *Journal of Sea Research*, vol. 76, pp. 222–226, 2013.

References

[58]   D. D. Nguyen, H. H. Ngo, Y. S. Yoon, S. W. Chang, and H. H. Bui, "A new approach involving a multi transducer ultrasonic system for cleaning turbine engines' oil filters under practical conditions," *Ultrasonics*, vol. 71, pp. 256–263, 2016.

[59]   K. Gotoh and K. Harayama, "Application of ultrasound to textiles washing in aqueous solutions.," *Ultrason Sonochemistry*, vol. 20, no. 2, pp. 747–53, 2013.

[60]   A. G. Juarez, G. R. Corral, G. N. V. de Parga, F. V. Martinez, and P. van der Vlist, "Process and device for continuous ultrasonic washing of textile," 2001.

[61]   G. Mazue, R. Viennet, J.-Y. Hihn, L. Carpentier, P. Devidal, and I. Albaïna, "Large-scale ultrasonic cleaning system: Design of a multi-transducer device for boat cleaning (20kHz).," *Ultrason Sonochem*, vol. 18, no. 4, pp. 895–900, 2011.

[62]   A. Yap and W. Bagnall, "High power ultrasonics: a new and powerful tool for removing tartrate deposits and killing viable Brettanomyces cells in barrels," *Wine Industry Journal*, vol. 25, pp. 29–39, 2009.

[63]   S. Lin and F. Zhang, "Measurement of ultrasonic power and electro-acoustic efficiency of high power transducers," *Ultrasonics*, vol. 37, no. 8, pp. 549–554, 2000.

[64]   C. E. Brennen, *Cavitation and bubble dynamics*. Cambridge University Press, 2013.

[65]   MISSING:imagecav, "MISSING:imagecav," 2019.

[66]   K. Yasui, "Acoustic Cavitation," in *Acoustic Cavitation and Bubble Dynamics*, Springer, 2018, pp. 1–35.

[67]   M. P. Brenner, S. Hilgenfeldt, and D. Lohse, "Single-bubble sonoluminescence," *Reviews of Modern Physics*, vol. 74, no. 2, p. 425, 2002.

[68]   R. Esche, "Untersuchung der schwingungskavitation in flüssigkeiten," *Acta Acustica united with Acustica*, vol. 2, no. 6, pp. 208–218, 1952.

[69]   M. S. Plesset and A. Prosperetti, "Bubble dynamics and cavitation," *Annual Review of Fluid Mechanics*, vol. 9, no. 1, pp. 145–185, 1977.

[70]   M. H. Azhdast, H. Haleh, P. Pouladzadeh, A. Azhdast, and M. Soltanabadi, "Theoretical and experimental analysis of beating and cavitation phenomenon on erosion in ultrasonic cleaning process," in *2009 IEEE/ASME International Conference on Advanced Intelligent Mechatronics*, 2009, pp. 624–629.

[71]   N. S. M. Yusof, B. Babgi, Y. Alghamdi, M. Aksu, J. Madhavan, and M. Ashokkumar, "Physical and chemical effects of acoustic cavitation in selected ultrasonic cleaning applications," *Ultrasonics Sonochemistry*, vol. 29, pp. 568–576, 2016.

[72]   M. O. Lamminen, H. W. Walker, and L. K. Weavers, "Mechanisms and factors influencing the ultrasonic cleaning of particle-fouled ceramic membranes," *Journal of Membrane Science*, vol. 237, no. 1, pp. 213–223, 2004.

References

[73]   D. Peregrine, "The Acoustic Bubble. By TG LEIGHTON. Academic Press, 1994. 613 pp.\pounds 95. ISBN 0-12-441920-8.," *Journal of Fluid Mechanics*, vol. 272, pp. 407–408, 1994.

[74]   L. A. Crum, "Comments on the evolving field of sonochemistry by a cavitation physicist," *Ultrasonics Sonochemistry*, vol. 2, no. 2, pp. S147–S152, 1995.

[75]   K. S. Suslick, *Ultrasound: its chemical, physical, and biological effects*. VCH Publishers, 1988.

[76]   J. L. Laborde, C. Bouyer, J.-P. Caltagirone, and A. Gérard, "Acoustic bubble cavitation at low frequencies," *Ultrasonics*, vol. 36, no. 1–5, pp. 589–594, 1998.

[77]   S. Guo, B. C. Khoo, S. L. M. Teo, and H. P. Lee, "The effect of cavitation bubbles on the removal of juvenile barnacles," *Colloids and Surfaces B: Biointerfaces*, vol. 109, pp. 219–227, 2013.

[78]   S. K. Sankaranarayanan and V. R. Bhethanabotla, "Identifying the Removal Mechanism of Fouling Proteins In a Surface Acoustic Wave Biosensor: A Numerical Study and Comparison to Experiments," in *2008 AIChE Annual Meeting*, 2008.

[79]   S. Muthukumaran, K. Yang, A. Seuren, S. Kentish, M. Ashokkumar, G. W. Stevens, and F. Grieser, "The use of ultrasonic cleaning for ultrafiltration membranes in the dairy industry," *Separation and Purification Technology*, vol. 39, no. 1, pp. 99–107, 2004.

[80]   M. Legay, Y. Allibert, N. Gondrexon, P. Boldo, and S. Le Person, "Experimental investigations of fouling reduction in an ultrasonically-assisted heat exchanger," *Experimental Thermal and Fluid Science*, vol. 46, pp. 111–119, 2013.

[81]   "Hilsonic." [Online]. Available: http://www.hilsonic.co.uk/. [Accessed: 14-Aug-2017]

[82]   "Ultrawave." [Online]. Available: http://www.ultrawave.co.uk/. [Accessed: 14-Aug-2017]

[83]   G. Harvey, A. Gachagan, and T. Mutasa, "Review of high-power ultrasound-industrial applications and measurement methods," *IEEE transactions on ultrasonics, ferroelectrics, and frequency control*, vol. 61, no. 3, pp. 481–95, 2014.

[84]   T. J. Mason, "Ultrasonic cleaning: An historical perspective," *Ultrasonics Sonochemistry*, vol. 29, pp. 519–523, 2016.

[85]   N. I. Marinescu, D. Ghiculescu, and O. Alupei, "Aspects concerning FEM modelling of an ultrasonic horn used at micro-EDM drilling," *Nonconventional Technologies Review*, vol. 20, no. 4, 2016.

[86]   A. S. Nanu, N. I. Marinescu, and D. Ghiculescu, "Study on ultrasonic stepped horn geometry design and FEM simulation," *Nonconventional Technologies Review*, vol. 4, pp. 25–30, 2011.

[87]   K.-M. Shu and J.-W. Chen, "The design of acoustic horns for ultrasonic aided tube double side flange making," *International Journal of Mechanical, Aerospace, Industrial, Mechatronic and Manufacturing Engineering*, vol. 9, no. 5, 2015.

References

[88]   Y.-J. Choi, K.-H. Park, Y.-H. Hong, K.-T. Kim, S.-W. Lee, and H.-Z. Choi, "Effect of ultrasonic vibration in grinding; horn design and experiment," *International Journal of Precision Engineering and Manufacturing*, vol. 14, no. 11, pp. 1873–1879, 2013.

[89]   M. R. Rani and R. Rudramoorthy, "Computational modeling and experimental studies of the dynamic performance of ultrasonic horn profiles used in plastic welding," *Ultrasonics*, vol. 53, no. 3, pp. 763–772, 2013.

[90]   M. Na\vd, "Ultrasonic horn design for ultrasonic machining technologies," *Applied and Computational Mechanics*, vol. 4, no. 1, pp. 68–78, 2010.

[91]   S. Lin, "Analysis of multifrequency Langevin composite ultrasonic transducers," *IEEE transactions on ultrasonics, ferroelectrics, and frequency control*, vol. 56, no. 9, pp. 1990–8, 2009.

[92]   D. M. Donskoy and B. A. Cray, "Acoustic particle velocity horns," *The Journal of the Acoustical Society of America*, vol. 131, no. 5, pp. 3883–3890, 2012.

[93]   P. Harkness, M. Lucas, and A. Cardoni, "Coupling and degenerating modes in longitudinal-torsional step horns," *Ultrasonics*, vol. 52, no. 8, pp. 980–988, 2012.

[94]   W. Colclough, "The chemistry of solvents used for ultrasonic cleaning," *Ultrasonics*, vol. 6, no. 1, pp. 21–23, 1968.

[95]   O. Antony, "Technical aspects of ultrasonic cleaning," *Ultrasonics*, vol. 1, no. 4, pp. 194–198, 1963.

[96]   M. Ibisi and B. Brown, "Variation of the relative intensity of cavitation with temperature," *The Journal of the Acoustical Society of America*, vol. 41, no. 3, pp. 568–572, 1967.

[97]   B. Niemczewski, "A comparison of ultrasonic cavitation intensity in liquids," *Ultrasonics*, vol. 18, no. 3, pp. 107–110, 1980.

[98]   A. Henglein and M. Gutierrez, "Chemical effects of continuous and pulsed ultrasound: a comparative study of polymer degradation and iodide oxidation," *Journal of Physical Chemistry*, vol. 94, no. 12, pp. 5169–5172, 1990.

[99]   D. McQueen, "Frequency dependence of ultrasonic cleaning," *Ultrasonics*, vol. 24, no. 5, pp. 273–280, 1986.

[100]   A. Mathieson, N. Cerisola, and A. Cardoni, "Nonlinear characterization of half and full wavelength power ultrasonic devices," *Physics Procedia*, vol. 87, pp. 125–131, 2016.

[101]   V. Raman, A. Abbas, and S. C. Joshi, "Mapping local cavitation events in high intensity ultrasound fields," in *Excerpt from the Proceedings of the COMSOL Users Conference, Bangalore, India*, 2006, pp. 1–6.

[102]   S. L. Peshkovsky and A. S. Peshkovsky, "Matching a transducer to water at cavitation: acoustic horn design principles.," *Ultrason Sonochem*, vol. 14, no. 3, pp. 314–22, 2007.

[103]   Z. Wei, J. A. Kosterman, R. Xiao, G.-Y. Pee, M. Cai, and L. K. Weavers, "Designing and characterizing a multi-stepped ultrasonic horn for enhanced sonochemical performance,"

Ultrasonics Sonochemistry, vol. 27, pp. 325–333, 2015.

[104]   L. E. Kinsler, A. R. Frey, A. B. Coppens, and J. V. Sanders, "Fundamentals of acoustics," *Fundamentals of Acoustics, 4th Edition, by Lawrence E. Kinsler, Austin R. Frey, Alan B. Coppens, James V. Sanders, pp. 560. ISBN 0-471-84789-5. Wiley-VCH, December 1999.*, p. 560, 1999.

[105]   S. H. Kristensen, "Design, construction and characterization of high power ultrasound sources," *Master's thesis, Univ. of Southern Denmark*, 2009.

[106]   "Augment Your COMSOL Multiphysics® Models with Material Properties from the Material Library." [Online]. Available: https://uk.comsol.com/material-library. [Accessed: 18-May-2019]

[107]   H. Lais, P. S. Lowe, T.-H. Gan, and L. C. Wrobel, "Numerical modelling of acoustic pressure fields to optimize the ultrasonic cleaning technique for cylinders," *Ultrasonics Sonochemistry*, vol. 45, pp. 7–16, 2018.

[108]   "Resolving time-dependent waves." [Online]. Available: https://www.comsol.com/support/knowledgebase/1118/. [Accessed: 11-Jun-2016]

[109]   "4294A Precision Impedance Analyzer." [Online]. Available: https://www.keysight.com/gb/en/home.html. [Accessed: 18-May-2019]

[110]   "Beijing Ultrasonics." [Online]. Available: https://www.bjultrasonic.com/. [Accessed: 07-Aug-2019]

[111]   "Polytec PSV-400 3D Laser Scanning Vibrometer ." [Online]. Available: https://www.polytec.com/uk/. [Accessed: 18-May-2019]

[112]   G. L. Chahine, A. Kapahi, J.-K. Choi, and C.-T. Hsiao, "Modeling of surface cleaning by cavitation bubble dynamics and collapse," *Ultrasonics Sonochemistry*, vol. 29, pp. 528–549, 2016.

[113]   C.-T. Hsiao, A. Jayaprakash, A. Kapahi, J.-K. Choi, and G. L. Chahine, "Modelling of material pitting from cavitation bubble collapse," *Journal of Fluid Mechanics*, vol. 755, pp. 142–175, 2014.

[114]   R. Jamshidi, *Modeling and Numerical Investigation of Acoustic Cavitation with Applications in Sonochemistry*. Papierflieger Verlag, 2014.

[115]   J. Lewis, S. Gardner, and I. Corp, "A 2D finite element analysis of an ultrasonic cleaning vessel: results and comparisons," *International Journal of Modelling and Simulation*, vol. 27, no. 2, pp. 181–185, 2007.

[116]   V. Moholkar, V. Nierstrasz, and M. Warmoeskerken, "Intensification of mass transfer in wet textile processes by power ultrasound," *Autex Research Journal*, vol. 3, no. 3, pp. 129–138, 2003.

[117]   M. Hodnett, B. Zeqiri, N. Lee, and P. Gélat, "Report on the feasibility of establishing a reference cavitating medium," *NPL Report CMAM 58, National Physical Laboratory, Teddington, UK*, 2001.

References

[118]   R. E. Caflisch, M. J. Miksis, G. C. Papanicolaou, and L. Ting, "Effective equations for wave propagation in bubbly liquids," *Journal of Fluid Mechanics*, vol. 153, pp. 259–273, 1985.

[119]   K. W. Commander and A. Prosperetti, "Linear pressure waves in bubbly liquids: Comparison between theory and experiments," *The Journal of the Acoustical Society of America*, vol. 85, no. 2, pp. 732–746, 1989.

[120]   I. Tudela, V. Sáez, M. D. Esclapez, M. I. Díez-García, P. Bonete, and J. González-García, "Simulation of the spatial distribution of the acoustic pressure in sonochemical reactors with numerical methods: a review.," *Ultrason Sonochem*, vol. 21, no. 3, pp. 909–19, 2014.

[121]   C. Vanhille and C. Campos-Pozuelo, "Numerical simulations of three-dimensional nonlinear acoustic waves in bubbly liquids," *Ultrasonics Sonochemistry*, vol. 20, no. 3, pp. 963–969, 2013.

[122]   C. Vanhille, "A two-dimensional nonlinear model for the generation of stable cavitation bubbles," *Ultrasonics Sonochemistry*, vol. 31, pp. 631–636, 2016.

[123]   D. Fuster and T. Colonius, "Modelling bubble clusters in compressible liquids," *Journal of Fluid Mechanics*, vol. 688, pp. 352–389, 2011.

[124]   Z. Wei and L. K. Weavers, "Combining COMSOL modeling with acoustic pressure maps to design sono-reactors," *Ultrasonics Sonochemistry*, vol. 31, pp. 490–498, 2016.

[125]   L. Zhong, "COMSOL Multiphysics Simulation of Ultrasonic Energy in Cleaning Tanks ," in *COMSOL Conference 2014, Boston, USA*, 2014.

[126]   O. Louisnard, "A viable method to predict acoustic streaming in presence of cavitation," *Ultrasonics Sonochemistry*, vol. 35, pp. 518–524, 2017.

[127]   O. Louisnard, "A simple model of ultrasound propagation in a cavitating liquid. Part I: Theory, nonlinear attenuation and traveling wave generation," *Ultrasonics Sonochemistry*, vol. 19, no. 1, pp. 56–65, 2012.

[128]   H. Dogan and V. Popov, "Numerical simulation of the nonlinear ultrasonic pressure wave propagation in a cavitating bubbly liquid inside a sonochemical reactor," *Ultrasonics Sonochemistry*, vol. 30, pp. 87–97, 2016.

[129]   R. Jamshidi and G. Brenner, "Dissipation of ultrasonic wave propagation in bubbly liquids considering the effect of compressibility to the first order of acoustical Mach number," *Ultrasonics*, vol. 53, no. 4, pp. 842–848, 2013.

[130]   R. Mettin, P. Koch, W. Lauterborn, and D. Krefting, "Modeling acoustic cavitation with bubble redistribution," in *Sixth International Symposium on Cavitation*, 2006, vol. 75, pp. 1–5.

[131]   B. Han, K. Köhler, R. Mettin, and A. Vogel, "Numerical simulation of bubble interaction," *Fortschritte der Akustik-DAGA*, pp. 453–454, 2012.

[132]   K. Yasui, Y. Iida, T. Tuziuti, T. Kozuka, and A. Towata, "Strongly interacting bubbles under an ultrasonic horn," *Physical Review E*, vol. 77, no. 1, p. 016609, 2008.

References

[133]   V. S. Moholkar, S. P. Sable, and A. B. Pandit, "Mapping the cavitation intensity in an ultrasonic bath using the acoustic emission," *AIChE journal*, vol. 46, no. 4, pp. 684–694, 2000.

[134]   M. Ashokkumar, *Handbook of Ultrasonics and Sonochemistry*. Springer, 2016.

[135]   K. Yasui, T. Kozuka, T. Tuziuti, A. Towata, Y. Iida, J. King, and P. Macey, "FEM calculation of an acoustic field in a sonochemical reactor," *Ultrasonics Sonochemistry*, vol. 14, no. 5, pp. 605–614, 2007.

[136]   I. M. G. de C. Esteban-Infantes, "Fundamentals of Pipeline Cleaning with Acoustic Cavitation," *PhD Thesis, Brunel University London, UK*, 2016.

[137]   "Viaduct Trading LTD." [Online]. Available: http://viaducttrading.com/. [Accessed: 31-May-2018]

[138]   P. Wilcox, M. Lowe, and P. Cawley, "The effect of dispersion on long-range inspection using ultrasonic guided waves," *NDT & E International*, vol. 34, no. 1, pp. 1–9, 2001.

[139]   P. Lowe, R. Sanderson, N. Boulgouris, and T. Gan, "Hybrid active focusing with adaptive dispersion for higher defect sensitivity in guided wave inspection of cylindrical structures," *Nondestructive Testing and Evaluation*, vol. 31, no. 3, pp. 219–234, 2016.

[140]   K. Yasui, T. Tuziuti, J. Lee, T. Kozuka, A. Towata, and Y. Iida, "Numerical simulations of acoustic cavitation noise with the temporal fluctuation in the number of bubbles," *Ultrasonics Sonochemistry*, vol. 17, no. 2, pp. 460–472, 2010.

[141]   M. O. Lamminen, H. W. Walker, and L. K. Weavers, "Effect of fouling conditions and cake layer structure on the ultrasonic cleaning of ceramic membranes," *Separation science and technology*, vol. 41, no. 16, pp. 3569–3584, 2006.

[142]   M. Cai, S. Zhao, and H. Liang, "Mechanisms for the enhancement of ultrafiltration and membrane cleaning by different ultrasonic frequencies," *Desalination*, vol. 263, no. 1, pp. 133–138, 2010.

[143]   S. Muthukumaran, S. E. Kentish, M. Ashokkumar, and G. W. Stevens, "Mechanisms for the ultrasonic enhancement of dairy whey ultrafiltration," *Journal of Membrane Science*, vol. 258, no. 1–2, pp. 106–114, 2005.

[144]   Y. Chang, J. H. Bae, and H.-C. Yi, "Ultrasonic cleaning of used plastic parts for remanufacturing of multifunctional digital copier," *International Journal of Precision Engineering and Manufacturing*, vol. 14, no. 6, pp. 951–956, 2013.

[145]   A. P. Mairal, A. R. Greenberg, and W. B. Krantz, "Investigation of membrane fouling and cleaning using ultrasonic time-domain reflectometry," *Desalination*, vol. 130, no. 1, pp. 45–60, 2000.

[146]   E. Ando and Y. Kagawa, "Finite element simulation for the design of an ultrasonic cleaning tank," *Electronics and Communications in Japan (Part III: Fundamental Electronic Science)*, vol. 72, no. 7, pp. 43–57, 1989.

References

[147]   M. Hill and R. J. Wood, "Modelling in the design of a flow-through ultrasonic separator," *Ultrasonics*, vol. 38, no. 1–8, pp. 662–665, 2000.

[148]   E. Heikkola and M. Laitinen, "Model-based optimization of ultrasonic transducers.," *Ultrason Sonochem*, vol. 12, no. 1–2, pp. 53–7, 2005.

[149]   N. Bretz, J. Strobel, M. Kaltenbacher, and R. Lerch, "Numerical simulation of ultrasonic waves in cavitating fluids with special consideration of ultrasonic cleaning," in *Ultrasonics Symposium, 2005 IEEE*, 2005, vol. 1, pp. 703–706.

[150]   J. Jordens, A. Honings, J. Degrève, L. Braeken, and T. Van Gerven, "Investigation of design parameters in ultrasound reactors with confined channels.," *Ultrason Sonochem*, vol. 20, no. 6, pp. 1345–52, 2013.

[151]   "STS Defence." [Online]. Available: https://www.sts-defence.com/. [Accessed: 07-Aug-2019]

[152]   "Brunel Innovation Centre." [Online]. Available: https://www.brunel.ac.uk/bic. [Accessed: 04-Aug-2019]

[153]   "InnoTecUK." [Online]. Available: https://www.innotecuk.com. [Accessed: 04-Aug-2019]

[154]   "Teletest Focus+." [Online]. Available: https://www.teletestndt.com/focus-guided-wave-inspection/. [Accessed: 04-Aug-2019]

[155]   "ESSAR." [Online]. Available: https://www.essar.com/. [Accessed: 04-Aug-2019]